Geochemistry of Gardar Intrusions in the Ivigtut area, South Greenland

Kathryn M. Goodenough

Doctor of Philosophy

University of Edinburgh

1997

Declaration

I declare that this thesis is my own original work, except where otherwise stated, and has not been submitted for any other degree.

K

Acknowledgments

There are many people to thank for their help during the term of this PhD. Firstly, my supervisors, Brian Upton, Ian Parsons and Adrian Finch, have provided lots of encouragement and advice along the way, which has been greatly appreciated. They also managed to read my thesis drafts with incredible speed! Adrian Finch, Denise Stirling, Ian Parsons and Bill Brown were all great field companions. Rob Ellam and Godfrey Fitton have given up large amounts of time to help with isotope and XRF analysis respectively, and to discuss the results; their assistance is greatly appreciated. Many other people contributed to the analytical work. At Edinburgh, Mike Hall made the thin sections, Dodie James was incredibly helpful both with XRF analysis and advice on parts of the thesis, and Simon Burgess, Pete Hill and Stuart Kearns all assisted with the electron probe study. At SURRC, Rob Ellam, Adrian Boyce, Anne Kelly, and Vinny Gallagher taught me everything I know about isotope analysis. Sarah James and Nick Walsh at RHBNC helped with the REE analysis. John Bailey provided the samples from Ivigtut drill cores. Tom Andersen helped me make sense of my Pb isotope data. And before all this, John Reavy must be thanked for inspiring my interest in igneous petrology.

There are lots of other people who have made my years at Edinburgh enjoyable; far too many to mention everyone individually. Many people in the Department should be thanked for some good times, particularly those that kept me going whilst writing-up: Amanda Voase, Alison Sowerbutts, Lynne Chambers, Martin Purvis and Jason Smith, as well as many others. The other staff and drinkers in the Argyle Bar reminded me that there is life outside a PhD, and generally helped preserve my sanity. My flatmates, Gavin Legg, Laura Kosidowski, Viv Bailey, Andy Farrell and Tim Fagge have all been great. Finally, my parents deserve the most thanks of all: without their support and self-sacrifice over the years, this PhD would never have been written.

Abstract

The Gardar Alkaline Igneous Province is a Proterozoic, rift-related, province in south-west Greenland. It consists of lavas, central complexes and dyke swarms, dating from between 1350 and 1150 million years ago. The majority of the intrusives were emplaced into a Proterozoic mobile belt which formed during the Ketilidian orogeny at ~1850-1740 Ma, but the north-western part of the province transgressed onto the edge of the South Greenland Archaean craton, and it is this area which has been investigated in this work.

The Gardar intrusives within the craton include three central complexes, Grønnedal-Íka, Ivigtut and Kûngnât, as well as many dykes. Grønnedal-Íka is the oldest of the complexes, and consists of nepheline syenites cut by a carbonatite plug. The oldest dykes in the area are lamprophyres; these were succeeded by various groups of basic and alkaline salic dykes, including a major set of olivine dolerites known as the "Brown Dykes". The Ivigtut stock is an alkali granite which, prior to mining, contained the world's largest deposit of cryolite, and the granite shows a distinctive pattern of alteration related to the fluids from which the ore deposit formed. The Kûngnât Complex consists of saturated and over-saturated syenites with an alkali gabbro ring-dyke. The petrography of the different rock-types is described together with the mineralogy of the Ivigtut granite.

The Gardar rocks of the subject area represent a wide spectrum of SiO_2 contents, from 35 wt% in the lamprophyres to 75 wt% in the granites, indicating a range from magmas of primitive compositions to highly evolved granites. The lamprophyre dykes have normalised trace element patterns similar to those of Ocean Island Basalts (OIB), whereas the patterns for the basaltic dykes suggest interaction with crust or sub-continental lithospheric mantle (SCLM). The trace and rare earth element patterns for the salic rocks

show evidence of evolution by fractionation from basic magmas. The altered rocks of the Ivigtut stock show large amounts of enrichment in highly incompatible elements (including the HREE). In general, all the granitic rocks have the characteristics of A-type granites.

Selected samples were analysed for Nd-, Sr- and (in some cases) Pb-isotopes in order to investigate the petrogenesis of the Gardar magmas. Nd- and Sr-isotope data show that the basic magmas were derived from a mildly depleted mantle source; and support the conclusion that the salic rocks evolved by fractionation of these basic parents, with accompanying crustal contamination in the silica over-saturated examples. Pb- isotope data provide further confirmation of these conclusions. Magmatic carbonates occur within each of the central complexes, as well as in the lamprophyric dykes; C- and O- isotope data imply a mantle source for the carbonates at Grønnedal-Íka and Ivigtut, but indicate crustal contamination at Kûngnât.

Comparison with data from Gardar rocks emplaced in the Ketilidian mobile zone to the south suggests that magma sources were similar and indicates that the magmas intruded through the Archaean craton were not sourced in a different, older component of lithospheric mantle. Geochemical differences between the intrusives within the craton and those to the south can be attributed to the nature of the crustal contaminant.

It is concluded that the Gardar lamprophyre magmas formed as volatile-rich small-degree partial melts within the asthenosphere, which were intruded with minimal lithospheric contamination. Larger melt volumes were derived from lithospheric mantle which had been selectively enriched in incompatible elements, possibly through the action of fluids derived from a subducting slab at the close of the Ketilidian orogeny. These melts were

intruded as primitive dykes, or evolved through fractionation and variable crustal contamination to produce the spectrum of Gardar magmas.

The mountain of Kûngnât, seen from the Grønnedal-Íka complex

South Greenland

Chapter 1: Introduction

1.1 The Alkaline Rocks

The alkaline rocks have been extensively studied and various volumes have been published specifically on this subject, in particular those edited by Sørensen (1974) and Fitton & Upton (1987). They are of major interest due to their mineralogical diversity and their extreme enrichment in the large-ion lithophile elements (LILE) and high field strength elements (HFSE), and therefore studies of their magma genesis have become widespread. Alkaline rocks are generally considered to originate by fractionation of a mantle source, rather than by melting of crustal material (Menzies, 1987), but the nature of that mantle source does not appear to be consistent for alkaline rocks throughout the world. Many authors (reviewed by Bailey, 1987) have invoked a source of metasomatised, LILE-enriched mantle within the continental lithosphere. However, Fitton & Dunlop (1985) showed that alkali basalts erupted in oceanic and continental settings from the Cameroon line have identical chemistry, implying a source in the asthenosphere. A superb area in which to study these immensely variable rocks is provided by the Gardar province of South Greenland, which is a well exposed, mid-Proterozoic alkaline province.

1.2 The Gardar province

The Gardar igneous province was formed during a period of intra-plate alkaline magmatism related to rifting, with intrusive activity occurring between about 1350 and 1150 million years ago (Ma). The area has been visited by geologists since the early 19th century but since 1954 has been extensively mapped by geologists working under the auspices of the

Greenland Geological Survey, e.g. Upton (1960), Berthelsen (1962). Reviews have been published by Upton (1974), Emeleus & Upton (1976) and Upton & Emeleus (1987).

Gardar igneous rocks occur as relict lava successions interbedded with continental sandstones, and as intrusive complexes and dykes. These were mostly emplaced into Proterozoic basement formed during the Ketilidian orogeny, although the northwest part of the complex lies on the South Greenland Archaean craton (Fig. 1.1). The Gardar intrusives include about ten central complexes, which crop out in a belt roughly 70km by 200km (Emeleus & Upton, 1976). These vary in size, from the Ivigtut stock which is about 300m across, to Nunarssuit, which crops out over an area of greater than 1000km^2.

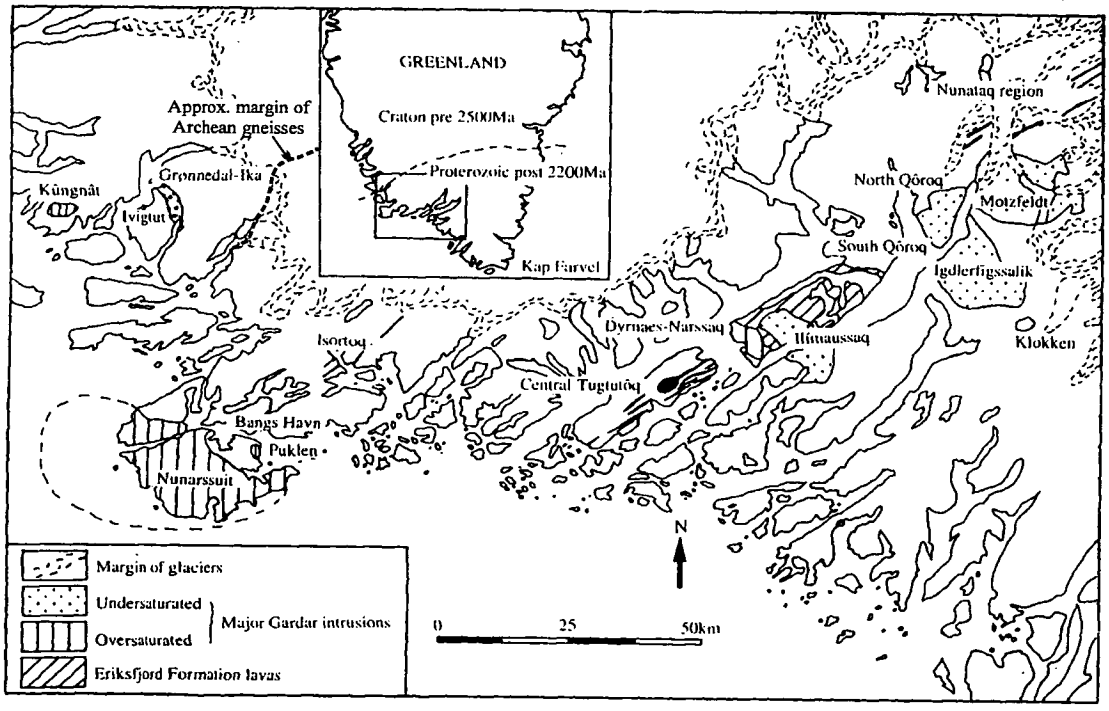

Fig. 1.1: Map of the Gardar Province, after Upton & Emeleus (1987). Inset shows the relationship to the Greenland basement rocks.

Upton & Emeleus (1987) considered that igneous activity in the Gardar can be divided essentially into three periods: early-, mid-, and late- Gardar. Each period represents a magmatic cycle, which commenced with a large-scale uprise of olivine basalt or hawaiite magmas during phases of crustal attenuation and ended with emplacement of central complexes.

The oldest rocks of the Gardar province appear to be those of the Eriksfjord Formation, which consists of clastic sediments interbedded with lavas and subordinate pyroclastics. This formation is now only found *in situ* in the eastern part of the region, where a thickness of 3000-5000m is preserved in the Ilímaussaq fault block, although the presence of Eriksfjord xenoliths in other parts of the province suggests that coverage was once much more extensive. The Eriksfjord Formation is considered to date from between 1600 Ma and the onset of Gardar intrusive activity at approximately 1350-1300 Ma (Blaxland, 1976). Early Gardar intrusions are the large, undersaturated syenite complexes of Motzfeldt and N. Qôroq to the east, and Grønnedal-Íka to the west (Fig. 1.1).

Mid-Gardar activity began with the emplacement of swarms of basic dykes, mostly lamprophyric or doleritic. In the eastern part of the province, a major group of trachytic and phonolitic dykes, the Fox Bay swarm, was intruded. This was followed by the intrusion of the Kûngnât and Ivigtut complexes in the northwest of the area (Fig. 1.1), which are generally believed to date from about 1220 Ma (Blaxland 1976).

In the late-Gardar, magmatic activity migrated southwards away from the margin of the Archaean craton with dyke swarms developing sub-parallel to the craton margin, concentrated in two main zones, a more northerly Nunarssuit-Isortôq zone and a more southerly Tugtutôq-Ilímaussaq zone. (Macdonald & Upton, 1993). Some "giant dykes" were intruded in both

zones. Central complexes included Nunarssuit, central Tugtutôq, Ilímaussaq, Dyrnaes-Narssaq, S. Qôroq, Early and Late Igdlerfigssalik, and Klokken (Fig. 1.1). The Motzfeldt, Qôroq and Igdlerfigssalik complexes are referred to collectively as the "Igaliko Complex".

1.3 Area of study

This project focuses on the Gardar geology of the area around Ivigtut, in the northwest of the province, as summarised by Berthelsen & Henriksen (1975) and as shown on the geological map Ivigtut 61 V.1 Syd, mapped at 1:100 000. A sketch map of this area, showing the major Gardar intrusives, is given in Fig. 1.2. The only settlements in the area of study are Grønnedal, a Danish naval base on the shores of the Arsuk fjord; Ivigtut, an old mining village two miles west along the same fjord; and Arsuk, further to the west on the open sea, below the mountain of Kûngnât. Recently, Ivigtut has been renamed to Ivittuut, and Kûngnât to Kuunnaat: but the spellings used in this study will be those originally used on the geological map. The area is cut by two major fjords, the Arsuk and Íka fjords, and the area between the two, south of Grønnedal, is described as the "Ivigtut peninsula".

The Gardar rocks in this area include three intrusive complexes; Kûngnât, Ivigtut and Grønnedal-Íka; and various swarms of dykes of differing compositions. These intrusives were emplaced into Archaean gneisses which were extensively faulted and deformed during the Gardar period. The earliest of the three complexes is Grønnedal-Íka, a nepheline syenite complex cut by a carbonatite plug, which lies between the Arsuk and Íka fjords as shown on the map. The Kûngnât complex, the most westerly of all the Gardar complexes, consists of three successive stocks of silica-saturated to oversaturated syenite which are cut by a gabbroic ring-dyke. The Ivigtut granite is a small (300m in diameter), alkali granite stock, on the edge of the

Arsuk fjord, which once hosted the worlds largest body of cryolite. This deposit has been entirely mined out. Gardar dykes are exposed throughout the area, but are most easily studied on the Ivigtut peninsula.

All the intrusives studied are fully described in the next chapter.

1.4 Fieldwork

Fieldwork in the area was carried out during July-August 1995, and July 1996. A large part of the 1995 field season was based around the deserted mine at Ivigtut, studying the Ivigtut stock itself and the many minor intrusives in the area. A brief trip to Kûngnât was undertaken and samples from both East and West sides of the complex were collected. The mountain of Kûngnât, west of Ivigtut, rises 1418m above sea-level and its slopes are exceptionally steep, making collection difficult. The 1995 field season was completed with a short visit to the Grønnedal-Íka complex. In 1996, again a short time was spent around Ivigtut but during the majority of the field season a base was set up at Jernhat, in the centre of the Grønnedal-Íka complex. This complex forms rolling hills around a bowl-shaped green valley. Jernhat lies at the top of the valley, providing a convenient base from which to study the geology but necessitating a long climb up the hill from the Danish naval base at the foot of the valley with food and gear. During the 1996 trip minor intrusives within the Archaean basement were studied on the 600m-high plateau which forms most of the Ivigtut peninsula.

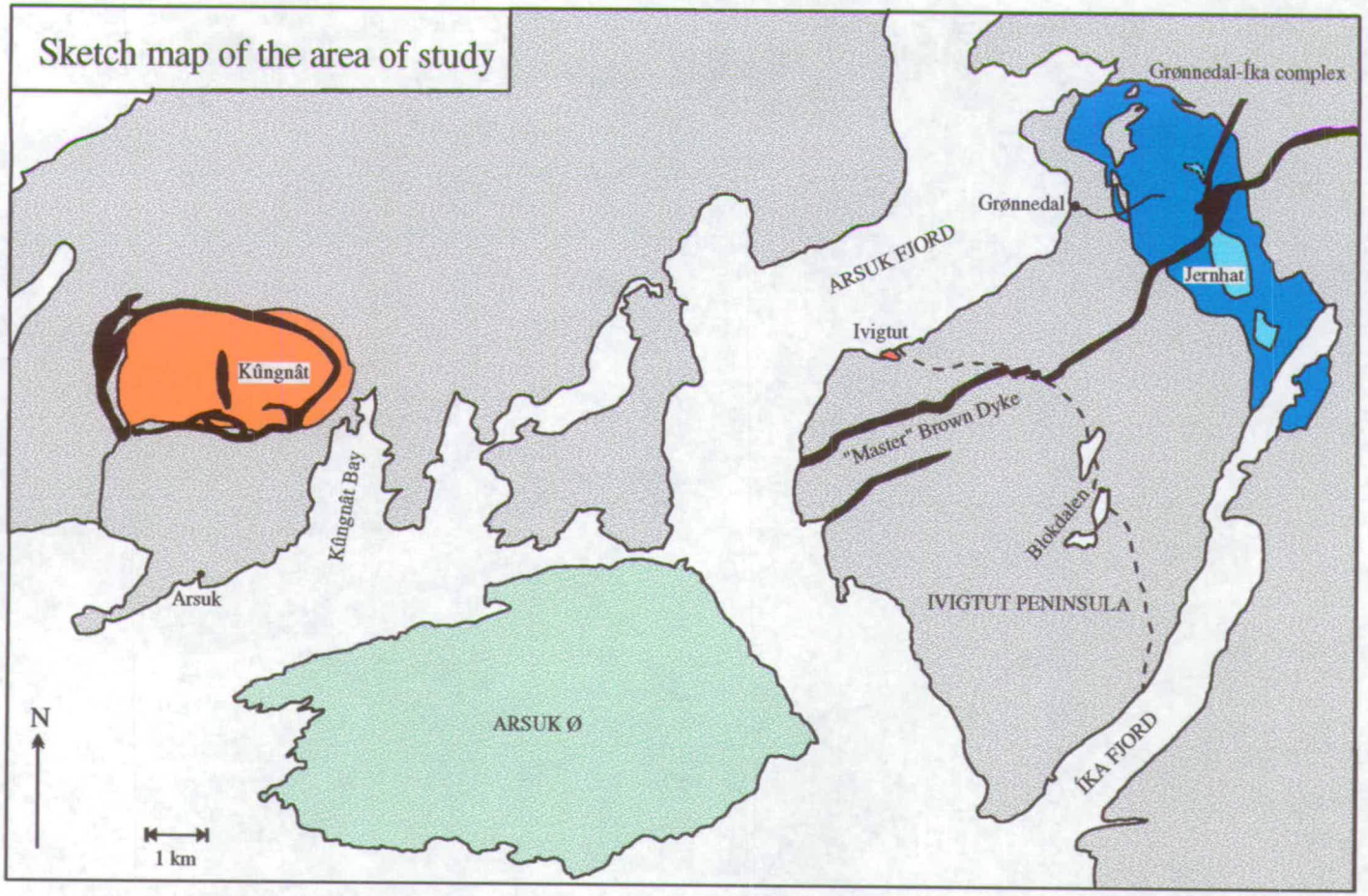

Fig. 1.2: Sketch map of the area of study, showing the major Gardar intrusives. The Grønnedal-Íka complex is shown in blue (dark blue for the syenites, pale blue for the carbonatite); the Ivigtut granite in red and the Kûngnât syenites in orange. Doleritic rocks are in black. The country rocks are Archaean gneisses, except on the island of Arsuk Ø, where basic metavolcanics of Ketilidian age overlie sediments. The dashed line across the Ivigtut peninsula represents a thrust within the Archaean rocks.

1.4 Rationale and objectives

Upton & Emeleus (1987) suggested a model for Gardar magmatism by which the sub-continental lithosphere was infiltrated by volatile-rich fluids rising from the deep mantle, with small degree partial melting of this metasomatised mantle producing ultramafic lamprophyres and carbonatites, and larger degree melting subsequently producing the parental Gardar magmas. The more evolved magmas were formed by fractionation and minor degrees of crustal contamination of the basic parent. It was noted that the dykes of the Ivigtut region showed some differences in chemistry when compared with those of the southeastern part of the Gardar and this was suggested to be related to the effect of the Archaean craton.

The work presented here has therefore had three main aims:
i) To study the geochemistry of all the Gardar intrusives in the Ivigtut region, and investigate the relationships between the complexes and dykes.
ii) To present a model for the genesis of these magmas based on geochemical and isotopic studies.
iii) To compare the magmas intruded on the edge of the Archaean craton with those intruded into the Proterozoic mobile belt to the south, and to identify the role of the craton in controlling petrogenesis.

1.5 Layout of this thesis

Much previous work has been carried out on the petrology and mineralogy of this area of the Gardar and this is described in Chapter 2. Chapters 3 and 4, respectively, present a summary of the fieldwork carried out for this project and a description of the petrography of all the rock-types concerned. A small electron probe study has been carried out, chiefly on the Ivigtut intrusion, to investigate the effects of fluids on mineral compositions, and the

results from this are described in Chapter 5. Chapter 6 presents the results of an extensive major and trace element study on samples from all rock-types in the area. A subset of selected samples was analysed for REE and the results from this are also given in this chapter. Various conclusions are drawn from these data which are then expanded upon in Chapter 7 in which the results of a radiogenic isotope study (Rb-Sr, Sm-Nd and common Pb), on a set of representative samples, are given. Generally, isotope studies were carried out with the aim of studying petrogenesis rather than obtaining dates for the rocks and therefore no conclusive dates are presented. Chapter 8 concludes the geochemical study with results of stable isotope analyses on carbonates from the area. In Chapter 9, previously published and unpublished results from the southeastern Gardar are compared with the results from this study, to try and identify the role of the Archaean craton in the petrogenesis of the rocks of the Ivigtut area, and conclusions are given in Chapter 10.

Chapter 2: Previous work

2.1 Country rocks

All three of the Gardar complexes discussed here lie within, but close to the edge of, the Archaean craton, with the Ketilidian mobile belt to the south (see Fig. 1.1); the Archaean gneisses on the craton margin have been affected by Ketilidian deformation. The gneisses have an age of about 3000 Ma (Taylor & Kalsbeek, 1986), and the Ketilidian rocks of the mobile belt date from about 1800 Ma (Windley, 1991).

The gneisses of the Ivigtut area were described by Berthelsen & Henriksen (1975), in the accompaniment to the geological map of the area, as mentioned in section 1.1. They divided the gneisses into four series. In the northeast of the area, between the settlement of Grønnedal and the Íka fjord, gneisses of the Fladland series are exposed; these are banded biotite and garnet-biotite gneisses with veins showing "pinch-and-swell" structures. Across the centre of the Ivigtut peninsula runs a belt of Nordland biotite gneisses characterised by enclaves of gabbro-anorthosite. These gneisses are also found in the area around Kûngnât. On the western edge of the Ivigtut peninsula, banded and veined biotite and biotite-hornblende gneisses are exposed. Pre-Ketilidian basic intrusives (Iggavik dykes), metamorphosed to amphibolite, cut the gneisses.

2.2 Chronology of the Gardar rocks.

A general chronology of the Gardar rocks in the study area, based mostly on cross-cutting relationships and some radiogenic dating, was provided by Berthelsen & Henriksen (1975). The oldest Gardar intrusion in the area is the

Grønnedal-Íka complex, which was dated by Blaxland (1978), using a whole-rock Rb-Sr isochron, at 1299 ± 17 Ma*. Emplacement of this complex was followed by intrusion of swarms of dykes including lamprophyres, olivine dolerites, and trachytes. Patchett (1977) dated lamprophyres from the region at 1227 ± 29 Ma* and 1249 ± 29 Ma.*, and olivine dolerites at 1250 ± 18 Ma* and 1238 ± 18 Ma*. Associated with the lamprophyres and alkaline dykes are various mineralisations, variously including sulphides, carbonates and crocidolite.

Both the Ivigtut and Kûngnât intrusions are believed to postdate virtually all the Gardar dykes of the region. Blaxland (1976) dated both complexes using Rb-Sr whole-rock isochrons, giving ages for Ivigtut of 1222 ± 25 Ma* , and Kûngnât 1218 ± 17 Ma*. More recently, J. Bailey (pers. comm.) has obtained an Rb-Sr mineral date on biotites from Ivigtut of 1170 Ma. L. Heaman (pers. comm.) has obtained a U-Pb baddeleyite date on Kûngnât of 1268 Ma. A much later magmatic event in the area is represented by a suite of Mesozoic dykes which cross-cut the Gardar rocks.

Faulting took place intermittently throughout the Gardar period in this region. Some faults were active between generations of Brown Dykes, while others postdate all the Brown Dykes. The Grønnedal-Íka complex has been extensively faulted, whilst the Kûngnât complex has been relatively undeformed. Many of the faults are mineralised, some having high levels of radioactivity.

---

* : Recalculated for decay constant of $\lambda = 1.42 \times 10^{-11}$ a^{-1}.

2.3 The Grønnedal-Íka complex

The Grønnedal-Íka nepheline syenite and carbonatite complex lies some 20km east of Kûngnât, between the Arsuk and Íka fjords. The complex was first described by Callisen (1943), mapped in detail by Emeleus (1964), and studied by Bedford (1989) (Fig. 2.1). It consists of two major series of laminated and layered nepheline syenites (the Upper and Lower Series), separated by a gneiss sheet. The intrusion originally formed an ovoid structure with steep inward-dipping layering defined largely by feldspar lamination, but the shape has since been disrupted by faulting. The northwestern margin of the complex is defined by a curving granular syenite body, considered by Emeleus (1964) to be an incomplete ring dyke. These syenites were cut by a steep-sided body of xenolithic, porphyritic nepheline syenite. A central plug of xenolithic carbonatite was then forcibly intruded into the syenites.

The two main syenite series form two distinct suites, with the Lower Series being the earlier. This series consists mostly of well-laminated foyaites which Emeleus (1964) considered to have formed by settling and bottom accumulation of feldspar and nepheline. Internal structure is mostly represented by feldspar lamination.The series is partly rimmed by a mostly structureless belt of coarse-grained brown syenite. Emeleus (1964) noted that in the field, the fresh foyaite can be seen to pass into dull brown syenite, which is altered and less well laminated, along and across the strike of the lamination. The differences in these rocks were postulated to be brought about by variation in the amounts of late-crystallising liquid trapped within the primocrysts of the syenite. A slight, steady movement of the magma was suggested to account for the close packing of the crystals in the well laminated rocks. Small sheets and dykes of porphyritic microsyenite cut the Lower Series syenites.

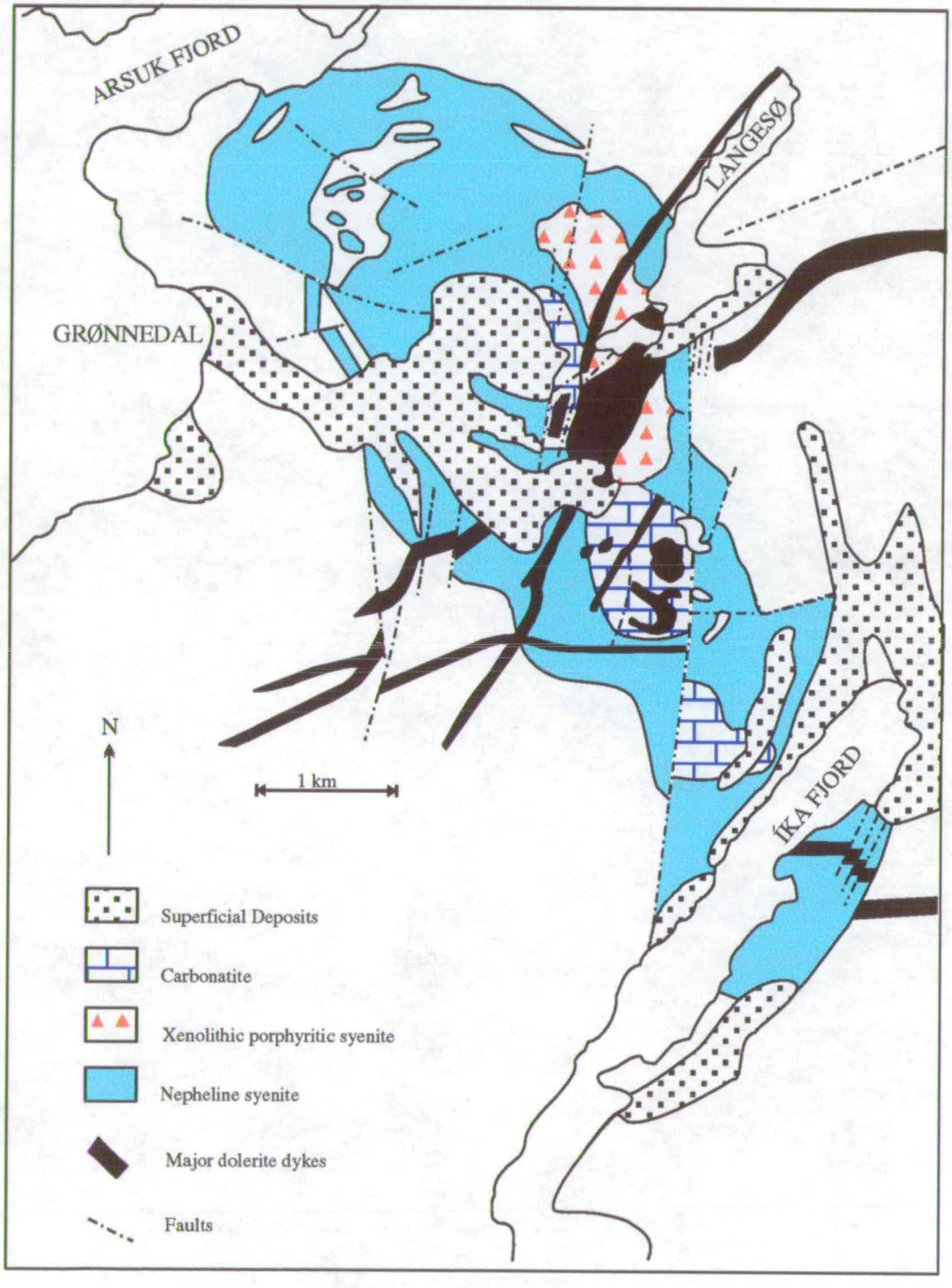

Fig. 2.1: Sketch map of the Grønnedal-Íka complex, after Pearce *et al.* (1997)

The Upper and Lower Series are separated by a gneiss raft which appears to have subsided through the magma during crystallisation, settling on the upper surface of the lower syenite sequence (Emeleus, 1964). The Upper Series, which accumulated on the floor provided by the gneiss sheet, was described by Emeleus (1964) as consisting of foyaites grading into pulaskites. The term "foyaite", once taken to describe any nepheline-syenite containing alkali pyroxenes and/or amphiboles, is now used to describe those nepheline syenites with a trachytic texture caused by the presence of platy alkali feldspars (Le Maitre 1989). Pulaskites are syenites which are less rich in nepheline. A unit of pyroxene-rich syenite is present within the Upper Series, in which thin layers and inclusions rich in aegirine-augite and apatite are common. A large enclave of coarse-grained syenite is also present within the Upper Series. Marginal, chilled rocks of the Upper Series were considered by Emeleus (1964) to be contemporaneous with the microsyenites cutting the Lower Series. A central plug of porphyritic syenite, which represents the latest syenite intrusion, contains numerous angular xenoliths of earlier syenites, trachytes, and rare gneisses at its margins. The matrix of the rock is porphyritic, with alkali feldspar phenocrysts.

After intrusion of the porphyritic syenite plug, the central carbonatite was forcibly emplaced into the Upper Series, leading to brecciation, metasomatism, and impregnation of the surrounding rocks with carbonate. The carbonatite is zoned, with calcite-rich margins passing into a siderite-rich core, and a small metasomatic magnetite-rich body at the centre. It can be seen where fresh to be xenolithic and flow-banded. Bedford (1989) described the effects of alteration related to the intrusion of the carbonatite. Close to the carbonatite, syenites are impregnated with calcite and recrystallised, and zircon is more common than in the fresh syenites. Gneisses included within,

and adjacent to, the complex have been metasomatised, with the growth of alkali amphibole and pyroxene.

The origin of the carbonatite has been discussed by Bedford (1989) and Pearce *et al.* (1997). Bedford (1989) noted two possible methods of origin: either by fractionation from small degree alkaline melts from a mantle source; or by liquid immiscibility. The occurrence of calcite and cancrinite in the syenites indicates the presence of carbonate-rich late - stage liquids and was taken to suggest an origin by liquid immiscibility from the syenite magma. Pearce *et al.* (1997) have presented evidence to show that the carbonatite magma may have separated by liquid immiscibility from magmas represented by the regional lamprophyre dyke swarms, rather than the syenites.

2.4 Dykes.

Berthelsen (1962) summarised a general chronology of the dyke swarms in the Ivigtut valley, whilst Emeleus (1964) studied the dykes in the vicinity of the Grønnedal-Íka complex. The most comprehensive review of all the dyke swarms in the area is provided by Berthelsen & Henriksen (1975).

The oldest Gardar dykes in the Ivigtut region are lamprophyres, mostly trending between NE and E, and generally 1-5m wide. Around Kûngnât the lamprophyres are all older than other dykes, but near Grønnedal-Íka Emeleus (1964) noted some lamprophyres postdating the dolerites. North of Arsuk Fjord the dykes can be traced for up to nearly 5 km, but south of the fjord they are less persistent. Berthelsen (1962) noted that the lamprophyres are most abundant in an ENE-trending zone crossing the Ivigtut peninsula which is also rich in mineralised crush zones, faulting and jointing. Berthelsen & Henriksen (1975) summarised the lamprophyres as intensely

weathered, melanocratic, fine-grained augite spessartites and kersantites, generally slightly chilled at the margins. Many of the dykes are porphyritic, with phenocrysts of the dominating mafic minerals (frequently biotite), and plagioclase, and characteristically contain small druses, filled with calcite and/or epidote.

Between the intrusion of the lamprophyres and the main dolerite swarms, some thin alkaline dykes were emplaced. Also generally predating the main olivine dolerites is a group of porphyritic dolerites known as the "Big Feldspar Dykes" (BFDs) (Berthelsen 1962). They contain plagioclase megacrysts up to 15cm across, and anorthositic inclusions, in a fine or medium-grained groundmass. These inclusions may make up over 40% of the rock in some dykes (Emeleus 1964). The BFDs are usually less than 10m in width and are mostly found in two major swarms, usually trending ENE: within the area of the present study there are few examples.

The major group of dykes in the study area are olivine dolerites, known as Brown Dykes (BDs) due to their typical weathering. They vary in width from 1-200 metres, and Berthelsen & Henriksen (1975) estimated that the total sum of dyke thicknesses across the area shown on the Ivigtut map sheet corresponds with a general crustal widening of about 3%. Berthelsen (1962), working in the Ivigtut valley, divided the dykes into 3 generations (BD0, BD1 and BD2), each with a characteristic trend. Dykes of all three generations cut the Grønnedal-Íka complex. The BD_0 dykes, the oldest generation, were intruded along zones of weakness striking roughly E-W, and then shifted dextrally along NNE-trending faults. The second generation was intruded with an ENE trend and further movement on the faults occurred before the intrusion of the BD2 dykes trending NE. Trends also vary between different sub-areas in the Ivigtut region. The changes in trend can be seen to follow each other in such a way that the oldest (BD0) generation is always that with

the greatest angle of bearing measured from true North, whilst the youngest generation has the lowest bearing (Berthelsen & Henriksen 1975).

The brown dykes are mostly regular intrusions, with chilled margins, all vertical or very steeply inclined. Contacts with the country rock are generally sharp, though Winstanley (1975) noted that some rheomorphism and brecciation of the gneisses around large dykes can be observed near Kûngnât. Emeleus (1964) also noted examples of contact metamorphism by an olivine dolerite at Grønnedal-Ika, leading to the production of magnetite accumulations. Internal structures within the Brown Dykes may include trough banding and pegmatitic patches up to 50cm across.

The various remaining groups of dykes found in the Ivigtut region can be less easily resolved into a chronological pattern. They can be divided into two sub-groups; basic dykes and alkaline, salic dykes. The basic dykes include a widespread group of micro-porphyritic basalts, which are younger than the olivine dolerites but older than the alkaline dykes (Berthelsen & Henriksen 1975). Emeleus (1964) described these dykes, in the area around Grønnedal-Íka, as fine-grained dark grey rocks with micro-phenocrysts of plagioclase tablets 1-2mm in length. The plagioclases may show a trachytoid texture or may be grouped in stellate clusters. The groundmass is composed mostly of augite and andesine, with olivine only occurring rarely, suggesting that these dykes are less basic than the Brown Dykes. The micro-porphyritic dykes are typically thin (up to 2m) and are mostly intruded along fault and crush zones, often forming multiple intrusions, with fine-grained chilled margins being a characteristic feature. They are most abundant in the Main Fault Zone on the Ivigtut peninsula, but are also found within the Grønnedal-Íka complex. Other basic dykes include a hornblende-bearing group which seems to have been intruded over a wide time span in the early part of the Gardar period.

Alkaline salic dykes occur over a wide area in the central and eastern parts of the Ivigtut region, being especially abundant in the NE-trending Main Fault Zone south of Arsuk fjord. They can be divided into two distinct groups, one older than the Brown Dykes but younger than the lamprophyres, and the other younger than all the dykes so far mentioned. Berthelsen (1962) described all the alkaline salic dykes in the Ivigtut valley as trachytes. They are generally 1-5m wide and can mostly only be traced for a few hundred metres. These dykes are typically leucocratic, pale-coloured, fine-grained, often with small feldspar phenocrysts. They vary in composition, including silica-oversaturated, saturated and undersaturated types. Gill (1972) reviewed the chemistry of peralkaline phonolite dykes in the Grønnedal-Ika area. The last Gardar dykes to be intruded in the area were a set of thin granophyric dykes, which appear to be associated with the Ivigtut granite, and which cut the Brown Dykes.

2.5 The Ivigtut stock

The Ivigtut intrusion consists of an alkali granite stock, 300m in diameter, which has been chiefly studied due to the presence of a cryolite (Na_3AlF_6) - bearing ore-body within the top of the granite. The first European scientist to visit Ivigtut was Giesecke, in 1806, and since then a wealth of mineralogical information has been published on the cryolite body.

The petrography of the granite was first treated by Callisen (1943), who described it as an alkaline granite containing phenocrysts of quartz and feldspar with scarce biotite, aegirine-augite and soda amphibole. The nature of the granite, as given below, was summarised by Bailey (1980). A chilled porphyritic microgranite roof capped the cryolite deposit. Close to the deposit, the fresh roof zone granite passes through mildly hydrothermally

altered variants into albitised granite and greisen (Fig. 2.2). Below the deposit the intensity of the alteration diminishes down to 550m below sea level. A distinction can be made between the roof granite, which is a hornblende biotite leucogranite, and the deep two-feldspar granite.

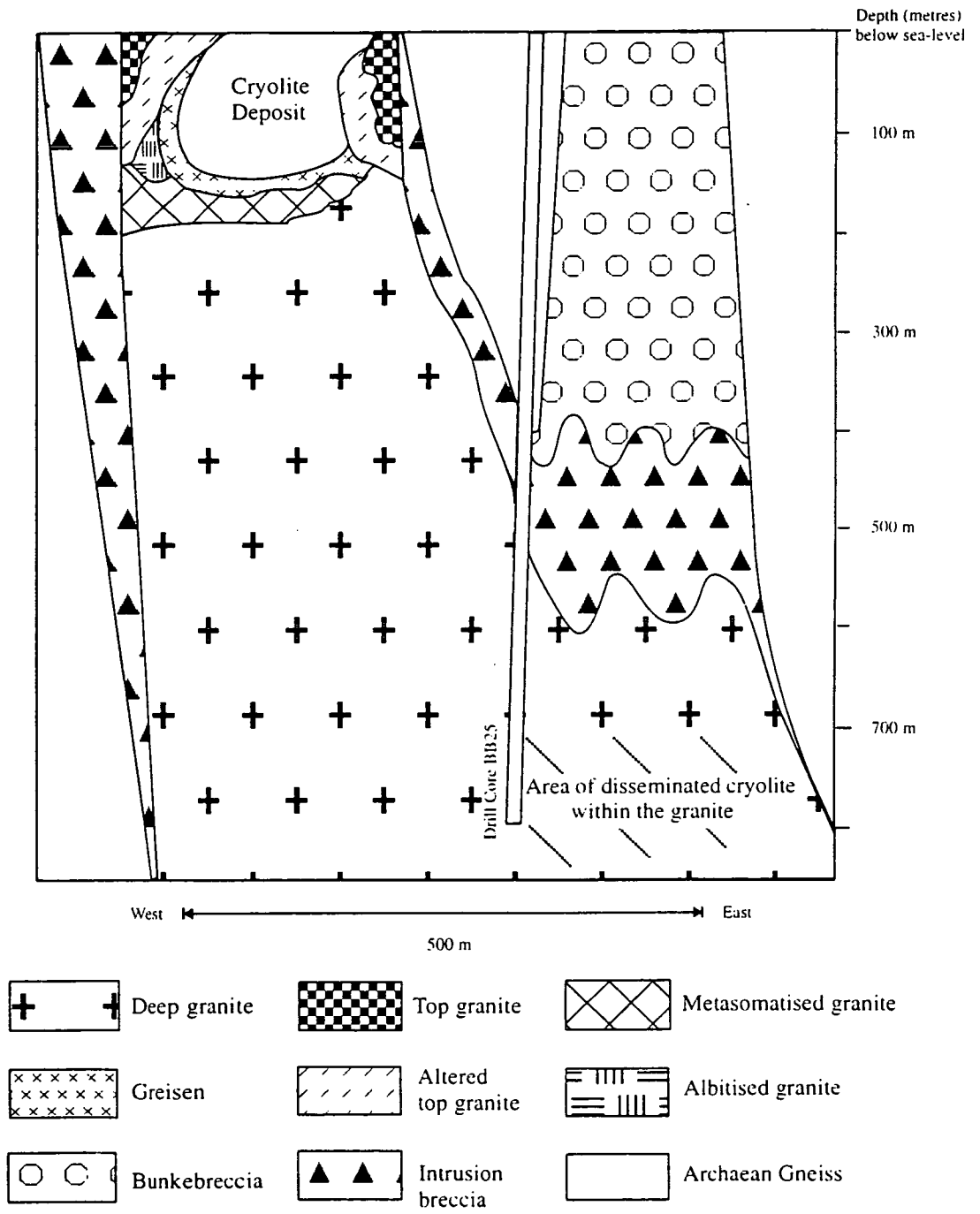

Fig. 2.2: Cross-section through the Ivigtut granite, after Karup-Møller & Pauly (1970), Bailey (1980) & Bondam (1991).

The roof granite consists of perthitic alkali feldspar and quartz with biotite, sparse amphibole and olivine and accessories including zircon, magnetite, ilmenite, fluorite and siderite. Hydrothermal alteration led to sericitisation of perthites, increased quartz contents and breakdown of mafic silicates. Albitisation has occurred in some parts of the granite with albite up to 65 vol%. In greisenised granites most feldspars have been converted to a yellowish phengitic mica (which has been termed "ivigtite") and accessories may include siderite, fluorite, cryolite, sulphides, topaz, zircon, and cassiterite. The deep granite, by contrast with the roof granite, is a two-feldspar leucogranite, with zircon, columbite, phengite, siderite and fluorite as the main accessories (Pauly & Bailey, in press.). Recent drilling has shown that disseminated cryolite is present at depth within the granite stock, between about 700 and 800m below sea level (Bondam 1991). (Fig. 2.2).

Mining of the cryolite deposit found within the stock commenced in 1855 and was described by Tayler (1856). Commercial mining of the cryolite continued from 1858 to 1962 and recommenced for a brief period during the 1980s, until virtually all the cryolite had been removed. Summaries of the structure of the cryolite deposit are given by Bailey (1980) and Karup-Møller and Pauly (1979). It consisted of a lens-shaped cryolite body about 200m across, overlying a quartz-rich cylindrical body, within the top of the granite stock. A quartz-feldspar pegmatite partly covered the top of the cryolite body (Fig. 2.3).

The cryolite body was dominated by siderite-cryolite rock, which was described in detail by Pauly (1960) as a coarse, granular material, with rounded lumps of cryolite, 5-50 cm across, within a network of siderite crystals. Contents of siderite and cryolite varied throughout, and in some parts of the body distinct layers were formed. On average siderite constituted about 20% of the material, with quartz and sulphides as

abundant accessories. The most abundant sulphides were sphalerite, chalcopyrite and galena, but many others were present in small quantities (Karup-Møller & Pauly, 1979).

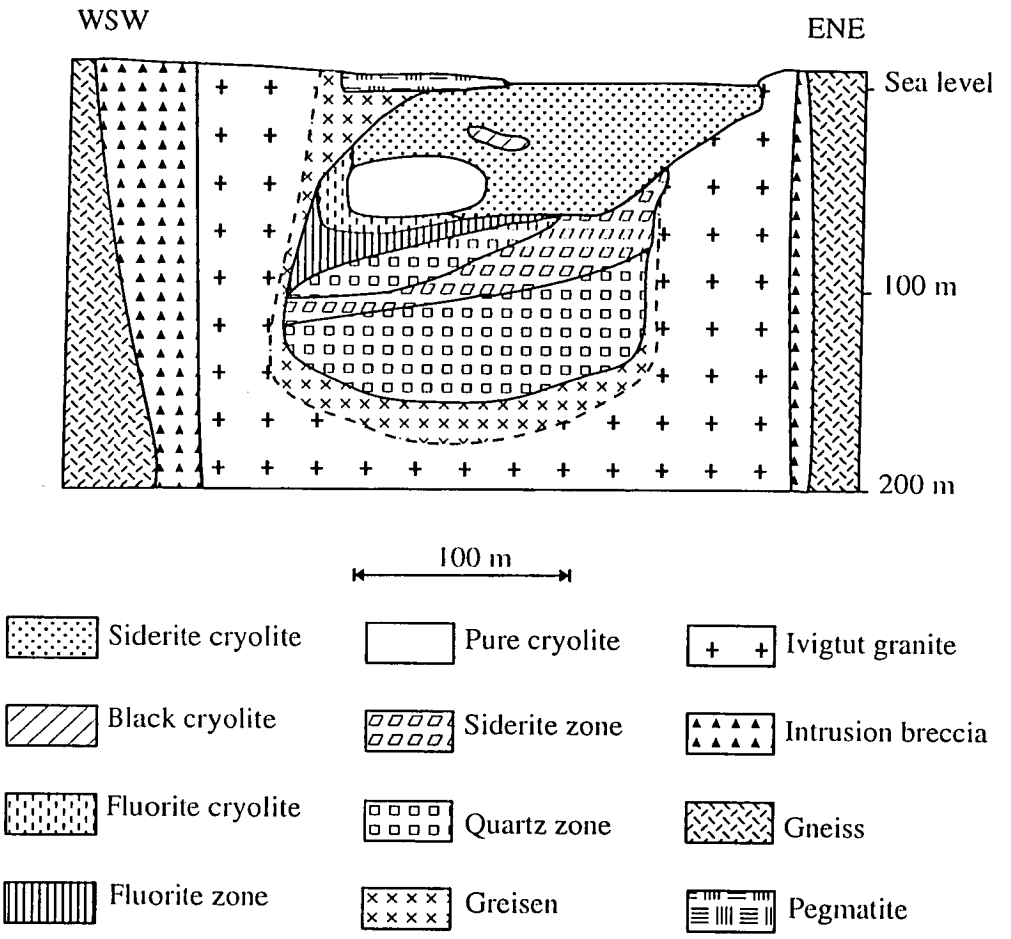

Fig. 2.3: Cross-section through the Ivigtut cryolite deposit, from Karup-Møller & Pauly (1979)

Below and to the west of the cryolite mass lay a shell of fluorite-cryolite rock, consisting of cryolite and fluorite interwoven with veins of cryptocrystalline topaz and spherulitic K-mica ("ivigtite") (Pauly 1986). Many rare minerals have been described from this part of the body, including weberite ($(Na,K)_2MgAlF_7$) (Pauly & Petersen 1981); chiolite ($Na_5Al_3F_{14}$) (Pauly 1986); and jarlite ($NaSr_3Al_3F_{16}$) (Pauly 1993). Beneath this shell lay the fluorite zone,

which consisted of the above minerals but lacked cryolite. Pauly (1992) suggested that gas-driven explosions, occurring after the cryolite body had formed, produced breccias with topaz and fluorite veins, with cryolite in the upper part. The surrounding granite was also brecciated, leaving large (>1m) granite xenoliths embedded in cryolite, pointing to the ductile nature of this mineral at high temperatures. Below the fluorite zone lay the quartz zone, which extended down to about 150m below sea-level. This zone consisted mostly of quartz, with up to 20% siderite plus some mica and sulphides, and was cut by a siderite-rich sheet dipping to the southwest.

Fluid inclusion studies (Prokof'ev *et al.*, 1991) indicate a temperature of formation of the cryolite deposit as 335-555°C. This correlates with temperatures obtained by Pauly (1960) whose studies of quartz forms in the deposit indicated that formation occurred near, or under, the inversion point of quartz (573°C at 1 bar).

Berthelsen (1962) described an intrusion breccia shell which surrounds the granite stock. This contains angular country rock fragments enclosed in fine-grained granite. About 100m to the east of the granite is a distinct breccia cylinder, the Bunkebreccia, which has a matrix of shattered wall rock, and was considered by Berthelsen (1962) to have originated through gas drilling. It is cut by a swarm of small, irregular dykes which Berthelsen (1962) described as tinguaites. Later studies of exploration drill cores (Bondam 1991) have revealed that the Bunkebreccia merges at depth into the intrusion breccia and the granite itself, indicating that two conical offshoots formed from one deep-seated alkali granite intrusion. Berthelsen (1962) also described a set of "tiny granophyric dykes" which cut the Brown Dykes and appeared to be cut by the Ivigtut granite. These seem to radiate out from the granite and were assumed to represent dyke intrusion immediately preceding the granite emplacement.

2.6 The Kûngnât Complex

The Kûngnât Complex was first mapped and described by Upton (1960). The ferromagnesian mineralogy has been reviewed by Stephenson & Upton (1982). The complex consists of two, possibly three steep-sided stocks of silica-saturated to oversaturated syenite, with an alkali gabbro ring-dyke (Fig. 2.4). The syenite stocks were intruded with a progressively eastward shift of centre, with the smallest and earliest body appearing to be the southwestern marginal syenite. These rocks are commonly xenolithic quartz syenites, containing blocks of dolerite and gabbro.

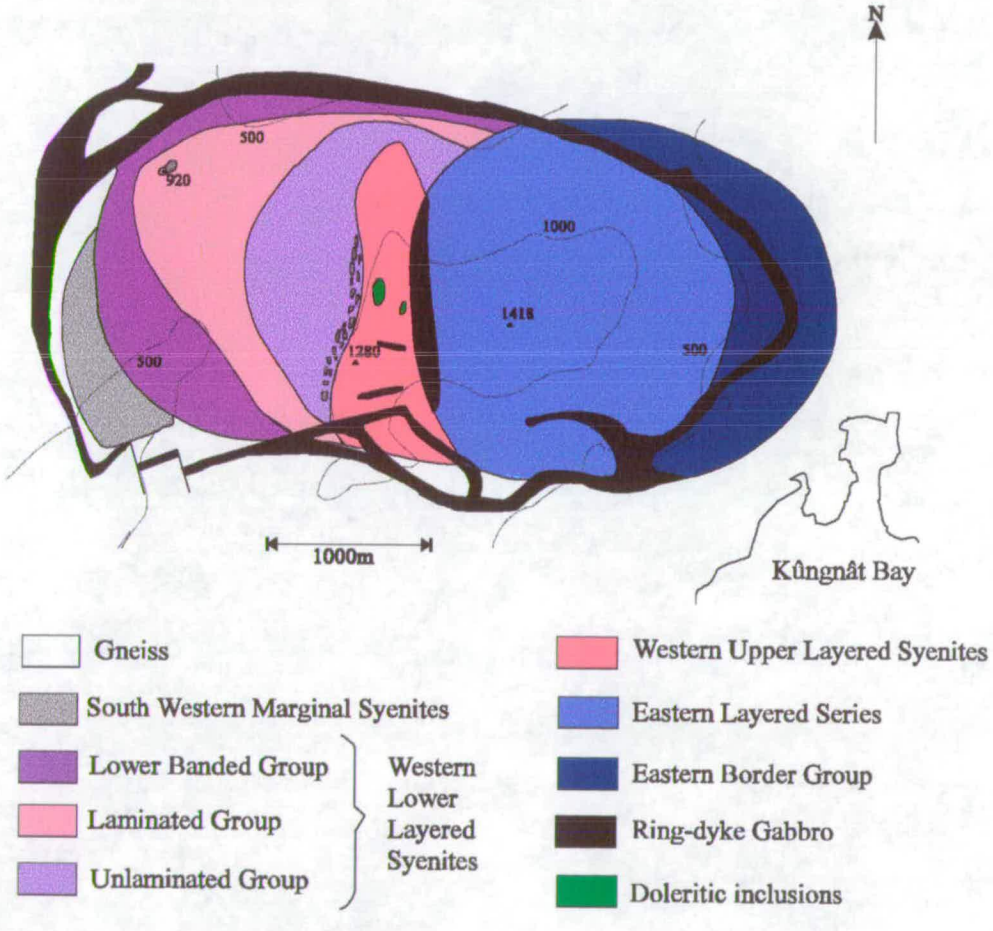

Fig. 2.4: Geological map of the Kûngnât complex, after Upton (1960). All heights given in metres.

The second intrusion, the western layered syenites, is divided into an upper and a lower series by a raft of foreign gneissic blocks. The syenites of this stock show inward-dipping rhythmic banding and feldspar lamination (Fig. 2.5). The western lower layered syenites (WLLS) are divided into three sub-series, which grade smoothly into each other. The lowest is the lower banded group, which is about 400m thick. These rocks are rhythmically layered, with dark layers rich in olivine, pyroxene and ilmenomagnetite grading upwards from sharply defined bases into more feldspathic layers over a distance of up to a metre or more. Upton (1960) considered this layering to have considerable areal extent, and to be related to gravity stratification, with trough-banding and apparent current bedding providing evidence for magmatic flow. Upton *et al.* (1996) interpreted the consistent "way-upness" of grading, cross-bedding, troughs and cryptic layering in the syenites as indicating that the stock accumulated upwards from an inwardly-inclined floor. The layers extend virtually to the contacts between syenites and country rocks, with no marginal border group. Hodson & Finch (1997) described the trough structures in the lower banded group and suggested that they were formed erosively by streams of "mafic crystal slurry" which had crystallised on the chamber walls and flowed down them.

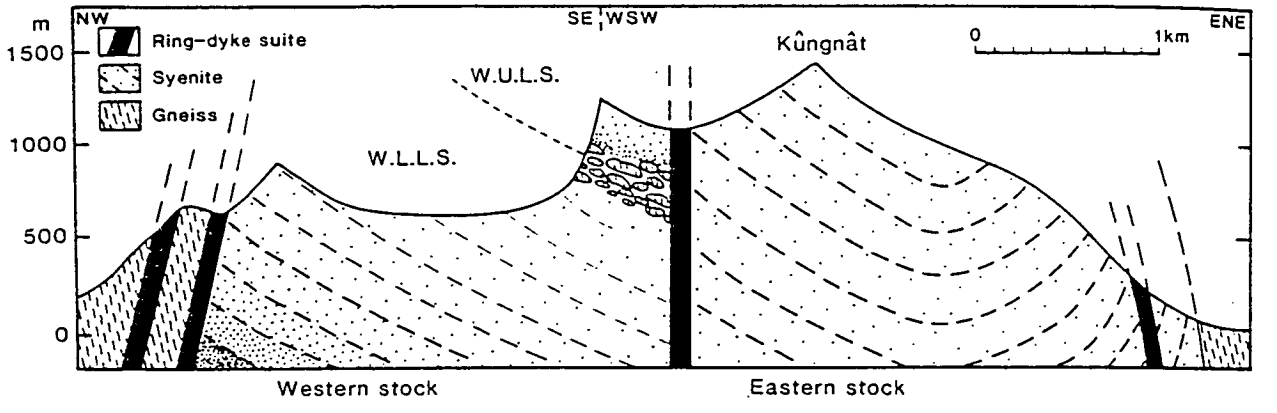

Fig. 2.5: Diagrammatic cross-section of the Kûngnât Complex, from Upton *et al.* (1996). Vertical scale=horizontal scale. Attitude of cumulate layering shown schematically by dashed lines.

The lower banded group grades up into the lower laminated group, which is devoid of modal layering but shows a clear feldspar lamination. The highest part of the WLLS is represented by the lower unlaminated group, highly feldspathic quartz syenites with no modal layering or clear lamination. Approaching the gneiss blocks, the syenites appear drusy and coarsely pegmatitic, with the appearance of riebeckite, fluorite, siderite, zircon and astrophyllite. Overall thickness of the WLLS is some 1500 metres.

The western uppered layered series (WULS) shows modally layered syenite units up to 10m thick near the base, with banding being lost further up the sequence. Lamination appears best in the middle parts of the WULS, but is lost in the uppermost rocks where the feldspars show a more equant habit. The upper rocks of the WULS are extremely leucocratic quartz syenites. The highest rocks become coarsely drusy and pegmatitic, and were considered by Upton (1960) to have formed relatively close to the roof of the intrusion. Many fine-grained basic inclusions are contained within the WULS.

The eastern syenite stock consists of an eastern border group (EBG), and a layered series (ELS). The border group represents a marginal belt of syenite at the eastern edge of the complex, with steep-angled layering, interpreted to have grown *in situ* on the steep boundary layer of the cooling magma chamber (Upton *et al.* 1996). The layered series, which includes Kûngnât peak itself, makes up most of the eastern stock. It consists of syenites which are somewhat more basic than those to the west, with intermittent layering dipping into the centre of the intrusion rather more steeply than that of the western centre. The eastern intrusion, similarly to the west, is surrounded by a feldspathic pegmatite.

Following the consolidation of the syenites, but whilst residual granitic and pegmatitic fluids were still mobile (Upton, 1960), a new episode of ring-

fracturing allowed intrusion of an iron- and alkali-rich gabbroic magma, forming a complete ring-dyke, with its focus at a more westerly point than that of the final syenite intrusion. The ring-dyke dips outwards at roughly 50° around the south and east of the complex, but in the southwest the angle of dip is much shallower, possibly as low as 20°. Angular masses of gneiss within the dyke provide evidence for its emplacement by stoping. The width of the ring-dyke is typically about 100m.

After the intrusion of the ring-dyke, large numbers of acid sheets were injected into the complex. These late sheets are considered as residua from the salic magmas (Upton 1960). Macdonald *et al.* (1973) divided the sheets of the western stock into four groups: quartz syenites; granite with anhedral amphibole; micro-granites with riebeckitic amphibole; and aplites and zoned pegmatite aplites bearing aegirine. In the east, quartz syenites and microgranites were intruded. Macdonald *et al.* (1973) described the metasomatism of gabbroic rocks cut by late peralkaline sheets, and showed that the metasomatism involved addition of K, F, and H_2O to the gabbros, presumably from a hydrous fluid lost from the granite sheets. Where the peralkaline sheets come into contact with syenites, no metasomatism is observed, and it was suggested that this contrasting behaviour is due to the existence of strong chemical gradients at the gabbro - granite contacts. It was also noted that there is no apparent transfer of Na or Cl from the granites to the gabbros, and it was postulated that Na and Cl were partitioned into a fluid phase which was expelled at an early stage of cooling of the melt.

Upton (1960) noted that the major intrusive units of the Kûngnât complex were emplaced in order of increasing basicity and suggested that the magmas were tapped off from successively deeper levels of an already-differentiated parental magma. A large body of alkali olivine basalt was envisaged as remaining in a non-convecting state through most of the Gardar

period, with diffusion of volatiles, silica and alkalis leading to higher concentrations of these materials in the uppermost part of the magma chamber, thus producing a syenitic melt with an internal composition gradient. Fractionation by crystal settling was envisaged as continuing in the main body of the magma. Isotopic evidence presented by Blaxland (1976) indicated that all units of the Kûngnât complex were comagmatic. The model for intrusion, as summarised by Stephenson & Upton (1982) suggested three successive "heaves" of less fractionated magma; firstly trachyte, followed by more mafic trachyte, producing the western and eastern syenite stocks, and finally hawaiite, producing the gabbroic ring-dyke.

2.7 Mineralisations

The Ivigtut peninsula is an extremely heavily faulted zone and Berthelsen & Henriksen (1975) described various different types of mineralisation associated with faults and shear zones in the area. U- and Th- enriched veins were found in some mineralised faults. Other mineralisations were found in fractures and mylonite zones, or associated with lamprophyres and alkaline dykes. The field relations and mineralogy of these mineralisations suggested that they were related to Gardar magmatic activity; they included sulphides, carbonates, fluorite and sodalite. Ayrton & Masson (1972) also reported small veins and impregnations of crocidolite along joints, faults and shear zones in the country rocks and suggested that these were genetically related to the alkaline massifs at some distance, describing them as a "low-temperature equivalent of fenitisation".

Chapter 3: Fieldwork and sample collection

3.1 The Grønnedal-Íka Complex

The Grønnedal-Íka complex lies partly under the vegetated slopes of Grønnedal, the "green valley", where exposure is very poor, but better exposure is found in the surrounding hills (Fig. 3.1). Many parts of the complex (streams, ridges, etc.) were given names by Emeleus (1964) and these names are shown on the map included in that publication, and on the sample location map in Appendix A.

The syenites of the complex are mostly heavily weathered to a feldspar gravel, making sampling of fresh rocks difficult. The best exposures of the main Upper and Lower Series syenites are found on the Cirkus ridge which encircles the valley, and in streams such as the Radioelv. In both Upper and Lower Series foyaites, lamination of feldspars can clearly be seen. These rocks are often pink in colour, due to the alteration of nepheline. The Lower Series foyaites may also contain prominent blue sodalite. Within the Upper Series, a band of pyroxene-rich syenite is notable for thin (<5cm), wispy, dark-green, aegirine-augite-rich layers within relatively normal syenite (Fig. 3.2). The gneiss raft separating the two series can be seen in the northwest of the complex, although the contact between gneiss and syenite is seldom exposed. The granular syenite and coarse-grained brown syenite are exposed on the ridge above the Grønnedal naval base. The later xenolithic, porphyritic syenite is exposed as outcrops in the scree slopes around the 530m peak of the Cirkus.

The central carbonatite is well exposed in the stream by the hut at Jernhat, although elsewhere it is difficult to obtain a fresh, *in situ* sample.

Fig. 3.1: The Grønnedal-Íka complex, with the Jernhat hut in the foreground, on the edge of the low area formed by the carbonatite, and syenites exposed on the Cirkus ridge in the background.

Fig. 3.2: Outcrop of pyroxene-rich syenite. The dark layers cutting the rock are extremely rich in aegirine-augite.

At Jernhat, metasomatism related to the intrusion of a Brown Dyke into the carbonatite has produced a magnetite deposit which has been partially mined out. Within this area the carbonatite can be seen to be inhomogeneous: the majority of exposures show a pale grey rock with flow banding defined by iron oxides, but some patches of coarse søvite are seen. Also of interest at Jernhat is a xenolithic basic dyke, packed with angular xenoliths of gneiss and syenite up to 10cm across (Fig. 3.3), which cuts the carbonatite.

The Grønnedal-Ika complex was visited during both the 1995 and 1996 field seasons and samples of most of the major rock types were collected.

3.2 Dykes

The Brown Dykes are reasonably well exposed in the area around Ivigtut, particularly in the hills above the mine. They vary in width from 5-30m across and are typically weathered to a brown rubble (Fig. 3.4). Where fresh, they appear gabbroic in the centre, with chilled margins. The largest of these dykes, the "Master Dyke" of the Ivigtut peninsula, which is 30m wide and runs approximately ENE-WSW, is clearly visible in the hills to the south of the Ivigtut valley. This dyke cuts the Grønnedal-Íka complex and is highly sheared by the associated faulting. Where it cuts the complex, it appears to have melted the syenites slightly, giving rise to lobate contacts and zones of mixing.

Some miscellaneous basic dykes are found, particularly around Ivigtut, where they may be rich in sulphides or carbonate. These dykes are often thin and impersistent. Ultrabasic lamprophyre dykes are also found throughout the area, though typically only 1-2m wide. These generally appear porphyritic, with phenocrysts of biotite or hornblende. Some of them are carbonate-rich and have a characteristic orange - brown weathering colour.

Fig. 3.3: Xenolithic dyke at Jernhat. Xenoliths of gneiss and syenite, approx. 10 cm across.

Fig. 3.4: A Brown Dyke, with characteristic rubbly weathering, cutting gneisses on the Ivigtut peninsula.

The lamprophyres have often been heavily brecciated by mineralising veins, with blocks of carbonated basic rock held together by a quartz cement. (Fig. 3.5)

Fig. 3.5: Blocks from a mineralised and brecciated lamprophyre on the Ivigtut peninsula.

Various alkaline dykes, chiefly trachytes and phonolites, are scattered around the area. These are mostly narrow (< 1m wide) and impersistent. They frequently show a green or pink colour.

Throughout both field seasons samples were collected from representative examples of all types of Gardar dykes within the area.

3.3. The Ivigtut stock

Due to the mining operations, exposure of the Ivigtut granite is limited. (Fig 3.6), and therefore the present study draws heavily on previous work for an understanding of the relationships within the stock. The granite pipe has been drilled down to depths of about 900m, and samples from the deeper granite have been taken from the drill cores which are now stored at GGU in Copenhagen.

The top granite is exposed in isolated outcrops around the edges of the mine. The lowest outcrop is on the north side of the mine, at the edge of the dam where part of the concrete has collapsed. The granite here is dark in colour and heavily weathered, showing columnar jointing which dips at ~45° into the centre of the granite (Fig 3.7). Similar columnar jointing is seen in an exposure on the W side of the mine behind the mine house, dipping into the mine at 50°. At a greater distance from the mine, the jointing becomes shallower (10° near the contact with the intrusion breccia on the W side), whilst in the outcrops on the S side of the mine, which are roughly 20m above sea-level, jointing is not apparent, and the granite is paler in colour. Exposures of granite found close to its margin against the intrusion breccia are clearly chilled porphyritic microgranites. All exposures of granite have been very altered and surfaces are typically heavily iron-stained, making it difficult to distinguish many characteristics in the field.

The mine tips which fill most of the Ivigtut valley provide sources of samples of relatively fresh granite and the cryolite deposit. However, there is the distinct drawback that the original location of this material cannot be identified. Samples were collected from *in situ* exposures of the top granite where possible; additional samples were collected from the tips.

Fig. 3.6: Ivigtut seen from the surrounding hills, showing the mine, which has been filled with water, and the cleared area around it.

Fig. 3.7: Outcrop of dark, weathered granite on the edge of the Ivigtut mine, showing columnar jointing.

The intrusion breccia which surrounds the granite is exposed in a few outcrops, chiefly on the shore to the west of the mine. It contains angular xenoliths of varying rock types, including gneiss, dolerite, and granite, in a micro-granitic groundmass.

The Bunkebreccia is now exposed as slabs typically about 2m high at the back of the gravel beach along the shoreline at Ivigtut. This exposure extends about 130m eastwards along the beach. To the south, the rest of the Bunkebreccia is hidden under the houses of Ivigtut village, with outcrops being sparse. The dimensions of the Bunkebreccia are reported to be 167 by 89m (Bondam 1991).

The most complex outcrop of the Bunkebreccia is at its western end, ~ 250m from the eastern side of the mine. This outcrop forms a face up to about 5m high and 20m across, and demonstrates many of the features of the breccia. (Fig 3.8). This outcrop was investigated during both the 1995 and 1996 field seasons and samples of all the rock types were collected.

The typical Bunkebreccia material consists of gneissic and amphibolite xenoliths in a gneissic groundmass. Included within the groundmass are regions of a darker felsitic breccia which typically has interfingered, lobate contacts with the gneissic material. This breccia is greenish-grey in colour, with abundant angular xenoliths, mostly gneiss, varying from 5-10cm across. Some fine-grained felsitic xenoliths are also present. The greenish colour of the groundmass is imparted by epidote and chlorite.

Fig. 3.8: Outcrop of the Bunkebreccia, showing dykes cutting across the gneissose groundmass. Scale provided by Dr A. Finch. Height of rock-face approx. 4m.

Fig. 3.9: Porphyritic basaltic dyke cutting and brecciating gneissose groundmass in the Bunkebreccia.

The brecciated groundmass is cut by basaltic, feldspar-phyric dykes which vary in width from over 2m down to 20cm, and strike roughly N-S. Contacts with the gneissic groundmass are relatively sharp and gneissose layering is clearly cross-cut in many places. However, there are zones of lobate contacts where rheomorphism of the gneissic material may have taken place. The basaltic dykes send off apophyses into the gneissic groundmass and enclose xenoliths of the gneiss. It appears that the dykes were intruded into the gneissic breccia soon after its formation and some rebrecciation occurred (Fig 3.9).

The latest activity within the Bunkebreccia involved the intrusion of narrow feldspar - phyric trachytic dykes. These have typically sharp contacts with the gneissic breccia, but again some lobate contacts indicate possible evidence for rheomorphism. They are generally about 20cm wide, and their margins are bluish in colour. One of these dykes, which lies along the face of the main outcrop, is blue-grey in colour and appears to have been mostly weathered away, leaving only the margin parallel to the rock face. It has lobate contacts with the gneiss and appears to contain many gneissic xenoliths; however its contacts with the basaltic material are sharp.

3.4. Granophyre dykes

Berthelsen (1962) described a set of tiny granophyric dykes in the Ivigtut valley, which cut the Brown Dykes and appear to radiate out from the Ivigtut Granite. Many alkaline dykes are found in the valley, cutting the gneisses, but the majority of these are trachytes and phonolites. About 5 or 6 granophyre dykes were found during the 1995 and 1996 field seasons. These dykes are generally 25-50cm wide, although some have widths up to 1m, and they typically strike into the granite. In most cases it is difficult to follow them for more than a few metres due to variable outcrop. They are mostly weathered to a yellow-white colour and heavily sheared, being broken into many shards of rock, so that obtaining a fresh sample is very difficult.

The study carried out by Berthelsen (1962) showed that the granophyres cut the Brown Dykes but are cut by the Ivigtut granite. Due to the mining out of the granite, plus limited outcrop around Ivigtut village, it is no longer possible to see where the granite cuts these dykes. However, a granophyre dyke has been found cutting the Bunkebreccia on its southeast side. Berthelsen (1962) suggested that xenoliths of granophyre are found in the Bunkebreccia, but Berthelsen & Henriksen (1975) mention an unpublished GGU report (Jacobsen 1966) in which the granophyres are noted to cut the Bunkebreccia and all other dykes within it. The granophyre dyke has sharp contacts where it cuts the Bunkebreccia, indicating that the breccia was fully consolidated before the dyke intrusion.

On the south side of the main Ivigtut reservoir, a 30cm wide granophyre cuts the gneisses and can also be seen cutting the BD0 dyke. This granophyre dyke can be traced for at least 50m on a strike of 100°. In the hills to the west of the mine, another granophyre cuts both the gneisses and a BD0. The

largest of the dykes is exposed on the shore in a small bay just west of the mine. It is approximately 1 m wide and has weathered out into a gully. Samples were collected from all the granophyre dykes, although fresh samples were difficult to extract (Fig. 3.10).

Fig. 3.10: Granophyre dyke cutting gneisses at Ivigtut. Contacts are sharp, but the dyke has been heavily weathered out, making collection of fresh samples difficult.

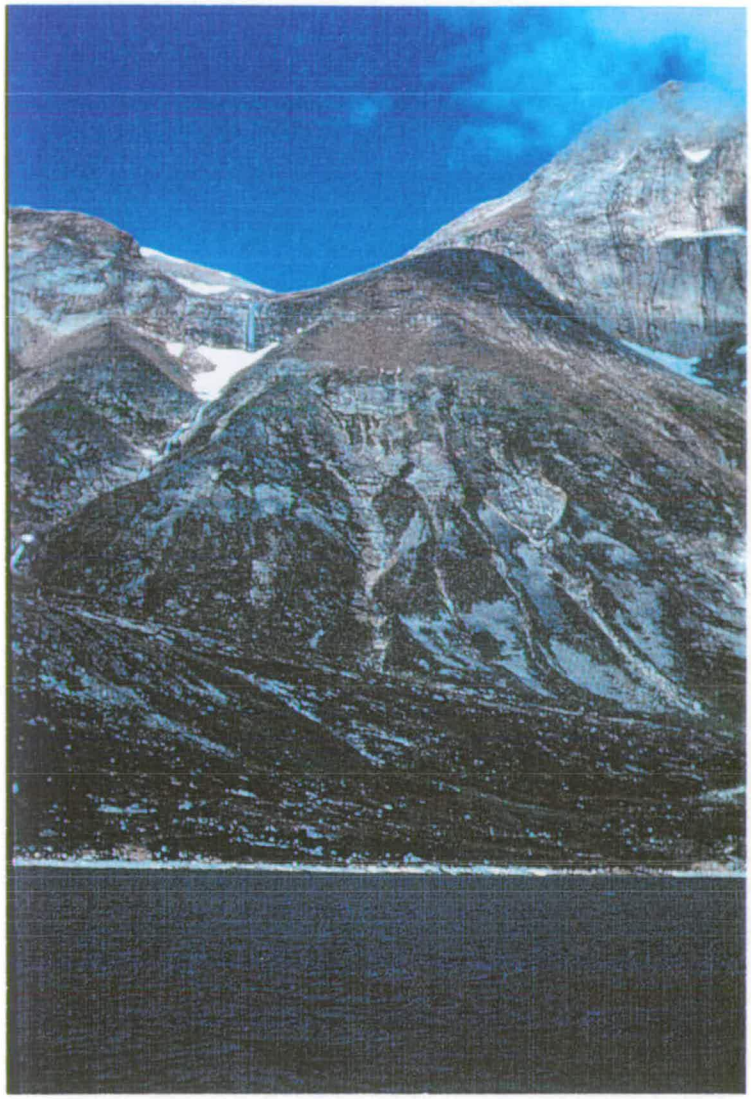

Fig. 3.11: The mountain of Kûngnât, seen from Kûngnât Bay. The grassy slopes are underlain by gneiss; the gabbro ring-dyke can be seen as a band of brown rubble cutting across the slope above the grass, and the peaks behind are formed by the syenites.

3.5 The Kûngnât Complex

The Kûngnât complex is seen from a distance as a steep sided mountain rising over 1400m above the surrounding fjords (Fig. 3.11). Its minor peaks were named by Upton (1960) and these names are shown on the map in that publication and on the location map in Appendix A. The peak of Kûngnât itself is formed by the Eastern Layered Series syenites, and the Eastern Border Group forms steep slabs on the east side of the mountain, so that the most easily accessible exposures are those in stream gullies. The lower parts of the slopes are formed by the Archaean gneisses, so that a climb of up to 500m is necessary before reaching parts of the syenite stock. The junction between the eastern and western syenite stocks lies within a col separating the peak of Kûngnât itself and the Røverborg-Nisseborg ridge. The western side of this ridge is a sheer wall of syenite about 500m high, rising above a small glacier (Fig. 3.12), below which the WLLS syenites are exposed in the area around 920m Peak.

At the contact between the Eastern Border Group syenites and the gneisses, extensive veining of the syenites into the country rocks can be seen. As reported by Upton (1960), pegmatitic patches are present in the marginal syenites and large, iridescent, cryptoperthite alkali feldspars can be collected. Siderite and sulphides are also found in these pegmatites.

The Eastern Layered Series syenites are exposed as slabs in the hanging valley between the peaks of Røverborg and Kûngnât, although these outcrops show little evidence of layering. In contrast to the syenites, the gabbro ring-dyke has chiefly been weathered out to a brown rubble, forming a wide gully around the mountain. The gabbro is back-veined at its margins by syenite, indicating that rheomorphism has occurred. Some "blebs" of mafic magma, with lobate contacts, are also found in the gneisses near the

contact with the gabbro. A lens of alkali gabbro is exposed in the valley to the east of the Røverborg peak, but the majority of the outcrop has been weathered to gravel.

The western syenites are accessible from Pâtussoq bay on the seaward side of the mountain. The southwestern marginal syenites are very poorly exposed, being almost entirely hidden under glacial moraine. The western layered syenites form the Røverborg wall and thus the WULS can only be sampled at its top, on the Røverborg ridge, where some layering can be seen in the syenites. Large exposures of the WLLS are found within the moraine in the valley below the Røverborg. These syenites are part of the lower banded group (Upton 1960) and are clearly layered, with leucocratic layers about 10cm wide separated by narrow (1cm), more mafic bands. Some of these outcrops show trough layering, as described by Upton (1960), Hodson (1994), and Upton *et al.* (1996) (Fig. 3.13). The trough layers average about 50cm high. Pegmatite veins and patches are again common in the syenites. Moving up the succession, the lower laminated group of the WLLS is exposed on the slopes of 920m Peak to the west. The unlaminated syenites are only exposed at the foot of the Røverborg wall and were not sampled in the present study.

The late-stage granites are found cutting the syenites and gabbros throughout the complex. Sheets of quartz syenite are also found within the gneisses close to the eastern contact. In the western stock, v-shaped outcrops of the granite sheets are well exposed around the main glacier river which runs through the valley between the Røverborg wall and 920m Peak. Some of these granitic sheets show banding, and are pegmatitic in places.

Kûngnât was visited during the 1995 field season and samples were collected from most of the main rock-types. Further samples come from Brian Upton's collection.

Fig. 3.12: The Røverborg wall, Kûngnât. The peak of the Røverborg is formed of Western Upper Layered Series syenites, whilst the Lower Series are exposed at the base of the wall.

Fig. 3.13: Trough layering in the Western Lower Layered Series syenites of the Kûngnât complex. Mafic layers approx. 50 cm high. Sketch below indicates scale and shape of the mafic layers.

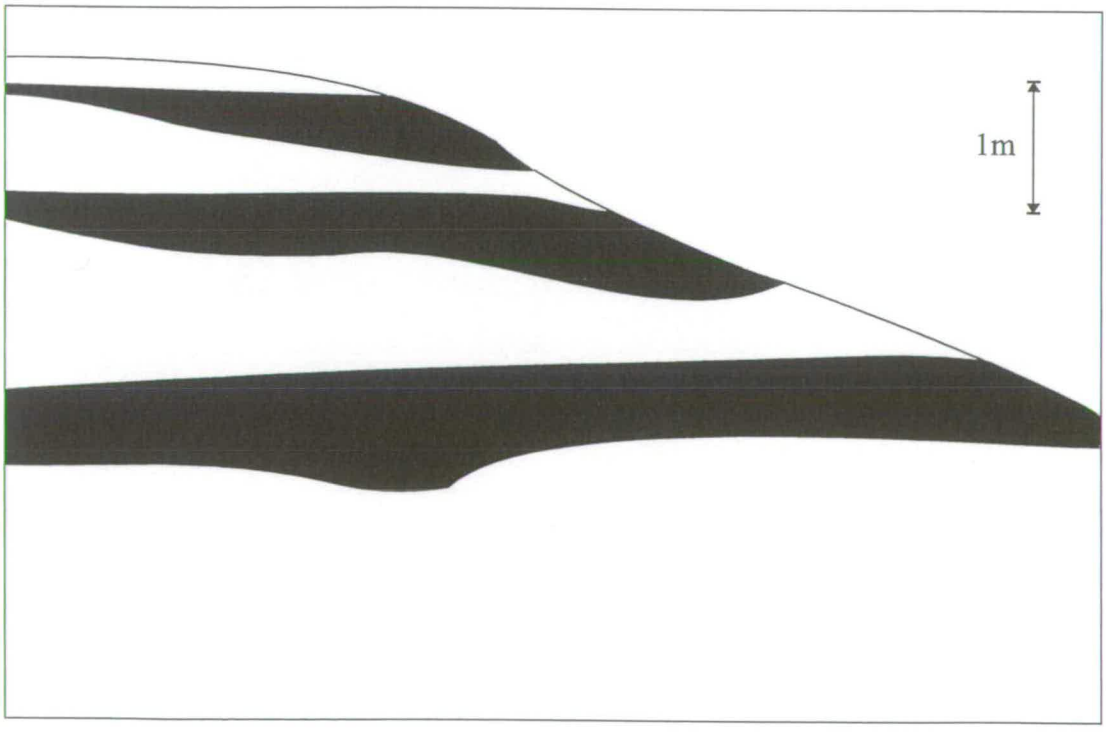

3.6 Mineralisations

Various examples of the mineralised zones described previously were studied on the Ivigtut peninsula during the field seasons of 1995-1996 A good example of a crocidolite zone was discovered in Blokdalen ("Boulder Valley") SE of Ivigtut. This zone is associated with a Gardar lamprophyre and consists of many bright blue-green veins, rich in alkali amphibole, around the dyke contact, with the veins averaging about 50 cm wide. In some places the vein material forms a breccia with xenoliths of carbonated gneiss. Thin (10 cm wide), more altered veins have blue, alkali amphibole-rich edges fading through green into brown, corroded centres,and veins of this type are found cutting sharply through the country rocks in Blokdalen, typically heavily weathered out and trending uniformly SW-NE.

A portable Geiger counter was carried during the 1996 field season but no radioactive mineralisations were located.

Fig. 3.14: Mineralised breccia on the Ivigtut peninsula

Chapter 4: Petrography

4.1 Introduction

This chapter aims to describe the general petrography of all the major Gardar intrusive rock types in the area. This work is based on the samples used in this study, but also draws on the work of others, particularly Bailey (1980) for Ivigtut, Upton (1960) for Kûngnât, and Emeleus (1964) and Bedford (1989) for Grønnedal-Íka. For Ivigtut in particular, generalisations have had to be made, due to the limited number of samples available for the deep granite. A table of average modal mineralogy for each major rock group is given in Appendix H.

4.2 The Grønnedal-Íka complex

4.2.1. The Lower Series Foyaites

The Lower Series Foyaites are well laminated nepheline syenites in which the lamination is defined by tabular alkali feldspars, which are exsolved to cloudy vein perthites up to 1cm long by 1-2mm wide (Fig. 4.1). They frequently show simple twinning, with a single Carlsbad twin along the (001) plane. The exsolution lamellae make an angle to this plane, giving a "herringbone" appearance. Complex intergrowths - "swapped rims" (Voll, 1960) - are present where two perthite crystals are adjacent to each other. This suggests the presence of an intergranular fluid subsequent to the coarsening of the perthite (Parsons, 1978). Some discrete crystals of antiperthite and microcline are also present.

Nephelines originally formed idiomorphic, hexagonal prisms about 2mm in diameter, but have now been variably altered to a fine-grained brownish aggregate of zeolites and micas, termed "gieseckite" (Bøggild 1953). In some samples the original nepheline has only been altered along cracks and at the rims of crystals, whereas in others it has been entirely replaced. Interstitial cancrinite is also present, indicating the presence of a late CO_2-rich fluid phase, and in places poikilitically encloses the altered nephelines.

The proportions of mafic minerals vary throughout the syenites, with the most important being an interstitial, bright green, moderately pleochroic aegirine-augite. Biotite is common, as ragged, green-brown, interstitial plates which may be found mantling pyroxene, and typically containing stringers of opaque oxides along cleavage planes. Opaque oxides are also found as discrete crystals and may poikilitically enclose small pyroxene crystals. The other major accessories are interstitial calcite, and apatite, which forms small (0.1-0.2mm diameter) clear prisms. Small zircons are also present. Bedford (1989) identified sodalite in the Lower Series syenites, and zircon was noted to increase in abundance with increasing degree of alteration.

4.2.2 The Lower Series granular syenite

No samples of this unit were collected in the present study, but Emeleus (1964) described it as an equigranular nepheline syenite with perthitic alkali feldspar, nepheline and aegirine-augite in crystals up to 5mm across. Bedford (1989) divided the unit into two facies: GS-A and GS-B. GS-A has stellate clusters of zoned alkali pyroxene prisms and laths of perthite, with interstitial nepheline. GS-B is the more typical granular syenite, with coarsely exsolved granular perthites and large poikilitic biotites.

4.2.3 Lower Series coarse-grained brown syenite.

This syenite is extremely altered. The alkali feldspars are large (up to 1cm long), tabular, turbid perthites which do not define any clear lamination. Originally subhedral nephelines have been entirely pseudomorphed by a fibrous aggregate ("gieseckite"), and pyroxenes have been chloritised. The only unaltered original minerals remaining are the accessory apatite and opaque ores. Some late interstitial calcite and cancrinite is also present. Zircons are present, as in all the altered rocks from Grønnedal-Íka (Bedford 1989).

4.2.4. Upper Series Foyaites

The Upper Series Foyaites have a similar mineralogy to those of the Lower Series; the alkali feldspars form rectangular plates often over 1cm long, but are less well laminated than those in the Lower Series. They are vein microperthites, which are variably twinned, and their exsolution lamellae are finer than in the Lower Series foyaites. Nephelines in the foyaites are subhedral-euhedral, varying from 0.5-4mm across, and in some cases are replaced by "gieseckite" or have rims altered to cancrinite. Aegirine-augite forms subhedral/interstitial crystals which are patchily zoned, and often contain inclusions of opaque oxides and apatite. Biotite forms ragged interstitial plates and interstitial cancrinite is also common. Again, Bedford (1989) noted the presence of zircons in the more altered samples.

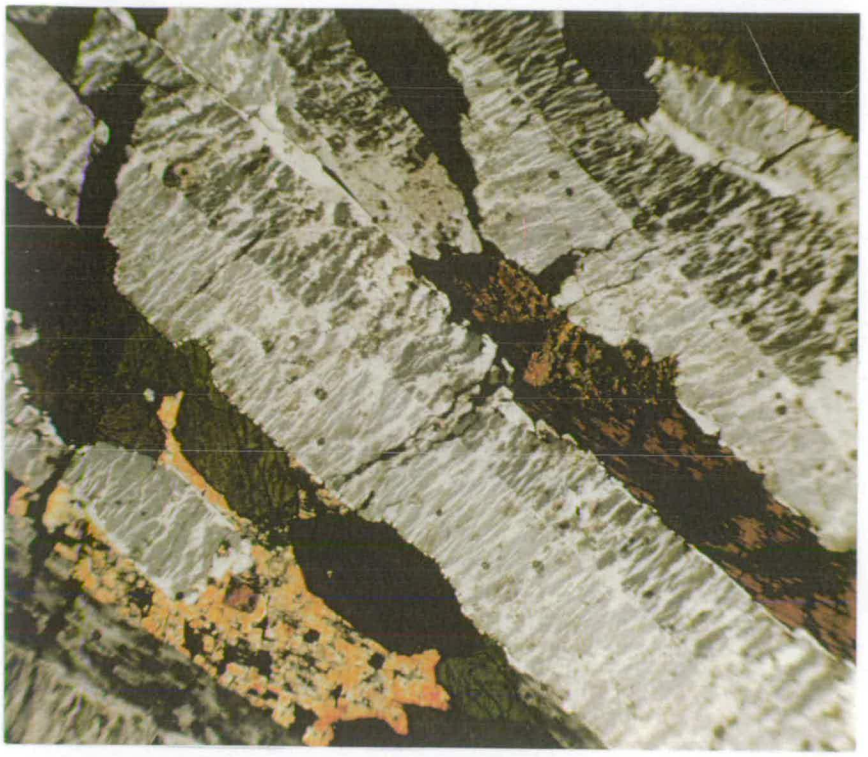

Fig. 4.1: Photomicrograph of sample 95/127 (L. Series foyaite). XPL; field of view approx. 3mm. Tabular, perthitic feldspars cross the picture. Aegirine-augites show anomalous, green interference colours; interstitial cancrinite shows yellow colours.

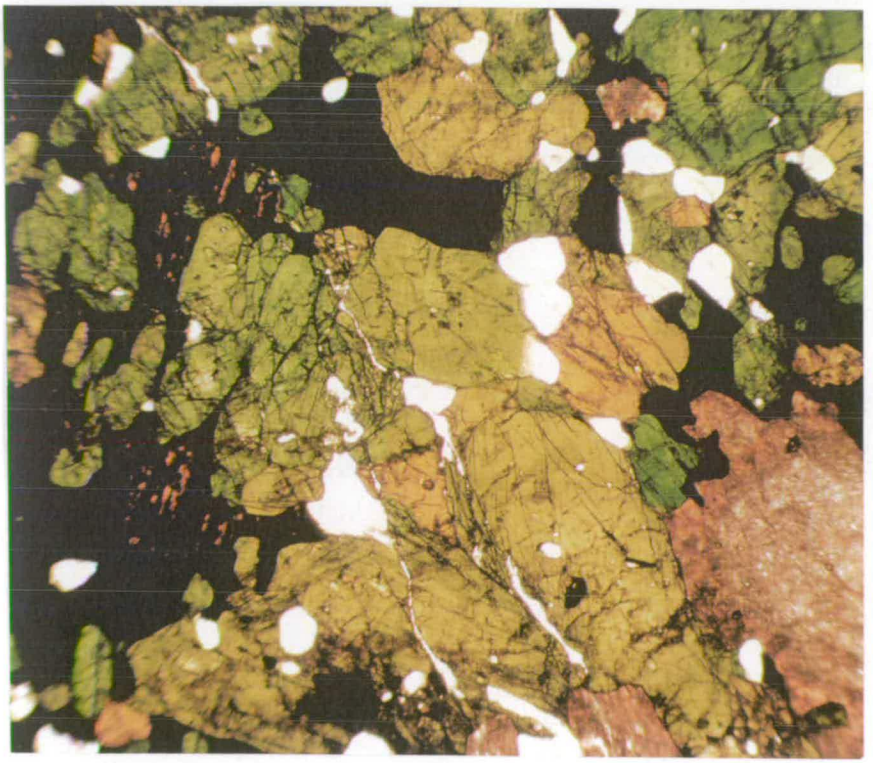

Fig. 4.2: Photomicrograph of sample 96/39 (pyroxene-rich syenite). PPL; field of view approx. 3mm. Green crystals of aegirine-augite and colourless apatite prisms, separated by interstitial opaque oxides replacing biotite. Dusty crystal at bottom right is altered nepheline.

4.2.5. Pyroxene-rich syenite of the Upper Series.

The pyroxene-rich syenite is rather variable in modal mineralogy due to the concentration of aegirine-augite in layers. The more mafic of these layers (Fig. 4.2) consist of subhedral aegirine-augite crystals, 1-2mm across, with interstitial biotite, opaque oxides, and nephelines (which have been replaced by gieseckite). Interstitial cancrinite, and small prisms of apatite, are common. The aegirine-augites frequently show zoning from bright green rims to paler green cores, as shown in Fig. 4.2. Where feldspars are present, they form coarse perthitic laths.

4.2.6. Upper Series coarse syenite.

This is a heavily altered syenite, with original large (5mm) euhedral nephelines, which make up about 50% of the rock, now entirely pseudomorphed by "gieseckite" (Fig. 4.3). Perthitic feldspars are interstitial. Although some remnants exist of original pyroxene, it has typically been broken down and altered to chlorite and a green amphibole, with many inclusions of opaque oxides. Biotite forms ragged plates and common accessories include apatite and interstitial calcite.

A sample taken from an outcrop alongside one of the streams running into Bryggerens Elv, which Emeleus (1964) mapped as coarse syenite, is actually a much fresher rock (Fig. 4.4). Bedford (1989) recognised that this rock-type differed from the coarse syenite and instead grouped it with the main Upper Series syenites. The alkali feldspars are tabular, simply twinned and up to 1.5cm long. They are vein perthites which grade via "pleated rims" (Parsons 1978, Lee *et al.* 1997) into areas of clear braid perthite in the core of the crystal.

Fig. 4.3: Photomicrograph of sample 95/105 (U. Series coarse syenite). XPL; field of view approx. 3mm. Heavily altered nephelines occupy the top of the picture, with interstitial biotite and perthitic feldspar in the centre.

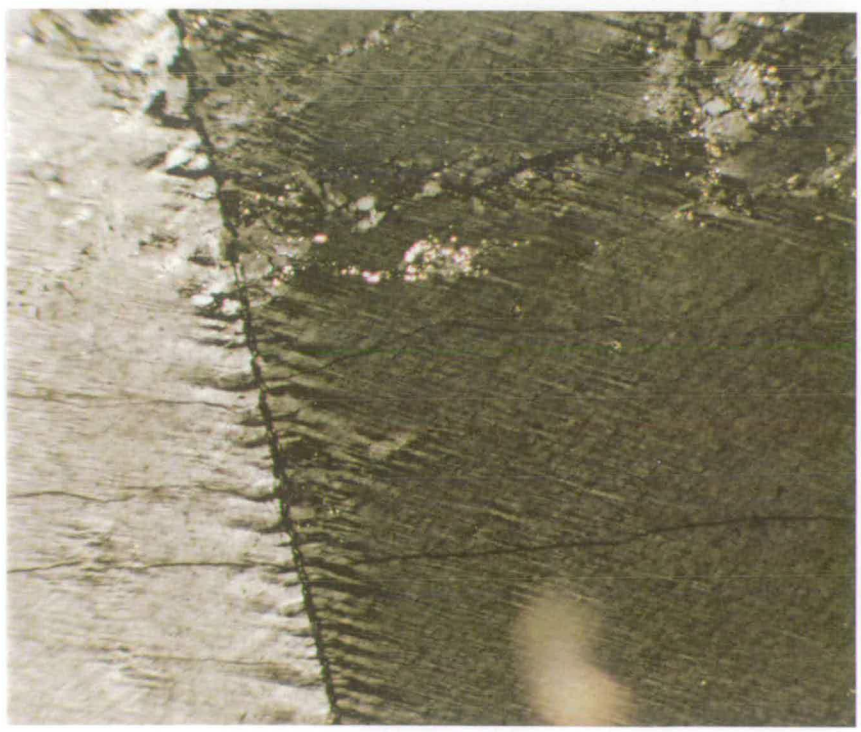

Fig. 4.4: Photomicrograph of sample 96/26 (U. Series syenite). XPL; field of view approx. 0.6mm. Perthitic alkali feldspars have clear cores of regular braid perthite, grading into "pleated rims".

Under cathodoluminescence, these clear feldspar cores can be seen to luminesce blue, suggesting that they have been relatively unaffected by alteration, whilst feldspars from all the other syenites luminesce a dark red colour, possibly due to hydrothermal alteration (D. Stirling, pers. comm.). Idiomorphic nephelines are 2-5mm across and fairly fresh, typically altered at the rims and along cracks. Alteration in some cases is to micaceous aggregates ("gieseckite"), but some crystals are replaced at their rims by narrow prisms of an unusual colourless, low relief, low birefringence mineral growing inwards perpendicular to the margin of the crystal. Aegirine-augite forms fresh, sub-euhedral crystals 1-2mm long which may be zoned. Prisms of pyroxene and apatite are frequently found within large plates of poikilitic biotite which are up to 5mm across. Opaque oxides are also present.

4.2.7. Porphyritic microsyenites

Emeleus (1964) described the rocks of the microsyenite sheets and dykes as "very fresh". However, samples of microsyenite sheets found during the present study are more altered. They contain tabular alkali feldspars 1-5mm in length, which do not show any preferred orientation. Perthitic exsolution textures are only clearly visible in the broader feldspar plates - some narrower laths appear only simply twinned. Small (1mm across) subhedral nephelines have been altered. Interstitial green-brown amphibole, aegirine-augite, and biotite are all present, as well as opaque oxides and apatite. Bedford (1989) noted that some of the sheets may show flow banding.

4.2.8. Xenolithic porphyritic syenite

This is a very altered rock with many angular xenoliths of earlier syenite, trachyte, gneiss and amphibolite included at its margins (Emeleus 1964). Phenocrysts of perthitic feldspar about 1cm long are common. The matrix consists of ragged, sericitised, feldspar plates 2-5mm long, nephelines which have been entirely replaced by gieseckite, and highly altered pyroxenes. Bedford (1989) noted that, in fresher samples from this syenite, aegirine-augites may form overgrowths on augitic cores. Accessories include calcite, cancrinite, opaque oxides and apatite.

4.2.9. Carbonatite

The majority of the carbonatite consists of subhedral plates of calcite about 5mm across, and smaller siderite rhombs about 2mm across, in varying quantities (Fig. 4.5). Calcite shows clear rhombohedral twinning, whilst siderite is typically heavily altered to magnetite along margins and cleavages. There are few silicate minerals within the carbonatite (< 5%), with granular feldspar being the most common, although aegirine, chlorite and zircon have also been reported (Bedford 1989). Syenitic xenoliths may occur within the carbonatite and at its margins the carbonatite brecciates the surrounding syenites.

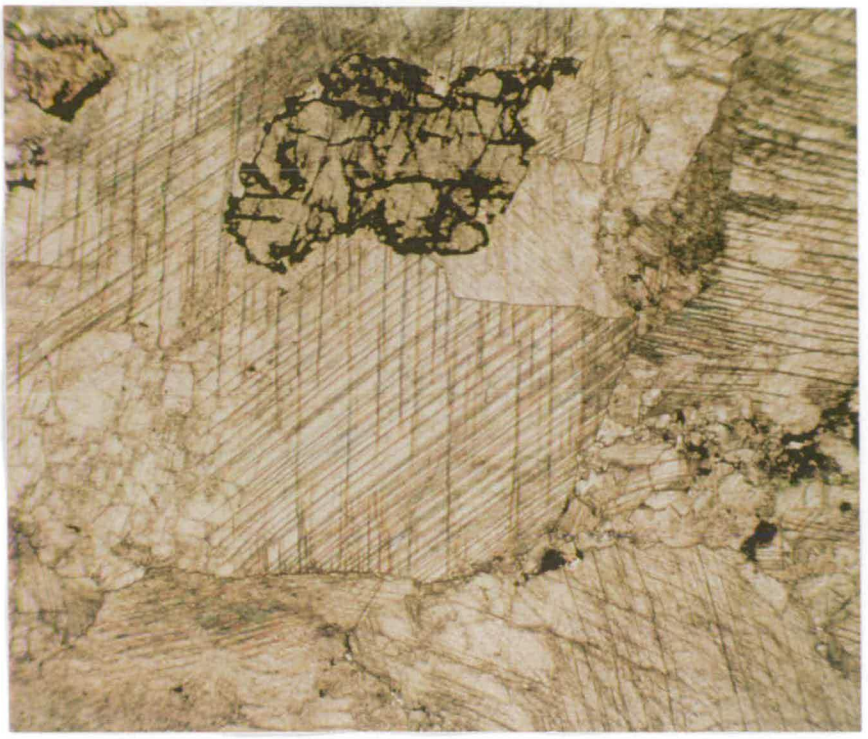

Fig. 4.5: Photomicrograph of sample 96/35 (carbonatite). PPL; field of view approx. 3mm. Chiefly composed of plates of calcite, but with a siderite rhomb, showing alteration to magnetite, at the top of the picture.

4.2.10. Metasomatised syenite

Where adjacent to the carbonatite, the syenites have been heavily altered. These rocks are fine-grained, probably due to recrystallisation, and all silicate minerals except the feldspars have been entirely replaced by micaceous aggregates. The feldspars have not been wholly replaced but are heavily corroded and sericitised. Interstitial carbonate is abundant.

4.3 Lamprophyre dykes

The lamprophyres of the region are mafic to ultramafic, typically porphyritic rocks. They vary in mineralogy and texture throughout the area but some generalisations can be made. The most common phenocrysts are plates of hornblende or biotite 2-3mm across, but euhedral, zoned augite (Fig. 4.6) or sericitised plagioclase feldspar are also occasionally found . In many dykes, original phenocrysts, probably olivine, have been pseudomorphed by a fine-grained aggregate of carbonate and chlorite.

The fine-grained groundmass of these dykes typically consists of biotite + hornblende + opaque oxides + chlorite + carbonate ± pyroxene ± apatite. Some contain small quantities of feldspar, but many are feldspar-free, and can be termed aillikites. The feldspar-bearing lamprophyres (spessartites and kersantites) appear to be more common in the area around the Kûngnât complex, although this may purely be a function of sampling. A characteristic of all the dykes is the presence of vughs, typically 1-5mm across, which are filled with carbonates, chlorite, or epidote. Some of the dykes are composite, indicating multiple intrusions.

Some of the lamprophyres, particularly those found on the plateau between Ivigtut and Íka fjord, are carbonated and mineralised. These lamprophyres are cut by many veins of carbonate and quartz, and they appear to have undergone recrystallisation (see section 4.9).

Fig. 4.6: Photomicrograph of sample 95/16 (lamprophyre). PPL; field of view approx. 3mm. Groundmass consists mostly of biotite, hornblende and opaque oxides, with calcite. Square phenocryst in the bottom right-hand corner is augite.

Fig. 4.7: Photomicrograph of sample 95/12C (Brown Dyke). XPL; field of view approx. 3mm. Composed mostly of fresh labradorite laths, with sub-ophitic augites and rounded olivines.

4.4. Brown Dykes

Where fresh, for example in the hills to the south of Ivigtut, the Brown Dykes are clean, coarse olivine dolerites (Fig. 4.7). Plagioclase (labradorite) forms narrow, idiomorphic laths up to 2mm long, but usually < 1mm, and showing no preferred orientation. Augitic pyroxene forms large (1-3mm) plates which partially enclose the plagioclase crystals , producing a sub-ophitic texture. Olivine forms small (0.1mm diameter), rounded crystals. Common accessories are opaque oxides, often fringed with biotite, and apatite. In the moderately altered BDs, such as those in the Ivigtut valley, the plagioclase has been sericitised and the olivine and augite have been replaced to varying degrees by fine-grained aggregates of chlorite and epidote. Where the "Master BD" of the Ivigtut peninsula intrudes the Grønnedal-Íka carbonatite, it is intensely altered: feldspars are highly sericitised and most other minerals are replaced by aggregates of carbonate and chlorite; only some remnant pyroxene remains.

4.5 Other Dykes

4.5.1. Basaltic dykes

There are various miscellaneous basic dykes within the area, including feldspar-phyric dolerites within the Grønnedal-Íka complex and within the Bunkebreccia. Those which cut the Grønnedal-Íka complex have euhedral phenocrysts, zoned from andesine to labradorite, generally about 1cm long. The groundmass contains randomly oriented labradorite laths up to ~2mm long, which have been sericitised. Clinopyroxene forms rounded sub-euhedral crystals up to 0.5mm across, which are heavily altered along cracks.

Biotite and hornblende are also present, with opaque oxides, calcite and epidote being common.

Also of interest at Grønnedal-Íka is the xenolithic dyke by the hut at Jernhat, which contains many angular xenoliths, up to 10cm across, of gneiss and syenite. The groundmass is doleritic, with randomly orientated plagioclase laths up to 1mm long, plus clinopyroxene, biotite, opaque oxides, apatite and chlorite. The gneissic xenoliths are altered; the feldspars are sericitised and other minerals have been chloritised.

The other main occurrence of porphyritic dolerites in the area is within the Bunkebreccia at Ivigtut. Heavily sericitised plagioclase (andesine) phenocrysts up to 1cm across are present within a doleritic groundmass. Also occasionally present are micro-phenocrysts: some of these are pale green aegirine-augite, others, possibly originally olivine, have been replaced by a fibrous aggregate of chlorite and white mica. The groundmass includes sericitised plagioclase laths up to 1mm long, with flakes of biotite and hornblende, and accessory apatite, calcite and opaque ores. Other basic dykes scattered throughout the area have similar mineralogy, consisting of plagioclase plus pyroxene, biotite, opaque oxides, chlorite and carbonate.

4.5.2 Alkaline dykes

The alkaline salic dykes throughout the region are mostly trachytic in composition but show quite considerable variation. The majority consist chiefly of needles of alkali feldspar, often orientated in the same direction to give a trachytoid texture. Some contain phenocrysts of perthitic alkali feldspar up to 5mm across. Grain sizes vary widely, the feldspars being from <0.1mm to 1mm long.

Some, fairly fresh dykes, have perthitic feldspars showing clear trachytic texture and flowing around micro-phenocrysts of alkali feldspar (micro-perthite). Aegirine-augite occurs as small ragged crystals which in more altered dykes have been replaced by fine-grained chloritic aggregates. Accessories include opaque oxides, white mica and zircon. With increasing degree of alteration the pyroxenes may be replaced by opaque oxides and the content of white mica increases. Some of the dykes contain abundant interstitial nepheline, whilst others are quartz rich. In the quartz-bearing samples, biotite is the prominent mafic mineral.

The trachytic dykes within the Bunkebreccia contain perthitic phenocrysts 2.4mm long in a groundmass of fairly randomly orientated perthite laths. Pyroxene (augite - aegirine-augite) is present as small rounded crystals. Accessories include apatites and opaque oxides.

4.6 The Ivigtut stock

The top granite at Ivigtut, which capped the cryolite deposit, is a sub-porphyritic hypersolvus granite (Fig. 4.8). Where fresh, it consists of phenocrysts of turbid vein microperthite and quartz around 0.5cm in diameter, set in a micro-granitic groundmass. The microperthitic plates often show "swapped rims". Quartz crystals tend to cluster together, forming masses of anhedral interlocking crystals with stable 120° triple junctions between grains. The groundmass consists of quartz and micro-perthite plus about 10-15% mafic silicates. The mafic minerals are found as clusters of small (0.2mm long) plates of green-brown biotite and a ferro-edenitic amphibole. Accessory minerals, which are typically associated with the clumps of mafic minerals, include abundant zircon, opaque ores, fluorite, and siderite. The granite is typically heavily fractured.

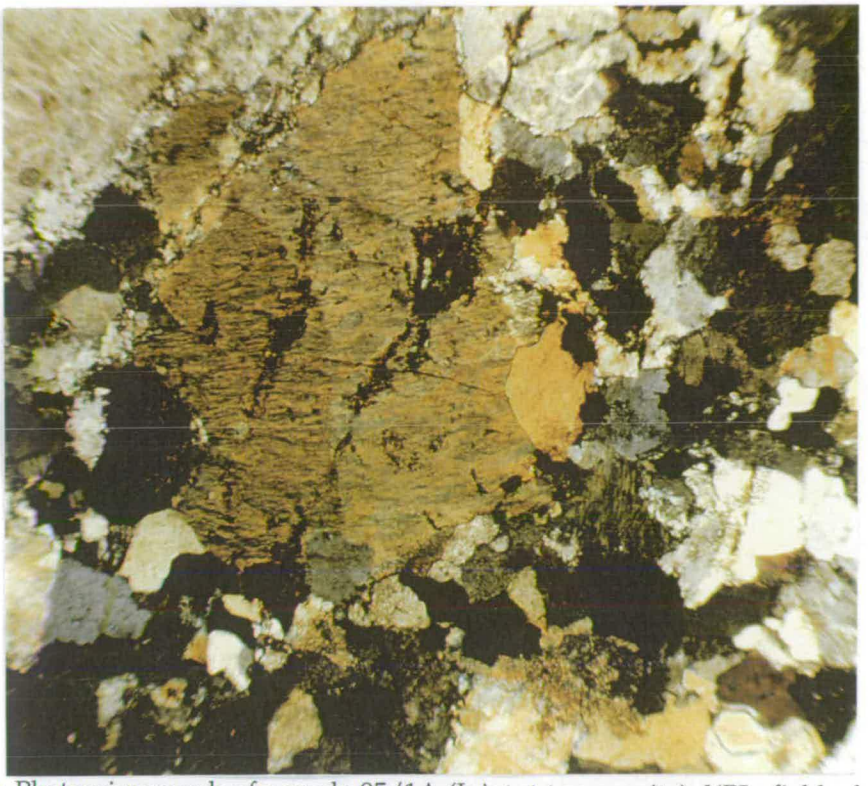

Fig. 4.8: Photomicrograph of sample 95/1A (Ivigtut top granite). XPL; field of view approx. 3mm. Phenocryst of perthitic feldspar in a groundmass of quartz and feldspar.

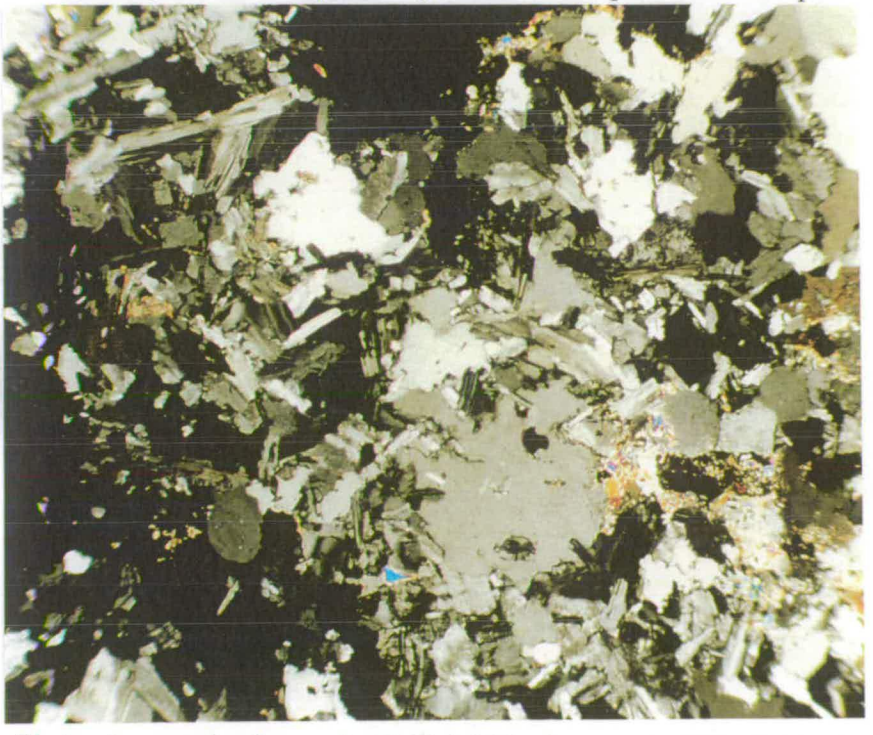

Fig. 4.9: Photomicrograph of sample 96/7 (albitised granite). XPL; field of view approx. 3mm. Original feldspar has been replaced by small laths of albite.

Pink, metasomatised varieties of the top granite have fresh quartz and relatively fresh feldspar, but mafic minerals have been broken down, being replaced by siderite and fluorite, which are more abundant than in the fresh granite. In samples believed to be taken from close to the ore body, the top granite has been albitised and sericitised, with late-stage albite laths replacing original perthitic alkali feldspar and quartz (Fig. 4.9). Remaining quartz shows evidence of strain, with undulose extinction patterns, whilst perthitic feldspars have a very patchy appearance. Original mafic minerals have entirely disappeared, with siderite, fluorite, white mica, and zircon the most abundant accessories. Some sulphides are also present (chalcopyrite and sphalerite). Zircons are up to 0.5mm across, typically heavily cracked and embayed.

In the immediate vicinity of the deposit, the albitised granite passes into greisen, with a yellowish phengitic mica ("ivigtite") replacing all original minerals except quartz and zircon. The mica occurs occasionally as ragged plates up to 2mm across but typically forms an aggregate of fine tablets. Zircons are abundant, large (1mm across) and typically zoned and embayed. Siderite, fluorite and cryolite are present within the greisen.

At depths of around 100 - 200m within the granite, at some distance below the deposit, the granite consists of anhedral quartz crystals averaging about 2mm across, in a groundmass of quartz plus small (0.5mm long) tablets of microcline, microperthitic alkali feldspar, and albite (Fig. 4.10). The main mafic minerals, making up less than 10% of the rock, are green biotite and hornblende. Zircon is present, along with late, interstitial cryolite, fluorite and siderite.

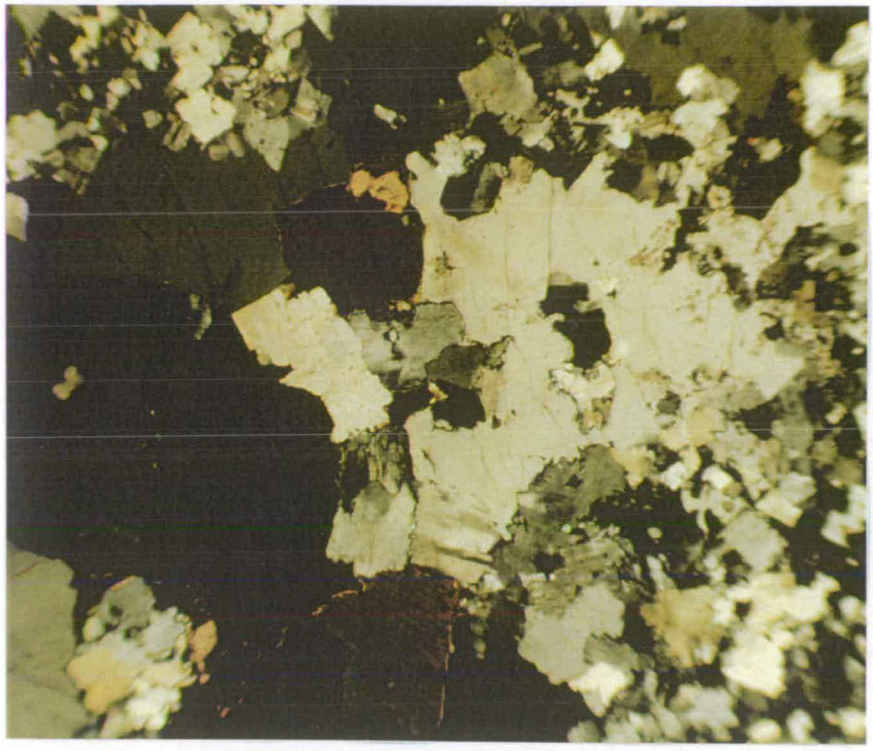

Fig. 4.10: Photomicrograph of sample J4 (vi) (Ivigtut granite). XPL; field of view approx. 3mm. Quartz plates in a groundmass of quartz and feldspar tablets. Hornblende shows green-brown anomalous interference colours.

Fig. 4.11: Photomicrograph of sample BB25 (v) (Ivigtut deep granite). XPL; field of view approx. 3mm. Feldspar with vein perthite textures cut by patches of coarsely-twinned albite.

A deep drill core, BB25, reached to a maximum depth of over 800m within the granite. Samples from around 600m vary in coarseness and some pegmatitic patches are present. Large (up to 5mm) anhedral plates of alkali feldspar show vein perthite textures which are cut by patches and veins of coarsely twinned albite (Fig. 4.11). Albitised ("swapped") rims are common and very broad in some samples. Abundance of quartz varies between samples. Mafic silicates are rare and the most abundant accessories are siderite and zircon, with fluorite and sulphides also being present.

A sample from a borehole depth of 781.4m is rich in interstitial cryolite and siderite, and has a texture similar to that of the albitised top granite. Quartz, vein perthite and microcline form plates averaging 2mm across which are typically partly replaced by albite. Small amounts of phengitic mica and the ubiquitous zircons are present. At 793.4m, textures are similar, but clumps of mafic minerals are abundant, the most prominent being greenish biotite and riebeckite. Some white, phengitic mica is also present. Accessories include zircon, siderite and an interstitial aluminofluoride.

Samples from 805m have quartz crystals up to 5mm across, with patch perthite and microcline forming anhedral plates 2-4mm in diameter. Again albite laths are present, replacing other feldspar crystals. Remnants of hornblende, and some phengitic mica, are present, but no alkali amphibole. Zircons are large, zoned, and heavily embayed. Interstitial fluorite and cryolite are present in small quantities.

4.7 Granophyre dykes

A set of "granophyre" dykes has been described (Berthelsen 1962, Bailey 1980) as radiating out from the Ivigtut granite stock. Bailey (1980) noted that some of them were altered, with the addition of cryolite, fluorite, siderite and muscovite. Samples from five such dykes have been studied: they are fine-medium grained and leucocratic. They typically have an equigranular groundmass consisting of anhedral quartz and dusty feldspar tablets (microperthite and microcline): crystal size varies between individual dykes, from about 0.1 - 0.5mm across. The coarsest of the dykes shows very prominent granophyric textures, with micrographic intergrowths of quartz and alkali feldspar often radiating out from a "core" of perthite (Fig. 4.12). In the finer dykes these intergrowths are less abundant, and one dyke appears to be a simple microgranite. However, all the dykes are considered as a related group on the basis of chemistry, being the only granitic (SiO_2 ~ 75%) dykes in the area (See section 6.2). Mafic silicates are rare, with some of the dykes containing hornblende ± biotite, which in some cases have been partly replaced by chlorite. Common accessories in all the dykes are opaque oxides, fluorite, and zircon, whilst some also contain siderite. However, no cryolite has been found in any of the granophyre dykes in the present study. One of the dykes, that which cuts the BD0 to the south of the Ivigtut village, is xenolithic, containing rectangular xenoliths of gneiss and trachyte up to or longer than 1cm. Many of the dykes contain tabular phenocrysts of perthitic alkali feldspar ± plagioclase, which are up to 2mm long.

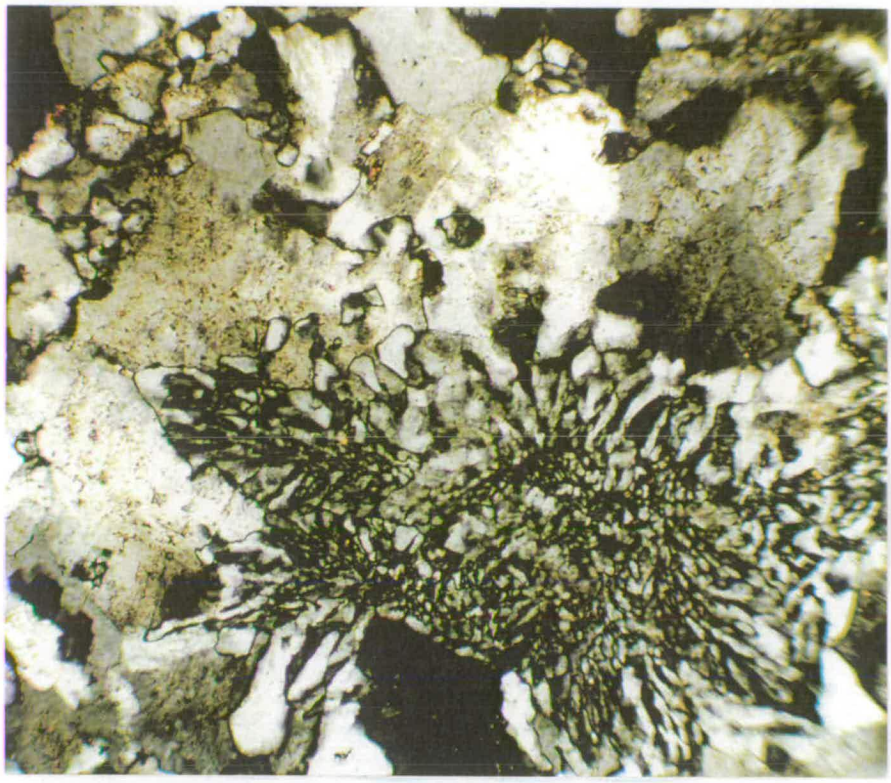

Fig. 4.12: Photomicrograph of sample 96/15 (granophyre). XPL; field of view approx. 0.6mm. Radiating granophyric intergrowth of quartz and feldspar.

Fig. 4.13: Photomicrograph of sample 95/77B (WLLS syenite, Kûngnât). PPL; field of view approx. 3mm. Clinopyroxenes in bottom left corner are zoned from augite cores to aegirine-augite rims, and associated with plates of brown amphibole. Perthitic feldspar, on the right of the photo, appears dusty. An olivine in the bottom of the photo is fairly altered.

4.8 The Kûngnât Complex

4.8.1. SW Marginal Syenites

No samples of the SW marginal syenites were collected in the present study but these rocks were described by Upton (1960). The feldspars are idiomorphic, 2-3mm long, vein micro-perthites; where twinned they have a "herring-bone" appearance, caused by perthite lamellae at an angle to the twin plane. Interstitial quartz makes up about 10% of the rock. Pyroxenes form subhedral, corroded, zoned crystals with cores of ferrohedenbergite and rims of green aegirine-augite. Interstitial hornblende and olivine, plus accessory fluorite, are present, but zircon and apatite are rare.

4.8.2. Western Lower Layered Syenites.

In the leucocratic syenite layers of the lower banded group (Fig. 4.13), feldspar makes up about 70% of the rock. These feldspars are coarse, turbid patch perthites and antiperthites which form laths or plates, averaging about 5mm × 2mm, but up to 2cm long. The majority of the feldspars are antiperthites, in which the clear, multiply-twinned plagioclase host contains patches of cloudy alkali feldspar. Textures vary, with the cores of some of the larger crystals being clear and showing little or no optically visible exsolution (cryptoperthites). The edges of the crystals have sutured grain boundaries and tend to interlock with each other. Lamination, if present at all, is poor.

Pyroxene in these syenites forms pale green, weakly pleochroic subhedral crystals up to 5mm across, which are heavily cracked, and are typically zoned from a colourless augitic core to a green aegirine-augite rim (Fig. 4.13).

These are associated with a green-brown hastingsitic amphibole, which mantles the pyroxene crystals, forming a fringe up to 2mm wide, and also penetrates cracks within the pyroxene. Some discrete, interstitial amphibole crystals are also present. The amphibole appears to have formed at the expense of the pyroxene. Fayalitic olivines form anhedral crystals 1-2mm across, which are altered along cracks to opaque ores and a mixture of smectite, chlorite, and goethite/haematite known as iddingsite (Deer *et al.* 1992). Apatite is a common accessory and typically occurs as inclusions in poikilitic pyroxene and amphibole.

The mafic layers in these syenites show similar textures to those of the leucocratic layers, but show an increase in mafic minerals to about 50%. Augite and olivine form clusters of subhedral crystals 1-2mm across. Amphibole and biotite are found chiefly as narrow, flaky fringes on pyroxenes, though large poikilitic patches of hastingsite also occur. Apatite and opaque oxides are common accessories, often as inclusions within amphibole. Marginal rocks from the WLLS contain small amounts of interstitial quartz, and in places the pyroxenes are highly altered.

The feldspars in the laminated group of the WLLS form laths about 2-5mm long which define some lamination. They appear to be patch perthites and microcline antiperthites, similar to those of the lower banded group. The mafic minerals are similar to those in the banded group, but the zoning in the pyroxenes is less pronounced and they appear more heavily replaced by amphibole. Olivine is rare and apatite is also less common than in the banded group. Zircon is rare, but can be found as unusually elongate crystals 2-3mm long.

In the unlaminated group at the top of the WLLS, the feldspars show finer exsolution lamellae and are relatively clear, vein perthites. The grain

boundaries are sutured and interlocking as in the lower groups. Pyroxenes are anhedral and zoned, from ferrohedenbergite cores to aegirine-augite rims, and tend to cluster with olivines. Interstitial brown amphibole and opaque oxides are common, but apatite is rare. Upton (1960) noted the presence of riebeckite and quartz in the top of the WLLS, increasing upwards.

4.8.3. Western Upper Layered Syenites.

The samples of the WULS used in this study were only collected from the top of the Røverborg ridge, therefore any description of the lower parts of the WULS is derived from Upton (1960).

Samples from the Røverborg peak have euhedral feldspar tablets 5-10mm long, separated by interstitial quartz (Fig. 4.14). The feldspars vary from cloudy vein perthites, some of which have single twins, to patchy antiperthites with clear albite twinning in the host. Upton (1960) noted that the feldspars lower in the sequence show less regular textures and have a greater aspect ratio. Pyroxene (pleochroic, green hedenbergite) is cracked and corroded, forming elongate crystals up to 5mm long. Many are mantled with hornblende, and in some cases the pyroxene is altered to needles of a blue-green mineral (riebeckite?). Biotite is present in small amounts, usually fringing opaque oxides. Olivine is rare and heavily altered to iddingsite where it does exist. Some interstitial calcite is present.

Fig. 4.14: Photomicrograph of sample 95/75 (WULS syenite, Kûngnât). XPL; field of view approx. 3mm. anhedral, interlocking plates of perthitic feldspar and quartz.

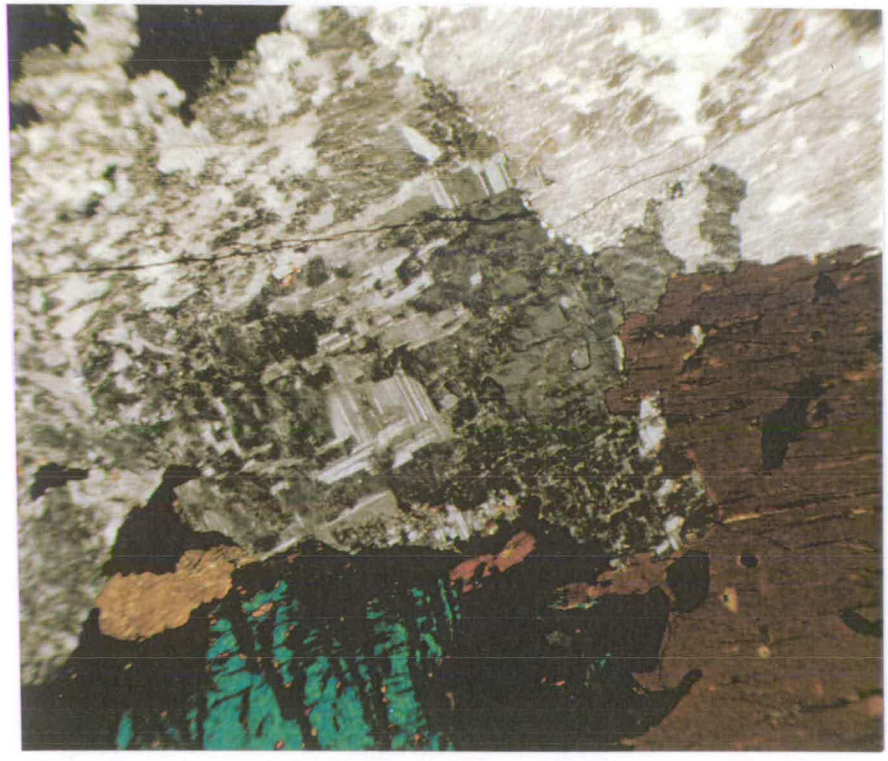

Fig. 4.15: Photomicrograph of sample 95/62 (E. syenite, Kûngnât). XPL; field of view approx. 3mm. Patchy perthitic feldspar with heavily altered olivine and brown hornblende.

4.8.4. Eastern syenites

The Eastern Border Group syenites are unlaminated, the feldspars forming anhedral crystals up to 5mm across (Fig. 4.15). The exsolution textures seen in the feldspars in thin section range from coarse patch antiperthites, in which the proportion of the albite-twinned host is much greater than that of the orthoclase, to finer patch perthites with approximately the same proportions of the two feldspars. Some clear feldspars showing little or no exsolution are also present, and Upton (1960) noted that these feldspars are particularly common in the more mafic syenites. The boundaries between feldspars tend to be interlocking, and some intergrowth of two crystals occurs in places.

Pyroxene is present as anhedral crystals 1-2mm across, which do not show the prominent zoning of those in the western syenites, but separate crystals vary from augite to hedenbergite. It is pervasively altered to green-brown hornblende which forms interstitial crystals up to 2mm across. Olivine is rare but, where present, forms anhedral crystals which are heavily altered to iddingsite. Accessories include opaque oxides, which are fringed with biotite, and abundant apatite, which forms slender prisms up to 2mm long. An interstitial carbonate is also present in some samples.

The Eastern Layered syenites are fairly similar in texture to the EBG syenites, although the pyroxenes tend to be smaller and more prismatic in the ELS.

4.8.5. Ring-dyke gabbro.

The Kûngnât ring-dyke is made up of fresh, sub-ophitic olivine gabbro and syenogabbro (Fig. 4.16). The plagioclase, of labradorite composition, forms large (10mm x 4mm), clear laths which do not show a preferred orientation.

In some marginal parts of the ring-dyke the plagioclases are strongly zoned. Interstitial, optically homogeneous alkali feldspar (possibly cryptoperthite) is present in the gabbros and becomes more highly developed in the more alkaline syenogabbros, in which the plagioclase is more sodic. Upton (1960) noted that perthite intergrowths coarsen to become microscopically visible in some of the most alkaline rocks. Olivine forms heavily cracked, rounded crystals about 2mm across, which cluster together, and augitic pyroxene forms sub-ophitic, interstitial crystals of a similar size. Apatite and opaque oxides are common accessories, the oxides being typically fringed by biotite.

Where the ring-dyke has been cut by the peralkaline granites of the western stock it has been metasomatised up to distances of 2-3cm from the granite contact (Macdonald *et al.* 1973). In the metasomatised gabbros, original mafic minerals have been replaced by fine-grained aggregates of green and brown biotite. Feldspars are preserved, but are altered and sericitised, and apatites are unaltered. At distances of a few cm from the contact, remnant pyroxene can be found.

4.8.6. Late-stage granites of the Western Stock

The "soda-granites" of W. Kûngnât are coarse-grained late sheets (Fig. 4.17). They contain laths of alkali feldspar: vein perthite, which may be simply-twinned, and patch antiperthite, up to 4mm long. Late-stage albite laths 0.1-0.2mm long are present in some of the granites. Interstitial quartz makes up ~ 25% of the rock and often forms rounded intergrowths within the perthites, appearing to have replaced them.

The most abundant mafic mineral is a sodic amphibole (riebeckite-arfvedsonite) which is pleochroic from a dark blue-green to a pale brown. This amphibole is typically interstitial and frequently encloses many crystals

Fig. 4.16: Photomicrograph of sample 95/64 (ring-dyke gabbro, Kûngnât). XPL; field of view approx. 3mm. In the bottom half of the picture are opaque oxide crystals with biotite fringes. High birefringence crystals are olivine. Labradorite laths fill the top half of the picture.

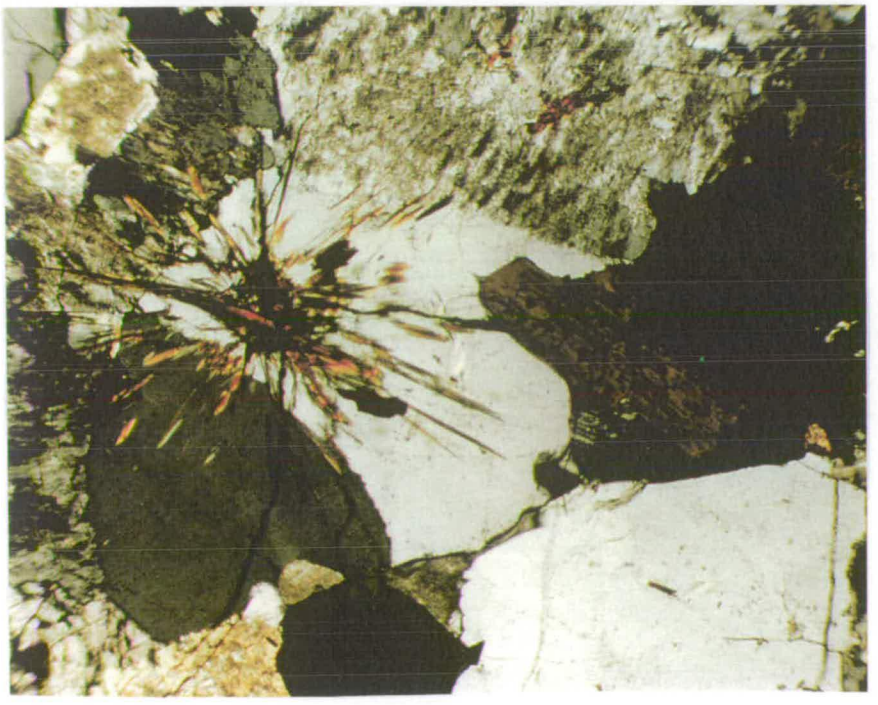

Fig. 4.17: Photomicrograph of sample 86184 (late granite, Kûngnât). XPL; field of view approx. 3mm. Astrophyllite forms a "star" shape of radiating needles; dark crystals on the right of the picture are riebeckite.

of quartz and feldspar, appearing poikilitic. Accessory minerals include astrophyllite, which forms radiating clusters of golden-brown needles; zircon; and opaque ores.

A second group of late sheets, the "grey-dykes", are banded rocks with 1mm-sized rectangular phenocrysts of perthite and microcline in a groundmass of albite and alkali feldspar laths 0.1-0.2mm long. The proportions of the differing feldspars vary between layers, but the smaller tablets tend to show a preferred orientation, producing a flow-banding. Interstitial quartz is present, and the major mafic mineral is again a sodic amphibole with pleochroism from a deep blue to a pale brown. Some green alkali pyroxene is also occasionally found in these rocks. Zircon and opaque ores are accessories.

4.8.7. Late sheets of the Eastern stock.

The late sheets of the eastern centre are microgranites and microsyenites with a less alkaline mineralogy than those to the west. Microperthite and plagioclase form cloudy, rectangular tablets up to 1mm long; the microperthite is more abundant and in some, syenitic, sheets the plagioclase is completely absent. Perthitic phenocrysts about 2mm across are present in some sheets and some are optically zoned. Interstitial quartz is present and varies from about 30% down to <10% in the microsyenite sheets.

Hornblende is the major mafic mineral and in some cases forms elongate crystals up to 1mm long, but is otherwise anhedral. Ragged plates of biotite are also commonly present, and some are partly chloritised. Opaque oxides are abundant accessories, along with zircon and late carbonate. One aplite sample from the eastern slopes contains remnant pyroxene, whilst another microgranite contains white mica.

4.9 Mineralisations

Two major types of mineralisation which appear to be associated with Gardar activity have been studied in this project. Both types are generally associated with Gardar basic dykes. The first type includes various mineralised breccias, which have highly carbonated clasts of varying rock-types in a cement of large prismatic quartz crystals. These clasts have generally been widely replaced by large crystals of calcite and siderite, but the precursors are assumed to be the associated basic dykes.

The second type of mineralisation has been described previously as crocidolite zones (Ayrton & Masson, 1972) (Fig. 4.18). In these zones, basic dykes are cut by veins of quartz and calcite ± albite, and have been highly altered, with the introduction of an alkali amphibole as well as large amounts of carbonate. The amphibole (magnesioriebeckite) forms clusters of tiny needles, which are pleochroic from pale blue-violet-straw yellow, and have replaced large parts of the dykes. Phenocryst phases in particular seem to have been entirely replaced by magnesioriebeckite and carbonate, although the amphibole is also abundant in the groundmass of the dykes. Gneiss adjacent to these altered dykes contains sprays of magnesioriebeckite needles, sodic pyroxene, and carbonate, replacing mafic minerals within the gneiss.

Fig. 4.18: Photomicrograph of sample 95/58D (crocidolite zone). PPL; field of view approx. 3mm. Groundmass of an ultramafic dyke is cut by calcite veins which include masses of magnesioriebeckite fibres.

Chapter 5: Mineral Chemistry

5.1 Introduction

Some mineral chemistry data for the study area have already been published: Bedford (1989) presented a comprehensive study of the mineralogy of the Grønnedal-Íka complex, whilst the mafic silicates of the Kûngnât Complex were described by Stephenson & Upton (1982), Hodson (1994), and Hodson & Finch (1997). The present study therefore concentrates on samples from the Ivigtut granite. Although the mineralogy of the Ivigtut cryolite body has been extensively studied in the past (e.g. Pauly 1992, 1993) the surrounding granite has been largely neglected. Analyses presented in the present work concentrate on the major silicate minerals. Although many other unusual minerals occur within the granite, study of the whole spectrum of these minerals represents a PhD project itself. The present study also included some analyses of samples from a single lamprophyre dyke and associated mineralisation, and these are summarised below. Analyses were made in the electron microprobe unit at Edinburgh University: operating conditions are given in appendix B and data tabulated in Appendix G. Fe in the analyses is expressed simply as a total FeO value.

5.2 Major minerals of the Ivigtut Granite

5.2.1 Feldspars

Since much of the feldspar in the granite is microperthitic alkali feldspar, it is difficult to obtain a bulk composition. The individual lamellae simply consist of almost pure albite and orthoclase. The feldspar in the altered granites was also shown to be virtually pure albite, the only impurity being up to 0.5% FeO, showing that they are highly fractionated and virtually Ca-free.

5.2.2 Micas

Both biotites and phengitic muscovites are found within the Ivigtut granite. The phengites only occur within altered granite, whereas Fe-micas are found throughout most of the stock. All the biotites studied in the samples of top granite, (IV53, KG95/1A and KG95/7) were compositionally similar. Recalculation of analyses for these samples does not imply any octahedral Al, hence the siderophyllite end member is zero, as has been observed elsewhere in the Gardar (Finch *et al.*, 1995). Although small amounts of tetrahedral Fe may be present, the biotites are most closely modelled by variation along the annite phlogopite solid solution. This variation can be expressed as Fe/(Fe+Mg), which for biotites from the Ivigtut top granite varies from 0.94-0.98; i.e. these biotites are all nearly pure annite ($K_2Fe_6[Si_6Al_2O_{20}](OH)_4$). Fluorine contents vary between samples: in KG95/1A they are about 0.3%, in IV53 about 0.9%, and in KG95/7 about 2.7%. F content appears to decrease with increasing Fe/(Fe+Mg) in biotites from these top granite samples, indicating an "Fe-F avoidance trend" (Mason, 1992). Due to the small number of samples and the small range of compositions of these biotites, it is difficult to quantify this trend; however, the Ivigtut micas have considerably higher F for given values of Fe/(Fe+Mg) than micas from other Gardar complexes (Finch *et al.*, 1995).

In the deeper granite samples, BB25(ii) and J4(vi), Fe/(Fe+Mg) for the biotites is almost exactly 1, and Si/Al ratios are > 4. Although Li has not been measured in these samples, the high Si/Al ratios, low total of ions in the octahedral site, and high F contents suggest that these micas are not true biotite, but that they tend towards zinnwaldite compositions. These micas contain virtually no Mg and they do not exhibit the Fe-F avoidance trend observed in the top granite samples, since they formed from the high-F late-stage fluids rather than primary magmatic melts.

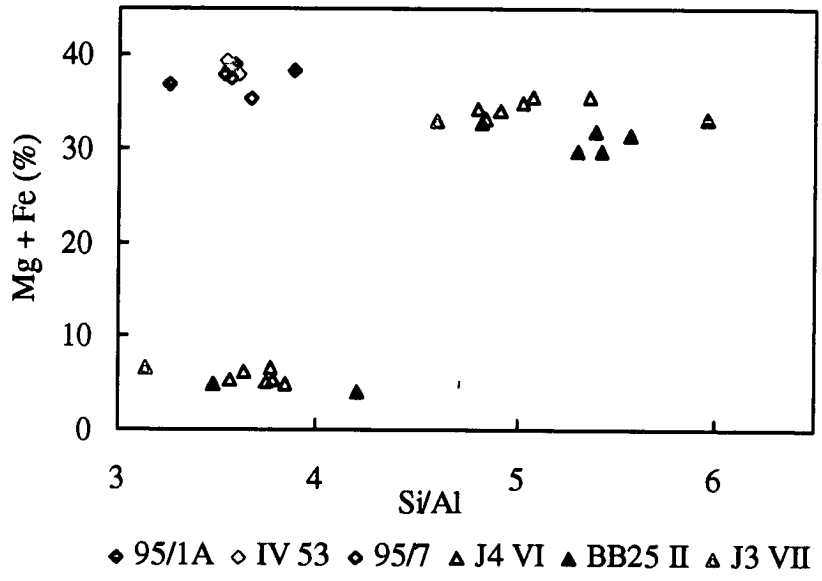

Fig. 5.1: Plot of (Mg + Fe_T) vs (Si/Al) for micas from the Ivigtut granite. Diamonds represent top granite samples: triangles represent deeper granite. Sample numbers shown below graph. Those with (Mg+Fe) > 20 are biotites; those with lower (Mg + Fe) are phengites.

Phengitic white micas were studied in samples of altered and albitised granite. They are typically very F-rich, with some containing enough fluorine to form the pure fluor-muscovite end-member, although F contents vary. Al_2O_3 contents in the Ivigtut white micas are low (14-16%) as compared with typical muscovite (~30%; Deer *et al.*, 1992), so that the Si:Al ratio is high(> 3), confirming that these micas are phengites. Again, the high F-content and apparent deficiency in the octahedral site suggest that Li may be present. Li is often associated with high F contents in rocks which have been affected by hydrothermal activity (Deer *et al*, 1992), and thus the presence of Li-bearing micas in the altered Ivigtut granites seems likely. Furthermore, Li-mineralisation has been reported in the cryolite deposit (Pauly, 1986). Curiously, in samples of the greisen, the closest zone of alteration to the cryolite body, the mica seems to be less exotic, having higher Al_2O_3 but lower F contents.

5.2.3 Amphiboles

Amphiboles are not as common as micas in the altered granite and, as mentioned in Section 4.6, there are distinct compositional differences between those in the top granite and those at depth. The top granite samples contain amphiboles approximating to $Na_{0.8}Ca_{1.7}Fe_{4.4}[Si_{6.3}Al_{1.3}O_{22}](OH)_2$ which is best described as ferro-edenite (Deer *et al.*, 1992). The most altered parts of the granite contain no amphibole but one sample from a depth of about 800m in a drill core (sample BB25 ii) contains riebeckite. The presence of riebeckite in the granite was previously reported by Callisen (1943).

5.2.4 Zircons

Zircons in the Ivigtut granite have been analysed for major- and trace-elements including Si, Zr, Th, Fe, Al, Y, Ca, Hf, Er and Yb. In a top granite sample (KG95/1A) the zircons are small (< 0.1mm across) and appear clear, with few inclusions, when studied using backscattered electron images (BSEI). They contain relatively few impurities, although HfO_2 may represent up to 4% of the total and Y_2O_3 1%. Some grains are patchily zoned and may contain up to 2.5% FeO in the zones which appear darker in BSEI. These zones have lower average atomic number, whereas the brighter zones have higher average atomic number: the substitution of Fe atoms for Zr clearly reduces the average atomic number of the zircon.

Zircons in a sample of altered, greisenised granite (J4 v) are much larger than in the top granite but heavily zoned and rich in inclusions. The zoning is typically patchy, only occasionally being concentric, and the zircons are typically heavily embayed. The darker zones under BSEI are again Fe-enriched, with up to 0.9% FeO, whereas the lighter zones are enriched in Y_2O_3 (up to 1%) and the HREE. In some grains HfO_2 makes up >5% of the total.

Some of the zircons in the greisen are cut by, or contain inclusions of, a mineral which appears very bright using BSEI. Although difficult to analyse quantitatively, it can be seen from energy dispersive spectra (EDS) that this mineral is a phosphate (possibly monazite or xenotime) which is rich in the HREE, and also to some extent in Th and U. The fact that this mineral cuts the zircons indicates that it must have formed late in the development of the rock and was clearly associated with the metasomatism.

5.4 Mineralised dyke

The electron probe study also included some samples from a zone of crocidolite mineralisation (described in section 4.9) associated with a lamprophyre dyke on the Ivigtut plateau. The blue amphibole, which is termed crocidolite because of its fibrous nature (Deer *et al.*, 1992) has a magnesioriebeckite composition: $Na_2Mg_3Fe_2[Si_8O_{22}](OH,F)_2$. K_2O varies from 3% in the cores of the crystals down to 0.5% in the rims, while CaO makes up less than 1% of the total of all analyses. Fluorine varies from low levels of 0.3% up to about 3%, and Cl levels are below detection limits. Associated with the amphibole are flakes of Ti-rich biotite with composition approximately $K_2Mg_{2.7}Fe_{2.7}Ti_{0.5}[Si_{5.7}Al_2O_{20}](OH,F)_4$. This is rather more Mg-rich than the Ivigtut biotites. The biotites of a relatively fresh sample from the lamprophyre are even more magnesian, having formula $K_{1.7}Mg_{4.3}FeTi_{0.5}[Si_{5.4}Al_{2.5}O_{20}](OH,F)_4$. Due to the presence of Ti in the octahedral sites, the micas from the lamprophyre are not true phlogopites, but they are richer in a phlogopite component than those from the mineralisation. These micas contain less than 0.5% F. Remnant cores of pyroxene exist in some samples, surrounded by amphibole. These are generally diopsidic ($CaMgSi_2O_6$), but variable amounts of Na substitution for Ca and Fe for Mg were noted. In diopsides from the fresh lamprophyre, FeO makes up ~ 5% of the total and Na_2O 0.5%.

The high magnesium contents of the minerals in this particular lamprophyre dyke suggest that it should be classified as an ultramafic lamprophyre (UML). The alkali- and fluorine- rich nature of the mineralisations associated with this dyke indicates alkali metasomatism (often termed "fenitisation"), which may have been caused by fluids related to the carbonate-rich veins. Magnesio-riebeckites are common constituents of "fenites" associated with carbonatites (e.g. Mian & Le Bas, 1986).

5.5 Discussion

No olivine has been reported within the Ivigtut granite in the present study, but Pauly & Bailey (in press) note the presence of sparse fayalite. Fayalite, ferro-hornblendes and annite are all typical minerals in rocks from A-type suites which are metaluminous-mildly alkaline (Eby, 1990). The presence of these Fe-rich minerals indicates the prevalence of reducing conditions (King *et al.*, 1997).

The biotites of the Ivigtut top granite appear to have higher fluorine contents at given values of Fe/(Fe+Mg) than those from the other Gardar centres reported by Finch *et al.* (1995), suggesting that the magma from which the Ivigtut granite formed was itself rich in fluorine. This result does not conform with the conclusions of Finch *et al.* (1995), who showed that, elsewhere in the Gardar, the undersaturated Gardar centres tend to have more F-rich biotites than the oversaturated. It is possible that the biotites of the top granite have had their F contents enhanced by fluorine from the late-stage metasomatic fluids. The micas of the altered granites have very high F contents which have clearly been imparted by these late-stage fluids, and the presence of such micas at hundreds of metres below the cryolite deposit indicates that fluids were not solely concentrated at one level. Lower levels of fluorine in the micaceous greisen (close to the cryolite deposit), than in the

albitised granites, suggest that fluorine- (and sodium-) rich fluids affected wider zones within the granite than K-rich fluids. This compares with the situation at Kûngnât, reported by Macdonald *et al.* (1973), in which K-rich fluids had metasomatised the rocks closest to the late-stage granites, but Na-rich metasomatism was not apparent.

The large zircons in the altered granites appear to have grown during hydrothermal activity in the granite, and the presence of HREE-rich veins cutting these zircons indicates that these F-rich hydrothermal fluids also transported the REEs.

The mineralisation of the crocidolite zone can be attributed to alkali-rich metasomatism, probably related to carbonates associated with the lamprophyre dyke. There is no evidence to confirm the suggestion of Ayrton & Masson (1972) that such metasomatism was related to alkaline massifs at some distance.

Chapter 6: Whole-rock Geochemistry

6.1. Introduction

The amounts of whole-rock major- and trace-element data that have previously been published vary between the intrusives from this area. Bedford (1989) presented data for the Grønnedal-Íka complex. Published data for the dykes from the area is limited(e.g. Upton & Emeleus 1987). Bailey (1980) listed some whole-rock analyses from the Ivigtut granite but did not discuss them in detail. Macdonald *et al.* (1972) published some data for parts of the Kûngnât complex (gabbros & granites) whilst Upton (1960) gave preliminary analyses of all the rock-types from Kûngnât.

In the present study a total of two hundred rock samples have been analysed by X-Ray fluorescence (XRF) at Edinburgh University for major and trace elements. These samples represent all the rock-types within the study area, including samples from the three main Gardar complexes as well as samples of the varying dyke swarms and the country rocks. Previously published analyses are mentioned where relevant: it was necessary to analyse samples from all rock-types both to ensure a consistent data-set and for selection of samples for isotopic analysis. A subset of thirty samples has been analysed for REE contents, using ICP-AES, at RHBNC, University of London. Analytical methods are described in Appendix B and all the results are tabulated in Appendix E. It should be noted that, as many of the rocks are cumulates, data from these samples do not necessarily represent the composition of the magmas from which the rocks crystallised.

This chapter presents the key features of these results and discusses their significance to the petrogenesis of Gardar rocks in the area. Four major rock

groups are considered; the three central complexes, and the dykes. The dykes are further divided into three subsets. The lamprophyres can be considered to be petrographically and geochemically distinct from all the other dykes, but the Brown Dykes are discussed as part of a group of "basaltic dykes" which also includes the BFDs and other miscellaneous dykes. The third subset contains all the salic alkaline dykes sampled from the study area.

6.2 Major element geochemistry

Fig. 6.1 shows selected Harker plots for all the rock-types from the area, except the carbonatites. Weight percentages of SiO_2 show a wide variation across the spectrum of rock-types, from 35-42 wt% in the lamprophyres up to 75 wt% in the granites. There is a continuous trend in SiO_2 contents from lamprophyres - dolerites - nepheline syenites - syenites - granites. The lamprophyres and basaltic dykes are distinguished as separate groups on the basis of petrographic observations, but they can also be effectively separated by a cut-off line of SiO_2 = 42 wt%. The Grønnedal-Íka carbonatites only contain 0.5-10 wt% SiO_2, depending on how much feldspar and other silicate material is present, and so are not plotted on these diagrams.

Plots of (Na_2O + K_2O) and Al_2O_3 against silica show an "anvil" shape, with a positive trend in the more mafic rocks, diverging at *c.* 60 wt% SiO_2 from trachytes towards granites (increasing SiO_2, decreasing Al_2O_3 and alkalis) and undersaturated syenites (decreasing SiO_2, increasing Al_2O_3 and alkalis). Magmatic evolution beyond the trachytic stage was chiefly controlled by fractionation of alkali feldspar, with the more extreme alkalic compositions representing the effects of feldspathoid accumulation (Upton, 1974). The granitoid rocks show high total alkali contents (7-11 wt%) which, with low CaO contents (<1.8 wt%) and high FeO_T/MgO ratios, typify A-type granites (Eby, 1990).

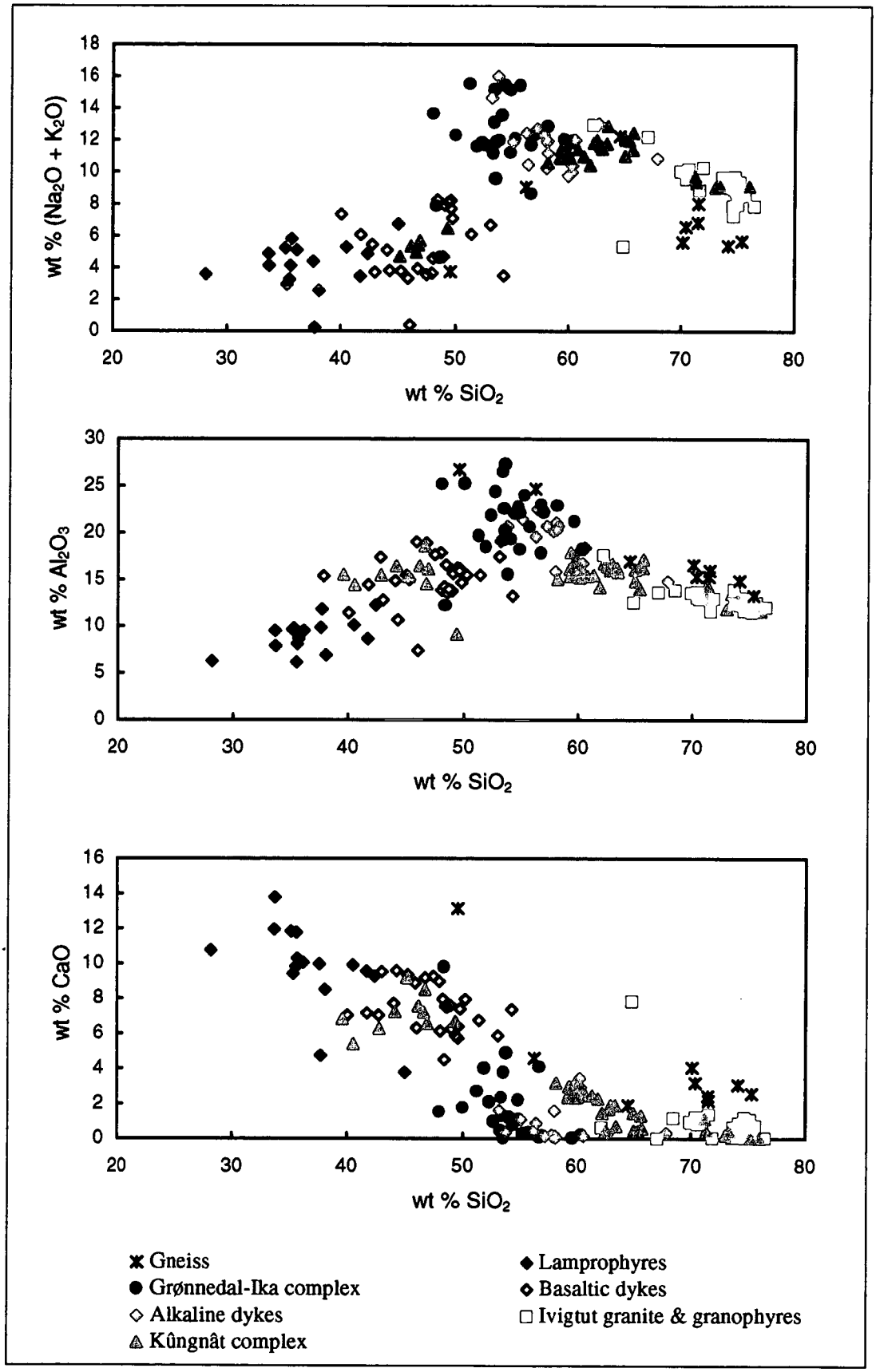

Fig. 6.1: Harker plots for all rock-types from this study

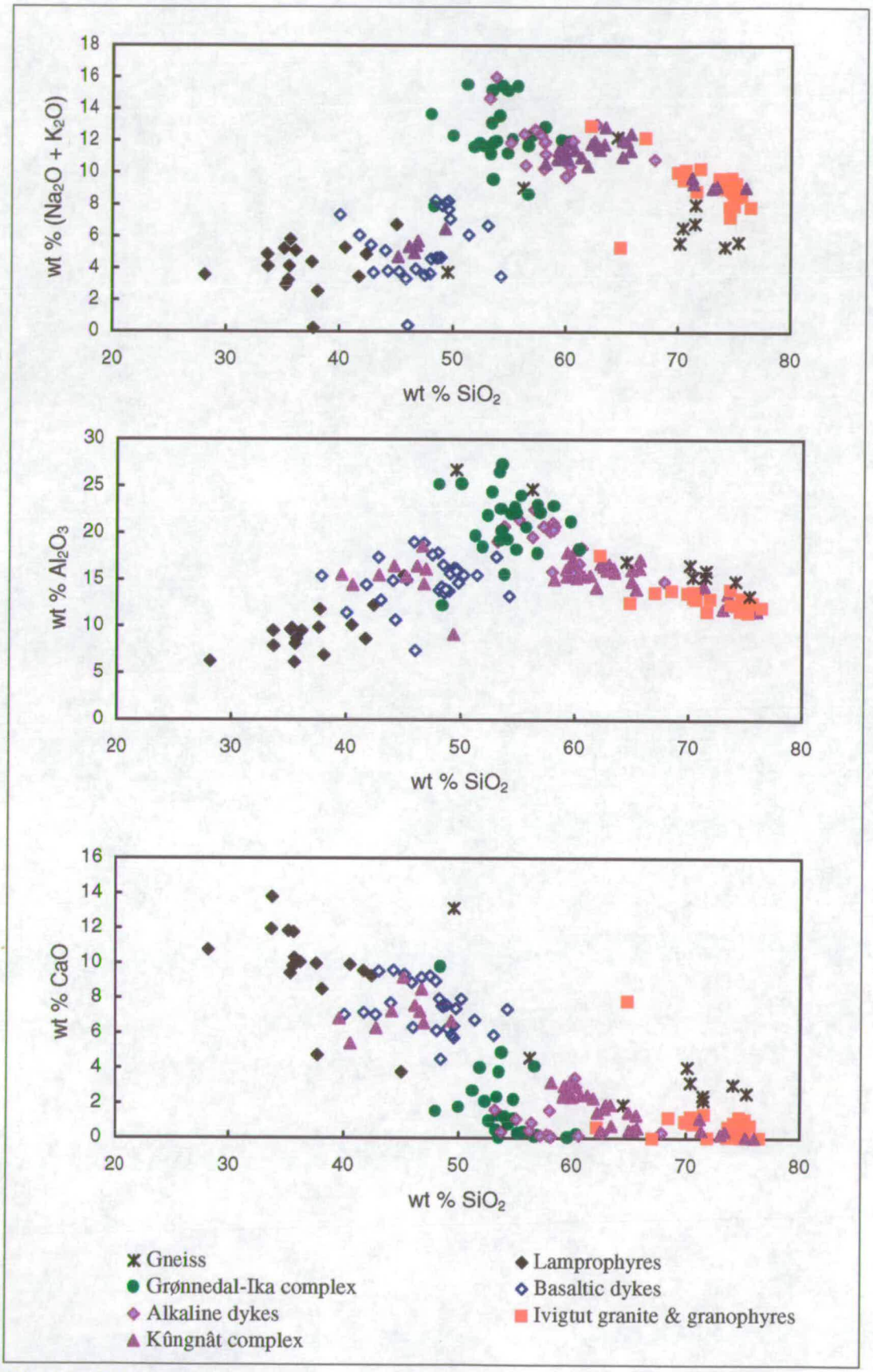

Fig. 6.1: Harker plots for all rock-types from this study

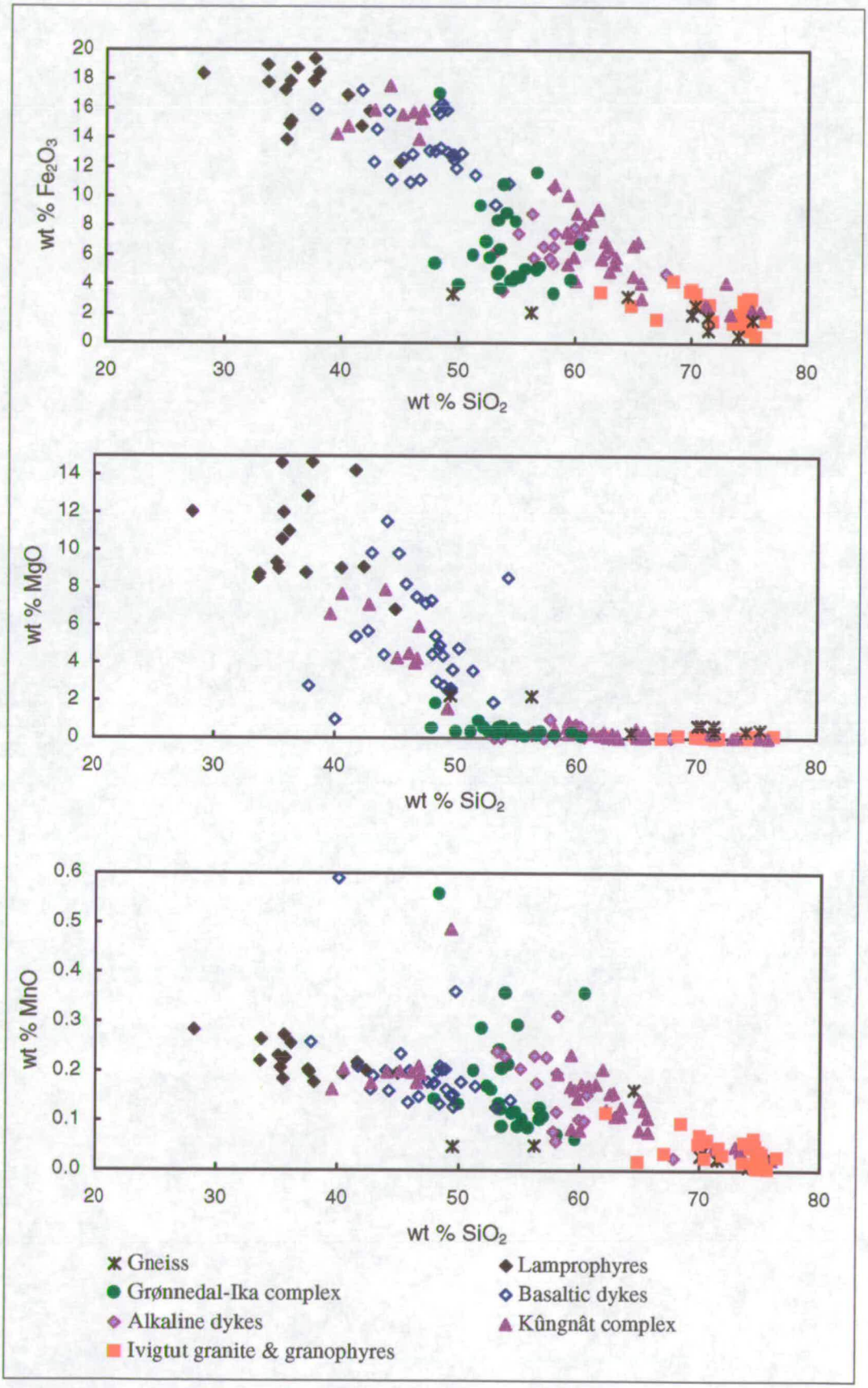
wt % Fe_2O_3
wt % SiO_2
wt % MgO
wt % SiO_2
wt % MnO
wt % SiO_2
Gneiss
Grønnedal-Ika complex
Alkaline dykes
Ivigtut granite & granophyres
Lamprophyres
Basaltic dykes
Kûngnât complex

Fig. 6.1 cont.

As expected, Fe_2O_3, CaO and MgO decrease with increasing SiO_2. MgO contents are up to 15 wt% in the lamprophyre dykes, whereas in the other basaltic dykes MgO < 8 wt%, and Upton & Emeleus (1987) noted that basaltic rocks more magnesian than this are rarely found in the Gardar Province. Virtually all the syenites, granites, and trachytes have MgO <1 wt% (the exception being the most pyroxene-rich syenite from Grønnedal-Íka). Similarly, only the basic rocks (SiO_2 < 50 wt%) have TiO_2 > 1 wt%. MnO is < 0.3 wt% in virtually all the rock-types and decreases with increasing SiO_2. The exceptions are mostly found among syenites from Grønnedal-Íka, which show MnO contents up to 0.6 wt%; and in the Grønnedal-Íka carbonatite, which is rich in MnO (0.5-3 wt%).

Mg-numbers are calculated as $100[Mg/(Mg+Fe_T)]$. The lamprophyre dykes, the most primitive rocks, have Mg-numbers of 30-50, whilst the Brown Dykes and other basaltic dykes show a wider variation from 15-45. If FeO/Fe_2O_3 is estimated (e.g.as 0.15 for all the basic dykes; see Appendix E)), and the Mg-number is calculated as $100[Mg/(Mg + Fe^{2+})]$, the values obviously increase (63-78 for the lamprophyres). In the three major complexes the salic rocks typically have Mg-numbers of less than 10. In Kûngnât the range is from 5-15 in the more basic eastern syenites, and from 0.5-7 in the western syenites. In Ivigtut Mg-numbers are very low, from 0.5-3, whilst the Grønnedal-Íka syenites have values ranging from about 1-10.

Peralkalinity data from the felsic rocks of the three main complexes have been plotted in Fig. 6.2, showing $Al_2O_3/(CaO + Na_2O + K_2O)$ vs. $Al_2O_3/(Na_2O + K_2O)$. Samples from Ivigtut are peralkaline or mildly metaluminous, with $Al_2O_3/(CaO + Na_2O + K_2O)$ and $Al_2O_3/(Na_2O + K_2O)$ < 1.1. The granophyre dykes from the Ivigtut valley generally show similar major element chemistry to the Ivigtut granite itself. Samples from the Kûngnât complex show a wider range, with the syenites being mostly metaluminous or weakly

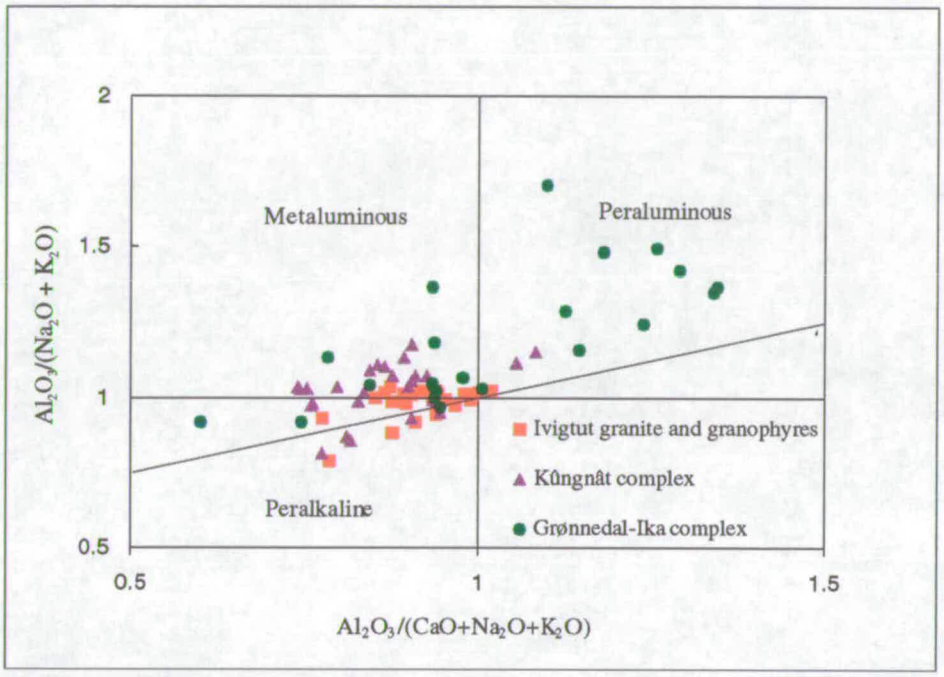

Fig. 6.2: Plot of Shand index for felsic rocks.

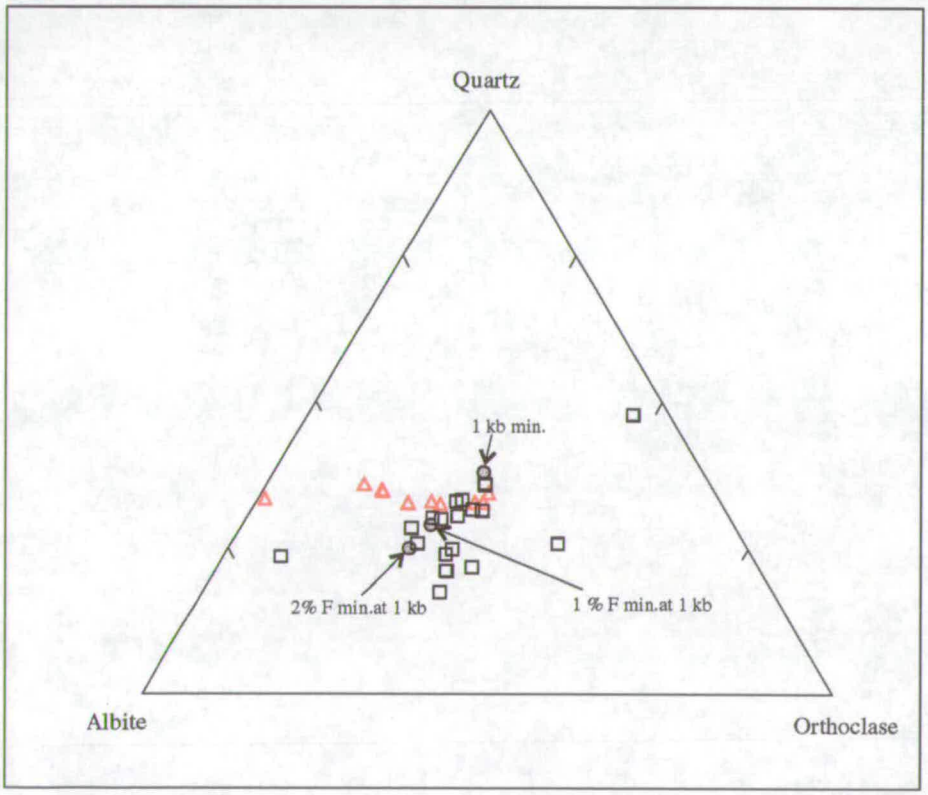

Fig. 6.3: Projection onto the plane quartz-albite-orthoclase from H_2O at 1 kb.
Minima are shown for the pure system and for 1% and 2% fluorine.
Open squares are samples from the Ivigtut granite; triangles represent granophyres.

peralkaline, whilst the majority of the granite sheets are peralkaline. Curiously, two of the late granite sheets from the east side of Kûngnât are metaluminous. The Grønnedal-Íka syenites are metaluminous to peraluminous, despite the fact that they contain aegirine-augite. Similar associations of rock-types are typical of many A-type suites such as the Topsails suite of Newfoundland (Whalen *et al.* 1996).

6.3 Normative geochemistry

CIPW norms are tabulated in Appendix E. Ratios of FeO/Fe_2O_3 for the varying rock types were estimated from data in existing literature (see end of Appendix E). Norms were calculated using the Chemcast 2.0 program (written by C.E. Ford, 1992), and methods and abbreviations are the same as those used in Cox *et al.* (1979).

6.3.1 The Grønnedal-Íka Complex

The Grønnedal-Íka syenites have up to 32 % normative nepheline, and some also have normative corundum; the pyroxene-rich syenites have diopside in the norm. Bedford (1989) plotted a broad spectrum of analyses from Grønnedal-Íka on the *Ne-Ks-Qz* diagram and showed that they tend to cluster around a point just above the *ne - k-feldspar* minimum at 1 kbar, with a general trend towards this minimum, and some samples lying below the phase boundary in the nepheline field. It was noted that, if crystallisation occurred at P_{H_2O} < 1kb, final liquid compositions would be displaced slightly further towards the undersaturated part of the system. Fractionation of alkali feldspar would drive the residual liquid towards the *ne - k-feldspar* phase boundary. Increasing volatile (F- and Cl-) contents in the magma tend to displace this phase boundary towards the *Ne-Ks* join, explaining those samples appearing to lie within the nepheline field (Bedford, 1989). Some

samples plot on the oversaturated side of the albite-orthoclase join and Bedford (1989) suggested that this was due to wall-rock contamination, or breakdown of nepheline to gieseckite, leading to increase of the Si/K ratio and loss of Na. The first explanation, however, is unlikely, since addition of quartz to a phonolitic magma would simply lead to the crystallisation of more alkali feldspar.

6.3.2 Dykes

The lamprophyres fall into two groups in terms of their normative assemblages. One group contains *or* + *ab* + *an* + *ne* + *di* + *ol* and these could be termed alkaline lamprophyres (Rock, 1987). These dykes tend to contain small amounts of feldspar, and have SiO_2 contents of 37-45 wt%. The second group, which includes only feldspar-free dykes with SiO_2 < 37 wt%, has a normative assemblage of *an* + *lc* + *ne* + *di* + *ol* + *la*. The presence of *la* (larnite, Ca_2SiO_4) indicates a gradation into ultramafic lamprophyres (Rock, 1987). The Brown Dykes and other basaltic dykes have typical normative assemblages of *or* + *ab* + *an* + *di*+ *ol*; they contain no normative *qz*, but all have either *ne* or *hy*. The trachytic dykes have norms mostly composed of *or* + *ab*, but many contain *co* or *ne*. Very few are *qz*-normative.

6.3.3 The Ivigtut stock

The Ivigtut granite samples have a norm made up almost entirely of *qz* + *ab* +*or*, and the top granite contains 18-34 % normative quartz. Fig. 6.3 shows all the samples plotted on the quartz - albite - orthoclase - H_2O diagram (Tuttle & Bowen, 1958). The majority of the samples from the relatively unaltered granites plot around the minimum for 1% F + excess H_2O at 1 kbar. (Manning, 1981), but the most strongly altered granites are scattered over the plot, albitised granites being shifted towards the albite apex, and greisen

towards the *qz-or* join. The trend of the apparently unmetasomatised granites towards the albite apex could be explained by the presence of 1-2% F in the magma. The high F contents in the biotites of the top granite (Section 5.2.2) also indicate that the magma from which the granite formed was rich in fluorine.

6.3.4 The Kûngnât Complex

The Kûngnât gabbros have a fairly uniform normative mineralogy, chiefly *ab* + *an* + *di* + *ol*. Most contain small (1-3%) amounts of normative nepheline, but the gabbros which have been metasomatised by fluids escaping from late-stage granites have 11-13% normative nepheline, and some have normative leucite, due to their high contents of K_2O. The syenites vary widely, with the most evolved, such as those from the top of the WULS, having *qz* + *hy* in their norm (silica over-saturated), in addition to the essential assemblage of *or* + *ab* + *di*. Some of the less evolved samples have normative assemblages containing *hy* + *ol* (silica saturated), whilst others contain small amounts (<2.5%) of normative *ne*, + *ol* (silica under-saturated). All the WULS samples analysed are over-saturated. However, samples from the WLLS show a coherent variation, from mildly *ne*-normative (although there is no modal nepheline present) in samples from the lowest outcrops, to *qz*-normative in samples from higher up the succession; this is probably attributable to the assimilation of SiO_2-rich country rocks as well as fractionation within the magma. Similarly, the eastern syenites are *qz*-normative near the margins of the stock, passing inwards to *ne*-normative. Samples of the late sheets are plotted on the *Qz-Ab-Or* diagram in Fig. 6.3b and two groups can easily be discerned, one with low normative *qz* (<8% - quartz syenites) and the other with >20% normative *qz*. Two late sheets from the eastern stock are metaluminous and contain normative *co*.

6.4 Trace element geochemistry

All the samples used in the present study have been analysed for Rb, Ba, Th, Nb, La, Ce, Sr, Nd, Zr, Ti, and Y. Many of the granitoid samples have also been analysed for Mo, U, Ta and Hf. A smaller set of samples, chiefly from Ivigtut, have been further analysed for Ga and Sn. The data are displayed on variation diagrams and normalised incompatible-element diagrams, and descriptions are given for each intrusion or group of intrusions. On the spidergrams all data are normalised to primitive mantle (normalising values from McDonough & Sun, 1995). Where a large number of samples from a rock unit with some internal variation have been analysed, such as at Kûngnât, the spidergrams show mean compositions for that unit; in other cases data for individual samples are plotted. Means and standard deviations are tabulated at the end of Appendix E. It should be noted that, although the trace element contents may vary between samples, the essential features of the patterns on multi-element diagrams are consistent.

6.4.1 The Grønnedal-Íka Complex

On a spidergram plot of representative samples from the different syenite units (Fig. 6.4), it can be seen that samples from the Upper and Lower Series foyaites are quite variable in trace element (TE) chemistry but have overlapping trace element concentrations. They show clear troughs at Ba, Sr and Ti, with the Lower Series foyaite tending to have the greater negative anomalies. The pyroxene-rich syenite unit of the Upper Series shows the same pattern, with troughs at Ba, Sr and Ti, but is relatively more enriched in these elements than the other syenites. The pyroxene-rich unit also has higher concentrations of La, Ce and Nd (i.e. the light rare earth elements (LREEs), which are discussed in section 6.6.1), but lower K and Rb concentrations, than the typical foyaites.

The coarse-grained brown syenite is notably enriched in Ba compared with the foyaites, whilst Sr contents are variable. Similar patterns were observed by Bedford (1989) and attributed to the effects of alteration and introduction of late stage carbonate. The xenolithic porphyritic syenite lacks the prominent Ba and Sr anomalies of the earlier units.

Samples of carbonatite are not plotted on the figure, but as might be expected they are very high in Sr (up to 2 wt%) and they also have high contents of Ba, Ce and Nd (all > 1000 ppm). Two samples of carbonatite contain ~ 400 ppm Nb.

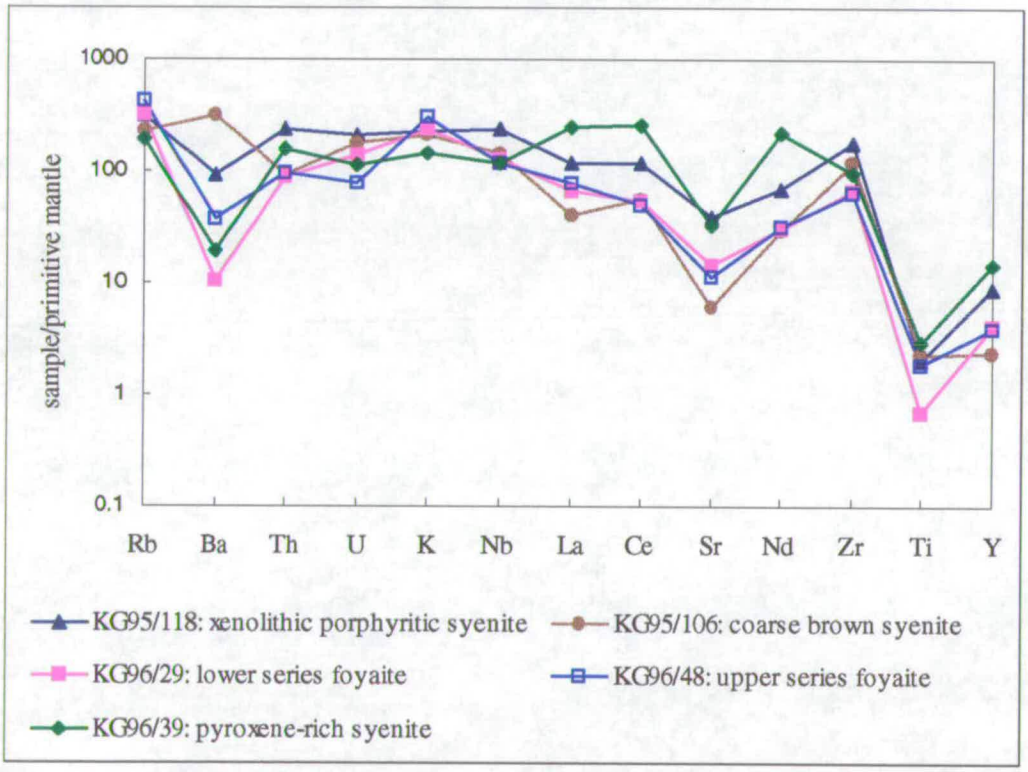

Fig. 6.4: Incompatible element normalised patterns for Grønnedal-Íka

6.4.2 Dykes

Selected inter-element variation diagrams are plotted on Fig. 6.5. On a plot of Zr vs. Nb (Fig. 6.5a) it can be seen that the lamprophyres and basic dykes fall into groups of varying Zr/Nb ratios. The lamprophyres have Zr/Nb about 4, and some other samples also fall into this group, notably those from the feldspar-phyric dykes within the Bunkebreccia. This Zr/Nb ratio accords with published values for lamprophyres in the eastern part of the Gardar Province (Upton & Emeleus 1987) and for basalts from the East African Rift (Zr/Nb ~ 3.5) (Wilson 1989) and also falls within the typical range for Ocean Island Basalts (OIB) of <10 (Wilson 1989). The remaining basaltic dykes (including the Brown Dykes) can be separated into two groups, one with Zr/Nb about 9, and one with Zr/Nb of 16-19. In general, those dykes with lower Zr/Nb are also *ne*-normative, whilst those with higher Zr/Nb are *hy*-normative, and it appears that dykes of the BD0 and BD1 swarms, B.F.D.s, and some miscellaneous dykes, have Zr/Nb >10, whilst BD2 dykes, micro-porphyritic basaltic dykes and some other dykes have Zr/Nb <10. There are some exceptions: for instance a sample of micro-porphyritic basalt cutting the Grønnedal-Íka complex has Zr/Nb of 18, but in general, the *hy*-normative dykes seem to be older than the *ne*-normative group. Plots of Zr/Nb vs. Y/Nb (6.5b) and Zr/Nb vs. Ce/Y (6.5c) (after Wilson 1989, and Fitton *et al.* 1988) show that lamprophyres and some samples of feldspar-phyric dykes plot in the field of OIB, whilst the other basaltic dykes, including the Brown Dykes, plot at the edge of, or outside, that area.

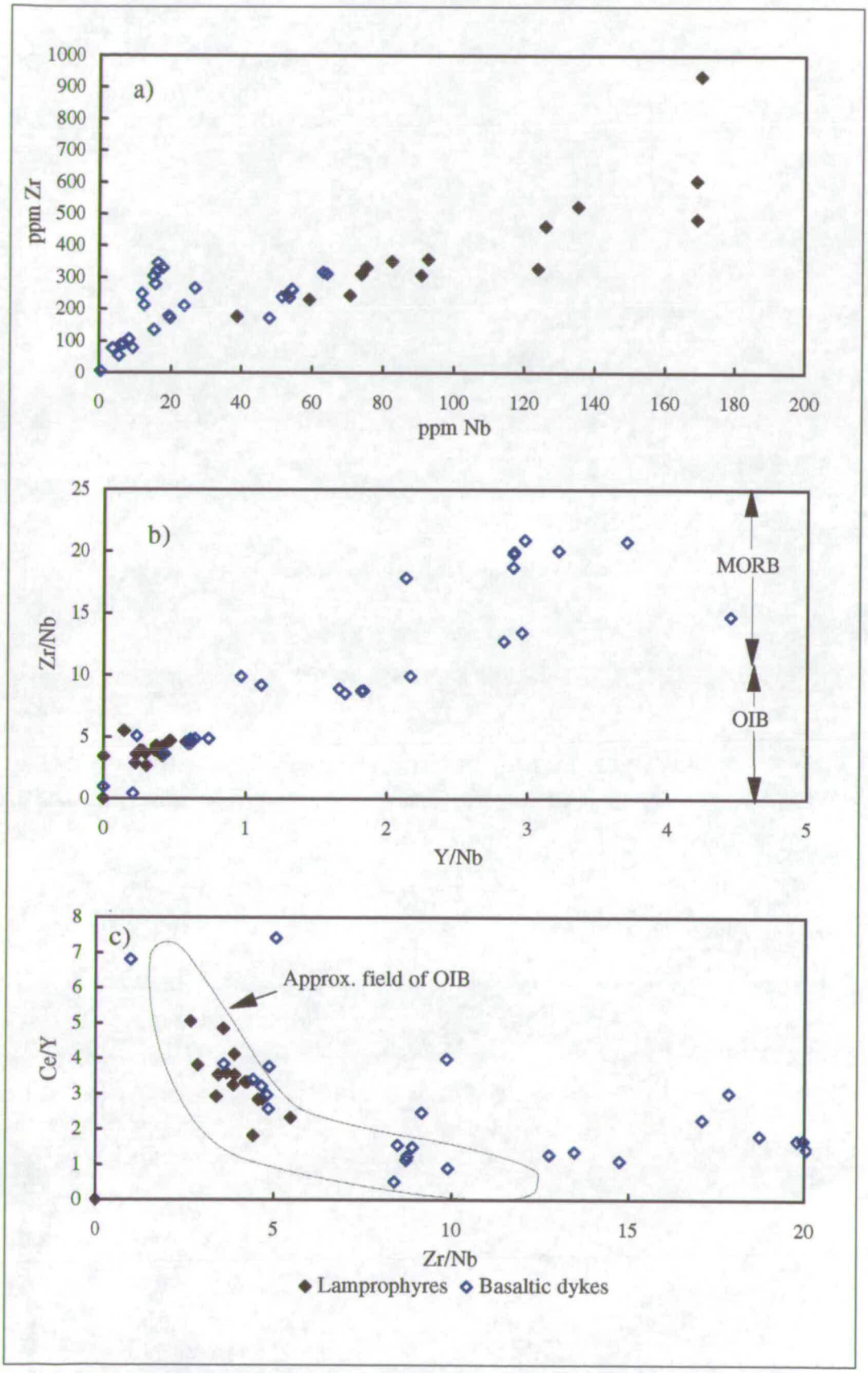

Fig. 6.5: Variation diagrams for lamprophyres and other basic dykes. OIB field on 6.5 c) from Fitton *et al.* (1988)

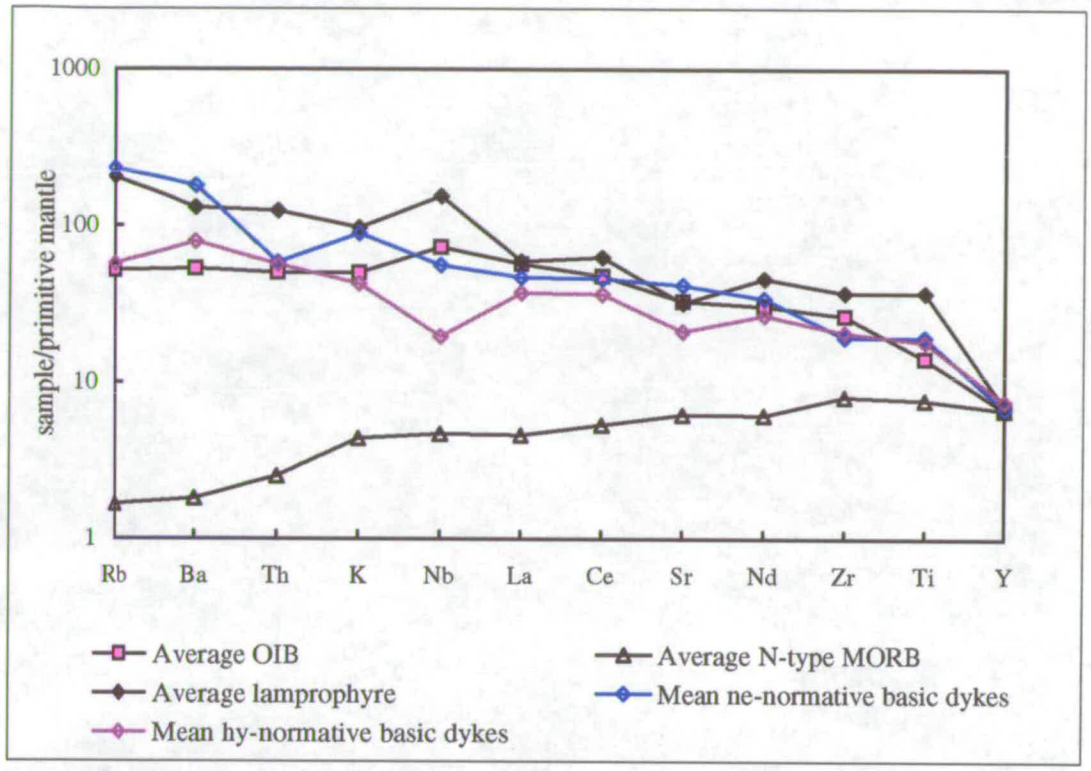

Fig. 6.6a: Comparison of basic dyke groups with average OIB and MORB

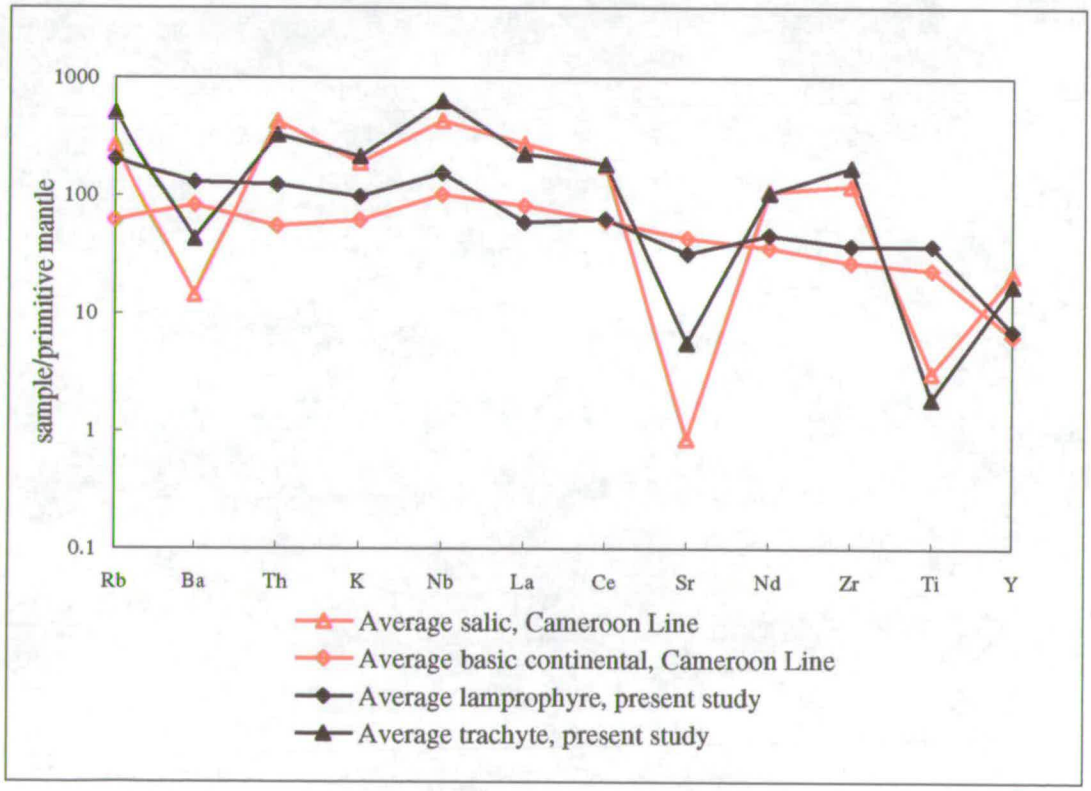

Fig. 6.6b: Comparison of dyke groups with Cameroon Line

The lamprophyres generally have higher incompatible element contents than the basaltic dykes, with higher Ni (>200 ppm) and Cr (>500 ppm) contents confirming their primitive nature.

Fig. 6.6a shows average normalised trace element compositions for the major basic dyke groups, as compared with standard OIB and Mid-Ocean Ridge Basalts (MORB) (data from Sun & McDonough, 1989). The lamprophyre pattern on the spidergram is similar to that of OIB, with strong enrichment in all the incompatible elements, and a peak at Nb, giving a very low La/Nb ratio (0.1-0.7). There are some minor differences from OIB: a small, negative Sr anomaly and a peak at Ti are present in the lamprophyre profile. This pattern is similar to that given by Rock (1987) for alkaline lamprophyres, although the Sr anomaly is unusual. The two sub-groups of lamprophyres (alkaline and ultramafic lamprophyres) are not separated on Fig. 6.6a, since their trace element patterns are very similar in shape, with the ultramafic group being slightly more enriched in all incompatible elements.

For the basaltic dykes, average profiles are shown on Fig. 6.6a for each of the two groups discussed above: *ne*-normative dykes, with low Zr/Nb, and *hy*-normative dykes, with high Zr/Nb. The pattern for the *ne*-normative dykes has a trough at Th but no Nb anomaly. That for the *hy*- normative dykes, however, has a negative Nb anomaly and a small positive Ba anomaly: otherwise the pattern for these dykes is relatively similar to that of the lamprophyres, but with lower concentrations of all incompatible elements. The *ne*-normative dykes are richer in all the incompatible elements than the *hy*-normative dykes.

Fig. 6.6b shows spidergrams for average lamprophyre and trachyte dykes from this study compared with data for average basic and more evolved rocks from the Cameroon Line (Fitton & Dunlop, 1985, and Fitton,

unpublished data). The Cameroon Line magmas are considered to have an asthenospheric mantle source (Fitton & Dunlop, 1985). It can be clearly seen from the figure that the two data-sets are similar, with the patterns for the more evolved rocks showing negative anomalies at Ba, Sr and Ti, indicating that these magmas formed by fractionation of a more basic parent. The patterns for the trachytic dykes from the Gardar also show a positive Nb anomaly.

6.4.3 The Ivigtut stock

All samples from the Ivigtut granite show the characteristics of A-type granites as described by Whalen *et al.* (1987), such as high contents of the High Field Strength Elements (HFSE) and high Ga/Al ratio ($1\text{-}5\times10^{-4}$), but metasomatism has had a pronounced effect on the trace element concentrations. The unmetasomatised top granite can be considered to represent compositions closest to those of the original granite, and differences between top granite and metasomatised variants can be clearly seen on a multi-element diagram (Fig. 6.7). Notably, all the samples show sharp troughs at Ba, Sr and Ti, indicating that fractionation of feldspars and one or more Ti-bearing minerals has played a part in the evolution of the granitic magma. Otherwise, the pattern for the top granite has a relatively smooth slope, with a slight peak at Ta. Albitised granites show clear enrichment in Th and U; Ta and Nb; Hf and Zr, and some enrichment in Rb. Ba, however, is more greatly depleted in the albitised granites, and Nd and La are also slightly depleted; the Ba, Sr and La depletions are probably due to the breakdown of alkali feldspar. Although not shown on the plot, Sn and Pb are also enriched in the altered granites, but Mo is not. The albitised granites around the main cryolite deposit and those at depths of about 800m, where disseminated cryolite is present, show similar patterns, although trace element concentrations vary.

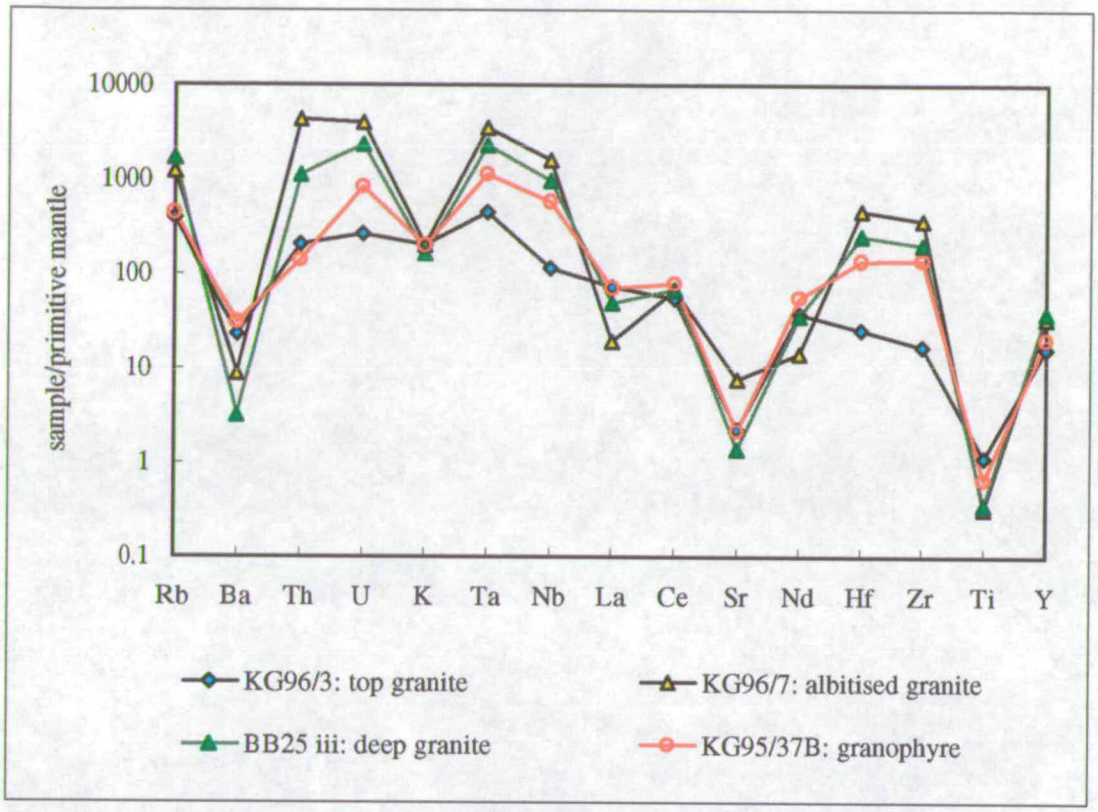

Fig. 6.7: Incompatible element normalised patterns for Ivigtut

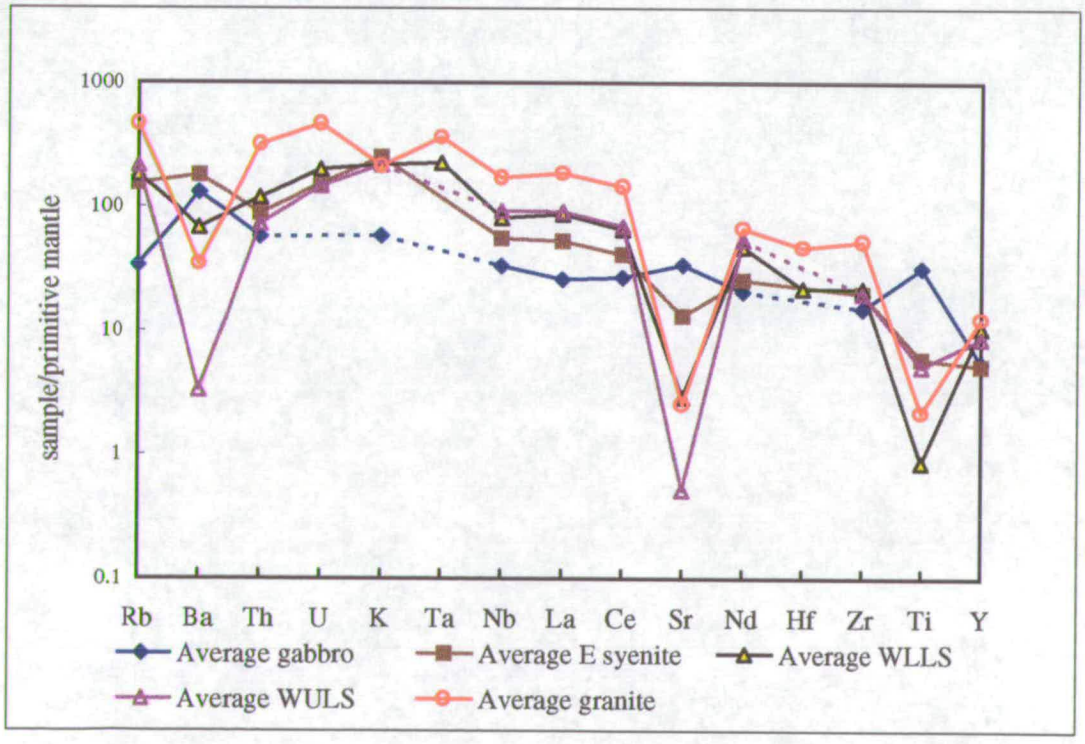

Fig. 6.8: Incompatible element normalised patterns for the Kûngnât complex

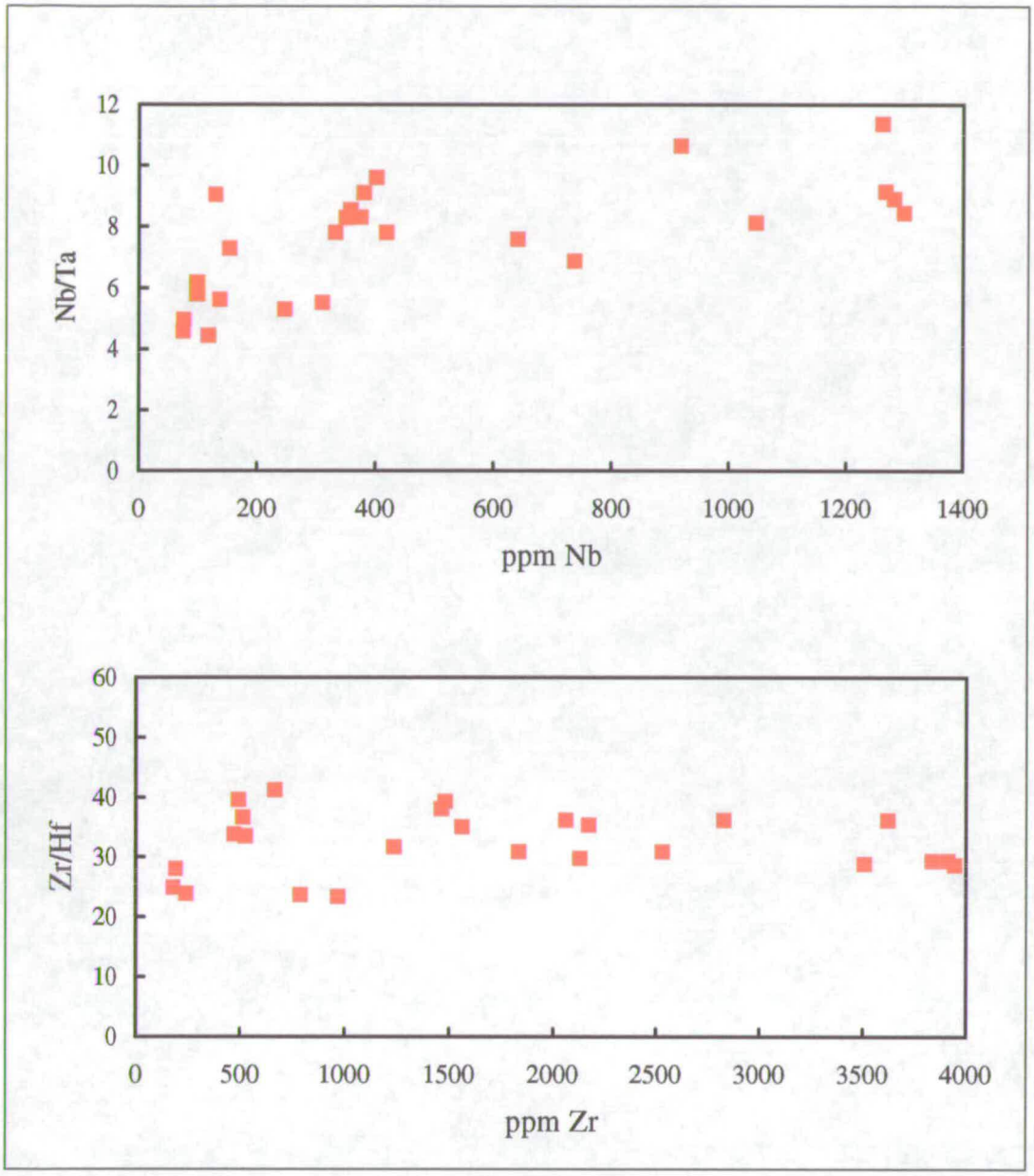

Fig. 6.9: Incompatible element variation diagrams for Ivigtut

The granophyre dykes associated with the Ivigtut granite show similar patterns on a spidergram to those of the albitised granites, although the peaks tend to be less prominent.

Fig. 6.9 shows variation diagrams for selected incompatible elements in the Ivigtut granite. It can be seen that most granite samples have Zr/Hf ratios of 30-40. This is close to the values of 31-35 given for primordial mantle by Weaver *et al.* (1987) and McDonough & Sun (1995). The same authors give values for Zr/Hf ratios in OIB ranging from 36 to 45.

Nb/Ta ratios in the Ivigtut granite range from 4-12 and increase slightly with increasing Nb content. The above authors give Nb/Ta values for OIB of 13-17. Chondritic values for Nb/Ta are ~ 17.5 (Green, 1995) and continental crust typically has lower values (~ 6 for Archaean crust in Greenland; Wedepohl *et al.* 1991) although some Archaean granites may have higher values.

6.4.4 The Kûngnât Complex

Average compositions of the different Kûngnât rock-types are plotted on a spidergram in Fig. 6.8. The ring-dyke gabbro shows a fairly flat pattern, with small peaks at Ba, Sr and Ti. The metasomatised gabbros, however, are slightly depleted in Ba, Sr and Ti but have very high K and Rb contents, as described by Macdonald *et al.* (1973). Only one of the metasomatised gabbro samples is notably enriched in Nb-Ta, Th-U and Zr-Hf, resembling the enrichment patterns in the altered granites at Ivigtut. All the metasomatised gabbros are fairly high in Ni and Cr, but in this respect they resemble a single sample of fresh ring-dyke gabbro which is also more Ni-, Cr- and Mg-rich than most gabbro samples. The gabbro ring-dyke has previously been noted to show some internal geochemical variation (Upton, 1960). The more basic

eastern syenites have a similar pattern to the average gabbros, with notable peaks at K and Ba, and small troughs at Sr and Ti. The plot for the WLLS has troughs at Ba, Sr and Ti but the WLLS are otherwise slightly more enriched than the eastern syenites. The pattern continues in the WULS, with large negative Ba, Sr and Ti anomalies. The late-stage granites also show deep troughs at Ba, Sr and Ti, but are enriched in all other incompatible elements, except K, relative to the syenites.

6.4.5. Trace element discrimination diagrams for granitic rocks.

On the tectonic discrimination diagrams of Pearce (1984) (Y vs. Nb and Y+Nb vs. Rb) (Fig. 6.10a) and Whalen (1987) (Zr vs. $(Ga*10^4)/Al$) (Fig. 6.10b) samples from the Ivigtut and Kûngnât granites clearly fall within the Within-Plate or A-type granite fields. It can be seen, on Fig. 6.10b, that $(10^4 * Ga)/Al$ increases with increasing ppm Zr. This is due to the fact that both Zr and Ga form complexes with fluorine (Whalen, 1987) and therefore the metasomatised granites, and the granophyres, are enriched in these elements. On the Ce/Nb vs. Y/Nb diagram of Eby (1992) (Fig. 6.11) all fresh samples from Ivigtut fall within the "OIB" field, indicating that the granites are representative of those formed in a rift-related environment. The metasomatised samples, being richer in Nb, fall below this field. Samples from Kûngnât plot within and slightly above this field, trending towards the field of continental crust.

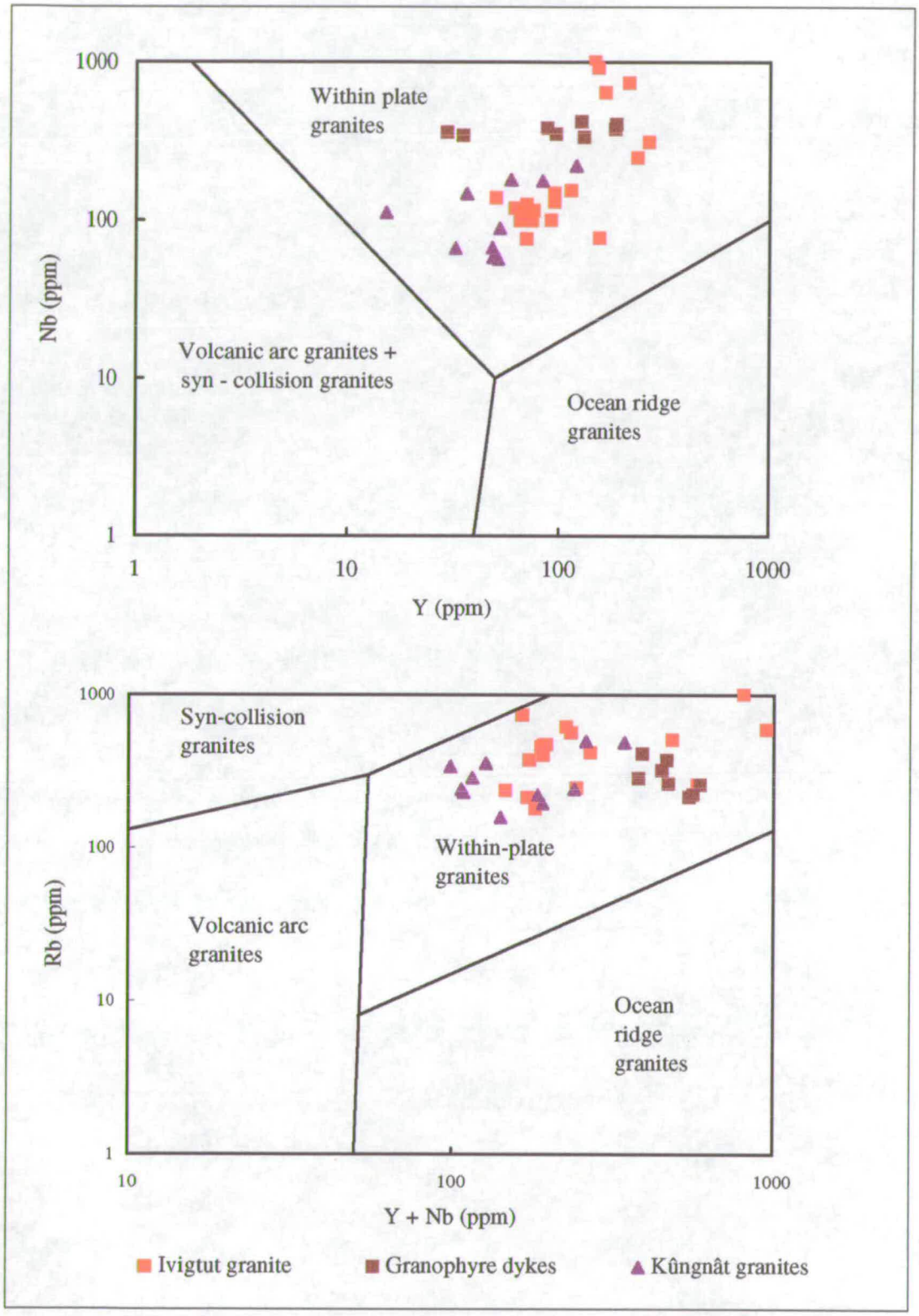

Fig. 6.10 a): Tectonic discrimination diagrams for granites after Pearce *et al.* (1984)

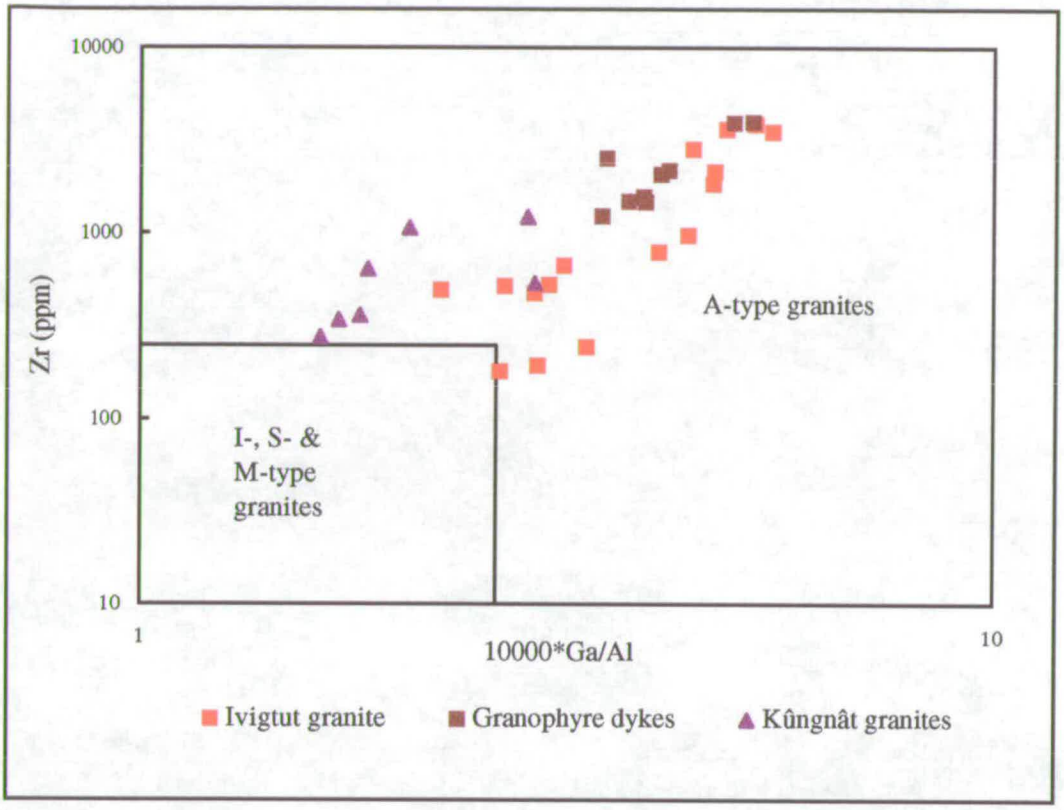

Fig. 6.10b: Tectonic discrimination diagram for granites (after Whalen *et al*., 1987a)

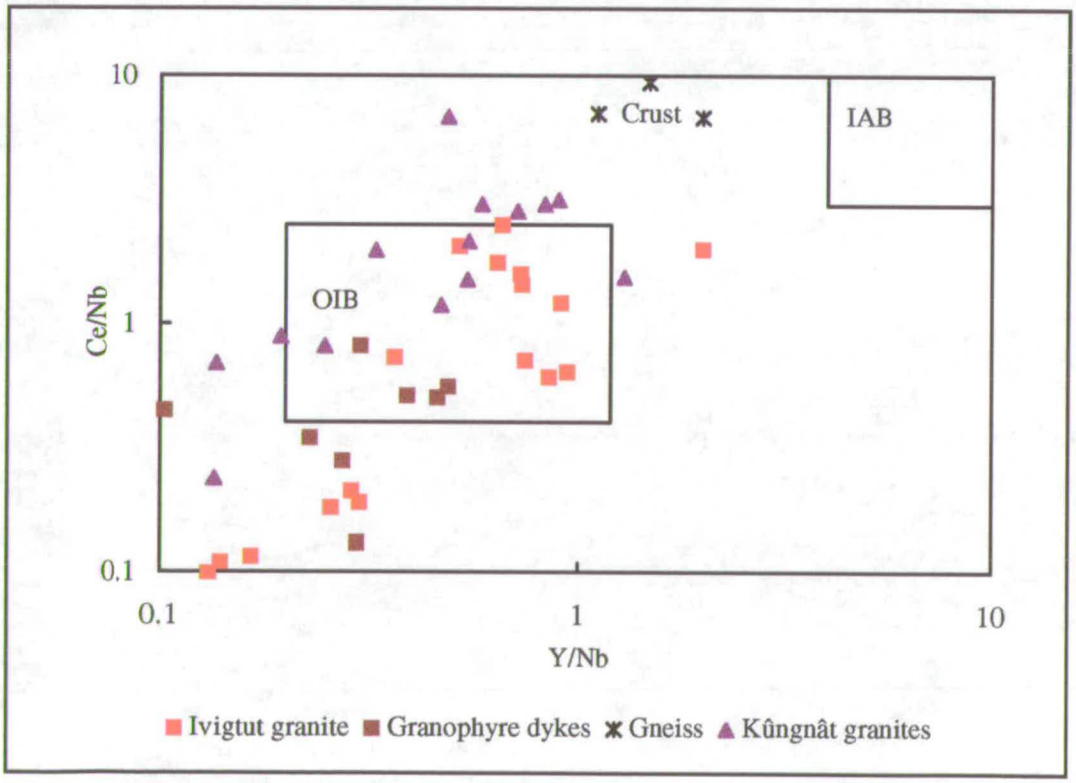

Fig. 6.11: Trace element discrimination diagram for granites after Eby (1992).
OIB = field of Ocean Island Basalts. IAB = field of Island Arc Basalts.
Gneiss analyses indicate position of continental crust on the diagram.

6.5 Interpretation of major and trace element geochemistry

6.5.1 The Grønnedal-Íka Complex

Incompatible element plots (Fig. 6.4) for fresh syenites from Grønnedal-Íka show clear evidence of fractionation of feldspars and Ti-bearing minerals from a more basic magma, but no obvious evidence of crustal contamination. The unusual patterns in the coarse brown syenite are likely to be due to alteration, whilst the lack of Ba and Sr anomalies in the xenolithic porphyritic syenite may be due to the presence of feldspar xenocrysts.

Bedford (1989) suggested that the syenitic magmas formed by fractionation of an alkali basaltic parent. Pearce *et al.* (1997) suggested on the basis of stable isotope work that the carbonatite at Grønnedal-Íka did not form through liquid immiscibility processes from the syenites, and may be associated with the lamprophyre suite. The data so far presented here do not provide any further geochemical evidence towards this hypothesis. There is also no clear geochemical indication of the nature of the parental magma from which the syenites formed, but on the basis of the trace element data the possibility of a genetic link between the syenites and the lamprophyres could not be ruled out. However, the very small volumes of lamprophyres seen in the area suggest that they are unlikely to represent parental material for the syenites.

6.5.2 Dykes

The lamprophyres represent the most primitive magmas in the region, having low silica (35-42 wt%) and high MgO, Ni and Cr contents, which suggest that they have been unaffected by crustal contamination. Although they are variably altered, the trace element profile on a spidergram remains

consistent in shape between differing samples. Nevertheless, the abundances of the alkali elements may have been affected by this alteration and therefore data for these elements are not discussed further.

There are essentially two possible sources for incompatible element enriched, primitive magmas such as these lamprophyres: small-degree partial melting of an asthenospheric source (i.e. similar to the source for OIB) or more extensive melting of metasomatised facies within the sub-continental mantle lithosphere (SCML). The SCML is considered to have been enriched through time by metasomatic fluids rich in LILE and volatiles rising from deeper parts of the mantle and becoming trapped (Brooks *et al.* 1976). The viscosity of the lithospheric mantle is high enough for it to retain this enriched signature over long periods of time, whereas similarly metasomatised domains in the asthenosphere become homogenized by convection over a few tens of millions of years.

The similarities of the incompatible element ratios and spidergram patterns of the lamprophyres to those of OIB (Figs. 6.5, 6.6a) suggest a similar mantle source. Low Zr/Nb (~4) is characteristic of OIB. Furthermore, since Ce and Nb are respectively more incompatible than Y and Zr in normal mantle phases, small degree partial melts from the mantle should show high Ce/Y and low Zr/Nb ratios (Fitton *et al.* 1988) and should fall into the OIB field in Fig. 6.5. Fitton et al (1988) also noted that OIB are characterised by low La/Nb ratios (<1.5) whilst magmas produced from lithospheric mantle sources tend to have higher La/Nb.

The evidence presented above (Section 6.4.2) thus suggests that the lamprophyre magmas originated as small-degree, partial melts in the asthenosphere. Very small-degree partial melt fractions (< 1%) would be required to produce the analysed levels of enrichment of the incompatible

elements. However, it has been shown (McKenzie, 1985) that removal of such small melt fractions is possible, particularly in the case of magmas with low viscosity. The presence of carbonate in the ultramafic lamprophyres indicates that removal of these melts could have been facilitated by the presence of CO_2 in the source. The alkaline lamprophyres may represent slightly larger-degree melts, although the possibility remains that these magmas could have undergone some interaction with the lithosphere during ascent.

James (1995) noted that high levels of Zr, Ti and Th in continental nephelinites could not be easily explained by partial melting models. It was suggested that small-degree partial melts from the asthenosphere did not penetrate the lithosphere but instead ponded near its' base. These were then remobilised shortly afterwards by further ascending melt fractions which thus became strongly enriched in the most highly incompatible elements. A similar process could be suggested to explain the high contents of e.g. Ti in the Gardar lamprophyres. The other notable difference between the lamprophyres and OIB is the negative Sr anomaly in the lamprophyres. Sr is highly partitioned into carbonate rather than silicate melts. The lamprophyres are frequently associated with carbonate veins and Pearce *et al.* (1997) have suggested the possibility of carbonatites being derived from lamprophyres through liquid immiscibility. Such a process would tend to deplete Sr in the residual melts.

The Brown Dykes and other basaltic dykes have higher SiO_2 contents (42-50 wt%) and lower Mg-numbers than the lamprophyres, indicating that they do not represent primitive magmas. As discussed above, the basaltic dykes can be divided, on the basis of their geochemistry, into two groups: a *ne*-normative group with Zr/Nb ~ 9, and a *hy*-normative group with Zr/Nb ~18. Due to the impersistence of many of the smaller dykes, it is difficult to be sure of their relative ages, but in general the *hy*-normative dykes appear to

be older than the *ne*-normative dykes. The basaltic rocks have higher SiO_2 contents but lower incompatible element contents than the lamprophyres, indicating that they could not have formed through fractional crystallisation of the same primitive magma. A Nb trough such as that seen in the *hy*-normative dykes is a typical feature of magmas which have interacted with crust or sub-crustal lithosphere (Thompson *et al.* 1983). Simple mixing models indicate that the observed Nb values in the basaltic dykes could not be produced by mixing of small amounts of crust with the lamprophyric magma, since the amount of crustal component required would produce a mixture with approximately 60% SiO_2. This suggests that the sources of the lamprophyres and the basaltic dykes were different. Upton & Emeleus (1987) suggested that the basic magmas were derived by partial melting of the SCML, initiated by infiltration of fluids from the deep mantle. The patterns for the *hy*-normative basaltic dykes show a negative Nb anomaly and a positive Ba anomaly: these features are often observed in subduction-related settings. Chadwick *et al.* (1996) have built up a model for the evolution of the ~ 1800 Ma Proterozoic mobile belt to the south of the study area, in which subduction occurred northwards, under the craton. It is possible, therefore, that fluids derived from the subducting slab ascended into the lithospheric mantle beneath the Proterozoic crust, where they became trapped, bringing about selective enrichment of the mantle in incompatible elements. Saunders & Tarney (1984) have noted that the Large Ion Lithophile elements (LILE) would be carried from the descending slab within supercritical fluid phases, leaving the HFS elements (particularly Nb) bonded within residual crystal lattices, and thus the lithospheric mantle above the slab would become enriched in the LILE. When Gardar rifting occurred, lithospheric mantle which had been enriched in this way was melted and mixed with varying amounts of an asthenospheric melt component to produce the observed spectrum of compositions of the basaltic dykes.

The pattern for the mean of all salic alkaline dyke samples analysed (Fig. 6.6b) compares reasonably with that for salic rocks from the Cameroon Line. The Cameroon Line magmas are believed to have been sourced in the asthenosphere (Fitton & Dunlop 1985) and to have been unaffected by crustal contamination. Thus the salic magmas are assumed to have formed by fractionation from a basic source, represented by the most primitive of the erupted magmas. The similarity between the patterns for the Cameroon Line and Gardar rocks leads to the inference that magmatic evolution of the two sets of rocks followed a similar path, and that the salic dykes from the Gardar may have formed by fractionation of a primitive source. The geochemical characteristics of the salic dykes suggest that they may possibly have evolved from a parental magma similar to that represented by the lamprophyre dykes - i.e. one with a large amount of asthenosphere-derived component.

6.5.3 The Ivigtut stock

The Ivigtut top granite shows trace element patterns and ratios which are typical of A-type granites (Whalen *et al.* 1987) and falls clearly within the rift-related A-type field on all the trace element discrimination diagrams shown in Figs. 6.10 and 6.11. Previous workers have considered that the Ivigtut granite magma formed by fractionation of a basic parent with some degree of crustal contamination (Blaxland, 1976, Bailey, 1980) and the incompatible element patterns presented here (Fig. 6.7) fit with this theory. The consistent, near primordial Zr/Hf ratio in altered and unaltered granites (Fig. 6.9) provides an argument against large degrees of crustal contamination, and in particular indicates that the hydrothermal fluids were unlikely to have leached incompatible elements from the surrounding crust. The Nb/Ta ratio of 6-8 is similar to that documented for other A-type granite suites (Green, 1995). Similar low ratios have been attributed to fluid/melt partitioning, with

preference for Ta in the fluid. This explanation fits with the observed increase of Nb/Ta ratio with increasing Nb, suggesting a Nb-Ta fractionation in the hydrothermal fluids.

Trace element enrichments similar to those of the altered Ivigtut granite have been documented for many peralkaline intrusions, such as the Bonifatto granites of Corsica (Egeberg *et al.*, 1993), peralkaline granites in Saudi Arabia (Harris, 1981), the Topsails suite of Newfoundland (Taylor *et al.*, 1981, Whalen *et al.*, 1987), and the Madeira granite of Brazil (Horbe *et al.*, 1991). These enrichments are chiefly attributed to volatile transfer through the medium of a highly peralkaline, F-rich residual fluid which has been greatly increased in its contents of certain incompatible elements during differentiation of the granite. At Ivigtut, the presence of the cryolite body provides evidence for such a fluid. Certain lines of evidence, including normative compositions, also indicate that the magma from which the granite formed was itself rich in fluorine. Previous workers (Pauly & Bailey, in press.) have suggested that the cryolite body formed after "waves" of hydrothermal fluids, including F- and CO_2-rich fluids, became trapped at the top of the granite stock and re-melted the granite, producing a liquid with the bulk composition of the whole ore deposit. This then became segregated to form the cryolite, quartz and fluorite bodies. However, the presence of cryolite at depth in the stock, and the similar trace element patterns of the altered granites at depth to those above, provide an argument contradicting this theory.

Fluorine in granites is often associated with Sn-Mo mineralisation (Bailey, 1977) but although Sn is enriched to some extent in the altered Ivigtut granites, this is scarcely so for Mo. However, Bailey (1977) noted that, where F-metasomatism is dominant over Cl-metasomatism, deposition of Sn and Li

is more effective than that of Mo. There is therefore little evidence for Cl as an important constituent of the hydrothermal fluids at Ivigtut.

The granophyre dykes show trace element patterns similar to those of the altered granites. If the dykes are considered as "offshoots" of the granite, then it is likely that they have undergone metasomatism, acting as channels for the escape of the hydrothermal fluids. However, the country rocks around the dykes do not appear to be metasomatised. This can be explained in two ways: either the fluids were trapped by the chilled margins of the dykes, or the granophyre dykes may represent late-stage liquids that were ejected out into the country rocks. More detailed study would be required in order to distinguish between these two hypotheses.

6.5.4 The Kûngnât Complex

Incompatible element plots for the Kûngnât complex (Fig. 6.8) support the theory that the syenite types within the complex formed by progressive fractionation of a trachytic parent magma (Upton, 1960). It appears that formation of a basic syenitic magma was controlled by fractionation of plagioclase, along with olivine and clinopyroxene, from basaltic parents. Alkali feldspar fractionation became important later in the evolution process. However, certain lines of evidence, such as the trend of the Kûngnât late sheets towards the field of continental crust on the Ce/Nb vs Y/Nb plot (Fig. 6.11), and the change in the syenites from mildly *ne*-normative to *qz*-normative moving towards the margins of the complex, suggest that crustal contamination of the magmas has played an important role in the petrogenesis of this complex.

Most of the Kûngnât granites have compositions which concur with the theory of their having formed as late-stage differentiates from the syenitic

magma. However, the peraluminous granites from the eastern stock have rather different compositions, and may represent crustal melts.

6.6 Rare earth element data.

Thirty samples representing a wide range of different rock-types from the study area have been analysed for REE using the ICP-AES method. The results are plotted as chondrite-normalised patterns (normalising values from Nakamura, 1974) in Figure 6.12.

6.6.1. The Grønnedal-Íka Complex

All the samples from Grønnedal-Íka show relatively smooth LREE-enriched patterns, with $(La/Lu)_N$ in the syenites ranging from 8-20. A sample of Lower Series foyaite shows a small negative Eu anomaly and a slight inflection at Er. The pyroxene-rich syenite has somewhat higher REE contents than the other syenites, due to the abundance of pyroxene and apatite, in which many of the REE are contained. The shape of the plot is similar to that of the foyaite, with small Eu anomalies and an Er inflection.

The coarse-grained brown syenite shows no Eu anomaly, but has a smooth pattern, whilst the sample of the xenolithic porphyritic syenite shows a small positive Eu anomaly. Bedford (1989) presented similar REE patterns and attributed this positive anomaly to the possible presence of xenocrysts from deeper levels of the complex into which Eu-rich cumulus phases had settled. The carbonatite sample has considerably higher REE contents than any of the syenites, and shows a strongly LREE-enriched pattern, with $(La/Lu)_N$ =72.

Bedford (1989) noticed slight upturns of the HREE "tail" in some of the patterns in his work. It was noted that $D^{Gt}_{Yb} > D^{Gt}_{Lu}$ and therefore very small

degree partial melting of a garnet rich source rock, in which garnet had not completed melting, would give rise to a liquid depleted in the HREE (Cullers & Graf, 1984) but relatively enriched in Lu. However, Bedford did not present data for Er, and in the present study the effect observed by Bedford can be seen as an inflection at Er, with a small relative increase in Yb and Lu contents. The above explanation does not explain this pattern so easily, since $D^{Gt}_{Yb} \approx D^{Gt}_{Er}$ (Henderson, 1984). However, high contents of Yb and Lu could be attributed to the presence of large zircon concentrations in the sample.

6.6.2 Dykes

Samples of the dykes on Fig. 6.12b show relatively smooth, LREE enriched patterns. The basaltic dykes have a small positive Eu anomaly, which is not present in the lamprophyres. The lamprophyres show the patterns typical for most rocks of this type (Cullers & Graf, 1984), being greatly enriched in the LREE and in the MREE compared to the basaltic dykes, but less enriched in the HREE: $(La/Lu)_N \sim 28$. The Brown Dyke sample (KG95/12C) has a much flatter profile ($(La/Lu)_N = 2.85$), with the result that it has higher Yb and Lu than the lamprophyres. The feldspar-phyric basaltic dyke from within the Bunkebreccia has an overall pattern similar to that of the BD, with a positive Eu anomaly, but has levels of enrichment similar to those of the lamprophyres.

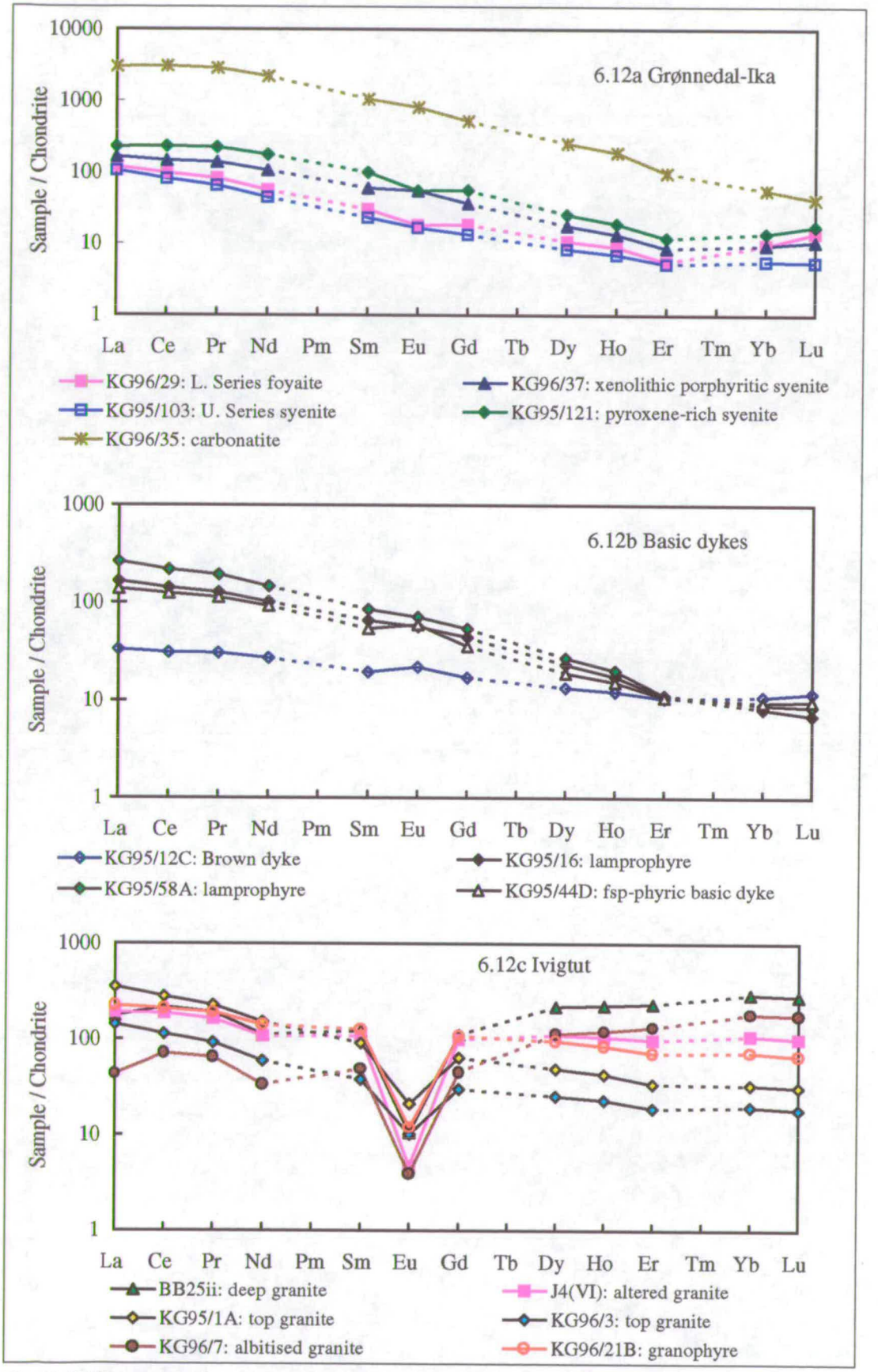

Fig. 6.12: Rare earth element plots, chondrite normalised

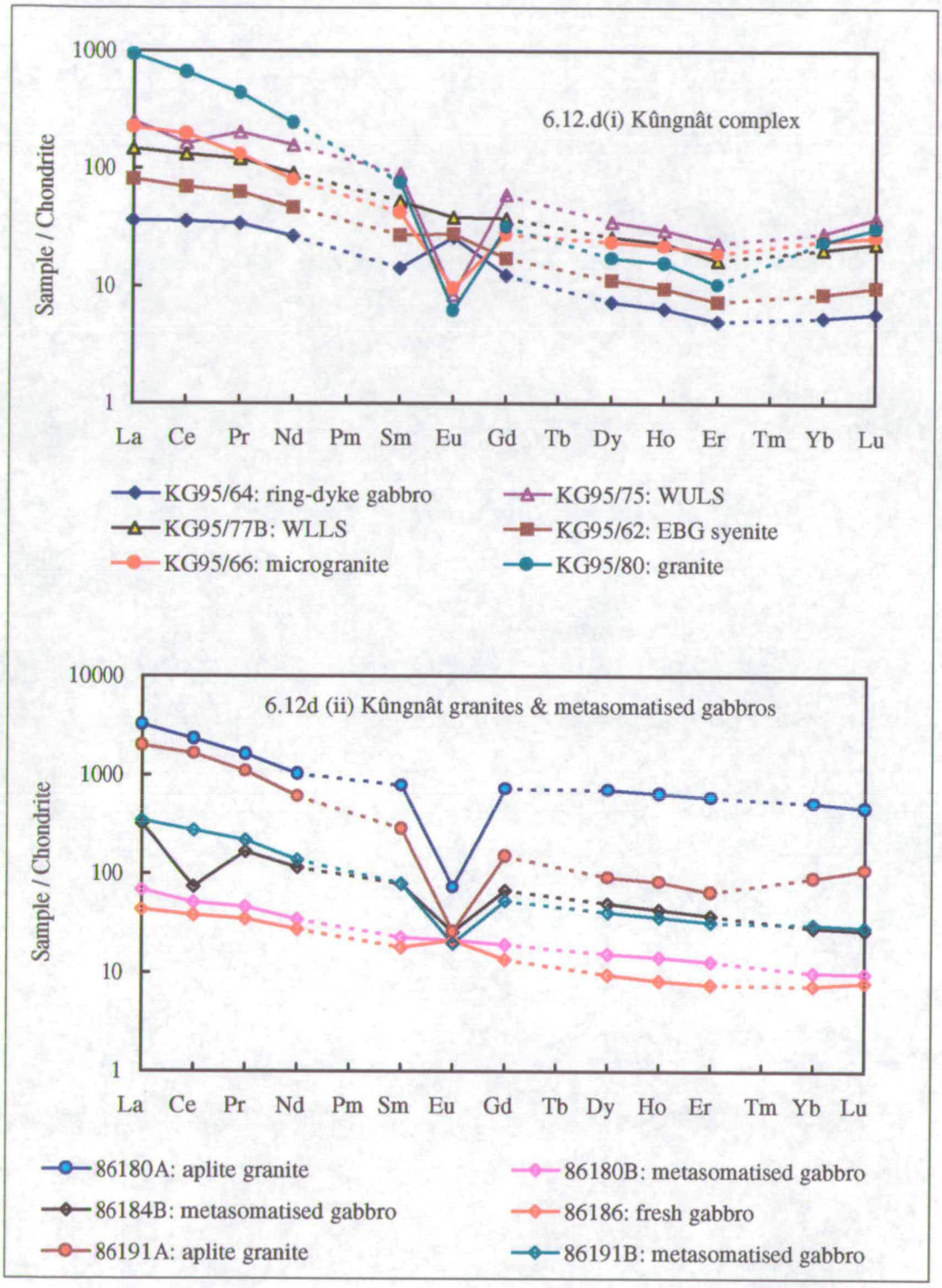
6.12.d(i) Kûngnât complex
Sample / Chondrite
1000
100
10
1
La Ce Pr Nd Pm Sm Eu Gd Tb Dy Ho Er Tm Yb Lu
KG95/64: ring-dyke gabbro
KG95/75: WULS
KG95/77B: WLLS
KG95/62: EBG syenite
KG95/66: microgranite
KG95/80: granite
6.12d (ii) Kûngnât granites & metasomatised gabbros
Sample / Chondrite
10000
1000
100
10
1
La Ce Pr Nd Pm Sm Eu Gd Tb Dy Ho Er Tm Yb Lu
86180A: aplite granite
86180B: metasomatised gabbro
86184B: metasomatised gabbro
86186: fresh gabbro
86191A: aplite granite
86191B: metasomatised gabbro

Fig. 6.12 cont.

6.6.3 The Ivigtut stock

Five granite (two top granite, two albitised granite, and one deep granite) and two granophyre samples from Ivigtut were analysed for REE. The top granite samples show LREE-enriched patterns ($(La/Lu)_N$ ~10), slightly convex towards the LREE (Fig. 6.12c), with a negative Eu anomaly ((Eu/Eu*)=0.27). This type of pattern is typical of the A-type granites (Collins *et al.*, 1982, Taylor *et al.*, 1981). However, all the metasomatised rocks show a very different pattern, with greater enrichment in the HREE and variable depletion in the LREE ($(La/Lu)_N$ =0.6-2), as compared with the top granite. In the albitised granites, dips in the pattern occur at La and Nd, whilst the other LREE appear less depleted, but the Eu anomaly has increased in size: (Eu/Eu*)=0.08. The HREE, however, are extremely enriched relative to the top granite samples, with the greatest enrichment (>> 100 x chondrite) in the sample from 793m depth in the drill core. Samples from the granophyre dykes also show enrichment in the HREE, although on a lesser scale than the altered granites. Electron probe analysis has shown (Section 5.3) that the HREE in the altered granites are resident chiefly within inclusions in zircons.

6.6.4 The Kûngnât Complex

A total of fourteen samples from Kûngnât were analysed. These included samples of fresh gabbro and the metasomatised gabbro described by Macdonald *et al.* (1972); the major syenite groups, and the differing late granite sheets, including the peralkaline granites from the study mentioned above. Representative samples are plotted in Fig. 6.12d (i & ii)

Samples of the fresh gabbro show a flat or slightly LREE enriched profile ($(La/Lu)_N$=6-8) with a small positive Eu anomaly. The metasomatised gabbros, by contrast, are typically uniformly enriched in the REE except Eu

(and in one case, Ce), thus giving a negative Eu anomaly ((Eu/Eu*)=0.35). A sample of the eastern syenites (KG95/62) shows a very similar pattern to the fresh gabbros, being slightly LREE enriched with a very small, positive Eu anomaly, whilst that from the WLLS has a flat, slightly LREE enriched pattern with no conspicuous anomalies. However, the more evolved sample from the top of the WULS shows pronounced differences, with a deep negative Eu anomaly ((Eu/Eu*)=0.11) and a smaller trough in the pattern at Ce, and a distinctly concave HREE profile. The late-stage granites show patterns similar to that of the Ivigtut top granite, enriched in the LREE over the HREE and having a negative Eu anomaly ((Eu/Eu*)=0.1). Profiles are typically convex for the LREE and concave for the HREE (Fig. 6.12d). The most enriched sample (86180A), a peralkaline granite from the western stock, has LREE contents up to 3000 x chondrite and shows a fairly flat pattern, except for the Eu anomaly.

6.7. Interpretation of REE geochemistry.

6.7.1 The Grønnedal-Íka Complex

Small negative Eu anomalies in the syenites (Fig. 6.12a) are associated with Ba and Sr negative anomalies in the trace element diagrams (Fig. 6.4) and indicate the fractionation of plagioclase and alkali feldspars from the primary magma: Eu is preferentially partitioned into plagioclase compared with the other REEs, due to its divalent state in conditions of low oxygen fugacity (fO^2). As mentioned above, Bedford (1989) believed that the observed pattern could be produced by very small-degree partial melting of a garnet-rich source rock, followed by feldspar fractionation. The carbonatite shows much greater LREE enrichment than the syenites and this could be the result of the carbonatite having evolved by liquid immiscibility from a different source, as suggested by Pearce *et al.* (1997).

6.7.2 Dykes

The lamprophyres are highly LREE enriched: these enrichments could have been produced by very small degree partial melting of a mantle source, containing garnet or an LREE-enriched component, for example fluorapatite (Cullers & Graf, 1984). The REE patterns for the lamprophyres are closer in shape and slope to those for the Grønnedal-Íka carbonatite than those for other rock-types in the study area; but this is not enough evidence to indicate a definite relationship. The Brown Dykes have a much flatter, less enriched pattern than the lamprophyres, which could be generated by larger degrees of partial melting. The lack of an Eu anomaly suggests that crustal contamination has had little effect on any of these rocks, and that removal or concentration of plagioclase has had little significance in their evolution.

6.7.3 The Ivigtut granite

Many authors have described patterns of REE mobilization in altered granites (Alderton *et al.*, 1980, Baker 1985, Ward *et al.*, 1992, Poitrasson *et al.*, 1995), but introduction of HREE during alteration, such as that at Ivigtut, is rare and typically only reported in albitised peralkaline granites (Bowden & Whitley, 1974, Taylor *et al.*, 1981, Horbe *et al.*, 1991). This effect is attributed to complexing of the REE with F^- or CO_3^{2-} ions in hydrothermal fluids. It has been shown (e.g. Wood 1990) that, due to the variation in stability constants for REE complexes, whilst the HREE are concentrated in F^-- or CO_3^{2-}- bearing fluids, the LREE are typically concentrated in Cl^--bearing fluids. The nature of the fluid which brought about the formation of the Ivigtut cryolite deposit (rich in fluorine and carbonate, but apparently poor in chlorine) would therefore explain the preferential enrichment in HREE. An increase in the size of the Eu negative anomaly has been explained in terms of break-down of feldspars, releasing Eu^{2+}, which at relatively high temperatures is not taken

up into secondary minerals (e.g. Alderton *et al.*, 1980). Removal of La can also be attributed to breakdown of feldspars.

The fluids which brought about metasomatism of the Ivigtut granite are inferred to have passed through virtually the entire granite (since the same effects are seen at a range of depths), but were trapped below the chilled top granite. Taylor *et al.* (1981) suggested that the hydrothermal fluids which produced similar effects on REE patterns in the Topsails suite were directly mantle-derived, and emphasised the importance of mantle degassing. It is possible that some of the carbonate-rich fluids at Ivigtut were also derived directly from the mantle.

6.7.4 The Kûngnât Complex

The fluids released from the Kûngnât granites, which brought about a striking metasomatism of the surrounding gabbros, were considered by Macdonald *et al.* (1973) to be rich in K and F. Although the REE contents of the metasomatised gabbros have increased substantially, the shapes of the profiles remain essentially the same, with the exception of the negative Eu anomaly, as those of the fresh gabbros. Thus in this instance it appears that complexing of the HREE with F^- ions has been of little importance. The Ce anomaly in one sample may be due to late weathering effects.

The variation in REE patterns within the Kûngnât complex can essentially be explained by crystal fractionation. $(La/Lu)_N$ ratios remain constant at about 6-8 within the gabbros and syenites, but increase in some of the granites.

6.8 Geochemical conclusions

Although some conclusions can be drawn from the geochemistry, the isotopic data presented in the next chapter will have a bearing on most ideas given here. Nevertheless, certain points have been established:

i) The lamprophyres are the most primitive Gardar rocks in this area and appear to have originated by small degree partial melting of an asthenospheric source, which may subsequently have undergone minor interaction with the lithosphere. The variation from ultramafic to alkaline lamprophyres may be simply related to degree of melting.

ii) The other basaltic dykes fall into two groups, both of which have geochemical signatures compatible with formation by partial melting of lithospheric mantle which had been enriched in the past by slab-derived fluids, but with variable amounts of asthenospheric contribution. Crustal contamination of the magma is a possibility, but there is no direct evidence for this.

iii) The trachytic dykes of the area, on the other hand, show incompatible element patterns which could have been produced by direct fractionation of a parental magma with geochemical similarities to the lamprophyres.

iv) All three of the central complexes show evidence of having formed by fractionation of a basic parental magma, agreeing with previous hypotheses (Emeleus & Upton, 1987). It is likely that a measure of crustal contamination was also involved, particularly in the case of Kûngnât.

v) Metasomatism in the Ivigtut granite was caused by a peralkaline, F-rich fluid, which introduced high contents of the HREE and LILE. This fluid has

generally been considered to represent residua from the formation of the granite, but some evidence suggests the possibility of the effect of a primitive, mantle-derived fluid. It can be shown that the magma from which the granite itself formed was rich in fluorine.

Chapter 7: Radiogenic Isotope Analysis

7.1 Introduction

Previous isotope work on Gardar rocks of the Ivigtut area has principally been concerned with attempting to date the intrusives (See Section 2.2). In the 1970s an extensive study was carried out, in which Rb-Sr whole-rock isochrons were presented for all the major Gardar central complexes (Blaxland, 1976, Blaxland, *et al.* 1978). The dates obtained have already been mentioned in Section 2.2. Blaxland *et al.* (1978) gave a low initial $^{87}Sr/^{86}Sr$ ratio (0.7032 ± 0.0004) for the Grønnedal-Íka complex which was identical for the syenites and the carbonatite. This was interpreted as showing a mantle source, with minimal crustal contamination, for all the rocks of the complex. An initial $^{87}Sr/^{86}Sr$ ratio of 0.7041 ± 0.0008 was obtained for an isochron based on five samples of Kûngnât syenite and the initial ratio calculated for two ring-dyke gabbro samples was identical within error. It was suggested on the basis of this ratio that crustal contamination of the Kûngnât magma took place before differentiation of the gabbro and syenite fractions.

The initial $^{87}Sr/^{86}Sr$ ratio obtained for the Ivigtut granite in the same study was 0.7125 ± 0.0048 (Blaxland, 1976), which was considered to be extremely high compared with the primitive Gardar, "mantle-type" ratio of about 0.703. The ore material from the Ivigtut granite was shown to have slightly lower initial ratios than the granite; however, interstitial cryolite from a granite sample had a much higher initial $^{87}Sr/^{86}Sr$ ratio than the granite whole-rock samples or the ore-body. It was therefore suggested that the high ratios were due to the introduction of hydrothermal fluids which had preferentially leached radiogenic ^{87}Sr from older crust. Recently, doubt has been thrown on the reliability of these results because rock populations which were initially isotopically variable were combined in the research (J. Bailey, pers. comm.).

More recent isotope work on this part of the Gardar is scarce. Taylor & Upton (1993) presented Pb isotope data for the Kûngnât complex, and the Tugtutôq Younger Giant Dyke in the eastern Gardar, and concluded that in both complexes crustal contamination had been important. Isotopic differences between the two complexes were attributed to the variation in the country rock contaminants. Pearce *et al.* (1997), as part of a study of the Grønnedal-Íka complex which included stable isotope data, gave initial $^{87}Sr/^{86}Sr$ ratios (recalculated to 1300 Ma) of 0.7030 ± 0.0001 for the carbonatites, and 0.7032 ± 0.0008 for the syenites. Initial $^{87}Sr/^{86}Sr$ ratios for the lamprophyre suite ranged from 0.7026-0.7029.

During the present study a set of forty-two whole-rock samples, representing all the rock types in the study area, was analysed by isotope dilution for the Rb-Sr and Sm-Nd isotopic systems. Nineteen of these samples were further analysed for Pb isotopes. Analyses were carried out at SURRC, East Kilbride. Analytical techniques are described in Appendix B and results tabulated in Appendix F. Isochron calculations were made using the Isoplot program, version 2.9 (Ludwig, 1991): details and explanations of terms are given in Appendix C.2.

7.2 Rb-Sr data

7.2.1 The Grønnedal-Íka Complex

Five samples of syenite and one of carbonatite were analysed for Rb and Sr isotopes. The carbonatite sample gives an initial $^{87}Sr/^{86}Sr$ ratio (corrected to 1300 Ma) of 0.70305 ± 0.00004, which agrees exactly with the initial ratios presented by Blaxland *et al.* (1978) and Pearce *et al.* (1997). The syenites give slightly lower initial ratios, from 0.6999-0.7019, averaging 0.7011 ± 0.0012; one altered sample gives an extremely low calculated initial ratio of 0.6444, which is lower than the chondritic meteorite value (BABI), considered to represent the initial $^{87}Sr/^{86}Sr$ ratio at the formation of the Earth. The ratio for this sample therefore cannot be considered reasonable and may be attributable to loss of radiogenic Sr during alteration or late-stage increase in the Rb/Sr ratio of the rock. An errorchron (Fig. 7.1) based on the five fresher samples gives an initial ratio of 0.7028 at an age of 1222 ± 130 Ma (Mean Square Weighted Deviation (MSWD) = 577). An errorchron is a regression line for which the observed scatter cannot be accounted for by the analytical errors: see Appendix C.2 for details. This date is much younger than that given by any other form of dating, but the errors are so large that it cannot be taken as a reliable age. In general, however, the Rb-Sr data given above agree with previous suggestions that the rocks of the Grønnedal-Íka complex formed from a mantle source with relatively little crustal contamination.

7.2.2 Dykes

Three samples of Brown Dykes, three of lamprophyres, one of a feldspar-phyric basic dyke, and two of salic alkaline dykes, were analysed for Rb-Sr. Samples of the Ivigtut granophyre dykes will be discussed later (7.2.4). All have been corrected to 1240 Ma, this being an average age for the dykes

based on the dates given by Patchett (1977). Of the lamprophyre samples, one is highly altered and field evidence (section 3.7) indicates the passage of mineralising fluids, which have mobilised the Rb-Sr system. The fresher lamprophyre samples have average initial $^{87}Sr/^{86}Sr$ of 0.7037 ± 0.0001. The Brown Dykes, which include one sample which is very altered but has similar isotopic ratios to the fresh samples, have an average initial $^{87}Sr/^{86}Sr$ ratio of 0.7033 ± 0.0001, and the feldspar-phyric basic dyke has an initial ratio of 0.7057. These results suggest a mantle source for all the basic dykes and lamprophyres, with minimal crustal contamination. The two samples of salic alkaline dykes have impossibly low (< BABI) calculated $^{87}Sr/^{86}Sr$ at 1240 Ma (0.6970 and 0.6945): this is only a very rough estimate of their age, but nevertheless this indicates that the Rb-Sr systematics in the alkaline dykes have been disturbed after emplacement.

7.2.3 The Ivigtut stock

It is evident from the trace element patterns (Fig. 6.7) that Rb and Sr have been exceptionally mobile under the effects of the hydrothermal fluid activity at Ivigtut, and it is therefore unlikely that an isochron could be obtained using samples of altered granite. Fourteen samples from Ivigtut have been analysed for Rb-Sr; four of granophyre dykes, five of top granite, and five of variably altered granites. $^{87}Sr/^{86}Sr$, calculated for 1200 Ma, ranges between 0.6628 and 0.8077, and it appears that the Rb-Sr system in all the samples has been strongly affected, suggesting that hydrothermal alteration affected the top granite as well as the granites which have been mineralogically altered. An errorchron based on the top granite samples (Fig. 7.1) gives an age of 1154 ± 350 Ma, and an initial ratio of 0.7062 ± 0.104, with an extremely large MSWD of 16600; the granophyre samples give an age of 1143 ± 230 Ma and an initial ratio of 0.7102 ± 0.084, with an MSWD of 7360.

Combining top granite and granophyre samples gives an age of 1147 ± 110 Ma, with an initial ratio of 0.7083 and MSWD = 9240. Clearly the errors are so large as to render these values practically meaningless. However, it should be noted that the "ages" fall close to the date obtained by J. Bailey (pers. comm.) of 1170 Ma.

The effects of the metasomatism seem to have been to variably increase contents of both Rb and Sr in the granite, so that the Rb/Sr ratio does not correlate strongly with the amount of alteration. Variable degrees of alteration would introduce an initial isotopic inhomogeneity, so that the samples could not lie on an isochron. However, if the metasomatic event had occurred over a fairly short period of time soon after the formation of the granite, it would be expected that the calculated initial ratios would give geologically reasonable numbers. The very low calculated initial values can be explained in two ways: either alteration occurred at a much later date than intrusion of the granite; or the Rb-Sr system remained open for some considerable period of time. (≥ length of the Gardar period). Removal of radiogenic strontium during metasomatism could not alone explain the observed values. It is possible that after the initial hydrothermal event the granite was so heavily altered, with the feldspars being extremely porous, that the Rb-Sr system was susceptible to a later, low-temperature alteration event; although oxygen isotope work indicates no evidence that such alteration has occurred elsewhere in the Gardar (Sheppard, 1986; Finch & Walker,1991, Finch *et al.* 1995).

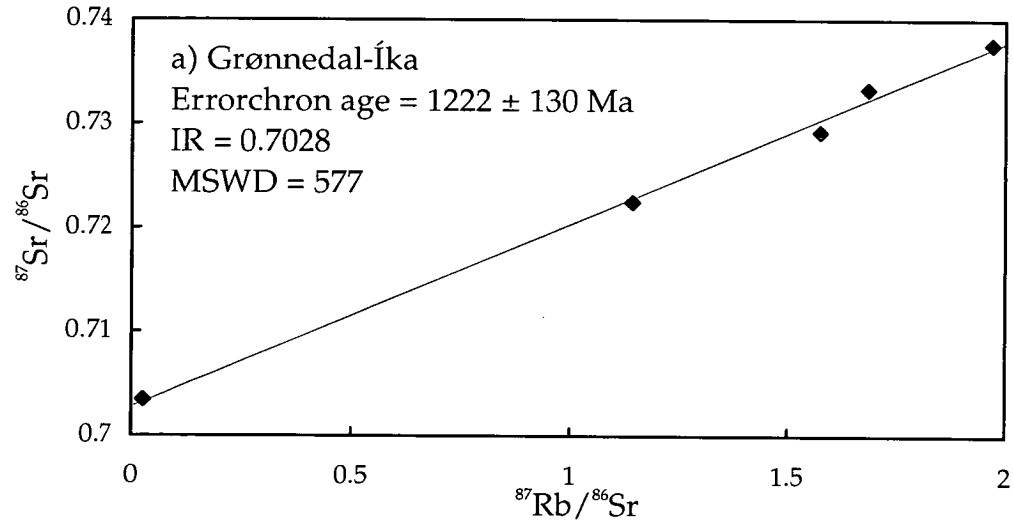

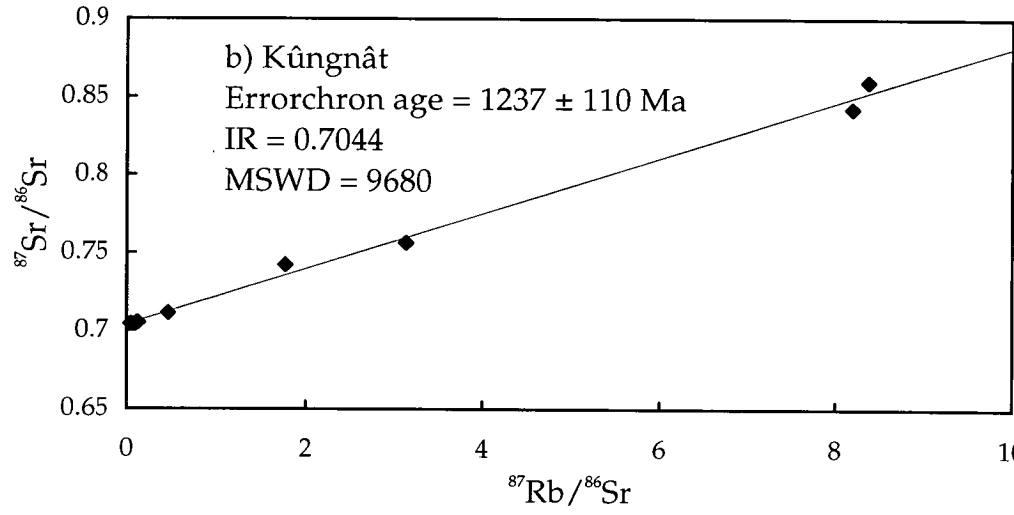

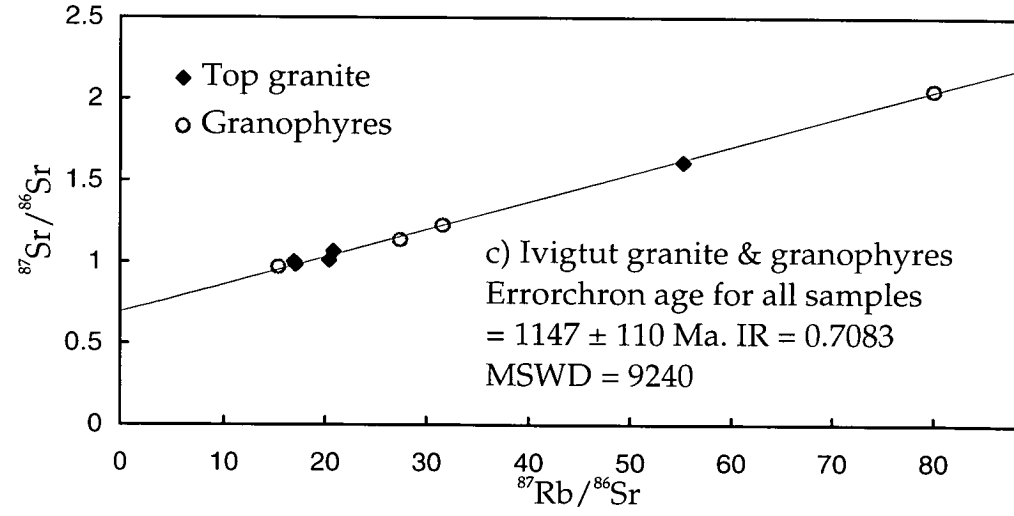

Fig. 7.1 Rb-Sr errorchron plots

7.2.4 The Kûngnât Complex

Two samples of ring-dyke gabbro, five of syenite, and three of late sheets were analysed. The initial ratios have been calculated for 1270 Ma after the dating of Heaman (pers. comm.). The gabbros have an initial $^{87}Sr/^{86}Sr$ ratio of 0.7033 ± 0.0001 - i.e. virtually identical to that of the Brown Dykes. The syenites show a wide variation in calculated initial $^{87}Sr/^{86}Sr$ ratio, from 0.7102 to 0.5291. The only sample which shows an initial ratio similar to that of the gabbros is a fresh, unaltered sample from the Eastern Layered syenites ($^{87}Sr/^{86}Sr_{(i)}$ = 0.7032), whilst a sample from the Eastern Border Group shows a higher initial ratio. This suggests that the syenites at the margin of the eastern stock were contaminated by assimilated crust, thus raising the initial $^{87}Sr/^{86}Sr$ ratios, whilst the syenites in the centre of the stock were relatively uncontaminated. The more evolved syenites of the western stock have much higher Rb/Sr ratios and give calculated initial $^{87}Sr/^{86}Sr$ ratios of <0.7. The effect of the high Rb/Sr ratios is to make these calculations very age-sensitive, so that use of Blaxland's date of 1220 Ma gives initial ratios for the WLLS samples of 0.7005 ± 0.0013. However, this value is still lower than expected, as is the initial ratio for the WULS sample of 0.5778. This latter ratio is clearly unrealistic and again indicates that the Rb-Sr systematics have been disturbed in these rocks. The feldspars in these syenites are turbid and pyroxenes have been largely replaced by amphiboles, indicating that alteration has occurred. Some of the low initial ratios could be explained by the removal of radiogenic Sr (which is in Rb lattice sites in the alkali feldspars and therefore may be more easily removed than stable Sr isotopes) from the rocks during alteration by a hydrothermal fluid circulating within the western stock. Alternatively, addition of Rb during alteration at some time after emplacement would lead to errors in the calculated initial ratios. A reasonable initial ratio is obtained for the most altered sample by setting a

date of approximately 1100 Ma, suggesting the possibility of a late-Gardar alteration event.

Of the three samples of late granitic sheets analysed, one, an aplite from southeast Kûngnât, has an initial $^{87}Sr/^{86}Sr$ ratio at 1270 Ma of 0.7074, which lies within the range of ratios for the eastern syenites. The other two granitic samples have calculated initial ratios <7, with that from the western stock having an exceptionally low ratio which can only be due to extensive alteration.

An errorchron plotted for Kûngnât using data from all the syenite and gabbro samples is controlled by KG95/75, a sample from near the top of the WULS with an extremely high Rb/Sr ratio. This gives a very young age of 1142 ± 120 Ma, with $(^{87}Sr/^{86}Sr)_{(i)}$ = 0.7057 ± 0.005 and MSWD = 461, using Model 1 of the Yorkfit program (see Appendix C.2). If the errorchron is produced using only data from those samples with $^{87}Rb/^{86}Sr < 10$ (Fig. 7.1), and Model 3 is used in order to try and take into account the effects of crustal contamination, the age given is 1237 ± 110 Ma, with initial $^{87}Sr/^{86}Sr$ of 0.7044 ± 0.005, and MSWD 9680. The errors are far too large for this to be considered as a meaningful date, although it does fall in the area of other available dates for Kûngnât.

7.3 Sm-Nd data

7.3.1 The Grønnedal-Íka Complex

Of the samples mentioned above, three of syenite and one of carbonatite were analysed for Sm and Nd. Sample 95/121 (pyroxene-rich syenite) was analysed, but was later found to have not dissolved completely (see appendix B for details). The three syenite samples have initial $^{143}Nd/^{144}Nd$ at 1300 Ma ranging from 0.51112 to 0.51116 (ε_{Nd} = +3.2 to +3.9, with an average of +3.6). The carbonatite has a much lower initial ε_{Nd} of −18, which is highly unusual, since this is a crustal value. However, the syenite values are compatible with derivation from a mantle source. The calculated initial ε_{Nd} for the carbonatite sample is very low due to the high Sm/Nd ratio in the sample: the present-day ε_{Nd} for the carbonatite is similar to that for the syenites. The high Sm/Nd ratio could be attributable to fractionation of the REEs into certain rare minerals in the carbonatite which may not have been evenly distributed throughout the sample. Since only one carbonatite sample was run, it is also possible that the unusual ε_{Nd} value may be due simply to analytical error. Clearly, further isotopic analysis of the carbonatite would be of interest.

7.3.2 Dykes

The lamprophyres have initial $^{143}Nd/^{144}Nd$ at 1240 Ma ranging from 0.51123 to 0.51139, giving positive values for ε_{Nd} of +3.8 to +6.9, averaging +5.1. The Brown Dykes have slightly lower initial $^{143}Nd/^{144}Nd$ of 0.51111 to 0.51126 (ε_{Nd} = +1.5 to +4.4, with an average of +2.6), whilst the feldspar-phyric basaltic dyke has initial $^{143}Nd/^{144}Nd$ of 0.51109 (ε_{Nd} = +1.0), and one sample of a trachytic dyke has initial $^{143}Nd/^{144}Nd$ = 0.51113 (ε_{Nd} = +1.8). All these values

fall within the range for OIB (Wilson, 1989), but there is clearly a difference between the lamprophyres and the other dykes. Sm-Nd systematics of the dykes do not appear to have been affected by the alteration process.

7.3.3 The Ivigtut stock

From the differences in the REE patterns (given in Fig. 6.12c) between the top and altered granites, it can be seen that Sm and Nd were mobile under the influence of the F- and CO_2-rich hydrothermal fluid in the Ivigtut granite. This mobility is shown in the range of present day ε_{Nd} values (+4.2 to -15.2); initial ratios calculated at 1200 Ma, however, fall within a relatively small range (0.51092 to 0.51112). Samples of relatively unaltered granite, including both top and deep granites, have initial ε_{Nd} ranging from 1.3 to -3.6, with an average of -2.7. The most altered granite samples have initial ε_{Nd} of +0.7 and -0.1, whilst the granophyres have values ranging from +0.3 to -1.37.

Fig. 7.2 shows an isotope evolution diagram for Ivigtut, with ε_{Nd} plotted versus time. The majority of the evolution lines meet at 1330 ± 40 Ma, with ε_{Nd} at this point of approximately -2. The location of this intersection suggests that the Sm-Nd system was reset at this time by a hydrothermal fractionation of the Sm/Nd ratio (Poitrasson *et al.*, 1995). However, this is a considerably older date than any previously obtained on the Ivigtut granite. This can be explained in one of three different ways:

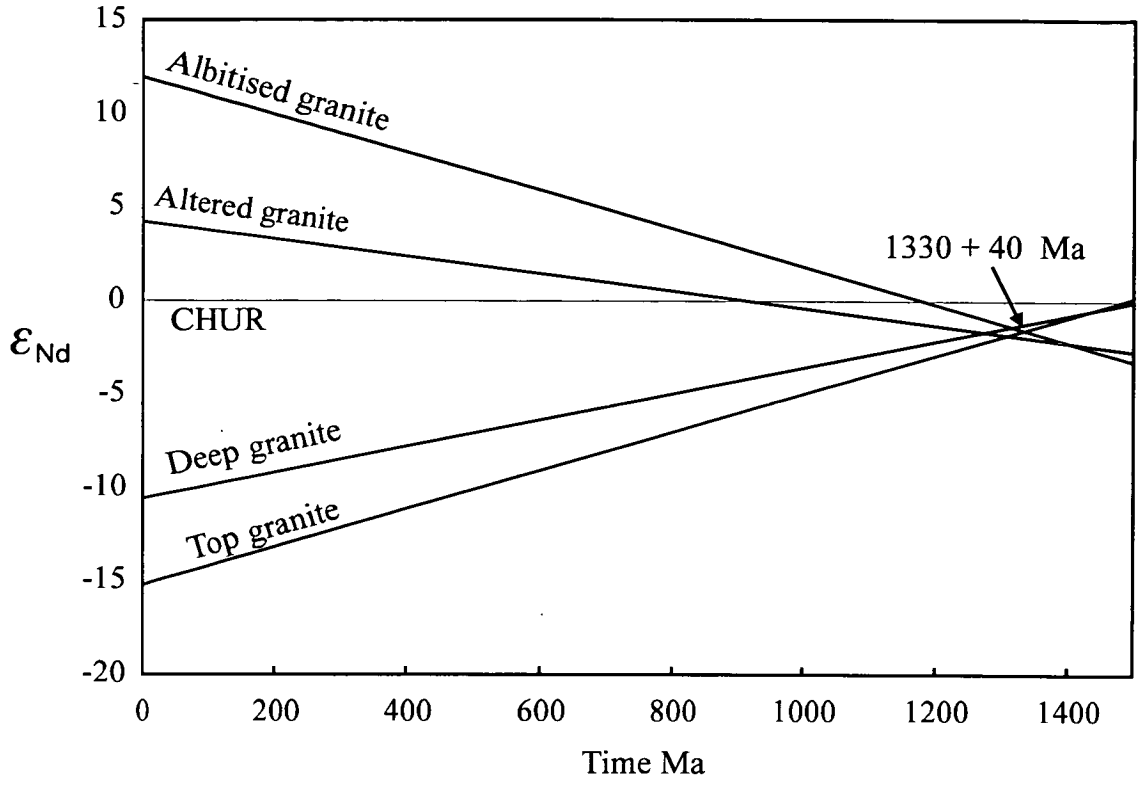

Fig. 7.2: ε_{Nd} evolution diagram for the Ivigtut granite.

i) Introduction of a fluid with a more radiogenic $^{143}Nd/^{144}Nd$ ratio at the time of hydrothermal fractionation. This is similar to the explanation used by Blaxland (1974) to explain the overly high $^{87}Sr/^{86}Sr$ ratio for Ivigtut. However, Blaxland invoked a fluid derived by leaching of radiogenic Sr from the crust, whereas in the present case the only potential fluid with the required $^{143}Nd/^{144}Nd$ ratio would have been primitive and mantle-derived.

ii) Two events of hydrothermal fractionation of Sm/Nd at widely differing times. There is no clear geological evidence for this having occurred at Ivigtut.

iii) This is a true date for the metasomatism of the Ivigtut granite and all previously obtained dates are artificially young, due to the resetting of all the isotope systems. However, age relationships would appear to argue against this hypothesis since the granophyre dykes, which are believed to be related to the granite (Berthelsen 1962), cut the Brown Dykes in the Ivigtut valley.

Sm-Nd errorchrons for the Ivigtut granite and granophyres again show very large errors (Fig. 7.3). The granophyres have the best fit errorchron, with an age of 1093 ± 130 Ma and an initial $^{143}Nd/^{144}Nd$ ratio of 0.5112 ± 0.0001, and an MSWD of 17.3. The six samples of relatively unaltered granite give an errorchron with age 1230 ± 140 Ma, initial $^{143}Nd/^{144}Nd$ 0.5109 ± 0.0001, and MSWD 45.7. Again, the large errors indicate that the calculated age is not significant.

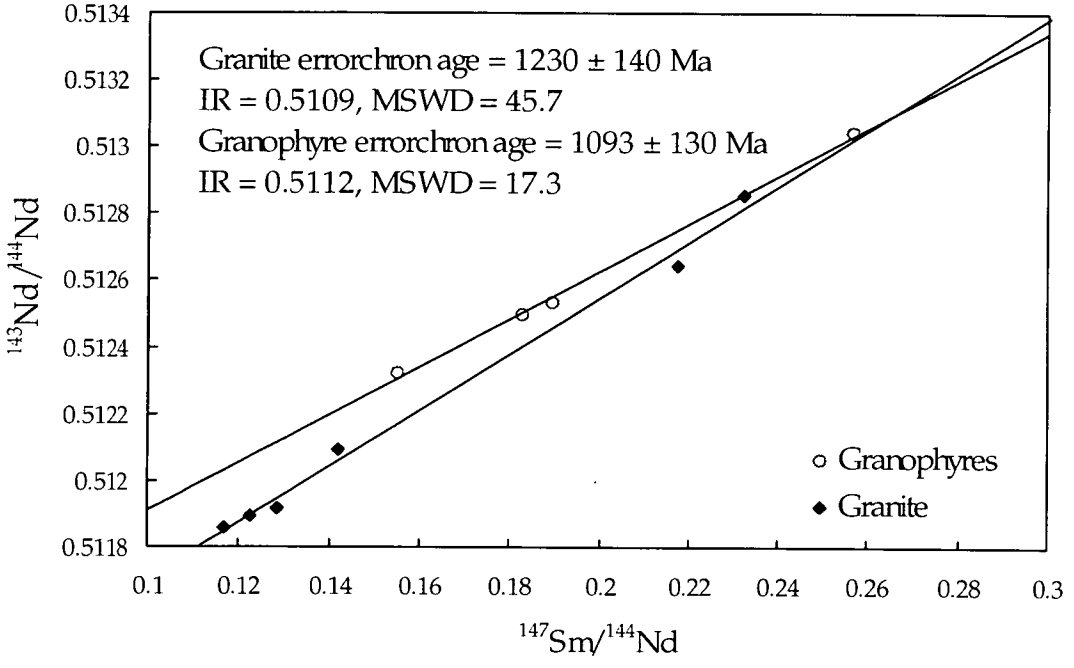

Fig. 7.3: Sm-Nd errorchrons for Ivigtut

Two samples of the ring-dyke gabbro have initial $^{143}Nd/^{144}Nd$ calculated at 1270 Ma of 0.51098 and 0.51095 (ε_{Nd} = -0.3 and -1.0). The eastern syenite samples have initial $^{143}Nd/^{144}Nd$ ratios of 0.51094 and 0.51097 (ε_{Nd} = -1 and -0.6), whilst those of the western syenites range from 0.51093 to 0.51089 (ε_{Nd} = -1.3 to -2.1). Two of the granites have similar initial ratios of 0.51086 and 0.51089 (ε_{Nd} of -2.6 and -2.2). However, the peraluminous late sheet from eastern Kûngnât (KG95/66) shows a much lower initial $^{143}Nd/^{144}Nd$ of 0.51070 (ε_{Nd} = -5.9). This adds weight to the hypothesis (6.5.4) that these peraluminous late sheets are products of crustal melting rather than late-stage differentiates from the evolving syenites. On a plot of ε_{Nd} vs. SiO_2 (Fig. 7.4) for all samples, it can be seen that initial ε_{Nd} decreases with increasing SiO_2. This would not be produced by fractional crystallisation alone, and it thus seems most likely that the magmas of the Kûngnât complex evolved by a process of crustal assimilation and fractional crystallisation (AFC).

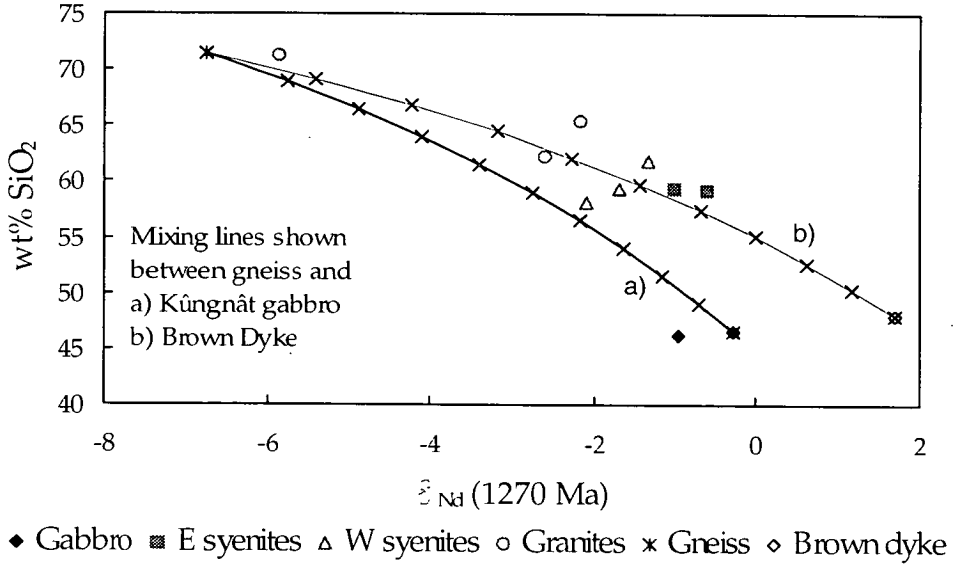

Fig. 7.4: Plot showing mixing between gneiss and basic precursors for Kûngnât. Crosses mark 10% intervals on the curves.

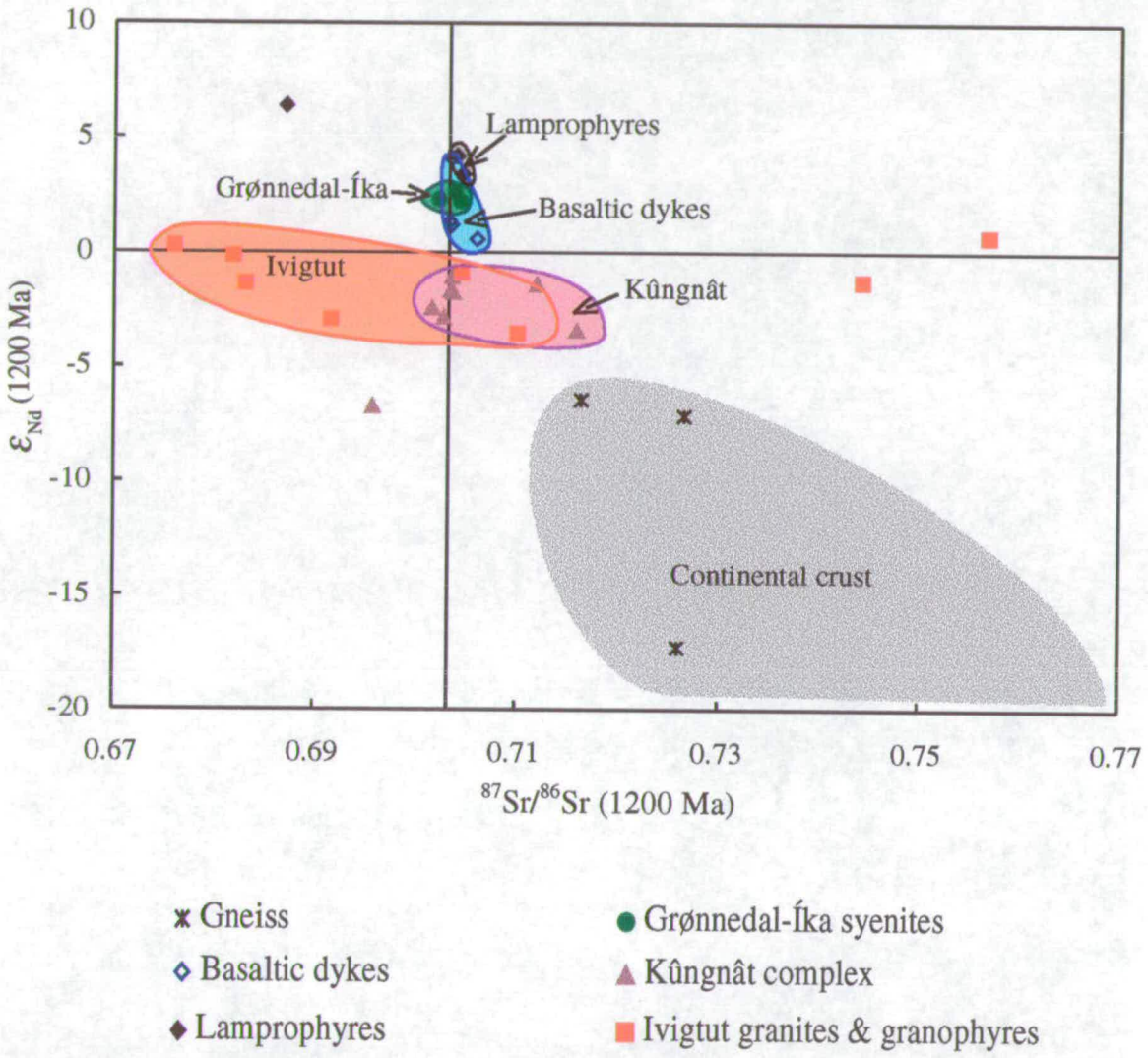

Fig. 7.5: Nd-Sr isotope correlation diagram for 1200 Ma

7.4 Nd-Sr isotope correlation

Fig. 7.5 shows initial $^{87}Sr/^{86}Sr$ plotted against initial ε_{Nd} for samples of all the rock groups. All the data are calculated back to 1200 Ma rather than the respective dates for the different complexes, to allow closer comparison. In practice, calculation of ratios to 1200 Ma or e.g. 1240 Ma makes very little difference to the plot.

Samples from all the dykes, with the exception of one altered lamprophyre, plot around the Bulk Earth line for $^{87}Sr/^{86}Sr$, but have small positive values of ε_{Nd}. On average, the lamprophyres have higher ε_{Nd} than the basaltic dykes. These samples therefore all fall within the OIB field (Wilson 1989), with the lamprophyres appearing to originate from slightly more depleted mantle than the other basic dykes. The Grønnedal-Íka syenites also fall within the OIB field, suggesting minimal crustal contamination of the magmas.

A field representing continental crust is shown on the diagram, based on the analysis of gneiss samples from the area and also on published fields on similar diagrams (e.g. DePaolo & Wasserburg, 1978). Data from rocks formed by mixing of depleted mantle and continental crust would trend from Bulk Earth towards this field, i.e. showing a negative correlation between ε_{Nd} and $^{87}Sr/^{86}Sr$. A similar trend could be formed by mixing of two mantle-derived magmas, one from a depleted mantle source and one from an enriched mantle source such as the EMII reservoir of Zindler & Hart (1986), but there is no evidence for the existence of such an enriched source in the Gardar. Despite the apparent effects of alteration on the $^{87}Sr/^{86}Sr$ ratios, the Kûngnât samples show this type of trend, and this is interpreted as being due to the mixing of continental crust with the evolving trachytic magma. Samples from Ivigtut are scattered about the diagram due to the extensive disturbance of the Rb-Sr system, as described above. Nevertheless, the freshest samples

seem to fall close to the cluster of data for Kûngnât, indicating that the magmas from which the Ivigtut granite formed have also undergone crustal contamination.

There is no apparent trend towards the low $^{87}Sr/^{86}Sr$, low $^{143}Nd/^{144}Nd$ EM1 reservoir of Zindler & Hart (1986) which is believed to represent the lithospheric mantle below some examples of Archaean cratons (Menzies & Halliday, 1988). If the lithospheric mantle was enriched in the LILE by ascending fluids, this must have occurred at a short time (on the geological time-scale) before Gardar activity commenced.

7.5 Nd Model Ages

Nd model ages have been calculated relative to depleted mantle (see Appendix C.3 for details of calculations and assumptions). These represent the time elapsed since the sample was removed from a depleted mantle source. The samples of gneiss give model ages of *ca.* 3000 Ma, which fit with previously measured dates for the gneisses in this area (Taylor & Kalsbeek, 1986). However, virtually all the samples of Gardar rocks give model ages older than the known emplacement ages. Values for the lamprophyres range from 1285 to 1574 Ma; for the basaltic dykes from 1520 to 1896 Ma; and for the Grønnedal-Íka syenites from 1550 to 1640 Ma. Samples from the Kûngnât and Ivigtut complexes show older model ages and have a greater amount of scatter.

The youngest model age for the lamprophyres is close to the emplacement age (1250 Ma; Patchett, 1977). This indicates that the lamprophyres could not have been formed from sub-continental lithospheric mantle that had been undergoing incompatible-element enrichment processes over a long period of time: instead, enrichment by volatile-rich fluids or small-degree partial

melts from deeper in the mantle could only have occurred shortly before separation of the magmas, if at all. The basaltic dykes and the Grønnedal-Íka syenites, which are considered to be relatively uncontaminated by continental crust, have model ages which mostly fall in the range 1740-1500 Ma. 1740 Ma is considered to represent the end of the Ketilidian orogeny (Windley, 1991) and the model ages therefore suggest that any enrichment of the mantle from which these magmas were drawn immediately postdated Ketilidian activity.

The scatter of model ages for Ivigtut can be related to the hydrothermal fractionation of Sm/Nd that occurred when the granite was metasomatised. The older model ages observed for Ivigtut and Kûngnât are probably due to the crustal contamination of the magma: the values obtained represent the average time that the Nd in the sample has formed part of the continental crust (Arndt & Goldstein, 1987).

7.6 Pb isotope data

7.6.1 Models

A total of nineteen whole-rock samples were analysed for Pb isotopes, including two gneiss samples, three from Grønnedal-Íka, one lamprophyre, two basaltic dykes, five samples from Kûngnât, and six from Ivigtut. The present day values are plotted on Fig. 7.6. These data have been calculated back to 1200 Ma, using U, Th and Pb concentration values measured by XRF (see Appendix C.4 for details of calculations) and the results are shown on Figs. 7.7a and b. It should be emphasised that these age-corrections depend on the assumption that the U/Pb and Th/Pb ratios have remained constant since the rocks were emplaced, but since these ratios may have been changed

due to late-stage, low-temperature U loss, the results can only be considered as approximate.

The Pb isotope system is more complicated than either the Rb-Sr or Sm-Nd systems, due to the number of radiogenic isotopes involved, and various models have been produced to explain the evolution of lead isotopes in the Earth over time. The simplest model, the Holmes-Houtermans model (described in detail by Faure, 1986) is a single-stage model in which lead in the Earth evolved from an initial meteoritic composition (Tatsumoto *et al.*, 1973) in reservoirs of varying U/Pb ratios. When a common lead mineral such as galena was formed, the lead was separated from uranium and thorium and thus its isotopic composition remained constant until the present day. However, this model is inappropriate for igneous rocks, which typically contain lead which has had a multi-stage history: i.e. the lead has resided in several systems with different U/Pb and Th/Pb ratios.

Lead data are frequently presented in terms of a two-stage model (e.g. Taylor & Upton, 1993; Andersen, 1997), in which lead evolved from an initial meteoritic composition with time-integrated $^{238}U/^{204}Pb$ (μ_1) until separation from that system at a time t. Lead was then extracted from the source reservoir(s) and evolved in a closed system with constant $^{238}U/^{204}Pb$ (μ_2) until the present. However, it is unlikely that Precambrian rocks will genuinely fit this model. The U/Pb ratio of the mantle reservoir is almost certain to have changed during formation of the continental crust, and contamination of magmas by older crust is also likely to have occurred. This introduces the necessity of three or more stages in the model (Taylor *et al.*, 1980). U/Pb ratios of the rock may have been disturbed at some point during its evolution (Doe, 1970), and decay of U and Th will also change the $^{238}U/^{204}Pb$ ratio over long periods of time (Faure, 1986).

Andersen *et al.* (1994) used a three-stage model to approximate the evolution of a Precambrian granitic intrusion in Norway. The first stage was considered to represent the mantle source; the second the crustal material which was extracted from the mantle at a time t_1, and the third the granite itself, which formed by crustal anatexis and was emplaced at time t_2. Each reservoir can be described in terms of a distinct μ value.

Ulrych (1964), in a study of galenas from Ivigtut, also concluded that a simplified three stage model was appropriate. In this model, ordinary lead was removed from a mantle reservoir with $\mu_1 = 8.99$ at a time t_1. The lead isotope ratios remained unaltered ($\mu_2 = 0$) until a time t_2, when uranium and thorium mineralisation occurred and radiogenic lead was added. Lead evolution then continued until emplacement at time t_3. Ulrych interpreted his model to indicate that "ordinary lead mineralisation" occurred, at latest, at 2980 ± 10 Ma; the radiogenic leads were derived from a source which came into existence between 1880 ± 60 Ma and 1100 ± 40 Ma; and the galenas were emplaced at, or after, 1100 ± 40 Ma.

This model can be used to suggest a generalised history of lead evolution in the Gardar complexes. Continental crust, which had a low U/Pb ratio (Taylor *et al.*, 1984), separated from its mantle source at ~ 3000 Ma. Lead continued to evolve in separate sub-reservoirs in the mantle through the late Archaean and early Proterozoic until a Gardar parental magma was removed from the mantle and concentrated lead from various sub-reservoirs. This parental magma may have subsequently been contaminated with relatively unradiogenic lead from the continental crust before emplacement. Lead isotope ratios continued evolving to the present; the $^{238}U/^{204}Pb$ ratio may have remained constant, but is likely to have been altered either by metasomatism at a short time after the intrusion of the rocks (as in Ivigtut) or by recent weathering.

Two different models have been used in the present study. A two-stage model, in which lead was separated from the mantle reservoir at 1200 Ma (approximate time of emplacement of Gardar intrusives) and then evolved in closed systems till the present day, allows calculation of a suitable μ_1 value which can be compared with the data of Taylor & Upton (1993). However, it is evident that this model is over-simplified, and thus a three-stage model has also been used. In this latter model, lead evolved in a mantle reservoir with a constant μ_1 value until separation of the continental crust at time t_1 (stage 1). The Gardar rocks are considered to be largely mantle derived and thus evolution of the lead continued in the depleted mantle reservoir with parameter μ_2 until time t_2, when the intrusion of the Gardar rocks occurred (stage 2). Lead then continued to evolve to the present day (stage 3). This has been modelled graphically using a program written by T. Andersen (in press). Clearly this model is still a simplification of the probable history, but it approaches a more reasonable solution than the two-stage model. Results of the modelling are given below, and the relevant calculations are described in Appendix C.4.

For all samples analysed in this study, present day $^{238}U/^{204}Pb$ ratios have been calculated from measured values (See Appendix C.4 for calculations). These can be applied to a two-stage model, assuming the age of the rocks to be 1.2 Ga in order to calculate a value for μ_1. For almost all the samples, the value obtained is very low (from 3.1 to 7.1) and does not correspond with the two-stage model values. These low apparent values are probably due to alteration of the U/Pb ratio in the rocks after emplacement.

7.6.2 Country rocks and magma sources.

Taylor & Upton (1993) presented data for Archaean gneisses from the Ivigtut area and the field of their typical analyses (corrected to 1200 Ma) is shown on Fig 7.7a. It can be seen that the two gneiss samples analysed in the present study are widely different: J3 (viii) lies within the field of typical gneiss from the area, whilst KG95/50A has relatively radiogenic Pb isotope ratios. Taylor & Upton (1993) also noted that some of the gneisses have unusually radiogenic leads, but in general the Archaean rocks are typified by low $^{207}Pb/^{204}Pb$.

Taylor *et al.*, 1980, studied the Archaean gneisses further north within the craton, in the area of Godthaab, and showed that their mantle source was characterised by a μ_1 value of 7.5-7.6. Assuming a date of 3 Ga for emplacement of the gneisses, and employing a two-stage model, sample J3 (viii) has a lower apparent model μ_1 of 7.3.

The location of "average mantle", from Zartman & Haines (1988) is shown on Fig. 7.6; this value, corrected to 1200 Ma, and the Northern Hemisphere Reference Line (NHRL) of Hart (1984) are also shown on Fig. 7.7a.

7.6.3 The Grønnedal-Íka complex

Three samples from Grønnedal-Íka have $^{206}Pb/^{204}Pb$ ranging from 15.9 to 23.8. These values appear to fall on a straight line on the present day $^{206}Pb/^{204}Pb$ vs. $^{207}Pb/^{204}Pb$ plot (Fig. 7.6) but the slope of this line does not correspond to a reasonable age. Using the two-stage model, they have apparent model μ_1 values of 7.3-7.7.

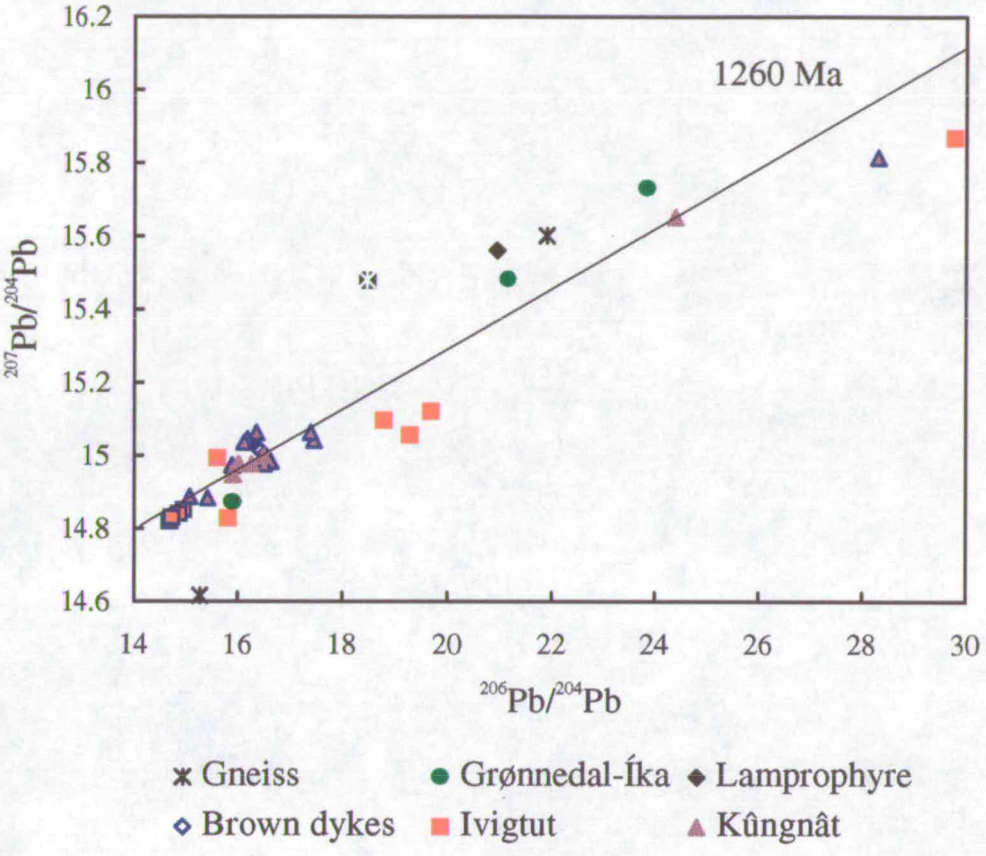

Fig. 7.6: Plot of present-day $^{206}Pb/^{204}Pb$ vs. $^{207}Pb/^{204}Pb$.
1260 Ma isochron for the Kungnat samples is shown for reference
White star on black represents average mantle (Zartman & Haines 1988)
Data for Ivigtut galenas (outlined squares) from Ulrych (1964) and for Kungnat (outlined triangles) from Taylor & Upton (1993) are also shown.

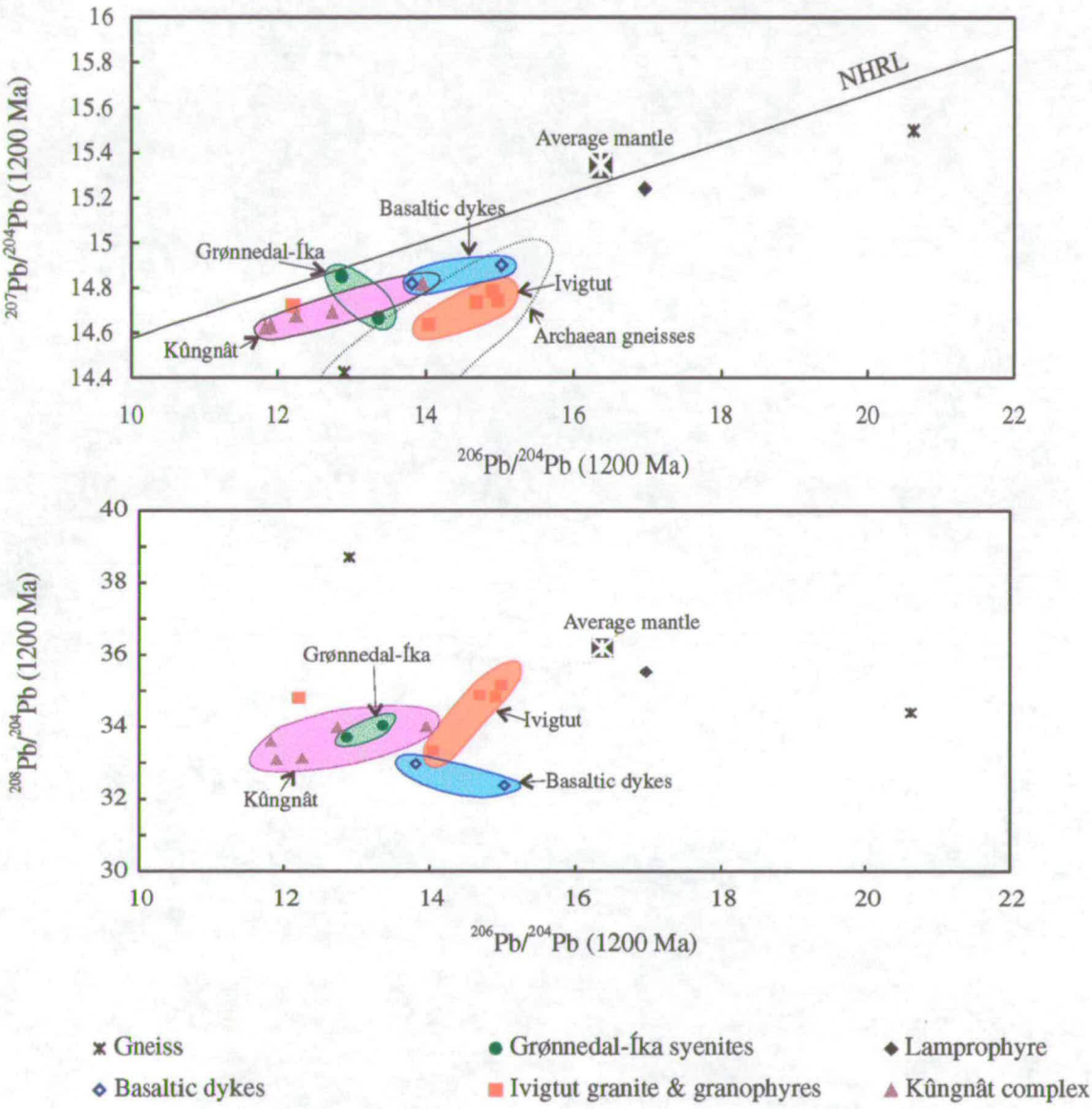

Fig. 7.7: Pb isotope correlation plots for 1200 Ma. Recalculated using present-day U values.

7.6.4 Dykes

On the plot of present day $^{206}Pb/^{204}Pb$ vs. $^{207}Pb/^{204}Pb$, the lamprophyre sample plots fairly close to the average mantle values taken from Zartman & Haines (1988) but with higher $^{206}Pb/^{204}Pb$, indicating U enrichment in the lamprophyres. The basaltic dykes plot close to samples from Kûngnât in the low $^{206}Pb/^{204}Pb$, low $^{207}Pb/^{204}Pb$ area of the diagram. On the age-corrected diagrams (Fig. 7.7), the lamprophyre sample remains close to the "average mantle" value, and the basaltic dykes appear to plot towards the crustal field. Using the two-stage model, the lamprophyre sample has model μ_1 = 7.8, whilst the basaltic dykes have values of 7.47 and 7.49. Similarly, in a three-stage model, the basaltic dykes fit the model for Kûngnât (see below) with μ_2 of 6.5-7, whilst the lamprophyre sample requires a μ_2 value approaching 8.

7.6.5 The Ivigtut stock

The samples from Ivigtut are widely scattered across the present day Pb-Pb plot, having a range in $^{206}Pb/^{204}Pb$ of 15.6 to 23.8, probably related to the introduction of U and Pb during metasomatism. Again, they do not define a sensible errorchron. On the age-corrected $^{206}Pb/^{204}Pb$ vs. $^{207}Pb/^{204}Pb$ diagram they show a mixing trend towards the continental crust, and their calculated two-stage model μ_1 values range from 7.08 to 7.55. The scatter of values makes even application of the three-stage model difficult, but a reasonable fit is achieved by using a typical mantle value for μ_1 of 7.5 (Taylor *et al.* 1980); μ_2 = 5, with t_1 = 3000 Ma and t_2 = 1150 Ma. μ_3 is, unsurprisingly, highly variable. 3000 Ma is an appropriate age for regional crust formation (Taylor *et al.*, 1980) and an emplacement date for the Ivigtut granite of 1150 Ma fits with the 1170 Ma age for Ivigtut obtained by Bailey (pers. comm.)

7.6.6 The Kûngnât Complex

The samples from Kûngnât fall in the same range as the data presented by Taylor & Upton (1993). Two samples of peraluminous granites from SE Kûngnât are shown on the plot: KG95/66, from the present study, and 81144, from the study of Taylor & Upton. These have markedly higher present day $^{206}Pb/^{204}Pb$ (24.4 and 28.3) and $^{207}Pb/^{204}Pb$ (15.6 and 15.8) than any other Kûngnât samples. These granites are believed to have formed by melting of the surrounding gneisses and the high ratios given here suggest that the precursors were rich in radiogenic Pb, similar to the gneiss sample KG95/50A. Of the other samples from this study, the gabbro has $^{206}Pb/^{204}Pb$ of 16.02 and $^{207}Pb/^{204}Pb$ 15.01, whilst the syenites have $^{206}Pb/^{204}Pb$ = 15.9 to 16.5 and $^{207}Pb/^{204}Pb$ = 14.9-15.0. A best fit errorchron has a slope of 0.0825, which corresponds with an age of 1256 ± 110 Ma, with an MSWD of 2.26. Although the MSWD is low, again the errors are too large for this to be a useful date.

Apparent two-stage model μ_1 values of 7.46 for the gabbro and 7.42-7.43 for the syenites cover a smaller range than those reported by Taylor & Upton (1993), and the value for the gabbro is similar to those for the basaltic dykes. The basaltic dykes also fit the apparent three-stage model for Kûngnât. Fitting t_2 = 1260 Ma, as this seems to be a reasonably certain age for the Kûngnât complex (unpublished data, Larry Heaman (pers. comm.)) and t_1 again = 3000 Ma, with μ_1 of 7.5, gives μ_2 = 6.5 and $\mu_3 \approx 8$.

7.7 Discussion of isotope data

No real isochron ages have been obtained from this isotope study, although the errorchron ages obtained for Kûngnât fall within the spread of dates obtained by other workers, which place Kûngnât at 1220 to 1270 Ma (mid-Gardar). However, the results presented above do provide petrogenetic information.

7.7.1 The Grønnedal-Íka Complex

Samples from the Grønnedal-Íka complex show positive initial ε_{Nd} and low $^{87}Sr/^{86}Sr$ isotope ratios similar to those of the basaltic dykes, and although there is a range in apparent two-stage model μ_1 values, two samples have model $\mu_1 > 7.6$. This would seem to indicate that the syenites of Grønnedal-Íka formed through fractionation from a relatively uncontaminated mantle-derived magma, probably from a source similar to that of the basaltic dykes. The third sample, which has lower model μ_1, was taken from a locality fairly close to the edge of the complex and may show the effects of some localised crustal contamination. The apparently low calculated initial Pb isotope ratios of these samples (Fig.7.7) are almost certainly due to post-emplacement alteration of U/Pb and Th/Pb ratios.

7.7.2 Dykes

All the isotope data confirm the origin of the lamprophyres from OIB-type mantle, with little contamination from lithospheric mantle or crust. In terms of Nd and Sr isotopes, the same appears to hold true for the basaltic dykes, which also appear to have formed from a mildly depleted source. However, Pb data show that, whilst the lamprophyres have relatively high μ_1 values, the basaltic dykes have rather lower μ_1, suggesting that the latter have either

been contaminated by the Archaean crustal material, which has unradiogenic Pb isotope ratios, or that they have formed from a different mantle reservoir to that of the lamprophyres. These data seem to confirm the conclusions, drawn in the previous chapter, that the lamprophyres and basaltic magmas were derived from differing sources. It also suggests that the lamprophyres may have been derived from a HIMU-type OIB source. However, further Pb isotopic data would be useful to confirm this hypothesis.

It is apparent that the observed initial isotopic ratios for the basaltic dykes are not appropriate for a magma formed from an old (> 3000 Ma), enriched sub-cratonic lithospheric mantle source, which might be expected to have negative ε_{Nd} but model $\mu_1 > 8$ (Hawkesworth *et al.*, 1986). The positive initial ε_{Nd} values and low initial $^{87}Sr/^{86}Sr$ ratios for the basaltic dykes indicate that any enrichment of this source in LILE could not have occurred as early as the Archaean. Nd model ages suggest that selective trace element enrichment of the mantle source from which the basaltic dykes were derived occurred following the end of Ketilidian activity. This supports the hypothesis that the basaltic dykes were derived from lithospheric mantle which had been enriched at ~ 1700 Ma by fluids rising from the subducting Ketilidian slab. There is thus no evidence for the involvement of old, LILE-enriched sub-Archaean lithospheric mantle in the genesis of the Gardar magmas. Instead, it appears likely that all the Gardar magmas were derived from mantle sources beneath the relatively young Proterozoic lithosphere.

7.7.3 The Ivigtut stock

Samples from the Ivigtut granite have clearly been strongly affected by metasomatism related to the cryolite body. Mobility of Rb and Sr over a lengthy period of time has led to a wide variation in apparent initial $^{87}Sr/^{86}Sr$

ratios which therefore give little clue to the petrogenesis. However, although the Sm-Nd and U-Th-Pb systems have also been affected by the metasomatism, models can be used to "see through" the scatter. The initial ε_{Nd} value for Ivigtut obtained from the evolution diagram (Fig. 7.2) is ≈ -2. This value suggests contamination by the crust which has strongly negative ε_{Nd} values at 1200 Ma. The three-stage lead model confirms this conclusion; although U/Pb ratios were altered by metasomatism, giving a variable set of μ_3 values, a very low model μ_2 of approximately 5 strongly suggests the effects of crustal contamination. The gneisses of the crust in the Ivigtut area are known to have low μ values (Taylor *et al.* 1984, Taylor & Upton 1993, and data from the present study).

The Nd evolution diagram provides some information about the nature of the fluids which caused the metasomatism of the granite. Cross-cutting relationships indicate that the granite must be younger than the Brown Dykes, and thus that metasomatism cannot have occurred at 1330 Ma. It is therefore suggested that, when metasomatism occurred in the granite, a component of fluid was introduced with a positive ε_{Nd} of about +5 - i.e. similar to the Nd composition of the lamprophyre dykes. It seems likely that this fluid had therefore been derived directly from the mantle.

7.7.4 The Kûngnât Complex

Isotopic evidence for crustal contamination in the Kûngnât complex is clear. $^{87}Sr/^{86}Sr$ > Bulk Earth and negative ε_{Nd} at 1200 Ma, with ε_{Nd} decreasing with increasing SiO_2, indicate the effects of contamination occurring during crystallisation. The three-stage Pb model for Kûngnât bears out this conclusion, giving model μ_2 of about 6.5. μ_3 is about 8 for most samples, but is considerably higher for the peraluminous granite samples, which are

believed to be the products of minor crustal anatexis. This may be attributed to the melting of small areas of crust which have more radiogenic Pb isotope values, which have been shown to exist in the area by Taylor & Upton (1993), or may be due to concentration of U in the partial melts.

7.8 Conclusions from radiogenic isotope data

i) The isotope data support the hypothesis that the lamprophyres represent primitive magmas derived from an OIB-type source, with higher U/Pb ratios than the other Gardar magmas in the area.

ii) The basaltic dyke swarms and the syenites of the Grønnedal-Íka complex appear to have been affected by, at most, minor crustal contamination of the magmas. However, the isotopic evidence confirms that they were derived from a young lithospheric mantle source which was enriched in incompatible elements no earlier than the closing stages of the Ketilidian orogeny.

iii) The magmas which formed the younger complexes of Kûngnât and Ivigtut have clearly been crustally contaminated. These complexes have been subject to late alteration which has disrupted the Rb-Sr system.

iv) At Ivigtut, the F- and CO_2- rich metasomatic fluids altered all the isotopic systematics in the granite. Nd data strongly supports a mantle derivation for a component of this fluid.

Chapter 8: Stable Isotopes

8.1 Introduction

Samples of carbonates from every carbonate-bearing rock type in the study area were analysed for C- and O- isotopes at SURRC, East Kilbride. The samples used included calcite and siderite from the Grønnedal-Íka carbonatite; whole-rock lamprophyre samples containing calcite; siderite from mineralised dykes; calcite and siderite from pegmatites at Kûngnât; and siderite from the Ivigtut ore body. Analytical techniques are summarised in Appendix B and results tabulated in Appendix G. The C-isotope results are presented relative to the PDB standard and the O-isotopes to the SMOW standard. Pearce *et al.* (1997) have recently published C- and O- isotope data on the Grønnedal-Íka syenites and carbonatites, and some lamprophyres, and their data will be compared with those obtained in the present study.

A small set of sulphides from Ivigtut, Kûngnât and Grønnedal-Íka were also analysed for S-isotopes in a preliminary study. Due to time constraints the data-set was not expanded, but the results provide an additional support for certain hypotheses and are discussed below. S-isotopes are reported relative to the Canyon Diablo Troilite (CDT) standard.

8.2 C- and O- isotope results

Five carbonate separates from the Grønnedal-Íka carbonatite have $\delta^{13}C_{PDB}$ ranging from -4.3 to -5.0 ‰, and $\delta^{18}O_{SMOW}$ ranging from +7.0 to +8.7 ‰. These are similar to the ranges given by Pearce *et al.* (1997) of $\delta^{13}C_{PDB}$ = -4.0 to -4.7 ‰ and $\delta^{18}O_{SMOW}$ = +6.7 to +7.9 ‰. The three calcite separates have higher $\delta^{13}C_{PDB}$ (-4.3 to -4.7 ‰) than the siderite separates (-4.9 to -5 ‰). Pearce *et al.*

(1997) also noted this effect, showing that $\delta^{18}O_{SMOW}$ and $\delta^{13}C_{PDB}$ decreased with increasing Fe_2O_3, and related it to fractionation of calcite from the melt.

Four lamprophyre samples have $\delta^{13}C_{PDB}$ of -4.7 to -5.7 ‰ and $\delta^{18}O_{SMOW}$ of +9.9 to +10.3 ‰. Pearce *et al.* (1997) had a wider spread of data but gave average values for lamprophyres of $\delta^{13}C_{PDB}$ = -5.34 ‰ and $\delta^{18}O_{SMOW}$ = +10.3 ‰, which fall within the range measured in the present study.

Seven samples of siderite from the Ivigtut stock, mostly from the ore body but including one of siderite from within the granite itself, have $\delta^{13}C_{PDB}$ ranging from -7.0 to -8.3 ‰, and $\delta^{18}O_{SMOW}$ from +7.8 to +9.2 ‰. Two siderite samples from mineralised dykes on the Ivigtut peninsula have $\delta^{13}C_{PDB}$ of -7.2 and -8.4 ‰,and $\delta^{18}O_{SMOW}$ of +7.6 and +7.5 ‰. These values fall close to the range of the samples from the Ivigtut ore-body.

Samples from Kûngnât include both siderite and calcite separates. Three samples come from pegmatites from the southeastern syenites, two from the western syenites, and one from within the ring-dyke gabbro. There is a wide variation in the results, $\delta^{13}C_{PDB}$ ranging from -3.9 to -7.2 ‰, and $\delta^{18}O_{SMOW}$ from +6.5 to +10.3 ‰.

8.3 Discussion of C- and O-isotope results

All the data are plotted on Fig. 8.1 and it can be seen that the samples from Ivigtut, Grønnedal-Íka, and the lamprophyres form three discrete groups. The samples from Kûngnât are more scattered. The two samples of siderite from the mineralised dykes on the Ivigtut peninsula plot close to the field of the Ivigtut siderites, suggesting that the mineralising fluid originated from the same source as that in the Ivigtut granite.

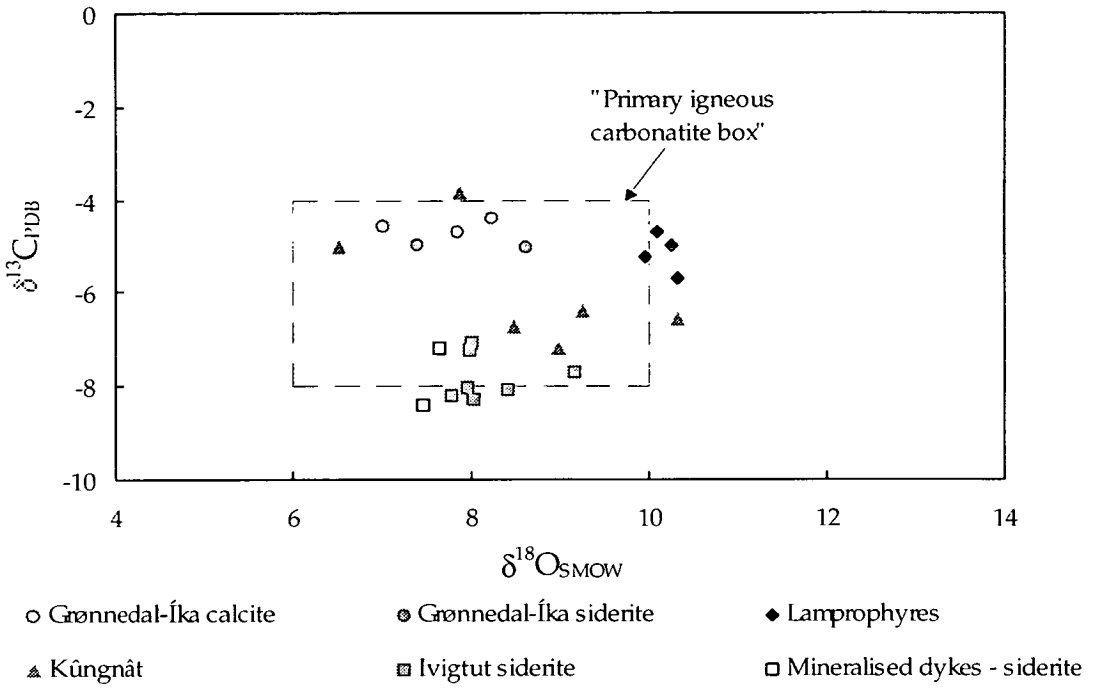

Fig. 8.1. Plot of $\delta^{13}C_{PDB}$ vs. $\delta^{18}O_{SMOW}$ for carbonates from the study area. "Primary igneous carbonatite box" from Deines (1989) and Keller & Hoefs (1993) represents the field of mantle-derived carbonatites.

The samples from the Grønnedal-Íka carbonatite clearly fall within the box for primary igneous carbonatites. The lamprophyre samples fall around the high $\delta^{18}O_{SMOW}$ edge of the box. Pearce *et al.* (1997) observed that this was also true for syenite samples from Grønnedal-Íka and attributed the heavy oxygen values to oxygen isotope fractionation accompanying fractional crystallisation during magmatic evolution. The lamprophyres are considered to be relatively primitive magmas, suggesting that fractional crystallisation has not been significant, but Pearce & Leng (1996) noted that fractionation may occur during the partial melting process in the mantle. This would lead to an increase in $\delta^{18}O_{SMOW}$ and $\delta^{13}C_{PDB}$. Although the lamprophyres have high $\delta^{18}O_{SMOW}$, their $\delta^{13}C_{PDB}$ values are typical for mantle-derived carbonates, suggesting that this explanation is not valid in this case. The samples analysed in the present study were whole-rock samples and may have contained a mixture of primary carbonate and secondary carbonate in vugs.

If the secondary carbonate was derived from fluids which had had a long period of residence in the crust, its $\delta^{18}O_{SMOW}$ would be high and would increase the $\delta^{18}O_{SMOW}$ value for the whole-rock. Alternatively, high $\delta^{18}O_{SMOW}$ may be a source characteristic.

Samples from Ivigtut have $\delta^{18}O_{SMOW}$ values within the range for mantle-derived carbonatite, but low $\delta^{13}C_{PDB}$ values. This has been observed before in other carbonatites associated with high F contents, such as carbonatite dykes from the Igaliko Complex in the east of the Gardar province (Pearce & Leng, 1996) and carbonatite lavas from Oldoinyo Lengai (Keller & Hoefs, 1993). It appears that light C may be preferentially incorporated in F-rich melts, probably due to fluor-carbonate complexing. However, it should be noted that at Ivigtut the high F contents are associated with high alkali contents. It has been shown (Rye & Ohmoto, 1974) that $\delta^{13}C_{PDB}$ decreases with increasing pH and, under reducing conditions, increases with decreasing fO_2. The low $\delta^{13}C_{PDB}$ values for Ivigtut therefore suggest formation from an alkaline fluid. Finch (1990) has shown that the fluids associated with the undersaturated Gardar intrusives are more alkaline (i.e. higher pH) than those associated with the oversaturated rocks. Based on the data above, it could be suggested that the fluids from which the Ivigtut ore body formed were not entirely derived by differentiation from the granite, but included a component of more alkaline fluid.

The Kûngnât data scatter across the diagram, with four of the samples continuing the vague positive correlation between $\delta^{18}O_{SMOW}$ and $\delta^{13}C_{PDB}$ shown by the Ivigtut samples. All the Kûngnât samples are taken from vugs in pegmatites, but their $\delta^{18}O_{SMOW}$ values are higher than would be expected for carbonates derived by interaction with meteoric waters, indicating that they are primary magmatic carbonates.

8.4 Origin of the carbonates

The Grønnedal-Íka carbonatite appears to be essentially mantle-derived, with fractionation of calcite producing the observed spread of values. Pearce *et al.* (1997) suggested that the carbonatite was genetically unrelated to the syenites, since the two formed markedly distinct groups in terms of their C- and O- isotope compositions, and proposed that the carbonatite was instead genetically associated with the lamprophyre dykes. It can be seen in the present study that the lamprophyres have similar $\delta^{13}C_{PDB}$ to the Grønnedal-Íka carbonatite, but $\delta^{18}O_{SMOW}$ is higher in the lamprophyres by about 3 ‰. If these heavy oxygen values can be attributed to the secondary carbonates in the lamprophyres, the initial C- and O- isotopic ratios of the carbonatite and the lamprophyres may have been very similar. However, there is no evidence to directly confirm the hypothesis mentioned above.

Although the samples of Ivigtut siderite fall outside the "mantle box" this may be due to the apparent effect of fluorine and/or alkalis in lowering the $\delta^{13}C_{PDB}$, and therefore it seems that the fluids from which this siderite formed were also mantle-derived. The implication is that an incursion of primitive hydrothermal fluids contributed to the genesis of the Ivigtut ore deposit. The Kûngnât samples, however, show some evidence of contamination, with the scatter of values suggesting exchange of C- and O-isotopes with crust or ground waters. Reported $\delta^{18}O_{SMOW}$ values for feldspars from Kûngnât are about + 6.5 ‰ (Sheppard, 1986), but the data given here for the carbonates extend to much higher values, indicating the likelihood of crustal contamination. The differences between Ivigtut and Kûngnât siderites are emphasised by electron probe data, which show that the Ivigtut siderites contain ~ 3% MnO but virtually no MgO, whereas the Kûngnât siderites contain ~ 3.5% MgO and < 1% MnO.

None of the $\delta^{18}O_{SMOW}$ values given above for the carbonates give any indication that these intrusions were affected by interaction with meteoric waters, since the likely effect of this would be to lower the $\delta^{18}O_{SMOW}$ values significantly (Sheppard, 1986). This agrees with the results obtained by previous workers for feldspars from igneous complexes throughout the Gardar (Sheppard, 1986; Finch & Walker, 1991; Finch *et al.* 1995). Oxygen isotopes in silicate minerals were not studied in the present work, but use of this technique on feldspars from the Ivigtut granite could be interesting for future study, since it appears possible that late, low-temperature alteration may have occurred (Section 7.2.3).

8.5 S-isotope ratios.

A small set of sulphides, including five galena samples, four chalcopyrites and a pyrite from Ivigtut, a sphalerite sample from Grønnedal-Íka, and a pyrrhotite sample from the Kûngnât ring-dyke, was analysed for S-isotope ratios. Average values of $\delta^{34}S_{CDT}$ for Ivigtut were -0.14 ‰ for galena, +1.56 ‰ for chalcopyrite, and +2.32 ‰ for pyrite. All these figures lie within the range of 0 ± 3‰ which Ohmoto (1986) defined as values for magmas generated by partial melting of the mantle, without significant crustal assimilation. Sphalerite from Grønnedal-Íka gave a $\delta^{34}S_{CDT}$ value of +1.15 ‰, which also lies within the magmatic field. $\delta^{34}S_{CDT}$ for the Kûngnât pyrrhotite was +3.72 ‰ , indicating the likelihood of contamination by crustal material.

Although the data-set is very small, these results agree with the conclusions drawn from other isotope studies, indicating that the magmas of the Grønnedal-Íka complex were mantle-derived, as was at least a component of the fluid from which the Ivigtut ore deposit formed. The Kûngnât magmas, however, were contaminated by crust.

Chapter 9: Comparison of the Ivigtut area with the rest of the Gardar Province

9.1 Introduction

Previous workers (e.g. Upton & Emeleus, 1987; Taylor & Upton, 1993) have suggested that the differences between the Gardar rocks of the Ivigtut area ("on-craton" intrusives) and those to the southeast ("off-craton") are controlled by the variation in the country rocks through which they were intruded. It has been suggested that these differences could either be attributed to crustal contamination of magmas which were initially derived from the same source, or to variations in the lithospheric mantle from which the magmas were thought to have been derived. In this chapter, the results obtained in the present study for samples of Gardar intrusives from the Ivigtut region are compared with published and unpublished geochemical data from other Gardar complexes, in order to investigate the above hypotheses.

9.2 Geochemistry: XRF data

9.2.1 Basic and ultrabasic rocks in the Gardar

Basic and ultrabasic rocks are found throughout the Gardar Province, as lavas, dykes and other minor intrusions; these occurrences were reviewed by Upton & Emeleus (1987), and the geochemical characteristics of specific examples in the eastern Gardar have been described by various authors. Larsen (1977) presented data for some late lavas within the Eriksfjord Formation, which included "ultramafic lavas", and Stewart (1970) studied the rocks of the Qassiarsuk Complex, which lies in the northeastern part of the Gardar, including carbonatitic and ultrabasic lavas and intrusions. The

ultramafic intrusives which have been studied (see Section 1.2 for locations) include those of the Tugtutôq-Nugarmiut region (Craven, 1985), dykes of the Tugtutôq-Ilímaussaq Dyke swarm (Upton & Fitton, 1985, Martin, 1985) and those in the area of the Igaliko Complex (Pearce & Leng, 1996). Upton (1991) investigated mantle xenoliths in an ultramafic lamprophyre intrusion on Igdlutalik island, part of the Tugtutôq-Ilímaussaq swarm. Data for basaltic rocks were included in many of the above papers; other studies include the work of Patchett (1977) on dolerite dykes and various papers on the Giant Dyke complexes (e.g. Upton *et al.* 1985).

Lamprophyres are essentially restricted to two regions in the Gardar, the Ivigtut area and the Tugtutôq-Ilímaussaq zone, and their geochemistry is similar for all occurrences across the province. The distinction between ultramafic lamprophyres (UML) and alkaline lamprophyres (AL) observed in the present study appears to be valid across the Gardar. UML intrusions have often been observed to be associated with carbonatites, whereas it has been suggested that the AL represent a transition to alkali basaltic compositions (Upton & Emeleus, 1987). Lamprophyres throughout the Gardar have low Zr/Nb and show similar incompatible element patterns, with high Nb and Ti, and low Y contents. Negative Sr anomalies, as observed in the present study, are seen in some other Gardar intrusives (e.g. Nugarmiut; Craven, 1985). There appears to be a similar source for all the Gardar lamprophyres.

In the present study, the basaltic dykes of the Ivigtut area have been divided into two groups: a *ne*-normative group with moderately low Zr/Nb of ~ 9, and a *hy*-normative group with higher Zr/Nb of 16-19 (Section 6.4.2). Basaltic rocks from the eastern Gardar (i.e. "off-craton") have been divided into two similar groups on the basis of geochemistry (Upton & Emeleus, 1987): the *ne*-normative dykes of the present study show similar characteristics

(Zr/Nb <10) to the Tugtutôq-Ilímaussaq-Nunataq Late Gardar dykes, whilst the *hy*-normative dykes correspond to the early- and mid-Gardar basalts and those of the Nunarssuit-Isortôq zone, with Zr/Nb ~ 18 (See Section 1.2 for location). The age relationships between the two groups observed in the Ivigtut area are similar to those observed on the larger scale, suggesting that basaltic rocks of the high Zr/Nb group were prevalent in the earlier stages of rifting but that, at later stages, the low Zr/Nb group became important.

The dykes of the Igaliko Dyke Swarm were divided into two similar groups by Pearce & Leng (1996); *ne*-normative dykes with Zr/Nb ~ 3.5 and *hy*-normative dykes with Zr/Nb ~6. In this case, the *ne*-normative group were considered to be related to the large, undersaturated syenite complexes, whilst the *hy*-normative dykes were suggested to be part of the Tugtutôq-Ilímaussaq dyke swarm. Similarly, Martin (1985) described late basic dykes which cut the main Tugtutôq-Ilímaussaq dykes. These late dykes were more silica-undersaturated and had lower Zr/Nb than those of the main swarm. In the Ivigtut area, a few late basaltic dykes with very low Zr/Nb (~ 4) are also observed, e.g. those cutting the Bunkebreccia.

Again, the evidence suggests that the geochemistry of the basic Gardar magmas in differing areas was not controlled by the age and nature of the crustal lithosphere into which they were emplaced, as has been previously suggested (Upton & Emeleus, 1987). The variation in geochemistry of these dykes can be explained by variation in amounts of asthenosphere- and lithosphere- derived melt making up the magma, which can be related to stages of rifting.

9.2.2 Gardar syenite complexes.

The syenite complexes represent the majority of the volume of the Gardar intrusives and are therefore the most studied (Upton & Emeleus, 1987, and refs. therein). It is generally agreed that the syenites were generated from a basic parent by fractional crystallisation, together with variable amounts of crustal contamination. Upton *et al.* (1971) presented a study of the chemical variation in three Gardar complexes, in which they concluded that the parental magmas were similar and that all the observed differences could be explained by varying conditions of fractionation. The geochemical data obtained for the Kûngnât and Grønnedal-Íka syenites in the present study do not indicate any significant features which could be used to argue against these conclusions.

9.2.3 Gardar granites

Gardar granites occur in the Dyrnaes-Narssaq complex, the Tugtutôq Central Complex, the Puklen stock, the Nunarssuit and Ilímaussaq complexes, and as the salic parts of some of the Giant Dykes (Bangs Havn intrusion and the Tugtutôq Younger Giant Dyke), as well as at Ivigtut and Kûngnât. Ivigtut is unusual in that it is the only Gardar intrusion known to be dominated by granite. Brief descriptions of all these intrusions are given by Emeleus & Upton (1976). Upton *et al.* (1971) included some data for granites in their discussion of the variation in major-element geochemistry between the Kûngnât, Central Tugtutôq, and Younger Giant Dyke Complexes; and Upton *et al.* (1990) presented further geochemical data for the Tugtutôq Central Complex, but overall few data have been published on granites from the eastern Gardar. A small set of new whole-rock major, trace, and rare earth element data, on granite samples from across the province, are presented here, and compared with data from the Ivigtut and Kûngnât granites. The

data, from samples from the Ilímaussaq and Nunarssuit granites, the Tugtutôq Central Complex, the Dyrnaes granite and the Giant Dykes, are tabulated in Appendix E.

In terms of major elements, there is little difference between the various granites. It is noticeable, however (Fig. 9.1), that the Ivigtut granite has higher SiO_2 (averaging ~ 74 wt%) and lower total alkalis (~9 wt%) than any of the other Gardar granites. On the trace element discrimination diagrams of Pearce *et al.* (1984) and Whalen *et al.* (1987a), as described in Section 6.4.5, all the granites fall in the "Within-Plate" or "A-type" fields. On the Ce/Nb vs. Y/Nb diagram of Eby (1992) (Fig. 9.2) the granites intruded into the Ketilidian crust all fall at or above the high Ce/Nb edge of the OIB field, indicating a trend towards the "crustal field" (Section 6.4.5).

Fig. 9.3 shows primitive mantle-normalised incompatible element patterns for the new analyses of "off-craton" granites compared with samples from the Ivigtut and Kûngnât granites. The majority of the granites show reasonably similar patterns, with distinct troughs at Ba, Sr and Ti and smaller K troughs. An exception to this is the sample from the Helene granite of Nunarssuit, which shows prominent Nb and U troughs, as well as Ba, Sr and Ti troughs. The presence of a Nb anomaly suggests that this granite may have assimilated a large amount of crust, or possibly even be formed through crustal anatexis, since crustal rocks tend to be deficient in Nb. All the granites show a small, positive Ta anomaly, and therefore have low Nb/Ta ratios, as is typical for A-type granites (Green, 1995).

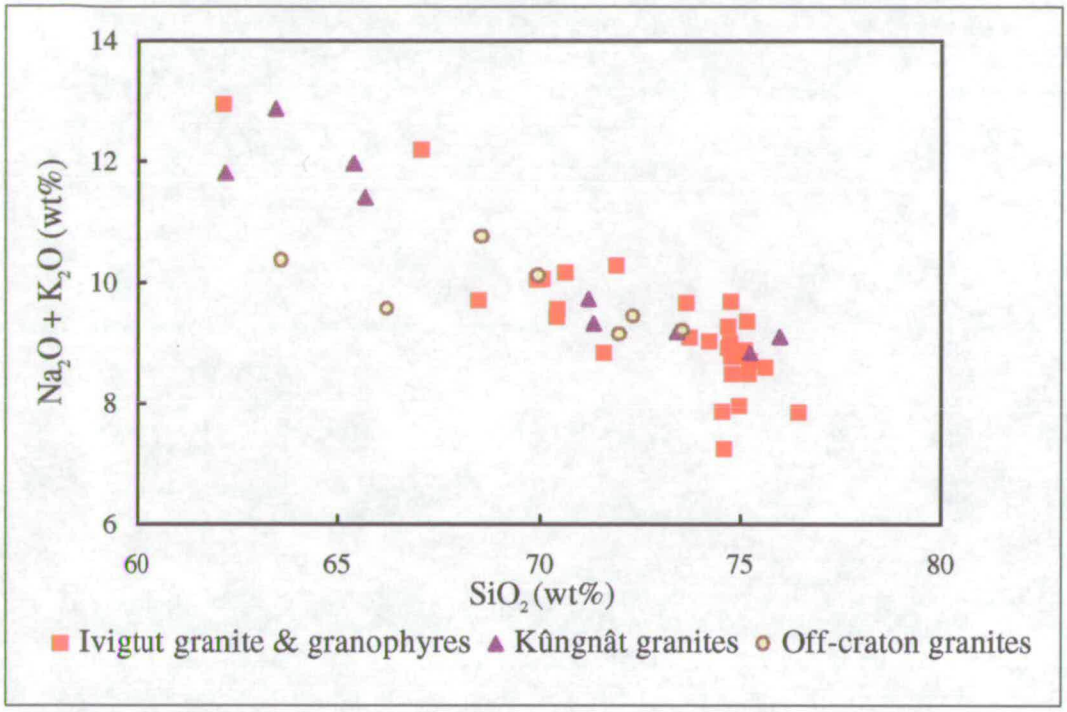

Fig. 9.1: Total alkalis vs. silica for Gardar granitoids

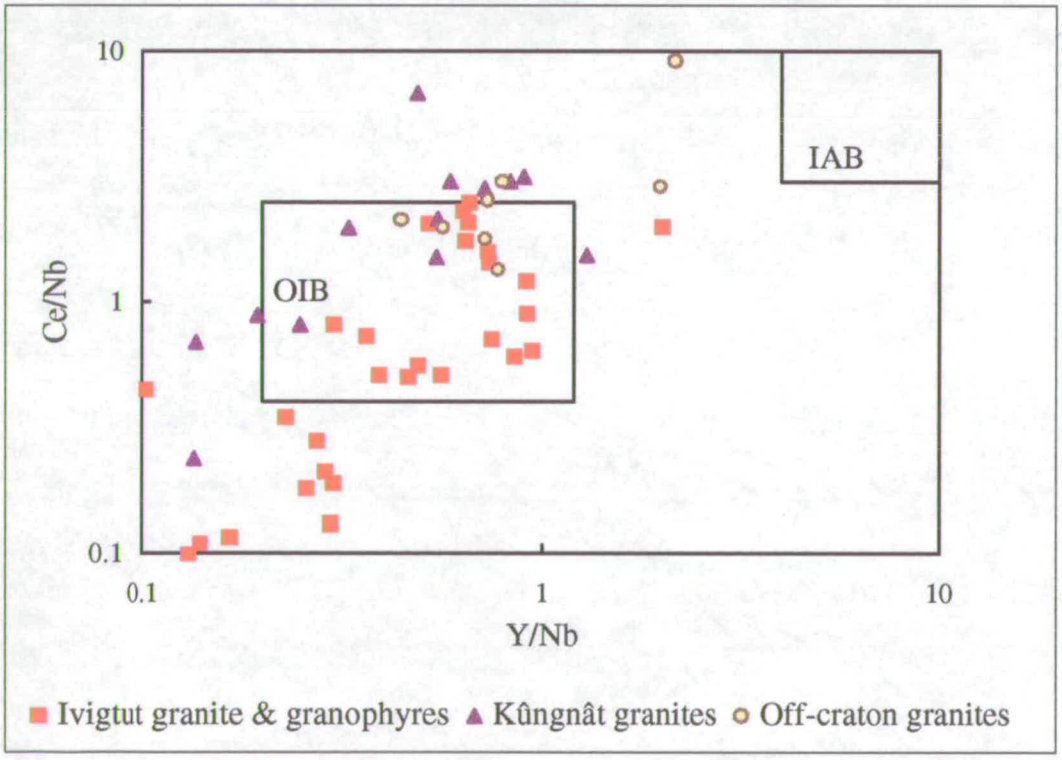

Fig. 9.2: Tectonic discrimination diagram for Gardar granites, after Eby (1992)
OIB: Ocean Island Basalt field, representing granites formed in a rift-related environment.
IAB: Island Arc Basalt field

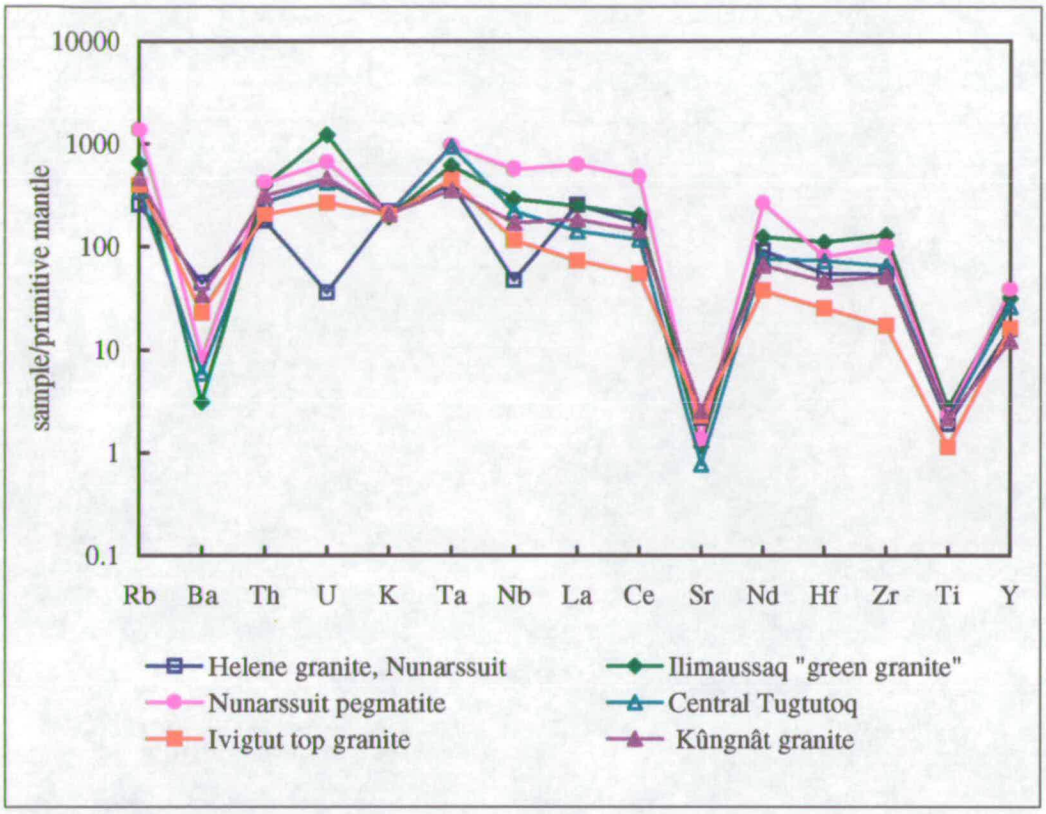

Fig. 9.3: Incompatible element normalised plot for Gardar granites

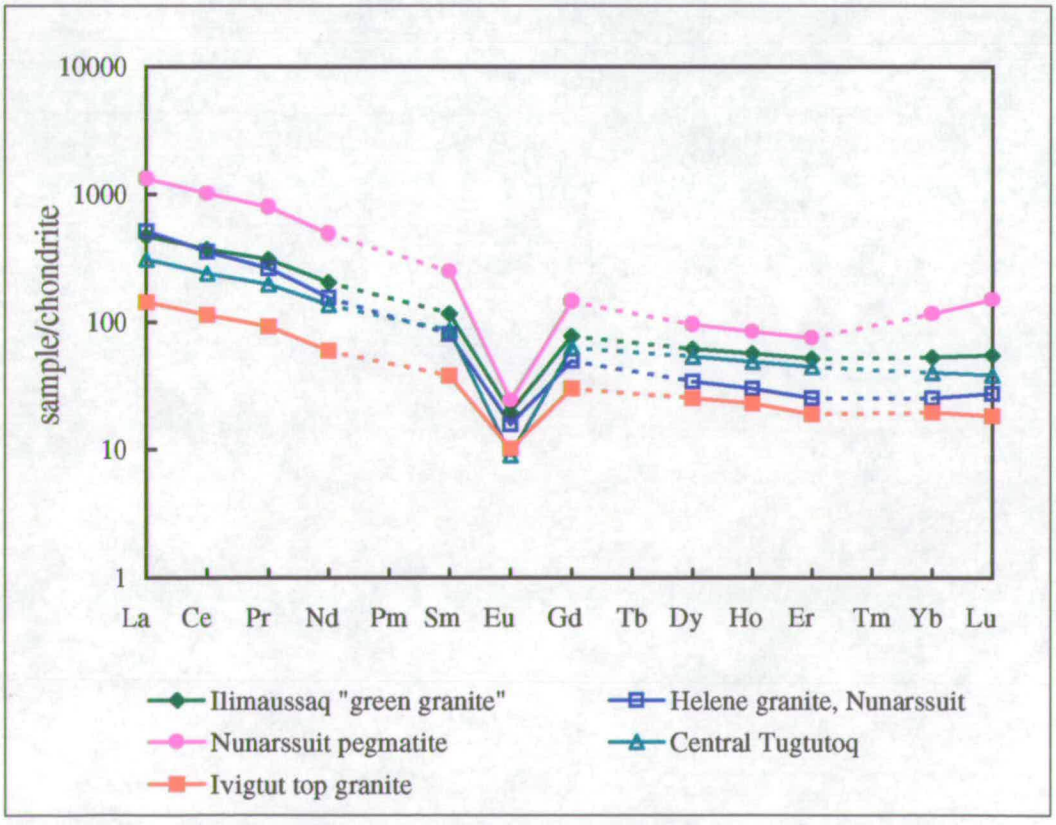

Fig. 9.4: Chondrite normalised REE plot for Gardar granites

The clearest distinction between the "on-craton" and "off-craton" granites relates to their uranium contents. Ivigtut top granite samples have no U anomaly and Kûngnât granites show a small peak; granites from Central Tugtutôq also only show a small U peak, but a granite pegmatite from Nunarssuit and the Ilímaussaq "green granite" sample, as well as a sample from Dyrnaes and a late-stage granite from within the Younger Giant Dyke Complex (YGDC), all have prominent U peaks. Kalsbeek & Taylor (1985) noted that some Ketilidian granites from the border zone of the mobile belt had higher U/Pb ratios than the Archaean gneisses. The U peaks in the incompatible element patterns may therefore be due to contamination by U-enriched crust, although this effect is extremely muted in the granites of the Tugtutôq Central Complex. This indicates that the Helene granite of Nunarssuit is unlikely to have formed through melting of a Ketilidian granite, due to its low U contents; further discussion of this is beyond the scope of this work.

Chondrite-normalised REE plots (Fig. 9.4) are fairly similar for all the granites, with some degree of LREE enrichment and prominent negative Eu anomalies. The most REE-enriched sample is a granitic vein from the Nunarssuit Complex: it shows consistent enrichment in all REEs rather than preferential HREE enrichment as at Ivigtut. However, it does show a small inflection at Er, with an upturn in the pattern towards Yb and Lu.

Again, the geochemical data for the granites suggest formation from similar basic sources by AFC processes, including fractionation of plagioclase, Fe-Ti oxides, and lesser amounts of alkali feldspar, with varying amounts of crustal contamination. The only apparent difference between the granites intruded into the different country rocks is the variation in uranium contents, which may be due to crustal contamination.

9.3 Radiogenic isotopes

9.3.1 Rb-Sr and Sm-Nd isotopes

Blaxland *et al.* (1978) showed, on the basis of initial $^{87}Sr/^{86}Sr$ ratios, that the majority of Gardar complexes could have been derived from upper mantle sources with minimal crustal contamination. These mantle sources were considered to be similar (initial $^{87}Sr/^{86}Sr$ ~ 0.703) for the whole Gardar province. Some complexes showed higher initial Sr ratios and it was believed that the magmas had been affected by crustal contamination, but no distinction was made between the types of crust involved. Later Sr isotope work on the Gardar (e.g. Winther, 1992) has corroborated these conclusions.

Coupled Nd and Sr isotope studies of the Gardar are scarce in the literature; the only published data are from the carbonatites, lamprophyres and phonolites of the Igaliko dyke swarm (Pearce & Leng, 1996) and the Qassiarsuk complex, which consists of a series of carbonatite and alkaline silicate tuffs and intrusives (Andersen, 1997). Paslick *et al.* (1993) used Sm and Nd data to date samples from the Motzfeldt and Ilímaussaq syenite complexes (Section 1.2 for location), but did not present Rb-Sr data. The data mentioned above are shown on a plot of initial $^{87}Sr/^{86}Sr$ vs. $\varepsilon_{Nd(i)}$ (Fig. 9.5) along with unpublished data of a) P.N. Taylor for the Tugtutôq Central Complex, giant dykes, and other dykes and b) A. N. Halliday for various dykes, lavas and carbonatites, together with data from the present study. These unpublished data, which have been corrected back to estimated dates for each particular intrusion, are tabulated in Appendix F.

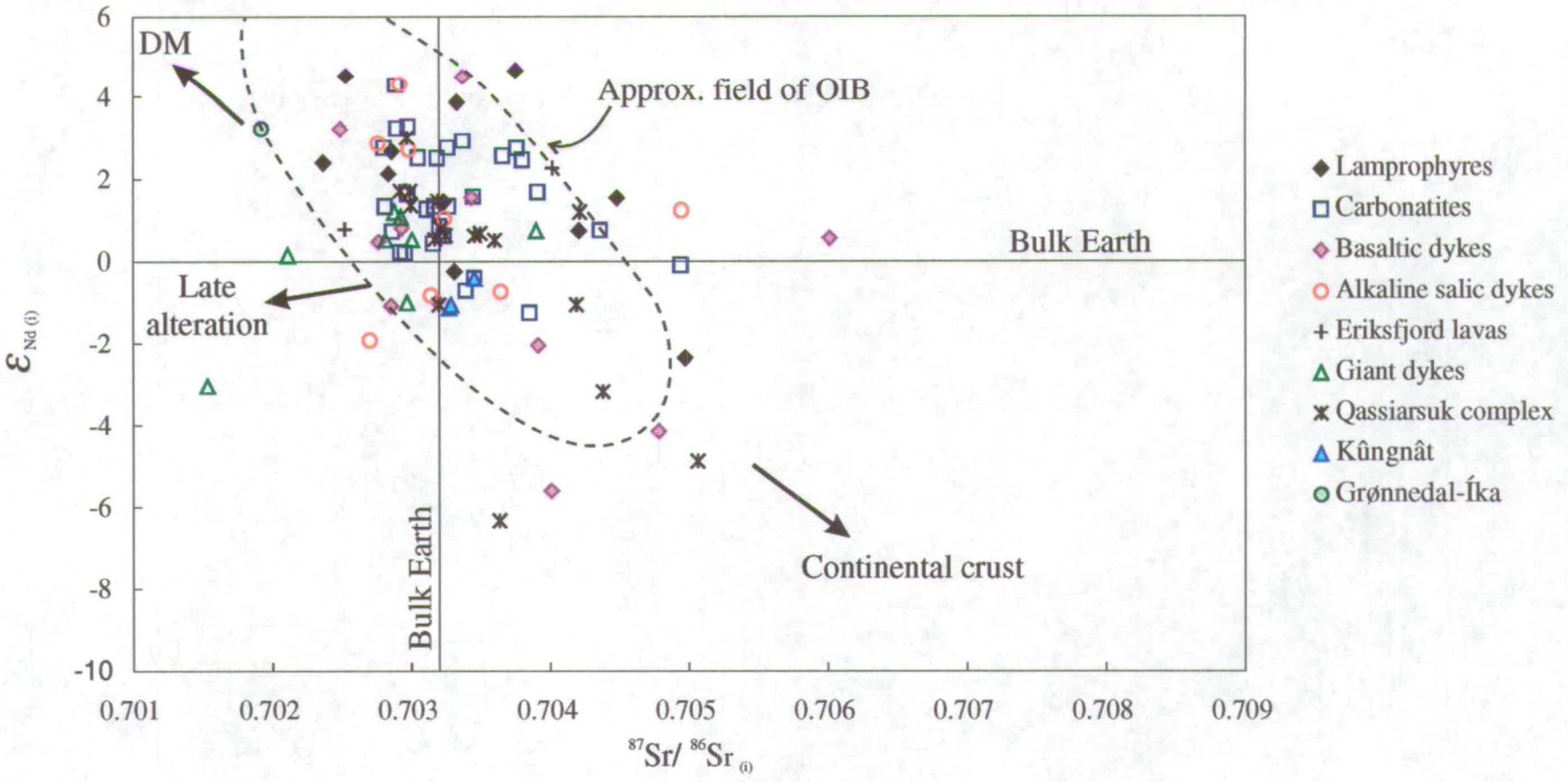

Fig. 9.5: Initial Nd-Sr isotope correlation diagram showing all available data for the Gardar. Dashed line shows field for Ocean Island Basalts, and arrows indicate the effects on the data of crustal contamination and late alteration. DM = depleted mantle.

A large part of the data on Fig. 9.5 form a cluster with initial $^{87}Sr/^{86}Sr \approx 0.703$ ("mantle-type" ratio for the Gardar; Blaxland, 1976) and initial ε_{Nd} of 0 to +3. These samples include almost all the analysed carbonatites, the basaltic dykes from the Ivigtut area, the Giant Dykes, and most samples from Qassiarsuk. The initial ε_{Nd} values observed agree with the figure of +2.4 given by Paslick *et al.* (1993) for the Eriksfjord lavas. The Ivigtut lamprophyres have higher initial ε_{Nd} (~ +4) than most of the samples: the only other samples with similar $\varepsilon_{Nd\,(i)}$ values are dykes from Igaliko, which also include lamprophyres. Generally, the lamprophyres have a higher average $\varepsilon_{Nd\,(i)}$ than the other rock-types. Overall, the positive initial ε_{Nd} values and initial $^{87}Sr/^{86}Sr$ ratios similar to Bulk Earth suggest derivation of all the basic Gardar parental magmas from a mildly depleted mantle. Samples from Kûngnât, as well as the alkaline dykes from Tugtutôq and Qassiarsuk, have lower initial ε_{Nd} and higher initial $^{87}Sr/^{86}Sr$, indicating the effects of crustal contamination. Stevenson *et al.* (in press) present initial ε_{Nd} values for the Ilímaussaq syenite complex of 0 to -6 and these low values are also attributed to crustal contamination. There is no consistent variation in initial Nd and Sr isotopic ratios between samples intruded into the Archaean craton and those intruded into the Ketilidian basement. Samples from Ivigtut and the Tugtutôq Central Complex show impossibly low initial $^{87}Sr/^{86}Sr$ ratios (i.e. lower than BABI, the $^{87}Sr/^{86}Sr$ ratio at the formation of the Earth, which is taken as 0.69897, the composition of basaltic achondrite meteorites), which indicate late-stage alteration of the complexes (as described in section 7.2.3).

9.3.2 Pb isotopes

Taylor & Upton (1993) presented Pb data for the Kûngnât and Tugtutôq complexes, and showed that the the overall differences in the Pb isotopic ratios between the two complexes reflect the differing country rocks. The

Archaean gneisses were shown to have relatively unradiogenic Pb isotope ratios, whilst the Proterozoic granites into which the Tugtutôq complex was intruded have more radiogenic signatures. Pb data have also been published by Andersen (1997) for the Qassiarsuk complex; and some Pb data for galenas from Ivigtut were given by Ulrych (1964).

Fig. 9.6 shows a compilation of all present-day Pb ratios available from the Gardar. As well as the published data mentioned above, some unpublished data on the Tugtutôq Central Complex and the Giant Dykes (B.G.J. Upton, pers. comm.) have been used, and these results are tabulated in Appendix F. It can be clearly seen on the figure that the "off-craton" intrusives form a separate group from those intruded into the Archaean craton. The latter group almost all have lower $^{206}Pb/^{204}Pb$ and lower $^{207}Pb/^{204}Pb$ than those intruded into the mobile belt. The two groups are separated by an isochron with two-stage apparent model μ_1 of 7.48: this represents the isochron for the basaltic dykes of the Ivigtut area. The "on-craton" intrusives have model μ_1 values < 7.48, whilst the "off-craton" intrusives have higher values. This result agrees with the hypothesis that the basaltic magmas were parental to the major Gardar complexes: it appears that the variations in lead isotope characteristics for all the major complexes studied could be explained by variable crustal contamination of a basaltic parental magma with model μ_1=7.48. Differences between the complexes intruded into the Archaean craton and those intruded into the Ketilidian country rocks are explained by the differing lead isotope ratios of the crustal rocks. The higher model two-stage model μ_1 for the lamprophyre dyke sample (~ 7.8) adds weight to the hypothesis that it originated from a different mantle source to that of the basaltic dykes: however it should be noted that more lead isotope data on the lamprophyres are required to confirm this hypothesis.

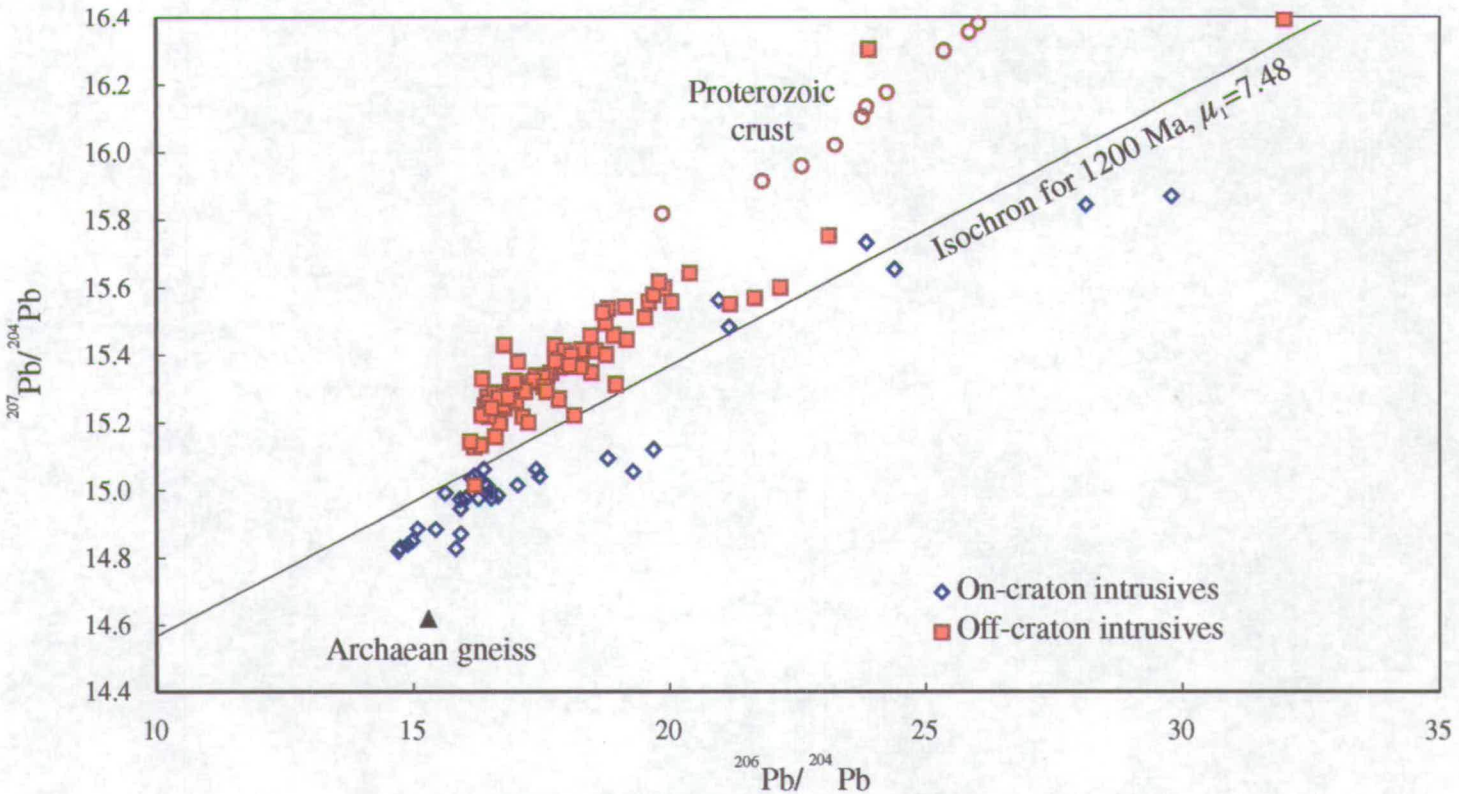

Fig. 9.6: Present day Pb isotope correlation diagram for all available Gardar data, showing that "on-craton" and "of f-craton" rocks fall on different sides of an isochron with μ_1=7.48

9.3.3 Discussion of isotope data

The Nd and Sr isotope data suggest that virtually all the Gardar magmas originated from a similar parent with initial $\varepsilon_{Nd} \approx +3$ and initial $^{87}Sr/^{86}Sr \approx 0.7030$. The spread of isotope ratios was achieved through variable amounts of crustal contamination and, in some cases, re-setting of the isotope system by hydrothermal alteration. Exceptions may include some lamprophyres and carbonatites, which appear to have slightly higher initial ε_{Nd} values than the rest of the Gardar intrusives. On the basis of Nd- and Sr- observations, Gardar parental magmas appear to have originated from a mantle source which was slightly depleted relative to Bulk Earth. It is apparent that, if metasomatic enrichment of this mantle source by a fluid with high contents of volatiles and trace-elements took place (Upton & Emeleus, 1987) it must have occurred a (geologically) short time before magma genesis.

Pb isotope data corroborate the above theory, but show that the majority of the magmas were contaminated to some extent by crustal material, with the Pb isotopic ratios being controlled by the nature of the contaminant. It appears that the Pb isotopes are more sensitive to the effects of crustal contamination than Sr and Nd isotopes. Again, the lamprophyre dykes from the Ivigtut area show some slight isotopic differences when compared with the other rock types.

9.4 Conclusions from comparison with other Gardar intrusives

i) The sources for the Gardar basic magmas were similar throughout the province. There is no evidence to indicate that the magmas of the Ivigtut area were derived from, or contaminated by, old, enriched sub-cratonic lithosphere: in other words, the margin of the Archaean craton does not appear to have provided a lithospheric control on the nature of the magmas.

ii) Although the basic rocks of the Gardar can be divided into several groups, these groups can then be identified throughout the province. If the ultramafic lamprophyres represented small-degree asthenospheric partial melts, it appears that the alkaline lamprophyres, *ne*-normative and *hy*-normative basaltic rocks were formed through varying degrees of partial melting and incorporation of young lithospheric mantle by asthenosphere-derived melts. It appears (Section 7.7.2) that the sub-Proterozoic lithospheric mantle had been fairly recently enriched in incompatible elements by the effect of fluids, and that these fluids were derived from the descending slab after Ketilidian subduction.

iii) Although the differences in age and chemistry of the crust do not appear to have affected the parental magmas, they have brought about some differences in the geochemistry of the contaminated salic rocks. The major differences are related to the U/Pb ratio, which is higher in the Proterozoic rocks than in the Archaean, leading to positive U anomalies and more radiogenic Pb ratios in all rocks contaminated by Proterozoic crust. This difference makes Pb isotope ratios very sensitive indicators of crustal contamination. The clear trends towards the respective country rocks, which are shown by the datasets on the $^{206}Pb/^{204}Pb$ vs. $^{207}Pb/^{204}Pb$ diagram, indicate that the majority of the rocks have actually been contaminated to some extent by continental crust.

10: Discussion and Conclusions

10.1 Individual complexes

10.1.1 The Grønnedal-Íka complex

The data suggest that the parental magmas from which the Grønnedal-Íka nepheline syenites formed were derived from the sub-Proterozoic lithospheric mantle, with essentially no crustal contamination. The syenites were produced by extensive crystal fractionation of basic parents. The Grønnedal-Íka carbonatite was also clearly derived from the mantle, though whether its origins lie with the lamprophyres or the nepheline syenites is uncertain. Further lead isotope study could be useful in investigation of this question. However, the conclusion of Pearce *et al.* (1997), that the carbonatite is genetically related to the lamprophyre dykes, is preferred, due to the clear association of abundant carbonates with the lamprophyres.

10.1.2 Dykes

10.1.2.1 Lamprophyres

The lamprophyres of the Ivigtut area include ultramafic types which can be considered to represent the most primitive Gardar magmas. They have normalised trace element patterns similar to those of OIB, with positive Nb anomalies, suggesting that they formed as small-degree partial melts from an asthenospheric source rather than from lithospheric mantle. The high carbonate contents in the rocks suggest that these small melt fractions may have been CO_2-rich. Alkaline lamprophyres probably represent larger degree melt fractions than the ultramafic group.

Initial Nd- and Sr-isotopic ratios for all the lamprophyres are also similar to those of OIB, therefore corroborating the above theory. Pb isotope data on one lamprophyre sample suggest a higher apparent model μ_1 value for these dykes than for other Gardar rocks, indicating the possibility of a HIMU-type OIB source. However, the Zr and Ti contents of the lamprophyres are higher than can be easily modelled for carbonate-rich melts derived directly from the asthenosphere. It has been suggested (James, 1995) that compositions such as these could have formed when early small-degree (possibly carbonatitic) melts were "frozen in" at the base of the lithosphere and were remobilised shortly afterwards by further ascending melts. This model would explain the high contents of the most highly incompatible elements without requiring a change in the isotopic ratios. Field, petrographic and geochemical evidence show that the lamprophyres are carbonate-rich rocks and indicate the possibility that some carbonate may have separated from the ultramafic lamprophyres by liquid immmiscibility. This is typically evident in the presence of carbonate veins associated with the dykes, but it is possible that the Grønnedal-Íka carbonatite may have formed through the same process.

10.1.2.2 Basaltic dykes

The basaltic dykes in the area include both *ne*- and *hy*- normative types, of which the *hy*-normative appear to be the earlier, and have the lowest contents of the incompatible elements. The *hy*-normative group show negative Nb anomalies on normalised multi-element diagrams, whereas the *ne*-normative dykes lack any Nb anomaly; neither group has patterns similar to those of OIB. All the basaltic rocks are less enriched in the incompatible elements than the lamprophyres but have higher SiO_2 contents, indicating that they could not have formed from the same magma as the lamprophyres through a process of crystal fractionation alone. Furthermore, it can be

shown on the basis of simple mixing models that the basaltic dykes could not have evolved from the lamprophyres by straightforward mixing with crust. However, the presence of negative Nb anomalies in the normalised incompatible element patterns of some of the basaltic dykes suggests either crustal contamination of the magma or origination in a lithospheric mantle source.

The isotopic data show that there has been no major crustal contamination of the basaltic magmas. Initial Nd- and Sr- isotope ratios suggest derivation from a source which was similar to that of the lamprophyres, and Pb-isotopic data suggest an apparent model μ_1 of ~ 7.48. However, Nd model ages for the basaltic dykes average *ca.* 1700 Ma. This date is considerably older than emplacement dates and suggests that a process of enrichment of the lithospheric mantle source in incompatible elements may have occurred at this time. This hypothesis accords with the normalised trace element patterns which suggest the involvement of enriched lithospheric mantle in the petrogenesis of the basaltic dykes. The isotopic data constrain the date of incompatible element enrichment to less than 1700 Ma,and thus it appears that the old lithospheric mantle beneath the Archaean craton is unlikely to have been involved. The date given by the Nd model ages of approx. 1700 Ma represents the end of the Ketilidian orogeny. Recent work (Chadwick & Garde, 1996) has shown that the Ketilidian slab probably subducted northwards, under the craton (Fig. 10.1). Fluids rising from this slab would probably have been enriched in some incompatible elements but lacking in others, such as Nb. These fluids may have been trapped by the sub-Proterozoic lithospheric mantle, which assimilated their trace element signatures. Melting of this lithospheric mantle during Gardar rifting and asthenospheric upwelling produced the basaltic dykes. Their varying characteristics could have been produced by variations in the amount of the asthenospheric mantle component involved.

10.1.2.3 Salic alkaline dykes

The salic alkaline dykes were produced by fractionation of basic parents, with some degree of crustal contamination. Incompatible-element normalised patterns for the salic dykes show similarities to those of the lamprophyres, but it should be noted that the lamprophyres only seem to represent very small volumes of melt. It therefore seems probable that the salic dykes evolved from a basic parent containing moderately large fractions of asthenospheric melt, similar to that represented by the *ne*-normative basaltic dykes.

10.1.3 The Ivigtut stock

In terms of geochemistry and mineralogy, the unaltered Ivigtut granite is a typical A-type. Geochemical and isotopic data indicate that the granitic magma formed through fractional crystallisation processes from large volumes of a fluorine-rich basic parent magma with associated crustal contamination. After the granite was emplaced, it seems that a fluor-carbonatitic melt derived from the underlying mantle rose through the conduit provided by the granite, possibly causing localised melting and metasomatism, and became trapped beneath the chilled carapace of the granite stock. Pauly & Bailey (in press) have suggested that the presence of this fluid led to melting of the granite, producing a fluid/melt rich in fluorine, CO_2 and alkalis; which separated into immiscible components (represented by the quartz- and cryolite- bodies) and solidified to produce the ore deposit. The fluids metasomatised the granitic stock itself and concentrated the HFSE and HREE. Isotopic ratios in the granite were altered as a result of hydrothermal fractionation, but whilst Rb and possibly Sr remained susceptible to hydrothermal alteration for a long time (at least the

length of the Gardar period) after metasomatism, Sm and Nd were fairly rapidly "frozen in".

10.1.4 The Kûngnât complex

Initial ε_{Nd} values decrease with increasing SiO_2 in the Kûngnât rocks, and this evidence, combined with geochemical data, indicates that the magmas of the Kûngnât complex formed by AFC processes, with fractionation of a basic parent (possibly represented by the most basic compositions of the gabbro ring-dyke) accompanied by varying amounts of crustal contamination. This evolution began in deep magma chambers, from which the magmas that formed the complex ascended through stoping and were emplaced at shallower levels, but continued during *in situ* crystallisation, so that the rocks in the centre of the complex show less evidence of crustal contamination than those at the margins. The most highly-evolved components produced the peralkaline granites, from which late-stage F-rich fluids were released, bringing about metasomatism of the gabbros. These fluids differ from those at Ivigtut in that they do not appear to have been CO_2-rich.

10.2 Model for the evolution of Gardar rocks in the Ivigtut area.

Chadwick & Garde (1996) suggested that, at about 1800 Ma, during the Ketilidian orogeny and accretion of the mobile belt, a crustal slab was subducted northwards beneath the Archaean craton. Fluids rising from this slab may have enriched the overlying young sub-continental mantle lithosphere (SCML) in the LILE. The area around the margin of the craton then remained relatively passive (in terms of magmatic activity) until the onset of Gardar rifting at about 1350 Ma.

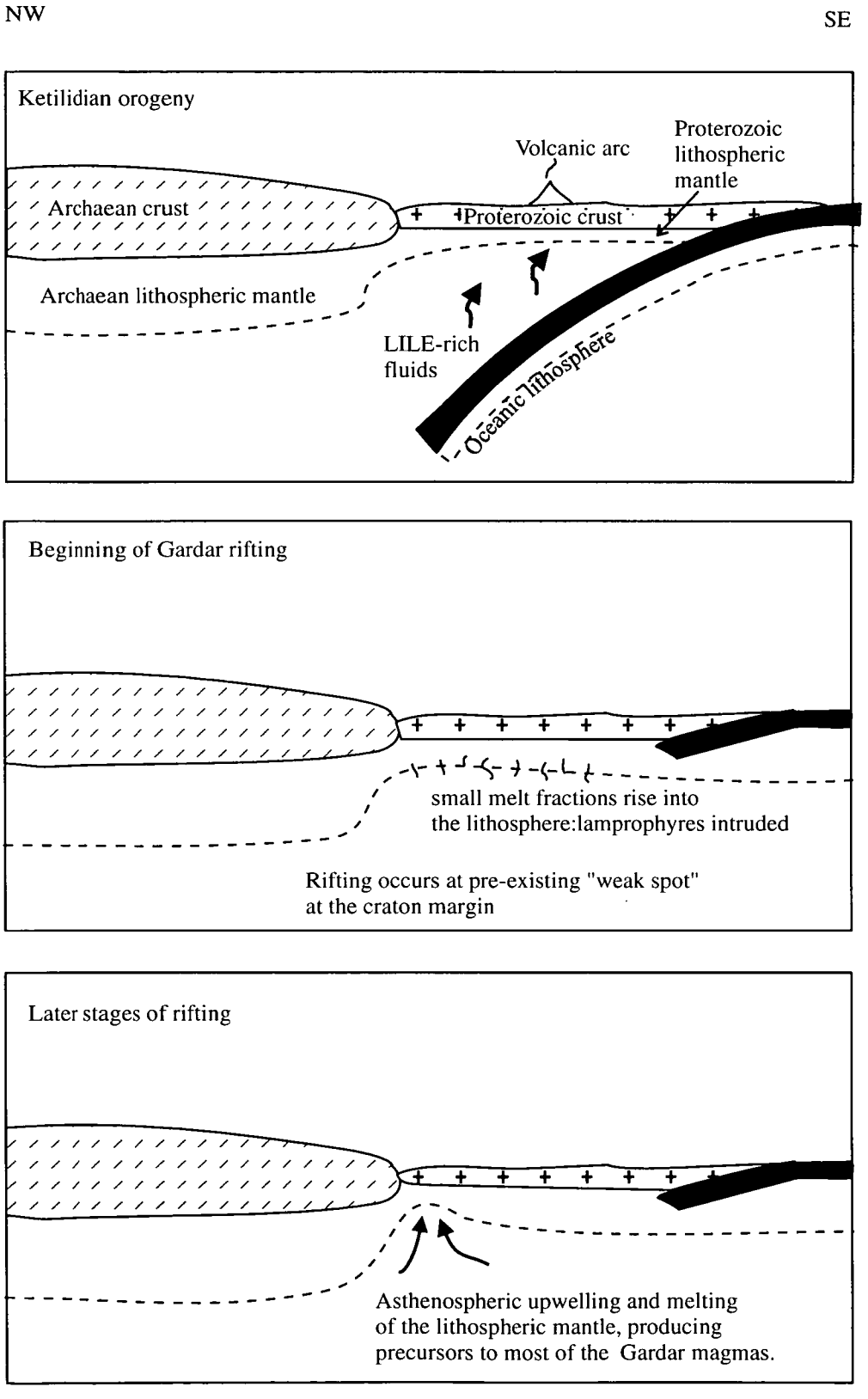

Fig. 10.1: Schematic diagram showing a model for source of the Gardar magmas. Not to scale. Model for the Ketilidian after Chadwick & Garde (1996).

Upton & Blundell (1978) suggested that Gardar magmatism involved three major magmatic cycles, each representing extensional phases. The majority of the intrusives of the Ivigtut area were included in the mid-Gardar cycle. However, the Grønnedal-Íka complex appears to date from the early Gardar (Blaxland, 1976), and the nepheline syenites probably evolved through fractional crystallisation from an alkali basaltic parent magma at the end of this first magmatic cycle.

Early in the mid-Gardar rifting, volatile-rich small-fraction partial melts separated from an OIB-like source within the asthenosphere and ascended into the lithosphere. The smallest melt fractions were probably carbonatitic, followed by silico-carbonatites. Such small volume melts are likely to have been rapidly frozen in within the lower parts of the lithosphere. They could then be remobilised by later melting episodes, since such remelting requires a smaller temperature rise, or a smaller amount of extension, than that required for dry melting of the mantle (McKenzie, 1989). These melt fractions eventually ascended through the lithosphere with very little further contamination and were emplaced at shallow crustal levels as lamprophyre dykes. The smallest melt fractions formed ultramafic dykes, whilst larger fractions are represented by the alkaline lamprophyres. Melt conduits are considered to be protected from the surrounding lithospheric mantle by reaction zones (Menzies, 1992), thus preventing large-scale contamination of the melts by the lithosphere. It appears that the silicate and carbonate portions of these melt fractions may have been separated by liquid immiscibility, so that the lamprophyres contain carbonate-rich ocelli or are cut by carbonate veins, with associated fenitisation of the country rocks. The Grønnedal-Íka carbonatite may also have been derived by liquid immiscibility from these lamprophyric melts, and was emplaced into a weakened zone provided by the recently-intruded syenite complex. This hypothesis accords with the conclusions of Pearce *et al.* (1997), who

suggested a cogenetic relationship between the carbonatites and lamprophyres, rather than between the carbonatite and the nepheline syenite, as originally postulated by Bedford (1989).

As rifting progressed, larger melt fractions formed within the asthenosphere and ascended into the lithospheric mantle. Thinning of the lithosphere led to partial melting of the lithospheric mantle, which had previously been selectively enriched in the incompatible elements by fluids rising from the Ketilidian slab. Melting thus produced primitive magmas which were enriched in the LILE. These magmas were ponded, probably at the base of the crust, and underwent fractionation of olivine ± clinopyroxene (Upton, 1996). This reduced density of the magmas, allowing ascent of the basalt residues which collected in large, mid-crustal magma chambers, or were intruded at higher crustal levels as dykes. Those magmas which were retained in magma chambers continued to evolve through fractional crystallisation, possibly with associated crustal assimilation, producing more salic magmas. Upton & Emeleus (1987) and Upton (1996) suggested that these magma chambers were stratified, with flotation cumulates formed of labradorite crystals at the roof, passing down through magmas of increasing density to the most basic compositions. The evolved magmas in the upper portions of these chambers were then themselves intruded as dykes, or ascended by stoping mechanisms, undergoing AFC evolution, to form the larger central complexes of the Gardar, including Kûngnât. *In situ* evolution of the magmas in the Kûngnât complex continued through AFC processes.

With time, as the lithospheric mantle became thinned, the lithospheric component of the primitive magmas became less important, and an asthenospheric signature began to prevail. The observed temporal variation in the magmatism in the Ivigtut region is unusual, since apparently-asthenosphere-derived magmas were intruded early in the rifting sequence.

This pattern has also been observed by Gibson *et al.* (1992) in the Rio Grande Rift, and it was suggested that this was related to the occurrence of previous rift-related volcanism, which had removed many fusible components from the lithospheric mantle. This explanation may also hold for the Gardar, since the emplacement of the lamprophyres was preceded by early-Gardar magmatic activity. It seems that in each Gardar cycle, small-degree, volatile-rich melts from the asthenosphere were introduced into the lithosphere; in some cases these ascended into the crust and were intruded as lamprophyre dykes, but in other cases they were frozen into the lithospheric mantle and served to increase the susceptibility of the lithosphere to melting under conditions of extension. During each cycle of magmatism, these fusible components were removed from the lithosphere.

J. Bailey (pers. comm.) has suggested a date of 1170 Ma for Ivigtut - i.e. late-Gardar. This places the Ivigtut granite as the only late-Gardar intrusive in the study area. It can be postulated that a similar sequence of melting events occurred during each Gardar cycle, but that in the late-Gardar small-degree carbonatitic melts never reached shallow crustal levels, but instead remained trapped in the lithospheric mantle. This SCML therefore became highly susceptible to melting and large volumes of alkali basaltic magma were produced which incorporated high volatile concentrations.This magma then ponded within the crust and evolved through AFC processes, producing large volumes of salic magma of low density and viscosity. Magma of this type rose through the crust to reasonably high levels, there to form the batholith which has been postulated to underlie the Ivigtut granite stock.

10.3 Sources and depths of melting

The earliest, small-degree mid-Gardar melts which produced the lamprophyres appear to have originated in the asthenosphere from an OIB-like source with a relatively high μ-value. The existence of HIMU-OIB sources has been attributed to the recycling of oceanic lithosphere into the mantle(Sun & McDonough, 1989; Ringwood *et al.*, 1992). Ringwood *et al.* suggested a model for generation of OIB-type magmas, whereby subducted oceanic crust was trapped at the 650 km discontinuity in the mantle to form a layer of garnetite. Partial melting of this layer produced melts with high LREE/HREE ratios, due to the controlling influence of garnet. These melts "re-fertilised" the overlying asthenospheric mantle which was then stored for ~10^8 to 10^9 years, before being reheated by rising convection currents, producing small degree partial melts. A model of this type may be appropriate for the sources of Gardar lamprophyres during early stages of rifting.

During later stages of rifting, OIB-like melts from the asthenospheric mantle mixed with melts derived from the lithospheric mantle (i.e from depths less than ~ 150 km). The LREE-enrichment observed in Gardar magmas indicates that this mantle source was probably composed of garnet lherzolite and that garnet was not completely consumed during melting.

10.4 Conclusions

i) The Gardar intrusives of the Ivigtut region represent a suite of rift-related, alkaline rocks which were formed over a period from about 1300 to 1150 Ma, intruded into the margin of the South Greenland Archaean craton.

ii) They include three central complexes, the Grønnedal-Íka nepheline syenite and carbonatite complex, the Kûngnât syenite and alkali gabbro complex, and the Ivigtut alkali granite, as well as a suite of dykes which includes lamprophyric, basaltic and salic alkaline examples.

iii) The oldest intrusion in the Ivigtut area is the Grønnedal-Íka complex. The nepheline syenites formed through fractional crystallisation of a basic parental magma which was similar to the source for the majority of the Gardar intrusives. The carbonatite, however, may have been derived from a different source.

iv) The lamprophyre dykes in the Ivigtut area include ultramafic, CO_2-rich compositions which appear to have been derived as small-degree partial melt fractions in the asthenosphere. The observed trace element compositions may have been produced by remobilisation of successive similar melt fractions which had crystallised within the lithospheric mantle.

v) The basaltic dykes of the area appear to have been derived from young, sub-Proterozoic SCML which had been enriched, ~ 500 Ma before Gardar activity, by fluids which were enriched in the LILE relative to the HFSE (especially Nb) rising from a subducting slab.

vi) The majority of other Gardar magmas also evolved, through AFC processes, from a parental magma which was derived from the SCML.

vii) None of the Gardar magmas were sourced in the old SCML below the Archaean craton. Differences between the "on- and off-craton" intrusives can be attributed to differing amounts of fractionation and contamination by different types of crust.

References

ALDERTON, D.H.M., PEARCE, J.A., & POTTS, P.J. (1980): Rare Earth Element Mobility during Granite Alteration: evidence from Southwest England. *Earth Planet. Sci. Lett.* 49, 149-165.

ANDERSEN, T. (1997): Age and Petrogenesis of the Qassiarsuk carbonatite-alkaline silicate volcanic complex in the Gardar rift, South Greenland. *Min. Mag.* 61, 499-513.

ANDERSEN, T., HAGELIA, P., & WHITEHOUSE, M.J. (1994): Precambrian multi-stage crustal evolution in the Bamble sector of south Norway: Pb isotopic evidence from a Sveconorwegian deep-seated granitic intrusion. *Chem. Geol.* 116, 327-343

ARNDT, N. & GOLDSTEIN, S. (1987): Use and abuse of crust-formation ages. *Geology* 15, 893-895.

AULT, W.U. & KULP,J.L. (1960): Sulfur Isotopes and Ore Deposits. *Econ. Geol.*55, 73-100

AYRTON, S. & MASSON, H. (1972): Les mineralisations en crocidolite de la cote SW du Groenland. Un example de metasomatose sodique. *Bull. Suisse. Min. Pet.* 52, 277-316.

BAILEY, D.K. (1987): Mantle metasomatism - perspective and prospect. *In*: FITTON, J.G., & UPTON, B.G.J. (eds.) *Alkaline Igneous Rocks* Geol. Soc. Sp. Pub. 30, 1-13.

BAILEY, J.C. (1977): Fluorine in granitic rocks and melts: A review. *Chem. Geol.* 19, 1-42

BAILEY, J.C. (1980): Formation of cryolite and other aluminofluorides: A petrologic review. *Bull. Geol. Soc. Denmark*, 29, 1-45.

BAKER, J.H. (1985): Rare Earth Element and other trace element mobility accompanying albitization in a Proterozoic granite, W.Bergslagen, Sweden. *Min.Mag.* 49, 107-115.

BEDFORD, C. (1989): Mineralogy, Geochemistry and Petrogenesis of the Grønnedal-Ika Alkaline Igneous Complex, SW Greenland. *PhD Thesis*, University of Durham (unpublished).

BERTHELSEN, A. (1962): On the Geology of the country around Ivigtut, SW Greenland. *Geol. Rundschau* 52, 269-280.

BERTHELSEN & HENRIKSEN (1975): Geological map of Greenland 1:100 000. Ivigtut 61 V.1 Syd. GGU, Copenhagen (*Meddr. om Grønland*)

BLAXLAND, A.B. (1976): Rb-Sr Isotopic Evidence for the Age and Origin of the Ivigtut Granite and Associated Cryolite Body, South Greenland. *Economic Geology* 71, 864-869.

BLAXLAND, A.B. (1976): Geochronology and Isotope Geochemistry of the Gardar Alkaline Complexes, South Greenland. *PhD Thesis*, Edinburgh University (unpublished).

BLAXLAND, A.B, VAN BREEMEN, O., EMELEUS, C.H. & ANDERSON, J.G. (1978): Age and Origin of the major syenite centres in the Gardar Province of South Greenland: Rb-Sr studies. *Geol. Soc. Am. Bull.* 89, 231-244

BONDAM, J. (1991): The Ivigtut Cryolite Deposit in South Greenland. *Open File Ser. GGU* No. 91/4.

BOWDEN, P. & WHITLEY, J.E. (1974): Rare-Earth patterns in peralkaline and associated granites. *Lithos* 7, 15-21.

BØGGILD, O.B. (1953): The Mineralogy of Greenland. *Meddr. om. Grønland* 149, No. 3.

BRIDGWATER, D. (1965): Isotopic Age Determinations from South Greenland and their Geological Setting. *Bull. Grønlands Geol. Unders.* 53 (also *Meddr. om Grønland* 179, No. 4).

BROOKS, C., HART, S.R., & WENDT, T. (1972): Realistic use of two-error regression treatments as applied to rubidium-strontium data. *Rev. Geophys. Space. Phys.* 10, 551-577

BROOKS, C., JAMES, D.E., & HART,S.R. (1976): Ancient lithosphere: its role in young continental volcanism. *Science* 193, 1086-1094

CALLISEN, K.(1943): Igneous Rocks of the Ivigtut Region, Greenland. Part 1. The Nepheline Syenites of the Grønne Dal-Ika area. *Meddr. om Grønland* 131, No.8.

CHADWICK, B. & GARDE, A.A. (1996): Palaeoproterozoic oblique plate convergence in South Greenland: a reappraisal of the Ketilidian Orogen. *In:* BREWER, T.S. (ed.): *Precambrian Crustal Evolution in the North Atlantic Region.* Geol. Soc. Sp. Pub. 112, 179-196.

COLLINS, W.J, BEAMS, S.D., WHITE, A.J.R., & CHAPPELL, B.W. (1982): Nature and Origin of A-Type Granites with particular reference to Southeastern Australia. *Contrib. Min. Pet.* 80, 189-200.

COX, K.G., BELL, J.D., & PANKHURST, R.J. (1979): The Interpretation of Igneous Rocks. *Unwin Hyman* 450pp.

CRAVEN, J.A. (1985): The Petrogenesis of some Ultramafic Rocks from the Gardar Province, SW Greenland. *PhD Thesis*, Edinburgh University (unpublished).

CULLERS, R.L., & GRAF, J.L. (1984): Rare Earth Elements in igneous rocks of the continental crust: predominantly basic and ultrabasic rocks. *In:* HENDERSON, P. (ed.): *Rare Earth Element Geochemistry*, 237-274. Elsevier.

DE JONGH, W.K. (1973): XRF-analysis using theoretical interference coefficients. *X-Ray Spectrometry* 2, 151

DEER, W.A., HOWIE, R.A., & ZUSSMAN, J. (1992): An Introduction to the Rock-Forming Minerals, Second Edition. *Longman.*

DEINES, P, (1989): Stable Isotope Variations in Carbonatites. *In*: BELL,K. (ed): *Carbonatites*, 301-359. Unwin Hyman.

DEPAOLO, D.J., & WASSERBURG, G.J. (1978): Petrogenetic mixing models and Nd-Sr isotopic patterns. *Geochim. et. Cosmochim. Acta* 43, 615-627.

DOE, B.R. (1970): *Lead Isotopes*. Springer-Verlag.

EBY, G.N. (1990): The A-type Granitoids: A review of their occurrence and chemical characteristics and speculations on their petrogenesis. *Lithos* 26, 115-134.

EBY, G.N. (1992): Chemical subdivision of the A-type granitoids: petrogenetic and tectonic implications. *Geology* 20, 641-644.

EGEBERG, A.T., BONIN, B., & SORENSEN, H. (1993): The Bonifatto peralkaline granites (NW Corsica): a possible case of evolution through volatile transfer. *Bull. Soc. Geol. France* 5, 739-758.

EMELEUS, C. H. (1964): The Grønnedal-Ika Alkaline Complex, South Greenland. *Bull. Gronlands Geol. Unders.* 45 (also *Meddr. om Grønland* 172, No. 3)

EMELEUS, C.H. & UPTON, B.G.J.(1976): The Gardar period in Southern Greenland. *In*: ESCHER, A. & WATT, W.S. (eds) *The Geology of Greenland*, pp. 153-81. The Geological Survey of Greenland, Copenhagen.

FAURE, G. (1986): *Principles of Isotope Geology*. 2nd Edition. Wiley.

FINCH, A.A. (1990): The Chemical and Isotopic Nature of Fluids Associated with Alkaline Magmatism, South Greenland. *PhD Thesis*, Edinburgh University (unpublished).

FINCH, A.A., & WALKER, F.D.L (1991): Cathodoluminescence and microporosity in alkali feldspars from the Blå Måne Sø perthosite, South Greenland. *Min. Mag.* 55, 583-589

FINCH, A.A., PARSONS, I., & MINGARD, S.C. (1995): Biotites as Indicators of Fluorine Fugacities in Late-Stage Magmatic Fluids: the Gardar Province of South Greenland. *J. Pet.* 36, 1701-1728.

FITTON, J.G., & DUNLOP, H.M. (1985): The Cameroon Line, West Africa, and its bearing on the origin of oceanic and continental alkali basalt. *Earth Planet. Sci. Lett.* 72, 23-38.

FITTON, J.G., JAMES, D., KEMPTON, P.D., ORMEROD, D.S., & LEEMAN, W.P. (1988): The Role of Lithospheric Mantle in the generation of late Cenozoic Basic Magmas in the Western United States. *J. Pet.*, Special Lithosphere issue, 331-349.

FITTON, J.G., & UPTON, B.G.J (eds.) (1987): *Alkaline Igneous Rocks* Geol. Soc. Sp. Pub. 30

GIBSON, S.A., THOMPSON, R.N., LEAT, P.T., MORRISON, M.A., HENDRY, G.L., DICKIN, A.P., & MITCHELL, J.G. (1993): Ultrapotassic Magmas along the flanks of the Oligo-Miocene Rio Grande Rift, USA: Monitors of the zone of Lithospheric Mantle Extension and Thinning beneath a Continental Rift. *J. Pet.* 34 I, 187-228.

GILL, R.C.O. (1972): Chemistry of peralkaline phonolite dykes from the Grønnedal-Íka area, South Greenland. *Contrib. Min. Pet.* 34, 87-100.

GOLDSTEIN, S.L., O'NIONS, R.K., & HAMILTON, P.J. (1984): A Sm-Nd study of atmospheric dusts and particulates from major river systems. *Earth Planet. Sci. Lett.* 70, 221-236.

GOVINDARAJU, K. (1994): 1994 compilation of working values and sample description for 383 geostandards. *Geostandards Newsletter* 18: Special Issue

GREEN, T.H. (1995): Significance of Nb/Ta as an indicator of geochemical processes in the crust-mantle system. *Chem. Geol.* 120, 347-359.

HARRIS, N.B.W. (1981): The role of Fluorine and Chlorine in the petrogenesis of a peralkaline complex from Saudi Arabia. *Chem. Geol.* 31, 303-310.

HART, S.R. (1984): A large-scale isotope anomaly in the Southern Hemisphere mantle. *Nature* 309, 753-757

HAWKESWORTH, C.J., MANTOVANI, M.S.M., TAYLOR, P.N., & PALACZ, Z. (1986): Evidence from the Parana of Southern Brazil for a continental contribution to Dupal basalts. *Nature* 322, 356-359

HENDERSON, P.(1984): General geochemical properties and abundances of the Rare Earth Elements. *In:* HENDERSON, P.(ed.): *Rare Earth Element Geochemistry* pp. 1-29. Elsevier.

HODSON, M.E. (1994): Igneous layering in the syenites of Nunarssuit and West Kûngnât, South Greenland: *PhD Thesis,* Edinburgh University (unpublished)

HODSON, M.E., & FINCH, A.A. (1997): Trough structures in the Western syenite of Kûngnât, S. Greenland: mineralogy and mechanism of formation. *Contrib. Min. Pet.* 127, 46-56

HORBE, M.A., HORBE, A.C., COSTI, H.T., & TEIXEIRA, J.T. (1991): Geochemical characteristics of cryolite-tin-bearing granites from the Pitinga Mine, NW Brazil - A review. *J. Geochem. Exploration* 40, 227-249

JACOBSEN, S.B., & WASSERBURG, G.J. (1980): Sm-Nd isotopic evolution of chondrites. *Earth Planet. Sci. Lett.* 50, 139-155.

JAMES, D.E. (1995): The Geochemistry of Feldspar-Free Volcanic Rocks. *PhD Thesis,* The Open University (unpublished).

KALSBEEK, F. & TAYLOR, P.N. (1984): Isotopic and chemical variation in granites across a Proterozoic continental margin-the Ketilidian mobile belt of South Greenland. *Earth Planet. Sci. Lett.* 73, 65-80.

KARUP-MØLLER, S. & PAULY, H. (1979): Galena and associated ore minerals from the cryolite at Ivigtut, South Greenland. *Greenland Geoscience* 2, 3-25

KELLER, J. & HOEFS, J. (1993): Stable Isotope Characterisitics of Recent Natrocarbonatites from Oldoinyo Lengai. *In:* BELL, K. & KELLER, J. (eds.): *Carbonatite Volcanism - Oldoinyo Lengai and the Petrogenesis of Natrocarbonatites.* IAVCEI Proceedings in Volcanology 4, 113-123.

KING, P.L., WHITE, A.J.R, CHAPPELL, B.W., & ALLEN, C.M. (1997): Characterization and Origin of Aluminous A-type Granites from the Lachlan Fold Belt, Southeastern Australia. *J. Pet.* 38, 371-391

KØNNERUP-MADSEN, J. (1984): Compositions of fluid inclusions in granites and quartz syenites from the Gardar continental rift province (South Greenland). *Bull. Mineral.* 107, 327-340

KROUGH, T.E. & HURLEY, P.M. (1968): Strontium Isotope Variation and Whole-Rock Isochron Studies, Grenville Province of Ontario.*J. Geophys. Res.* 73, 7107-7125.

KULP, J.L., AULT, W.U. & FEELY, H.W. (1956): Sulfur Isotope Abundances in Sulfide Minerals. *Econ. Geol.*51, 139-149

LARSEN, J.G.L. (1977): Petrology of the late lavas of the Eriksfjord Formation, Gardar Province, South Greenland. *Bull. Grønlands Geol. Unders.* 125

LE MAITRE, R.W. (ed.) (1989): A Classification of Igneous Rocks and Glossary of Terms. *Blackwell Scientific Pubs.*

LEE, M.R., WALDRON, K.A., PARSONS, I., & BROWN, W.L. (1997): Feldspar-fluid interactions in braid microperthites: pleated rims and vein microperthites. *Contrib. Min. Pet.* 127, 291-304.

LOISELLE, M.C. & WONES, D.R. (1979): Characteristics and origin of anorogenic granites. *Geol. Soc. Am. Abstr. Programs* 11, 468

LUDWIG, K.R. (1991): ISOPLOT; a plotting and regression program for radiogenic-isotope data; version 2.53. *U.S. Geol. Surv. Open File Report* 91-445, 39 pp.

LUGMAIR, G.W., & MARTI, K. (1978): Lunar initial $^{143}Nd/^{144}Nd$: differential evolution of the lunar crust and mantle. *Earth Planet. Sci. Lett.* 39, 349-357

MACDONALD, R., UPTON, B.G.J & THOMAS, J.E. (1972): Potassium and Fluorine-Rich Hydrous Phase coexisting with Peralkaline Granite in South Greenland.*Earth Planet. Sci. Lett.* 18, 217-222

MACDONALD, R. & UPTON, B.G.J. (1993): The Proterozoic Gardar rift zone, South Greenland: comparisons with the East African Rift System. *In:* PRICHARD, H.M., ALABASTER,T., HARRIS, N.B.W., & NEARY, C.R. (eds.): *Magmatic Processes and Plate Tectonics.* Geol. Soc. Sp. Pub. No.76, 427-442

MANNING, D.A.C. (1981): The effect of Fluorine on Liquidus Phase Relationships in the system Qz-Ab-Or with excess water at 1 kb. *Contrib. Min. Pet.* 76, 206-215

MARTIN, A.R. (1985): The evolution of the Tugtutôq-Ilímaussaq dyke swarm, Southwest Greenland. *PhD Thesis,* Edinburgh University(unpublished)

MASON, R.A. (1992): Models of order and iron-fluorine avoidance in biotite. *Canadian Mineralogist* 30, 343-354.

McDONOUGH, W.F., & SUN, S.-S. (1995): The Composition of the Earth. *Chem. Geol.* 120, 223-255

McKENZIE, D. (1985): The extraction of magma from the crust and mantle. *Earth Planet. Sci. Lett.* 74, 81-91.

McKENZIE, D. (1989): Some remarks on the movement of small melt fractions in the mantle. *Earth Planet. Sci. Lett.* 95, 53-72.

MENZIES, M. (1987): Alkaline rocks and their inclusions: a window on the Earth's interior. *In:* FITTON, J.G., & UPTON, B.G.J. (eds.): *Alkaline Igneous Rocks*. Geol. Soc. Sp. Pub. 30, 15-27

MENZIES, M.A. (1992): The lower lithosphere as a source for continental flood basalts: a re-appraisal. *In:* STOREY, B.C., ALABASTER, T., & PANKHURST, R.J. (eds.): *Magmatism and the Causes of Continental Break-up*. Geol. Soc. Sp. Pub. 68, 31-39.

MENZIES, M.A. & HALLIDAY, A. (1988): Lithospheric Mantle Domains beneath the Archaean and Proterozoic crust of Scotland. *J. Pet.* Special Lithosphere Issue, 275-302.

MIAN, I. & LE BAS, M.J. (1986): Sodic amphiboles in fenites from the Loe Shilman carbonatite complex, NW Pakistan. *Min. Mag.* 50, 187-197.

MOORBATH,S., WEBSTER, R.K. & MORGAN,J.W. (1960): Absolute Age Determinations in southwest Greenland. *Bull. Grønlands Geol. Unders.* 25 (also *Meddr. Grønland* 169, No. 9)

NAKAMURA, N. (1974): Determination of REE, Ba, Fe, Mg, Na and K in carbonaceous and ordinary chondrites. *Geochim. Cosmochim. Acta* 38, 757-775

OHMOTO, H. (1986): Stable Isotope Geochemistry of Ore Deposits. *In*: VALLEY, J.W., TAYLOR, H.P. & O'NEIL, J.R.(eds): *Stable Isotopes in high temperature geological processes*. Reviews in Mineralogy 16, 491-556.

PARSONS, I. (1978): Feldspars and fluids in cooling plutons. *Min. Mag.* 42, 1-17

PASLICK, C.R., HALLIDAY, A.N., DAVIES, G.R., MEZGER, K. & UPTON, B.G.J. (1993): Timing of Proterozoic magmatism in the Gardar Province, southern Greenland. *Geol. Soc. Am. Bull.* 105, 272-278.

PATCHETT, P.J. (1977): Rb-Sr Geochronology and Geochemistry of Proterozoic Basic Intrusions in Sweden and South Greenland. *PhD Thesis*, Edinburgh University (unpublished)

PAULY, H. (1960): Paragenetic Relations in the Main Cryolite Ore of Ivigtut, South Greenland. *N. Jb. Miner., Abh.* 94, 121-139.

PAULY, H. (1986): Chiolite in the cryolite deposit in Ivigtut, South Greenland. *In:* CRAIG et al (eds) *Mineral Parageneses*, Theophrastus Publ., S.A. Athens, Greece, 227-247

PAULY, H.(1986): Cryolithionite and Li in the Cryolite Deposit, Ivigtut, South Greenland. *Mat. fys. Meddr* 42:1 The Royal Danish Academy of Sciences and Letters.

PAULY, H. (1992): Topaz, prosopite, and closing stages of formation of the Ivigtut cryolite deposit, South Greenland. *Meddr. Grønland* 28

PAULY,H. (unpub.): Two vents from gas explosions in the Ivigtut cryolite deposit, S.Greenland.

PAULY, H.(1993): Columnar and radiating aggregates with jarlite from the Ivigtut cryolite deposit, South Greenland. *Bull. Geol. Soc. Denmark* 40, 272-279

PAULY, H. & PETERSEN, O.V. (1981): Weberite from Ivigtut, South Greenland: new data on paragenesis, twinning habit and optics. *N. Jb. Miner. Mh.* H.11, 511-519

PAULY, H. & PETERSEN, O.V. (1987): Acuminite, a new Sr-fluoride from Ivigtut, South Greenland. *N. Jb. Miner. Mh* 11,502-514

PAULY, H. & BAILEY, J.C. (in prep): The Ivigtut Cryolite Deposit.

PEARCE, J.A., HARRIS, N. B. W., & TINDLE, A.G. (1984): Trace Element Discrimination Diagrams for the tectonic interpretation of granitic rocks. *J. Pet.* 25, 956-983.

PEARCE, N.J.G, & LENG, M.J. (1996): The origin of carbonatites and related rocks from the Igaliko Dyke Swarm, Gardar Province, South Greenland: field, geochemical and C-O-Sr-Nd isotope evidence. *Lithos* 39, 21-40

PEARCE, N.J.G, LENG, M.J., EMELEUS, C.H., & BEDFORD, C.M. (1997): The origins of carbonatites and related rocks from the Grønnedal-Íka Nepheline Syenite complex, South Greenland: C-O-Sr isotope evidence. *Min. Mag.* 61, 515-529

PEUCAT, J.J., VIDAL, P., BERNARD-GRIFFITHS, J. & CONDIE, K.C. (1988): Sr, Nd and Pb isotopic systematics in the Archaean low- to high-grade transition zone of southern India: syn-accretion vs. post-accretion granulites. *J.* Geol. 97, 537-550.

POITRASSON, F., PIN, C., & DUTHOU, J.-L. (1995): Hydrothermal remobilisation of Rare Earth Elements and its effect on Nd isotopes in rhyolite and granite. *Earth Planet. Sci. Lett.* 130, 1-11

PROKOF'EV, V.Y., NAUMOV, V.B., IVANOVA, G.F. & SAVEL'EVA, N.I. (1991): Fluid Inclusion studies in cryolite and siderite of the Ivigtut Deposit (Greenland). *N. Jb. Miner. Mh.* H.1, 32-38.

RINGWOOD, A.E., KESSON, S.E., HIBBERSON, W. & WARE, N. (1992): Origin of kimberlites and related magmas. *Earth Planet. Sci. Lett.* 113, 521-538.

ROCK, N.M.S. (1987): The nature and origin of lamprophyres: an overview. *In:* FITTON, J.G., & UPTON, B.G.J. (eds.): *Alkaline Igneous Rocks.* Geol. Soc. Sp. Pub. 30, 191-226.

RYE, R.O. & OHMOTO, H. (1974): Sulfur and carbon isotopes and ore genesis. A review. *Econ. Geol.* 69, 826-842.

SAUNDERS, A.D., & TARNEY, J. (1984): Geochemical characteristics of basaltic volcanism within back-arc basins. *In:* KOKELAAR, B.P., & HOWELLS, M.F. (eds.): *Marginal Basin Geology.* Geol. Soc. Sp. Pub. 16, 59-76

SHEPPARD, S.M.F.(1986): Characterisation and Isotopic variations in natural waters. *In*: VALLEY, J.W., TAYLOR, H.P. & O'NEIL, J.R. (eds): *Stable Isotopes in high temperature geological processes.* Reviews in Mineralogy 16, 165-181

SHEPPARD, S.M.F.(1986): Igneous Rocks: III. Isotopic case studies of magmatism in Africa, Eurasia, and Oceanic Islands. *In*: VALLEY, J.W., TAYLOR, H.P. & O'NEIL, J.R. (eds): *Stable Isotopes in high temperature geological processes.* Reviews in Mineralogy 16, 319-368

SØRENSEN, H. (ed.) (1974): *The Alkaline Rocks.* 622 pp. Wiley, London

STEIGER, R.H., & JAGER, E. (1977): Subcommission on geochronology: convention of the use of decay constants in geo- and cosmochronology. *Earth Planet. Sci. Lett.* 36, 359-362

STEPHENSON, D. & UPTON, B.G.J. (1982): Ferromagnesian silicates in a differentiated alkaline complex: Kûngnât Fjeld, South Greenland. *Min. Mag.* 46, 283-300

STEVENSON, R., UPTON, B.G.J., & STEENFELT, A. (in press): Crust-Mantle interaction in the Evolution of the Ilímaussaq Complex, South Greenland: Nd isotopic studies. *Lithos*

STEWART, J.W. (1970): Precambrian alkaline-ultramafic/carbonatite volcanism at Qassiarsuk, South Greenland. *Bull. Grønlands. Geol. Unders* 84 (also *Meddr. Grønland,* 186 (4)).

SUN, S.-S., & McDONOUGH, W.F. (1989): Chemical isotopic systematics of oceanic basalts: Implications for mantle composition and processes. In: Saunders, A.D., & Norry, M.J. (eds.): *Magmatism in the Ocean Basins.* (Sp. Pub. Geol. Soc. Lon. 42), 313-345

TATSUMOTO, M., KNIGHT, R.J., & ALLEGRE, C.J. (1973): Time differences in the formation of meteorites as determined from the ratio of lead 207 to lead 206. *Science* 180, 1279-1283.

TAYLER, J.W. (1856): On the Cryolite of Evigtok, Greenland. *Proc. Geol. Soc. Lond.* 12, 140-144

TAYLOR, P.N., JONES, N.W., & MOORBATH, S. (1984): Isotopic assessment of relative contributions from crust and mantle sources to the magma genesis of Precambrian granitoid rocks. *Phil. Trans. R. Soc. Lond. Series A* 310, 605-625.

TAYLOR, P.N., & KALSBEEK, F. (1986): Pb isotopic evidence for early Archaean crust in South Greenland. In: ASHWAL, L.D. (ed.): *Early Crustal Genesis: The World's Oldest Rocks.* Lunar. Planet. Inst., Houston, Texas, Tech. Rep. 86-4, 103-106.

TAYLOR, P.N., MOORBATH, S., GOODWIN, R., & PETRYKOWSKI, A.C. (1980): Crustal contamination as an indicator of the extent of early Archaean crust: Pb isotopic evidence from the late Archaean gneisses of West Greenland. *Geochim. et Cosmochim. Acta* 44, 1437-1453

TAYLOR, P.N., & UPTON, B.G.J. (1993): Contrasting Pb isotopic compositions in two intrusive complexes of the Gardar Magmatic province of South Greenland. *Chem. Geol.* 104, 261-268

TAYLOR, R.P., STRONG, D.F., & FRYER, B.J. (1981): Volatile Control of Contrasting Trace Element Distributions in Peralkaline Granitic and Volcanic Rocks. *Contrib. Min. Pet.* 77, 267-271.

THOMPSON, R.N., MORRISON, M.A., DICKIN, A.P., & HENDRY, G.L. (1983): Continental flood basalts..... arachnids rule OK? *In:* HAWKESWORTH, C.J., & NORRY, M.J. (eds.) *Continental Basalts and Mantle Xenoliths* 158-85. Shiva.

TUTTLE, O.F., & BOWEN, N.L. (1958): Origin of granite in the light of experimental studies in the system $NaAlSi_3O_8$-$KAlSi_3O_8$-SiO_2-H_2O. *Mem. Geol. Soc. Am.* 74.

ULRYCH, T.J. (1964): The anomalous nature of Ivigtut lead. *Geochim. et Cosmochim. Acta* 28, 1389-1396.

UPTON, B.G.J (1960): The alkaline complex of Kûngnât Fjeld, South Greenland. *Bull. Grønlands Geol. Unders.* 27 (also *Meddr. Grønland*, 123).

UPTON, B.G.J. (1974): The Alkaline Province of Southwest Greenland. *In:* SØRENSEN, H. (ed.): *The Alkaline Rocks.* p. 231-238. Wiley, New York.

UPTON, B.G.J. (1991): Gardar mantle xenoliths: Igdlutalik, South Greenland. *Rapp. Grønlands Geol. Unders.* 150, 37-43.

UPTON, B.G.J. (1996): Anorthosites and Troctolites of the Gardar Magmatic Province. *In:* DEMAIFFE, D. (ed.): *Petrology and Geochemistry of magmatic suites of rocks in the continental and oceanic crusts.* Volume dedicated to Professor Jean Michot: 1996, 19-34.

UPTON, B.G.J, & BLUNDELL, D.J. (1978): The Gardar igneous province: evidence for Proterozoic continental rifting. *In:* NEUMANN, E.R. & RAMBERG, I.B. (eds.): *Petrology and Geochemistry of Continental Rifts,* 163-172. Reidel, Dordrecht.

UPTON, B.G.J. & EMELEUS, C.H. (1987): Mid-Proterozoic alkaline magmatism in southern Greenland: the Gardar province. *In*: FITTON, J.G. & UPTON, B.G.J. (eds) *Alkaline Igneous Rocks*, Geol. Soc. Sp. Pub. 30,pp. 449-471.

UPTON, B.G.J, MARTIN, A.R., & STEPHENSON, D. (1990): Evolution of the Tugtutôq Central Complex, South Greenland: a high-level, rift-axial, late-Gardar centre. *J. Volc. Geotherm. Res.* 43, 195-214.

UPTON, B.G.J, PARSONS, I., EMELEUS, C.H., & HODSON, M.E. (1996): Layered Alkaline Igneous Rocks of the Gardar Province, South Greenland. *In:* CAWTHORN, G. (ed.): *Layered Intrusions. Developments in Petrology 15*, 331-363. Elsevier Science B.V.

UPTON, B.G.J., STEPHENSON, D., & MARTIN, A.R. (1985): The Tugtutôq Older Giant Dyke Complex: mineralogy and geochemistry of an alkali gabbro-augite syenite-foyaite association in the Gardar Province of South Greenland. *Min. Mag.* 354, 623-642

UPTON, B.G.J, THOMAS, J.E. & MACDONALD, R. (1971): Chemical Variation within three Alkaline Complexes in South Greenland. *Lithos* 4, 163-184

VAN BREEMEN, O. & UPTON, B.G.J. (1972): Age of some Gardar Intrusive Complexes, South Greenland. *Geol. Soc. Am. Bull.* 83, 3381-3390

VOLL, G. (1960): Developments in petrofabrics. *Liv. & Man. Geol. J.* 2, 501-525

WARD, C.D., McARTHUR, J.M., & WALSH, J.N. (1992): Rare Earth Element behaviour during Evolution and Alteration of the Dartmoor Granite, SW England. *J. Pet.* 33, 785-815.

WEAVER, B.L., WOOD, D.A., TARNEY, J., & JORON, J.L. (1987): Geochemistry of Ocean Island Basalts from the South Atlantic: Ascension, Bouvet, St Helena, Gough and Tristan da Cunha. *In:* FITTON, J.G., & UPTON, B.G.J. (eds.): *Alkaline Igneous Rocks.* Geol. Soc. Sp. Pub. 30, 253-267.

WEDEPOHL, K.H., HEINRICHS, H., & BRIDGWATER, D. (1991): Chemical characteristics and genesis of the quartz-feldspathic rocks in the Archaean crust of Greenland. *Contrib. Min. Pet.* 107, 163-179.

WHALEN, J.B., CURRIE, K.L. & CHAPPELL, B.W. (1987): A-type Granites: geochemical characteristics, discrimination & petrogenesis. *Cont. Min. Pet.* 95, 407-419.

WHALEN, J.B., JENNER, G.A., LONGSTAFFE, F.J., ROBERT, F., & GARIEPY, C. (1996): Geochemical and Isotopic (O, Nd, Pb, and Sr) constraints on A-type granite petrogenesis based on the Topsails Igneous Suite, Newfoundland Appalachians. *J. Pet.* 37, 1463-1489.

WICKMAN, F.E. (1956): The Cycle of Carbon and the Stable Carbon Isotopes. *Geochim. Cosmochim. Acta* 28, 1389-1396

WILSON, M. (1989): Igneous Petrogenesis. *Chapman & Hall.*

WINDLEY, B.F. (1991): Early Proterozoic collision tectonics, and rapakivi granites as intrusions in an extensional thrust-thickened crust: the Ketilidian orogen, South Greenland. *Tectonophysics* 195, 1-10

WINSTANLEY, I. (1975): The Petrology of the Basic igneous Rocks of the Gardar Province, SW Greenland. *PhD Thesis,* Edinburgh University (unpublished)

WINTHER, K.T. (1992): Feldspar megacryst and anorthosite xenolith-bearing dykes in the Narssarssuaq area, South Greenland. *Rapp. Grønlands Geol. Unders.* 154, 49-59

WOOD, S.A. (1990): The aqueous geochemistry of the Rare Earth Elements and Yttrium, 2. Theoretical predictions of speciation in hydrothermal solutions to 350°C at saturation water vapor pressure. *Chem. Geol.* 88, 99-125

ZARTMAN, R.E., & HAINES, S.M. (1988): The plumbotectonic model for Pb isotope systematics among major terrestrial reservoirs - A case for bi-directional transport. *Geochim. et Cosmochim. Acta* 52, 1327-1339.

ZINDLER, A. & HART, S.R. (1986): Chemical Geodynamics. *Ann. Rev. Earth. Planet. Sci.* 14, 493-571.

Appendix A: sample list

The appendix shows the numbers of all samples used in this study, together with brief descriptions.
Coll. indicates collector of the sample:
KMG = K. Goodenough, BGJU = B. Upton, CHE = H. Emeleus, GGU = Greenland Geological Survey.
Sample location maps show the samples collected during the 1995 and 1996 fieldtrips
Types of analysis used are indicated:
T.S. denotes a thin section, P=probe data, X=XRF data, Sr=Rb-Sr isotope data,
Nd=Sm-Nd isotope data, Pb=Pb isotope data, REE = REE data, C=stable isotope data

Sample	Intrusion	Location	Description	Coll.	T.S.	P	X	Sr	Nd	Pb	REE	C
96/1	Ivigtut	Top of mine	Dark Granite	KMG	x		x					
96/2	Minor intrusive	Managers house, Ivigtut	Leuco. dyke	KMG	x							
96/3	Ivigtut	Loose block	Dark Granite	KMG	x		x	x	x	x	x	
96/4	Ivigtut	Loose block	Siderite zone	KMG								
96/6	Ivigtut	W side of mine	Foreign granite	KMG	x		x					
96/7	Ivigtut	Loose block	Albitised granite	KMG	x		x	x	x	x	x	
96/8	Bunkebreccia	Main face	Grey breccia	KMG								
96/9	Bunkebreccia	Main face	Porph. basaltic dyke	KMG	x		x					
96/10	Bunkebreccia	Main face	Blue trachytic dyke	KMG	x		x					
96/11	Bunkebreccia	E of main face	Porph. basaltic dyke	KMG	x		x					
96/12	Bunkebreccia	E of main face	Contact of basaltic dyke	KMG	x							
96/13	Ivigtut	Loose block	Granite	KMG			x					
96/14	Ivigtut	Loose block	Top granite	KMG	x		x	x				
96/15	Minor intrusive	Within Bunkebreccia	Granophyre	KMG	x		x					
96/16	Minor intrusive	Managers house, Ivigtut	Leuco dyke	KMG	x							
96/17	Brown Dyke	S Ivigtut valley	Margin, BD0	KMG	x		x					
96/18A	Minor intrusive	S Ivigtut reservoir	Granophyre	KMG	x		x	x	x		x	
96/18B	Minor intrusive	S Ivigtut reservoir	Xenolithic granophyre	KMG	x							
96/18C	Minor intrusive	S Ivigtut reservoir	Granophyre	KMG								
96/19	Gneiss	S Ivigtut reservoir	Gneiss adjacent to granophyre	KMG								
96/20	Minor intrusive	S Ivigtut reservoir	Granophyre	KMG	x		x					
96/21A	Minor intrusive	W edge Ivigtut valley	Granophyre	KMG	x		x					
96/21B	Minor intrusive	W edge Ivigtut valley	Granophyre	KMG	x		x	x	x	x	x	
96/21C	Minor intrusive	W edge Ivigtut valley	Granophyre	KMG								
96/22	Gneiss	W edge Ivigtut valley	Gneiss W of thrust	KMG	x		x					
96/23A	Minor intrusive	Bay opposite Ivigtut mine	Granophyre (margin)	KMG	x		x					
96/23B	Minor intrusive	Bay opposite Ivigtut mine	Granophyre (centre)	KMG	x		x	x	x			
96/24	Ivigtut	Top of mine	Microgranite	KMG	x							
96/25	Grønnedal-Íka	Hytteelv	U series syenite	KMG	x		x					
96/26	Grønnedal-Íka	Hytteelv	U. Series Coarse syenite	KMG	x							
96/27	Grønnedal-Íka	Radioelv	L. Series Foyaite	KMG	x		x					
96/28A	Minor intrusive	Radioelv	Composite dyke (felsitic core)	KMG	x		x					
96/28B	Minor intrusive	Radioelv	Composite dyke (near margin)	KMG								
96/28C	Minor intrusive	Radioelv	Composite dyke (basic margin	KMG	x							
96/29	Grønnedal-Íka	Radioelv	L. Series Foyaite	KMG	x		x	x	x	x	x	
96/30A	Brown Dyke	Radioelv	Gabbroic	KMG	x		x					
96/30B	Brown Dyke	Radioelv	Chilled margin	KMG								
96/31A	Minor intrusive	S of Jernhat	Fsp-phyric dyke	KMG	x		x					
96/31B	Minor intrusive	S of Jernhat	Chill of dyke	KMG								
96/32	Minor intrusive	S of Jernhat	Alkaline dyke	KMG	x		x					
96/33	Grønnedal-Íka	S of Jernhat	Carbonatite	KMG								x
96/34	Grønnedal-Íka	S of Jernhat	Microsyenite (nr. carbonatite)	KMG	x							
96/35	Grønnedal-Íka	S of Jernhat	Carbonatite	KMG	x		x				x	x
96/36	Grønnedal-Íka	Cirkus, S of 530m Pk.	Carbonatite	KMG	x		x					
96/37	Grønnedal-Íka	Cirkus, 530m Pk.	Xen. porph. sy. (matrix)	KMG	x		x				x	
96/38	Minor intrusive	Cirkus	Alkaline dyke	KMG	x							
96/39	Grønnedal-Íka	Toffelso	Pxy-rich syenite	KMG	x		x					
96/40	Grønnedal-Íka	Nedre Radioso	Microsyenite dyke	KMG	x		x					
96/41	Gneiss	Nedre Radioso	Green min. on surfaces	KMG								
96/42	Mineralised zon	Loose blocks, Blokdal.	Crocidolite zone	KMG	x							
96/42B	Mineralised zon	Loose blocks, Blokdal.	Crocidolite zone	KMG	x							
96/43A	Min. gneiss	Mineralised vn., Blokdal.	Crocidolite zone	KMG	x							
96/43B	Min. gneiss	Mineralised vn., Blokdal.	Crocidolite zone	KMG								
96/44	Min. gneiss	Mineralised vn., Blokdal.	Crocidolite zone	KMG								
96/45	Minor intrusive	Jernhat	Xenolithic dyke	KMG	x							
96/46A	Brown Dyke	Jernhat	Chill against carbonatite	KMG	x							
96/46B	Brown Dyke	Jernhat	Gabbroic, w/ calcite	KMG	x							
96/47	Grønnedal-Íka	585m Pk.	U. Series sy. nr. carbonatite	KMG	x		x					
96/48	Grønnedal-Íka	Radioelv	U. Series Foyaite	KMG	x		x					
96/49A	Minor intrusive	Radioelv	Alkaline dyke	KMG	x							

Sample	Intrusion	Location	Description	Coll.	T.S.	P	X	Sr	Nd	Pb	REE	C
96/49B	Gronnedal-Ika	Radioelv	Mafic syenite at dyke contact	KMG	x							
96/50	Minor intrusive	Rypefjeld	Pink alkaline dyke	KMG	x							
96/51A	Gneiss	Lojthanterens Elv	Gneiss contact w/ lamprophyı	KMG	x							
96/51B	Minor intrusive	Lojthanterens Elv	Carbonated lamprophyre	KMG	x							
96/51C	Minor intrusive	Lojthanterens Elv	Carbonated lamprophyre	KMG								
96/51D	Minor intrusive	Lojthanterens Elv	Carbonated lamprophyre	KMG								
96/51E	Minor intrusive	Lojthanterens Elv	Carbonated lamprophyre	KMG	x							
96/52A	Minor intrusive	S of Lojt. Elv	Basic dyke	KMG								
96/52B	Minor intrusive	S of Lojt. Elv	Lamprophyre	KMG	x							
96/52C	Minor intrusive	S of Lojt. Elv	Lamprophyre	KMG	x							x
96/53A	Minor intrusive	Lakes in plateau	Lamprophyre	KMG	x							
96/53B	Minor intrusive	Lakes in plateau	Lamprophyre	KMG	x							
96/54A	Minor intrusive	Lakes in plateau	Brecciated dyke	KMG	x		x					x
96/54B	Minor intrusive	Lakes in plateau	Brecciated dyke	KMG								
96/54C	Minor intrusive	Lakes in plateau	Brecciated dyke	KMG	x							
95/PG	Ivigtut	Loose block	Pink granite	KMG	x		x					
95/1A	Ivigtut	Bottom of mine	Dark granite	KMG	x	x	x	x	x	x	x	
95/1B	Ivigtut	Bottom of mine	Dark granite (alt. slightly)	KMG								
95/3A	Ivigtut	W side of mine	Top granite	KMG								
95/3B	Ivigtut	W side of mine	Top granite	KMG	x							
95/4	Ivigtut	W side of mine	Intrusion breccia	KMG	x							
95/6	Bunkebreccia	Main face		KMG	x							
95/6B	Bunkebreccia	Main face	Porph. basaltic dyke	KMG	x		x					
95/7	Ivigtut	W side of mine	Dark granite	KMG	x	x	x	x	x			
95/7B	Ivigtut	W side of mine	granite/int. breccia contact	KMG								
95/7C	Ivigtut	W side of mine	granite/int. breccia contact	KMG								
95/9A	Brown dyke	Hills SW of Ivigtut		KMG								
95/9B	Brown dyke	Hills SW of Ivigtut	gneiss xenolith (dyke edge)	KMG								
95/10	Brown dyke	Hills SW of Ivigtut	BD0	KMG			x					
95/11A	minor intrusive	Hills SW of Ivigtut	trachyte	KMG			x					
95/11B	minor intrusive	Hills SW of Ivigtut	trachyte	KMG	x		x					
95/11C	minor intrusive	Hills SW of Ivigtut	porph. basic dyke	KMG								
95/12A	Brown dyke	Hills SW of Ivigtut	Altered BD	KMG	x		x	x	x			
95/12B	Brown dyke	Hills SW of Ivigtut	granitic vein in BD	KMG	x							
95/12C	Brown dyke	Hills SW of Ivigtut	body of dyke (BD1)	KMG	x		x	x	x	x	x	
95/12D	Brown dyke	Hills SW of Ivigtut	marginal lamprophyre	KMG	x		x					
95/12E	Breccia	Hills SW of Ivigtut	siderite	KMG								
95/12F	Breccia	Hills SW of Ivigtut		KMG	x							x
95/13	minor intrusive	Point W of Ivigtut	lamprophyre	KMG	x		x	x	x			
95/14	minor intrusive	Point W of Ivigtut	lamprophyre	KMG								
95/15	minor intrusive	Point W of Ivigtut	basic dyke	KMG								
95/16	minor intrusive	Point W of Ivigtut	lamprophyre	KMG	x		x	x	x	x	x	
95/17	minor intrusive	Point W of Ivigtut	basic dyke	KMG								
95/18A	minor intrusive	Point W of Ivigtut	basic, trachytic texture;edge	KMG								
95/18B	minor intrusive	Point W of Ivigtut	basic, trachytic texture;cent	KMG	x		x					
95/18C	Brown dyke	Point W of Ivigtut	heavily altered	KMG	x		x					
95/19	minor intrusive	Point W of Ivigtut	pyrite? in basic dyke	KMG								
95/19B	minor intrusive	Point W of Ivigtut	central zone of basic dyke	KMG								
95/19C	minor intrusive	Point W of Ivigtut	lamprophyre	KMG			x					
95/20	minor intrusive	Point W of Ivigtut	?pyrite? in basic dyke	KMG								
95/20B	minor intrusive	Point W of Ivigtut	basic, trachytic texture	KMG								
95/22	gneiss	Point W of Ivigtut		KMG								
95/23	minor intrusive	SW Ivigtut valley	leucocratic dyke w/ sulphides	KMG	x		x					
95/24A	minor intrusive	SW Ivigtut valley	leuco dyke	KMG								
95/24B	minor intrusive	SW Ivigtut valley	most qtz rich part of dyke	KMG								
95/24C	minor intrusive	SW Ivigtut valley	contact w/ gneiss	KMG	x							
95/25A	minor intrusive	SW Ivigtut valley	granophyre	KMG	x		x					
95/25B	minor intrusive	SW Ivigtut valley	leucocratic dyke	KMG								
95/25C	minor intrusive	SW Ivigtut valley	poss. siderite? in dyke	KMG								
95/26	minor intrusive	Managers house	gneiss/meso. dyke contact	KMG	x							
95/27A	minor intrusive	Ivigtut graveyard	basic dyke	KMG								
95/27B	minor intrusive	Ivigtut graveyard	alkaline dyke	KMG								
95/28A	minor intrusive	Ivigtut graveyard	porphyritic trachyte	KMG			x					
95/28B	minor intrusive	Ivigtut graveyard	porphyritic trachyte	KMG	x							
95/29	minor intrusive	Managers house	leuco dyke	KMG	x							
95/30A	minor intrusive	Ivigtut village	alt. alkali dyke	KMG	x		x					
95/30B	minor intrusive	Ivigtut village		KMG								
95/31A	minor intrusive	Point W of Ivigtut	fairly leucocratic dyke	KMG			x					
95/31B	minor intrusive	Point W of Ivigtut	basic dyke/gneiss contact	KMG								
95/31C	minor intrusive	Point W of Ivigtut	lamprophyre	KMG			x					
95/31D	minor intrusive	Point W of Ivigtut	mesocratic dyke	KMG								
95/32	minor intrusive	Point W of Ivigtut	basic dyke	KMG								
95/33	minor intrusive	Point W of Ivigtut	lamprophyre	KMG	x		x					
95/34	minor intrusive	Point W of Ivigtut	lamprophyre	KMG								
95/34B	minor intrusive	Point W of Ivigtut	lamprophyre	KMG	x		x					

Sample	Intrusion	Location	Description	Coll.	T.S.	P	X	Sr	Nd	Pb	REE	C
95/34C	metagabbro	Point W of Ivigtut	pre Gardar	KMG			x					
95/35	minor intrusive	Point W of Ivigtut	porphyritic trachyte?	KMG								
95/37A	minor intrusive	Point W of Ivigtut	leuco dyke	KMG	x							
95/37B	minor intrusive	Point W of Ivigtut	whitish granophyre	KMG	x		x					
95/37C	minor intrusive	Point W of Ivigtut	sulphides in wht. grano.	KMG	x							
95/37D	minor intrusive	Point W of Ivigtut	basic dyke	KMG								
95/37E	minor intrusive	Point W of Ivigtut	mafic schlieren from'gran.'	KMG								
95/37F	minor intrusive	Point W of Ivigtut	mafic schlieren from'gran.'	KMG								
95/37G	gneiss	Point W of Ivigtut		KMG			minors					
95/37H	gneiss	Point W of Ivigtut		KMG	x		x					
95/38	minor intrusive	Point W of Ivigtut	leucocratic dyke w/ sulphs.	KMG								
95/39A	minor intrusive	Point W of Ivigtut	porph. trachyte	KMG	x		x					
95/39B	minor intrusive	Point W of Ivigtut	leuco dyke - granophyre?	KMG	x							
95/40A	minor intrusive	Point W of Ivigtut	mineralised dyke	KMG	x							
95/40B	minor intrusive	Point W of Ivigtut	mineralised dyke	KMG								
95/40C	minor intrusive	Point W of Ivigtut	mineralised dyke	KMG	x							
95/40D	minor intrusive	Point W of Ivigtut	fsp-phyric part of dyke	KMG	x							
95/41A	minor intrusive	Point W of Ivigtut	neph. sy. porph'	KMG	x		x					
95/41B	minor intrusive	Point W of Ivigtut	green facies of n.s.p.	KMG	x							
95/41C	minor intrusive	Point W of Ivigtut	basic dyke	KMG								
95/42	minor intrusive	Point W of Ivigtut	basic dyke	KMG			x					
95/43A	Ivigtut	Loose block	greisen	KMG								
95/43B	Ivigtut	Loose block	patchy dark granite	KMG	x		x	x	x			
95/43C	Ivigtut	Loose block	pink granite	KMG	x							
95/43D	Ivigtut	Loose block	pale granite	KMG	x							
95/43E	Ivigtut	Loose block	red fluorite in granite	KMG	x							
95/43F	Ivigtut	Loose block	greisen w/ blk. cry.	KMG	x							
95/43G	Ivigtut	Loose block	sid. cry. w/ sulphides	KMG								
95/43H	Ivigtut	Loose block	sid. cry. w/ sulphides	KMG								
95/44A	Bunkebreccia	Main face	trachyte	KMG	x							
95/44B	Bunkebreccia	Main face	Blue trachytic dyke	KMG	x							
95/44C	Bunkebreccia	Main face	Blue trachytic dyke	KMG	x							
95/44D	Bunkebreccia	Main face	Porph. basaltic dyke	KMG	x		x	x	x			
95/44E	Bunkebreccia	Main face	Grey breccia	KMG	x		x	x	x			
95/44F	Bunkebreccia	Main face	Blue trachytic dyke	KMG	x							
95/44G	Bunkebreccia	Main face	basic xenoliths	KMG	x							
95/44H	Bunkebreccia	Main face	basic xenoliths	KMG			x					
95/44J	Bunkebreccia	Main face	xenolith	KMG								
95/44K	Bunkebreccia	Main face	Blue trachytic dyke	KMG	x		majors					
95/44L	Bunkebreccia	Main face	gneissic groundmass	KMG	x		x					
95/44M	Bunkebreccia	Main face	breccia	KMG	x							
95/44N	Bunkebreccia	Main face	gneissic groundmass	KMG	x		x					
95/45	Minor intrusive	Road to Grønnedal	basic, trachytic texture	KMG			x					
95/46	Minor intrusive	Road to Grønnedal	basic, trachytic texture	KMG								
95/47	Brown Dyke	Road to Grønnedal	gabbroic	KMG			x					
95/48	Minor intrusive	Road to Grønnedal	trachyte	KMG	x		x					
95/49	Minor intrusive	Ivigtut shoreline	basic w/ sulphides	KMG			minors					
95/50A	Gneiss	Ivigtut shoreline		KMG	x		x	x	x	x		
95/51	Minor intrusive	E edge of Bunkebreccia	alt. porph. alkaline dyke	KMG	x		x	x	x			
95/52	Minor intrusive	E edge of Bunkebreccia	granophyre	KMG	x		x	x	x			
95/52B	Minor intrusive	E edge of Bunkebreccia	Blue trachyte contact	KMG	x							
95/52C	Minor intrusive	E edge of Bunkebreccia	blue trachyte	KMG								
95/53	Minor intrusive	Road to Grønnedal	basic dyke w/ bright sulphide	KMG								
95/54	Minor intrusive	SE Ivigtut valley	v. weathered dyke	KMG								
95/55	Minor intrusive	SE Ivigtut valley	trachyte	KMG	x		x					
95/56	minor intrusive	Hills E of Ivigtut	basic w/ megacrysts	KMG								
95/57	minor intrusive	Hills E of Ivigtut	trachyte	KMG	x		x	x	x			
95/58	mineralised zon	Blokdalen	siderite	KMG								x
95/58A	mineralised zon	Blokdalen	lamprophyre	KMG	x	x	x	x	x		x	
95/58B	mineralised zon	Blokdalen	granite pegmatite	KMG	x		x					
95/58C	mineralised zon	Blokdalen	inclusion w/in dyke	KMG								
95/58D	mineralised zon	Blokdalen	blue veins (crocidolite)	KMG	x	x						
95/58E	mineralised zon	Blokdalen	blue vein/dyke contact	KMG	x							
95/58F	mineralised zon	Blokdalen	brecciated blue vein	KMG	x	x						
95/59A	Kûngnât	Kûngnât Bugt	granitic sheet	KMG								
95/59B	Kûngnât	Kûngnât Bugt	granitic sheet	KMG			x					
95/59C	Kûngnât	Kûngnât Bugt	zircon peg. in granitic sheet	KMG			x					
95/60	minor intrusive	Kûngnât Bugt	lamprophyre	KMG			x					
95/62	Kûngnât	E Kûngnât	EBG Syenite	KMG	x		x	x	x	x	x	
95/63A	Kûngnât	E Kûngnât	EBG syenite	KMG	x		x					
95/63B	Kûngnât	E Kûngnât	siderite & moonsts., EBG	KMG								
95/64	Kûngnât	E Kûngnât	ring dyke gabbro	KMG	x		x	x	x	x	x	
95/66	Kûngnât	SE Kûngnât	microgranite sheet	KMG	x		x	x	x	x	x	
95/67	minor intrusive	SE Kûngnât	lamprophyre	KMG	x		x					
95/68A	Kûngnât	SE Kûngnât	late syenite sheet	KMG			x					

Sample	Intrusion	Location	Description	Coll.	T.S.	P	X	Sr	Nd	Pb	REE	C
95/68B	Kûngnât	SE Kûngnât	aplite	KMG	x		x	x	x			
95/68C	Kûngnât	SE Kûngnât	sheet/aplite contact	KMG	x							
95/70A	Kûngnât	SE Kûngnât	ring dyke gabbro	KMG								
95/70B	Kûngnât	SE Kûngnât	syenitic peg. veins in gabbro	KMG								
95/71	Kûngnât	SE Kûngnât	ELS syenite	KMG			x					
95/73	Kûngnât	Roverborg valley	Peg. vein in ELS	KMG								
95/73B	Kûngnât	Roverborg valley	ELS syenite	KMG	x		x	x	x			
95/74	Kûngnât	Roverborg valley	Gabbro lens	KMG	x		x	x	x		x	
95/75	Kûngnât	Roverborg peak	WULS	KMG	x		x	x	x	x	x	
95/76	Kûngnât	Below Roverborg wall	calcite from sy. blocks	KMG								x
95/77A	Kûngnât	Below Roverborg wall	WLLS, trough bands	KMG								
95/77B	Kûngnât	Below Roverborg wall	WLLS	KMG	x		x	x	x	x	x	
95/78	Kûngnât	River, W Kûngnât	aplite vein in WLLS	KMG								
95/79A	Kûngnât	River, W Kûngnât	microgranite sheet	KMG	x		x					
95/79B	Kûngnât	River, W Kûngnât	peg. bands in sheet	KMG			minors					
95/80	Kûngnât	River, W Kûngnât	banded late sheet	KMG	x		x	x	x		x	
95/81	Kûngnât	River, W Kûngnât	late sheet/syenite contact	KMG	x							
95/82	Kûngnât	River, W Kûngnât	WLLS	KMG								
95/83	Kûngnât	920m Peak	xenolith, 920m Pk.	KMG	x							
95/84	Kûngnât	920m Peak	lam. WLLS, 920m. Pk.	KMG			x					
95/85	Kûngnât	920m Peak	WLLS	KMG	x		x	x	x			
95/86A	Grønnedal-Íka	Jernhat	xenolithic dyke	KMG	x							
95/86B	Grønnedal-Íka	Jernhat	metasomatised BD	KMG			x					
95/86C	Grønnedal-Íka	Jernhat	dark carbonatite	KMG								
95/86D	Grønnedal-Íka	Jernhat	carbonatite	KMG	x		x					
95/86E	Grønnedal-Íka	Jernhat	coarse carbonatite	KMG								x
95/86F	Grønnedal-Íka	Jernhat	whitish carbonatite	KMG	x							
95/86G	Brown Dyke	Jernhat	altered BD	KMG	x							
95/86H	Brown Dyke	Jernhat	metasomatised dyke	KMG	x							
95/87	Brown Dyke	N of Jernhat	dolerite	KMG								
95/88	Brown Dyke	Langeso	dolerite (BD1)	KMG	x		x	x	x	x	x	
95/89A	Minor intrusive	Langeso	fsp-phyric, basic dyke	KMG			x					
95/89B	Grønnedal-Íka	Langeso	porph. syenite (v. alt)	KMG	x							
95/89C	Grønnedal-Íka	Langeso	syenite	KMG								
95/90	Minor intrusive	Skrallebunken	basic dyke	KMG								
95/91	Grønnedal-Íka	Skrallebunken	carbonated dyke rock?	KMG			x					
95/92	Grønnedal-Íka	Bryggerens Elv	U. Series coarse syenite	KMG	x		x					
95/93	Grønnedal-Íka	SE of Grønnedal	L. Series coarse brn syenite	KMG	x		x					
95/93B	Grønnedal-Íka	SE of Grønnedal	" " "	KMG								
95/94	Grønnedal-Íka	SE of Grønnedal	L. Series coarse brn syenite	KMG	x		x					
95/95	Grønnedal-Íka	SE of Grønnedal	L. Series foyaite	KMG	x							
95/96	Minor intrusive	SE of Grønnedal	green, fsp-phyric trachyte	KMG	x		x					
95/97	Grønnedal-Íka	SE of Grønnedal	unlam. syenite	KMG	x		minors					
95/98	Grønnedal-Íka	SE of Grønnedal	porphyritic syenite	KMG			x					
95/99A	Minor intrusive	Hytteelv	basic, fsp-phyric dyke	KMG								
95/99B	Minor intrusive	Hytteelv	magnetite	KMG								
95/100	Minor intrusive	Hytteelv	basic dyke	KMG	x		x					
95/101	Grønnedal-Íka	Hytteelv	coarse grey carbonatite	KMG			x					
95/102	Grønnedal-Íka	Xenolithso	carb.-impreg. rock?	KMG								
95/102E	Grønnedal-Íka	Xenolithso	carbonatite breccia	KMG	x							
95/103	Grønnedal-Íka	Xenolithso	laminated U. Series syenite	KMG	x		x	x	x	x	x	
95/104	Grønnedal-Íka	Xenolithso	xenolith'/syenite contact	KMG								
95/105	Grønnedal-Íka	Xenolithso	U. Series granular syenite	KMG	x		x					
95/106	Grønnedal-Íka	S of Xenolithso	brown syenite	KMG			x					
95/107	Grønnedal-Íka	S of Xenolithso	U. series foyaite/pulaskite	KMG								
95/108	Minor intrusive	Head of Urdal	mesocratic dyke w/ fluorite	KMG	x		x					
95/109A	Grønnedal-Íka	Head of Urdal	U. series foyaite/pulaskite	KMG	x		x					
95/109E	Grønnedal-Íka	Head of Urdal	microsyenite	KMG	x							
95/110	Grønnedal-Íka	Head of Urdal	carbonatite	KMG	x		x	x	x			
95/111	Grønnedal-Íka	E of Ovre Radioso	pyroxene-rich syenite	KMG	x		x					
95/112	Grønnedal-Íka	E of Ovre Radioso	porphyritic basalt	KMG	x							
95/113	Grønnedal-Íka	S of Jernhat	carb.-impreg. rock	KMG								
95/114	Grønnedal-Íka	S of Jernhat	porphyritic basalt	KMG			x					
95/115	Grønnedal-Íka	S of Jernhat	carbonatite breccia	KMG								
95/116	Grønnedal-Íka	Cirkus, 530m peak	U. Series foyaite/pulaskite	KMG								
95/117	Grønnedal-Íka	Cirkus, 530m peak	xenolithic' porphyritic sy.	KMG			x					
95/118	Grønnedal-Íka	Cirkus, 530m peak	xenolithic porphyritic sy.	KMG	x		x					
95/119	Grønnedal-Íka	Cirkus	U. Series foyaite/pulaskite	KMG	xx		x	x	x			
95/120	Grønnedal-Íka	Toffelso	pxy-richish syenite	KMG			x					
95/121	Grønnedal-Íka	Toffelso	pxy-rich syenite	KMG	x		x	x	x		x	
95/122	Grønnedal-Íka	Toffelso	base U. Series syenite	KMG			x					
95/123	Grønnedal-Íka	Toffelso	gneiss raft	KMG	x		x					
95/124	Grønnedal-Íka	Toffelso	U. Series syenite, nr. contact	KMG								
95/125	Grønnedal-Íka	Toffelso	porph. microsyenite	KMG	x		minors					
95/126	Grønnedal-Íka	NE of Grønnedal	L. Series foyaite	KMG			x					

Sample	Intrusion	Location	Description	Coll.	T.S.	P	X	Sr	Nd	Pb	REE	C
95/127	Grønnedal-Íka	NE of Grønnedal	L. Series foyaite	KMG	x		x	x	x	x		
95/128	Grønnedal-Íka	NE of Grønnedal	Grey, L. Series syenite	KMG			x					
81103	Kûngnât	W Kûngnât	WLLS, laminated	BGJU			x					
81108	Kûngnât	W Kûngnât	WLLS, unlaminated	BGJU	x		x					
81110	Kûngnât	W Kûngnât	WLLS, mafic horizon	BGJU	xxx		x					
81111	Kûngnât	W Kûngnât	Pegmatite	BGJU	x							
81113	Kûngnât	W Kûngnât	Veins	BGJU								
81126	Kûngnât	SE Kûngnât	Pegmatite	BGJU								x
81127	Kûngnât	SE Kûngnât	EBG syenite	BGJU	x		x					
81128	Kûngnât	SE Kûngnât	Microgranite	BGJU	x		x					
81129	Kûngnât		Ringdyke gabbro	BGJU			x					
81130	Kûngnât		Ringdyke gabbro	BGJU								
81132	Kûngnât	Roverborg	WULS	BGJU			x					
81133	Kûngnât	Roverborg	WULS	BGJU	x		x					
81134	Kûngnât	Roverborg	WULS	BGJU	x		majors					
81135	Kûngnât	Roverborg	WULS	BGJU								
81136	Kûngnât	W Kûngnât	microgranite	BGJU								
81137	Kûngnât	W Kûngnât	WULS basic inclusion	BGJU	x	x	x					
81138	Kûngnât	W Kûngnât	WULS basic inclusion	BGJU								
81139	Kûngnât	W Kûngnât	WULS basic inclusion	BGJU								
81140	Kûngnât	W Kûngnât	WULS basic inclusion	BGJU								
81142	Kûngnât	E Kûngnât	Basic inclusion	BGJU	x		x					
81143	Kûngnât	E Kûngnât	EBG syenite	BGJU			majors					
81144	Kûngnât	E Kûngnât	microgranite	BGJU	x		x					
81145	Kûngnât	E Kûngnât	EBG syenite	BGJU	x		x					
81146	Kûngnât	E Kûngnât	EBG syenite	BGJU	x							
81148	Kûngnât	E Kûngnât	Basic inclusion	BGJU	x		x					
81149	Kûngnât	SE Kûngnât	EBG syenite	BGJU								
81156	Kûngnât		syenite	BGJU								
86153	Kûngnât		granite sheet	BGJU	x							
86154	Kûngnât	W Kûngnât	Late granite	BGJU								
86157	Kûngnât	W Kûngnât	Late granite	BGJU								
86158	Kûngnât	W Kûngnât	Late granite	BGJU								
86159	Kûngnât	W Kûngnât	Late granite	BGJU								
86163	Kûngnât	W Kûngnât	Late granite	BGJU								
86164	Kûngnât	W Kûngnât	Astrophyllite granite	BGJU								
86174	Kûngnât	W Kûngnât	Riebeckite granite	BGJU	x							
86179	Kûngnât	W Kûngnât	Granite-pegmatite vein?	BGJU	x							
86180	Kûngnât	W Kûngnât	Gabbro contact	BGJU	x							
86180a	Kûngnât	W Kûngnât	Aplite granite	BGJU			x				x	
86180b	Kûngnât	W Kûngnât	Metasomatised gabbro	BGJU			x				x	
86184a	Kûngnât	W Kûngnât	Microgranite	BGJU	xx		x					
86184b	Kûngnât	W Kûngnât	Metasomatised gabbro	BGJU			x				x	
86185	Kûngnât	W Kûngnât	Peralkaline granite	BGJU	x		x				x	
86186	Kûngnât	W Kûngnât	Gabbro	BGJU	x	x	x				x	
86188	Kûngnât	W Kûngnât	WLLS	BGJU			minors					
86189	Kûngnât	W Kûngnât	Syenite	BGJU	x							
86190	Kûngnât	W Kûngnât	Late granite	BGJU			minors					
86191	Kûngnât	W Kûngnât	Gabbro/granite contact	BGJU	xxx							
86191a	Kûngnât	W Kûngnât	Aplite granite	BGJU			x				x	
86191b	Kûngnât	W Kûngnât	Metasomatised gabbro	BGJU			x				x	
86197	Kûngnât	W Kûngnât	Late granite sheet	BGJU	x							
86198	Kûngnât	W Kûngnât	Syenite	BGJU	x							
86200	Kûngnât	W Kûngnât	WLLS	BGJU			x					
58301a	Kûngnât		Ringdyke	BGJU								
58301b	Kûngnât		Ringdyke	BGJU	x		minors					
58304	Kûngnât	W Kûngnât	Astro. granite	BGJU								
58309	Kûngnât		Syenite	BGJU	xx							
26025	Kûngnât	W Kûngnât	soda granite	BGJU	x							
26094	Kûngnât	W Kûngnât	WULS	BGJU	x							
26110	Kûngnât	W Kûngnât	WULS	BGJU								
26135	Kûngnât	E Kûngnât	E.B.G. syenite	BGJU	x							
26415	Kûngnât		Layered syenite	BGJU								
26435	Kûngnât	W Kûngnât	WLLS	BGJU	x							
26443	Kûngnât	W Kûngnât	Unlam. gp. WLLS	BGJU								
26447	Kûngnât	W Kûngnât	Unlam. gp. WLLS	BGJU								
26457	Kûngnât	W Kûngnât	WLLS	BGJU	x							
27676	Kûngnât	W Kûngnât	WULS	BGJU	x							
K37	Kûngnât		Moonstone	BGJU	x							
KU12	Kûngnât		Olivine gabbro, ringdyke	BGJU	x		x					
KU15	Kûngnât		gabbro & granite contact	BGJU	x	x						
KU16	Kûngnât		Syenogabbro, ringdyke	BGJU	x		x					
10605	Kûngnât	W Kûngnât	Laminated WLLS	BGJU	x							
10624	Kûngnât	W Kûngnât	Riebeckite granite/gabbro	BGJU	x							
unno.	Kûngnât		Pyrrhotite-rich ringdyke	BGJU								

Sample	Intrusion	Location	Description	Coll.	T.S.	P	X	Sr	Nd	Pb	REE	C
KU1.92	Kûngnât	Moraine, W Kûngnât	Granitic pegmatite w/ siderite	BGJU	xxx							
KU2.92	Kûngnât	SE Kûngnât	Granitic pegmatite w/ siderite	BGJU	x							
KU5.92	Kûngnât	SE Kûngnât	Granitic pegmatite w/ siderite	BGJU	xx							
KU6.92	Kûngnât	SE Kûngnât	Granitic pegmatite w/ siderite	BGJU	xx	x						
KU7.92	Kûngnât	SE Kûngnât	Granitic pegmatite w/ siderite	BGJU	x	x						
81116	Minor intrusive	Kûngnât	Lamprophyre	BGJU	xx							
81117	Minor intrusive	Kûngnât	Chilled lamprophyre	BGJU	x							
81119	Minor intrusive	Kûngnât	Mica-rich lamprophyre	BGJU	x		x					
81120	Minor intrusive	Kûngnât	Lamprophyre contact	BGJU								
81121	Minor intrusive	Kûngnât	Lamprophyre	BGJU	x		x					
81123	Minor intrusive	Kûngnât	Lamprophyre	BGJU	x		x					
81159	Minor intrusive	Kûngnât	Lamprophyre	BGJU			x					
81162	Minor intrusive	Kûngnât	Lamprophyre	BGJU	x		minors					x
86166	Minor intrusive	Kûngnât	Lamprophyre	BGJU	x		minors					
86167	Minor intrusive	Kûngnât	Lamprophyre	BGJU	x		minors					x
86192	Minor intrusive	Kûngnât	Lamprophyre	BGJU	x		x					
81155	Minor intrusive	In Kûngnât bay	Dyke	BGJU								
81158	Minor intrusive		Dolerite dyke	BGJU								
81160	Minor intrusive		Dolerite dyke	BGJU	x							
81165	Minor intrusive	Patussoq Bay	BFD	BGJU			x					
81167	Minor intrusive	Laxelv valley	Basic dyke	BGJU			x					
86170	Minor intrusive	Patussoq Bay	Dolerite dyke contact	BGJU	x		x					
101409B	Minor intrusive	Kûngnât Bugt	Basic dyke	BGJU			x					
101414	Minor intrusive	Kûngnât Bugt	Basic dyke	BGJU			x					
104120	Minor intrusive	Tigssalup	BFD	BGJU			x					
KU11	Minor intrusive	~1km E of Kûngnât	Dolerite dyke	BGJU	x	x	x					
81141	Gneiss			BGJU			x					
KU13	Gneiss		Gabbro anorthosite	BGJU	x		x					
KU14	Gneiss		Archean grey gneiss	BGJU	x		x					
IV1	Ivigtut		Siderite-cryolite	BGJU	xxx	x						x
IV24	Ivigtut		Siderite & sulphides	BGJU								x
IV25	Ivigtut		Thomsenolite	BGJU								
IV26	Ivigtut		Thomsenolite	BGJU								
IV47	Ivigtut		Feldspar pegmatite w/ cryolit	BGJU	x							
IV50	Ivigtut		Greisen	BGJU	x							
IV52	Ivigtut		Mineralised greisen	BGJU	x							
IV53	Ivigtut		Dark porphyritic granite	BGJU	x	x	x					
IV54	Ivigtut		Porphyritic granite	BGJU	x		x					
IV55	Ivigtut		Siderite-cryolite	BGJU	x							
IV56	Ivigtut		Fluorite zone	BGJU	x							
IV57	Ivigtut		Siderite-cryolite	BGJU	x							
IV58	Ivigtut		Fluorite zone	BGJU	x							
IV59	Ivigtut		Top granite	BGJU	x		x					
IV60	Ivigtut		Altered granite	BGJU	x	x						
IV61	Ivigtut		Top granite	BGJU	x		x					
IV62	Ivigtut		Qtz-cryolite	BGJU	x							
IV63	Ivigtut		Qtz,siderite	BGJU	x	x						
IV64	Ivigtut		Granite w/ siderite bands	BGJU	x	x						
IV65	Ivigtut		Mineralised greisen	BGJU	x							
IV66	Ivigtut		Mineralised greisen	BGJU	x							
IV68	Ivigtut		Granite & fsp. pegmatite	BGJU	xx	x						
IV69	Ivigtut		Cryolite, fsp, qtz	BGJU	x							
IV71	Ivigtut		Granite w/ siderite bands	BGJU								
IV73	Ivigtut		Feldspar pegmatite	BGJU	x							
IV74	Ivigtut		Cryolite in granite	BGJU	x							
IV75	Ivigtut		Chiolite & cryolite	BGJU								
IV76	Ivigtut		Quartz zone	BGJU	x	x						
IV78	Ivigtut		Qtz-cryolite	BGJU	x							
IV79	Ivigtut		Fluorite-cryolite	BGJU	x							
IV80	Ivigtut		Fluorite zone	BGJU								
IV82	Ivigtut		Siderite-cryolite	BGJU	x	x						
IV84	Ivigtut		Qtz-cryolite	BGJU	x							
IV85	Ivigtut		Pegmatite w/ inclusion	BGJU	x	x						
IV86	Ivigtut		Altered granite?	BGJU	x							
IV87	Ivigtut		siderite	BGJU								
IV88	Ivigtut		Pegmatite	BGJU	x	x						
IV89	Ivigtut		Fluorite zone	BGJU								
IV91	Ivigtut		Sulphides & qtz	BGJU	x							
IV92	Ivigtut		Sulphides & qtz	BGJU	x							
IV93	Ivigtut		Sulphides & qtz	BGJU	x							
IV94	Ivigtut		siderite-cryolite	BGJU								
IV95	Ivigtut		Granite w/ siderite bands	BGJU	x							
IV96	Ivigtut		Feldspar pegmatite	BGJU								
IV100	Ivigtut		siderite-cryolite	BGJU								
IV101	Ivigtut		siderite-cryolite	BGJU								

Sample	Intrusion	Location	Description	Coll.	T.S.	P	X	Sr	Nd	Pb	REE	C
IV104	Ivigtut		siderite-cryolite	BGJU								
IV105	Ivigtut		siderite	BGJU								
IV106	Ivigtut		siderite	BGJU								
IV107	Ivigtut		siderite-cryolite	BGJU								
IV109	Ivigtut		cryolite & galena	BGJU								
IV110	Ivigtut		siderite-cryolite	BGJU								x
IV111	Ivigtut		siderite	BGJU								
IV113	Ivigtut		pegmatite	BGJU								
IV114	Ivigtut		banded porphyritic granite	BGJU								
IV115	Ivigtut		siderite	BGJU								
IV116	Ivigtut		dark granite	BGJU								
IV117	Ivigtut		pyrite rich	BGJU								x
IV118	Ivigtut		sulphide rich	BGJU								
IV119	Ivigtut		siderite	BGJU								
IV120	Ivigtut		veined granite	BGJU								x
J3 i)	Ivigtut	Drill core	Cryolite zone 5.69m	GGU								
J3 ii)	Ivigtut	Drill core	Fluorite zone 11.08m	GGU	x							
J3 iii)	Ivigtut	Drill core	Quartz zone 49.36m	GGU								
J3 iv)	Ivigtut	Drill core	Sid bands in qtz 54.75m	GGU	x							x
J3 v)	Ivigtut	Drill core	Quartz zone 74.8m	GGU								
J3 vi)	Ivigtut	Drill core	Greisen granite 82.1m	GGU	x	x	x					
J3 vii)	Ivigtut	Drill core	Granite 114.6m	GGU	x	x	x	x	x			
J3 viii)	Ivigtut	Drill core	Gneiss 153.14m	GGU	x	x	x	x	x	x		
J3 ix)	Ivigtut	Drill core	Gneiss 168.2m	GGU	x		x					
J4 i)	Ivigtut	Drill core	Cryolite zone 8.1m	GGU								
J4 ii)	Ivigtut	Drill core	Fluorite zone 36.1m	GGU	x							
J4 iii)	Ivigtut	Drill core	Quartz zone 62.43m	GGU								
J4 iv)	Ivigtut	Drill core	Greisen granite 88.11m	GGU	x	x	x					
J4 v)	Ivigtut	Drill core	Pink granite (alt.) 114.4m	GGU	x	x	x					
J4 vi)	Ivigtut	Drill core	Altered granite 171.5m	GGU	x	x	x	x	x		x	
J8	Ivigtut	Drill core	Siderite-cryolite 3.24m	GGU								
A	Ivigtut	Drill core	Siderite-cryolite 12.26m	GGU								
BB25 i)	Ivigtut	Drill core	Granite 805.82m	GGU	x	x	x					
BB25 ii)	Ivigtut	Drill core	Granite 793.4m	GGU	x	x	x	x	x	x	x	
BB25 iii)	Ivigtut	Drill core	Granite 781.4m	GGU	x	x	x					
BB25 iv)	Ivigtut	Drill core	Granite 629.75m	GGU	xx		x					x
BB25 v)	Ivigtut	Drill core	Granite/peg. 620.7m	GGU	xx	x	x	x	x	x		
IV 49	Grønnedal-Íka		carbonatite	BGJU								
14849	Grønnedal-Íka		carbonatite	CHE								x
101402	Minor intrusive	Jernhat	Basic dyke	BGJU			x					
Nun 1	Nunarssuit		Granite pegmatite vein	BGJU			x				x	
101433	Nunarssuit		Helene granite	BGJU			x				x	
85924	Dyrnaes		alkali granite	BGJU			x				x	
il 100	Ilimaussaq		green granite	BGJU			x				x	
101383	Bangs Havn		granite	BGJU			x				x	
40596	Tugtutoq	Central Complex		BGJU			x				x	
50260	Tugtutoq	Central Complex		BGJU			x				x	
85974	YGDC	Cuts syenogabbro	granitic vein	BGJU			x				x	
40553	OGDC	Central complex	microsyenite dyke	BGJU			x				x	

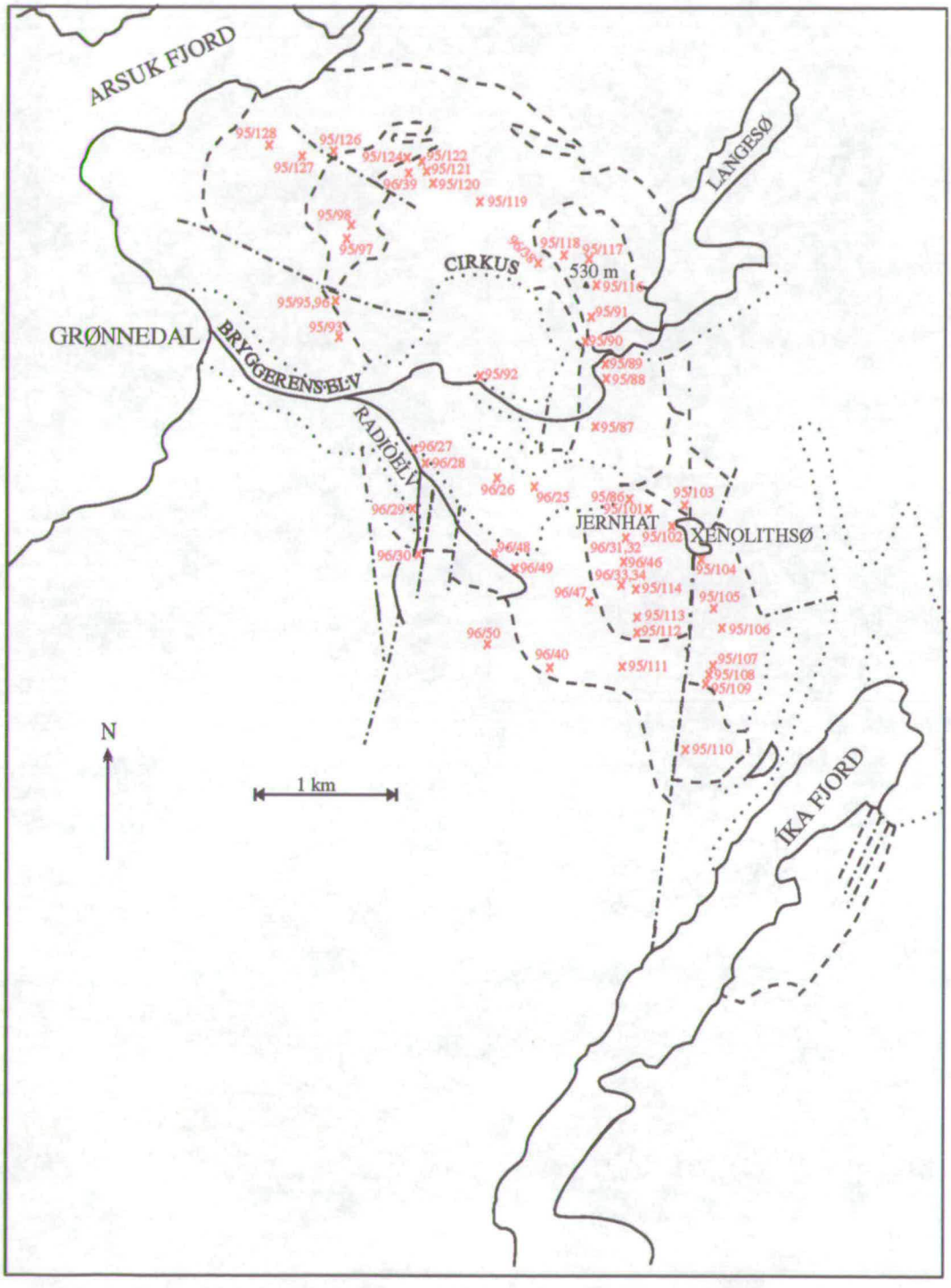

Fig. A.1: Sample location map for Grønnedal-Íka
Outlines of complex shown by dashed lines; superficial deposits by dotted lines.
Solid lines indicate geographical features. Sample locations shown in red.

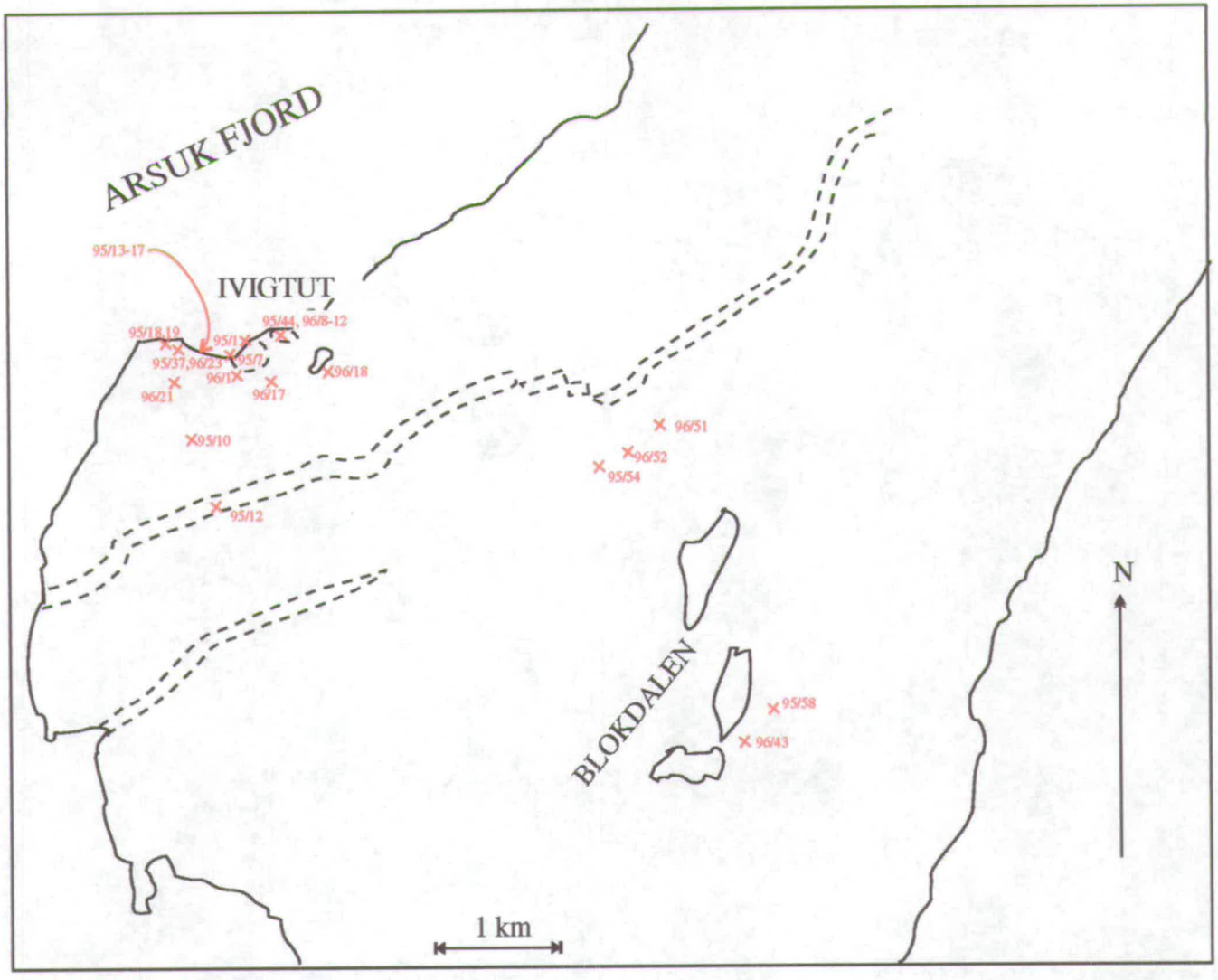

Fig. A.2: Sample location map for the Ivigtut peninsula.
Geological boundaries shown as dashed lines. Sample locations shown in red; only selected samples from Ivigtut shown due to space problems.

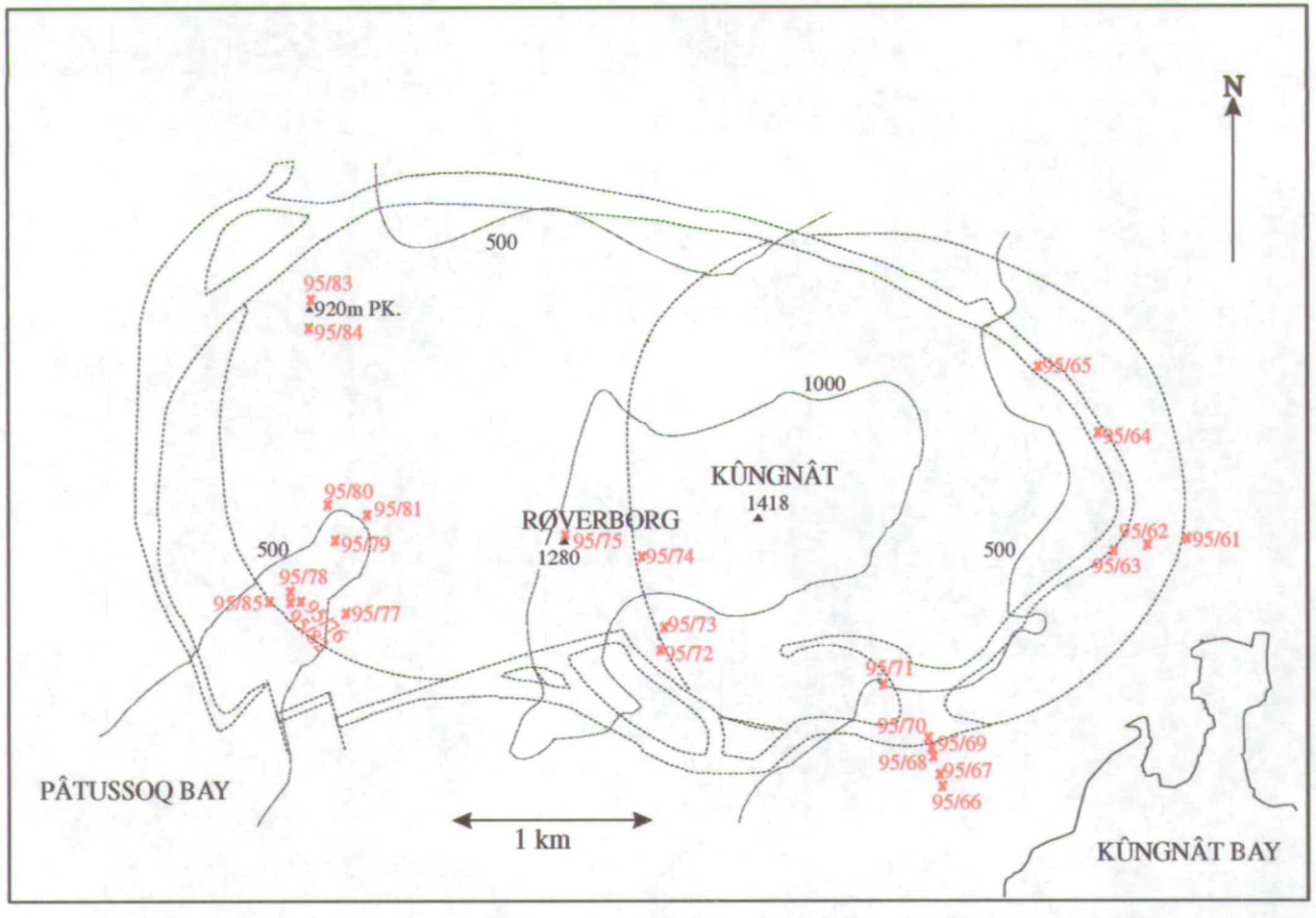

Fig. A.3: Sample location map for Kûngnât.
Outlines of major units shown by dashed lines. Solid lines are 500m contours and heights are given in metres.
Sample locations shown in red.

Appendix B: Analytical Techniques

B.1 Electron micro-probe analysis

Mineral analyses were made using the Cameca Camebax Microbeam electron probe at Edinburgh University. The Isis EDS system was used to study unusual minerals and to obtain qualitative estimates of their composition. Quantitative WDS analyses were made using an accelerating voltage of 20kV and a beam current of 20 nA, except for zircon analyses, for which a beam current of 60nA was used. Count times were 30 seconds on the peak and 10 seconds on the background.

Table B.1. Standards and crystals used.

PET = penta eurythritol, LIF = lithium fluoride, TAP = thallium acid phthalate.

Element	Standard	Crystal
Si	Wollastonite	TAP
Na	Jadeite	TAP
K	Orthoclase	PET
Fe	Metal	LIF
F	Magnesium fluoride	TAP
Al	Corundum	TAP
Ca	Wollastonite	PET
Ti	Rutile	PET/LIF
Mg	Periclase	TAP
Mn	Metal	PET/LIF
Ba	Baryte	LIF
Cl	Sodium chloride	PET
Cr	Metal	LIF
Zr	Zircon	PET
Th	Metal	PET
Y	Glass	PET
Yb	Glass	LIF
Hf	Metal	LIF

Element	Standard	Crystal
Er	Glass	LIF
Rb	$RbMnF_3$	TAP

B.2 Sawing, crushing and grinding

Approximately 50 g of material was cut from each rock sample to be analysed, using a diamond saw. The material selected was free, as far as possible, from alteration, veins and xenoliths. The cut pieces were crushed and the chips ground in a tungsten carbide barrel for 4 minutes to produce a fine powder.

B.3 XRF

Samples were analysed for major and trace elements at Edinburgh University on the Philips PW 1480 wavelength-dispersive, automatic, sequential X-Ray fluorescence spectrometer fitted with Rh anode side-window X-ray tubes. Monitors were used to update the current calibration before each batch of samples was analysed and samples were, routinely, measured once only.

Major-element analysis was carried out on fused glass discs, which were prepared as follows. Silicate rock powders were dried in an oven overnight at 110°C and approximately 1 g of each powder was measured into a Pt-5% Au crucible. The samples were then ignited for 20 minutes at 1100°C and a value for LOI (= H_2O loss + CO_2 loss - O_2 gain) was calculated from the weight change. The ignited powder was then fused for 20 minutes at 1100°C using a lithium borate flux (Johnson Matthey Spectroflux® 105) with a 5:1 (flux:sample) dilution. The molten material was poured from the crucible onto a graphite plate and pressed into a disc by lowering an aluminium

plunger onto the globule. The casting operation was carried out on a hotplate at 220°C and the glass disc allowed to anneal at this temperature for 10 minutes before cooling. Carbonatites were analysed for major elements, including as extras Sr, Ba, La, Ce and Nd, on fused glass beads made with a pure tetraborate flux (Johnson Matthey Spectroflux 100), made as follows. Batches of approx. 10 g of flux were dried overnight in a furnace at 400°C and transferred to an oven at 110°C. Rock powders were dried overnight at 110°C. Approx. 1 g of dried sample was fused in a Pt-5% Au crucible for 20 mins at 1200°C with dried flux, using a 10:1 (flux:sample) dilution. The molten material was poured from the crucible into a Pt-5% Au casting dish which had been heated over a Meker burner. The casting dish was then transferred to a hotplate at 220°C and the glass allowed to anneal at this temperature for 10 mins before cooling. Standards of suitable composition were made by the same method for calibration.

Trace element analysis was carried out on pressed pellets which were made from approximately 6g of rock powder mixed with 4 drops of binding agent (2% PVA in distilled water). The mixture was placed in a steel mould, surrounded and backed by boric acid powder, and compressed at 8 tons to form a 40 mm diameter pellet using a hydraulic press.

The spectrometer was calibrated for major- and trace-element analyses using USGS and CRPG standard samples. Calibrations were made using the concentrations given by Govindaraju (1994). Gradient, intercept, and root mean square deviation of the standards about the regression line for each element were checked for consistency between each batch of samples analysed.

Analytical lines were, in general, chosen to provide high intensity with minimal interference from other elements. Line overlap factors for trace

elements were calculated using normal standards and some synthetic glass standards. Line overlap corrections were made for Rb on Y, Sr on Zr, Y on Nb, V on Cr, Ce on Nd, Ca on Sc, V on Ti, and the back interference of Ti onV, Ti on La, and Ba on Ti.

The use of flux containing a heavy element absorber (La_2O_3) for major-element analysis produces glass discs with a relatively constant matrix composition. Linearity of major-element calibration lines was generally excellent but root mean square deviation could be improved by making matrix corrections, using theoretical alpha factors (de Jongh, 1973). Trace-element line intensities were corrected using a major-element analysis on the pressed pellet and theoretical alpha factors, or the RhKα Compton scatter peak for heavy trace elements.

Major-element data was screened by the total of the measured oxides plus LOI. The analysis of samples with totals lying outside the range 99.4 to 100.4 wt% were repeated using new glass discs to confirm the total or obtain an analysis in the expected range. In many cases, totals were low, due to high trace element concentration or likely presence of unmeasured elements such as fluorine. With each batch of samples analysed, international standards of suitable composition were included to ensure consistency between batches.

The samples analysed included some exotic, alkaline compositions which are not routinely analysed by XRF. The reproducibility of the major element measurements was checked using four repeats on one sample (J4 v))and trace element measurements were checked by analysing one pellet of the same sample five times. The results are tabulated below.

	Average	St. Dev.		Average	St. Dev.
SiO_2	64.5	0.43	Na_2O	0.51	0.23
Al_2O_3	12.65	0.09	K_2O	4.83	0.04
Fe_2O_3	2.55	0.02	TiO_2	0.029	0.002
MgO	0.21	0.04	MnO	0.014	0.003
CaO	7.82	0.05	P_2O_5	-0.005	0.016
Mo	3.92	0.10	Cu	0.18	0.82
Nb	819	1.4	Ni	0.06	0.51
Zr	2744	6.4	Cr	5.22	0.40
Y	155.6	0.5	Ce	101.5	2.6
Sr	803.2	1.3	Nd	21.66	1.52
U	63.08	0.52	La	15.20	2.01
Rb	761.5	2.1	V	4.46	0.24
Th	220.7	0.8	Ba	395.7	8.4
Pb	139.96	0.75	Sc	1.08	1.76
Zn	56.20	1.42			

B.4 REE analysis

REE analysis was carried out using the Phillips PV8050 simultaneous-sequential inductively coupled plasma-atomic emission spectrometer (ICP-AES) at Royal Holloway and Bedford New College, London. Samples were prepared as follows: 0.5 g of each sample were weighed into a Pt crucible which were then digested in a mixture of HF and $HClO_4$. The sample was dissolved in 5ml HCl and filtered with distilled H_2O. The residue and filter papers were fused with NaOH at 800°C in Ag crucibles, dissolved in HCl and combined with the filtrate. REE fractions were then separated on ion exchange columns using Dowex AG 50W x8 200-400 mesh resin, collected in 4 M HCl, and evaporated to dryness. Before being run on the ICP-AES, 5 ml 10% HNO_3 were added to the samples.

B.5 Isotope analysis

All radiogenic and stable isotope analyses were carried out at SURRC, East Kilbride.

B.5.1 Rb-Sr and Sm-Nd analysis

Samples were accurately weighed into PFA teflon screw-top beakers (Savillex®) and about 200 mg of sample were used. Samples were then dissolved using ultra-pure reagents in a HF-HNO_3-HCl digestion. The dissolved sample was accurately aliquoted (by mass) and spikes were quantitatively added by mass. The smaller (one fifth to one third) fraction was spiked with ^{145}Nd and ^{149}Sm spikes; the larger fraction was spiked with ^{87}Rb and ^{84}Sr. Rb and Sr were then separated in 2.5 M HCl using Bio-Rad AG50W x8 200-400 mesh cation exchange resin. A REE concentrate was collected by elution of 3 M HNO_3. Ba was then removed from the REE concentrate using elution of 1.5 M HNO_3 through Eichrom Industries' Sr Spec. resin. Nd and Sm were separated in a "cocktail" of acetic acid (CH_3COOH), methanol (CH_3OH) and nitric acid (HNO_3) using Bio-Rad AG1 x8 200-400 mesh anion exchange resin. Total procedure blanks for Rb, Sr, Sm and Nd were less than 0.5 ng.

In preparation for mass spectrometry, Sr samples were loaded onto single Ta filaments with 1 M phosphoric acid, Rb samples were loaded onto triple Ta filaments with ultra-pure H_2O, and Sm and Nd samples were loaded directly onto triple Ta-Re-Ta filaments with ultra-pure H_2O.

Sr samples were analysed either on a VG 54E single collector thermal ionisation mass spectrometer or a VG Sector 54-30 multiple collector mass spectrometer: both instruments were used during the course of this study.

On the 54E instrument ion beams were managed to give a total intensity of 1.5V (i.e. 1.5 x 10^{-11} A). On the Sector 54-30 a ^{88}Sr intensity of 1V (1 x 10^{-11} A) ± 10% was maintained. On both instruments, the $^{87}Sr/^{86}Sr$ ratio was corrected for mass fractionation using $^{86}Sr/^{88}Sr = 0.1194$ and an exponential law. On the VG 54E up to 6 sets of 25 ratios were collected and the mean and standard error computed until an internal precision better than ± 0.00004 (2 SE) was achieved. Repeat analysis of the NBS-987 standard gave $^{87}Sr/^{86}Sr = 0.710230 \pm 58$ (1 s.d., n=114), compared with a reference value of 0.710243. The VG Sector 54-30 mass spectrometer was operated in peak-jumping mode with data collected as 15 blocks of 10 ratios. For this instrument NBS-987 gave 0.710237 ± 10 (1 s.d., n=14). Rb samples were analysed on a VG 54E single collector mass spectrometer. 3 sets of 10 ratios were collected and the mean and standard error computed.

Sm and Nd samples were analysed on the VG Sector 54-30 instrument. $^{143}Nd/^{144}Nd$ ratios were measured with a ^{144}Nd beam of 1V (1 x 10^{-11} A). 12 blocks of 10 ratios were collected in the peak-jumping mode and corrected for mass fractionation using an exponential law and $^{146}Nd/^{144}Nd = 0.7219$. Repeat analyses of the internal laboratory standard (JM) gave $^{143}Nd/^{144}Nd = 0.511501 \pm 6$ (1 s.d., n=35) and repeats of the La Jolla standard gave 0.511851 ± 12 (1 s.d., n=47) compared with a reference value of 0.511859. Nd and Sm concentration (ID) runs were analysed as 3 blocks of 10 ratios with ion intensities of 5 x 10^{13} A for ^{143}Nd and ^{149}Sm respectively. Rb, Sr, Sm, and Nd ratios are adjusted for mass fractionation and spike contribution and concentrations calculated using adaptations of the standard algorithms of Krough & Hurley (1968).

B.5.2 Pb analysis

About 50 mg of sample were accurately weighed into PFA teflon screw-top beakers (Savillex®). The samples were then dissolved, using sub-boiling teflon-distilled reagents, in a HF-HNO_3-HCl-HBr digestion. The samples were loaded, in 1 M HBr, onto pre-cleaned 1 ml polypropylene pipette tips containing A61 x8 anion resin. 3 ml 1 M HBr and 1 ml 1.5 M HCl were eluted and Pb was collected in 2 ml 6M HCl. The procedure was repeated twice, giving total procedure blanks of less than 1 ng.

The samples were loaded onto single Re filaments using phosphoric acid (H_3PO_4) and silica gel. Analyses were carried out on the VG 54E single collector mass spectrometer with a total intensity of 1V (1×10^{-11} A). 5 blocks of 10 ratios were collected and corrected for mass fractionation using replicate analyses of NBS-981, giving a correction factor of 1.6 ‰ amu^{-1}. Repeat analyses of NBS-981 gave $^{206}Pb/^{204}Pb = 16.937$, $^{207}Pb/^{204}Pb = 15.491$, and $^{208}Pb/^{204}Pb = 36.721$, with a precision of 0.2%.

B.5.3 Stable isotope analysis

Most samples analysed for stable isotopes were carbonate or sulphide separates which had typically been picked from the rock samples as individual crystals and ground in a pestle and mortar. Some separates were drilled out from rock samples. Where the composition of the separate was uncertain, the X-Ray Diffraction (XRD) facility at Edinburgh University was used to make a check. The lamprophyre samples used were whole-rock powders.

For C- and O- isotope analysis, the carbonate samples were reacted with anhydrous phosphoric acid in vacuo overnight, at constant temperature

(25°C for calcite, 100°C for siderite). The clean CO_2 produced was separated from water vapour and purified on a vacuum line; the yield of CO_2 was measured and the gas was collected for analysis. Measurements were made on a VG SIRA II triple-collector mass spectrometer. Some samples gave a very small yield of CO_2 (<1, as compared with an expected value of 7-8) and these values were not used. The results are expressed as $\delta^{13}C$ and $\delta^{18}O$ per mil (‰) relative to the PDB and SMOW standards respectively. Overall analytical reproducibility was checked using a laboratory standard and was better than ± 0.2 ‰.

For S- isotope analysis, 5-10 mg of powdered sulphide were combusted with excess Cu_2O at ≥ 1060°C, producing SO_2. The extracted gas was purified cryogenically and analysed on the VG SIRA II triple-collector mass spectrometer. The results are presented as $\delta^{34}S$ per mil (‰) relative to the Canyon Diablo Troilite (CDT) standard. Analysis of an AgS_2 standard was used to check reproducibility and gave an error of better than ±0.2 ‰.

B.6 Data comparison

Some samples were analysed for Nd by three different methods: XRF at Edinburgh, isotope dilution (ID) at SURRC, and ICP-AES at RHBNC. The values measured by ID and ICP-AES typically agreed fairly closely with each other, but for some samples with Nd concentrations greater than about 40 ppm the concentrations measured by XRF varied from those measured by other methods by up to 20 ppm (but typically < 10 ppm). XRF data generally give slightly higher Nd concentrations than the other two methods.

The difference is based on the fact that XRF analyses are made on pressed powders, whilst the other two methods are solution-based. Where a single phase (such as zircon or apatite) concentrates particular trace elements, the

matrix correction based on the bulk rock composition may not be appropriate. This problem is acute at long wavelengths where X-ray penetration depths are not much greater than the average particle size.

Nd concentrations measured in one sample (KG95/121) by ID were much lower (~ 80 ppm) than the concentrations measured by the other two methods. This has been attributed to incomplete dissolution of the sample and therefore the Sm-Nd data for this sample have not been used in interpretation of the isotope results.

Appendix C: Isotope data calculations and presentation

C.1 Initial ratio calculation for Rb-Sr and Sm-Nd

Initial ratios for the Rb-Sr system were calculated from measured present-day ratios using the standard equations:

$$\left(\frac{^{87}Sr}{^{86}Sr}\right)_s = \left(\frac{^{87}Sr}{^{86}Sr}\right)_i + \left(\frac{^{87}Rb}{^{86}Sr}\right)_s \left(e^{\lambda t} - 1\right) \qquad [C:1]$$

where $(^{87}Sr/^{86}Sr)_s$ = strontium isotope ratio measured in the sample at the present day, $(^{87}Sr/^{86}Sr)_i$ = initial ratio, λ is the decay constant which is taken to be 1.42×10^{-11} a^{-1} (Steiger & Jager, 1977), and t is the age of the sample in years.

Similarly, for the Sm-Nd system, the equation used is:

$$\left(\frac{^{143}Nd}{^{144}Nd}\right)_s = \left(\frac{^{143}Nd}{^{144}Nd}\right)_i + \left(\frac{^{147}Sm}{^{144}Nd}\right)_s \left(e^{\lambda t} - 1\right) \qquad [C:2]$$

λ in this case is taken to be 6.54×10^{-12} a^{-1} (Lugmair & Marti, 1978).

C.2 Errorchron calculations

Slopes, initial ratios and Mean Square Weighted Deviation (MSWD) values for errorchron plots were calculated using the Isoplot program of Ludwig (1991). The MSWD value is a measure of the fit of the line within the limits of analytical error. If the line has an MSWD of <2.5 it can be deemed an isochron. For any greater value of MSWD, the line is termed an "errorchron" (Brooks *et al.* 1972). This implies that the scatter of points is due to a geological variation, i.e. the samples did not all have the same initial ratio, or the isotopes did not evolve in a closed system. This is the case for virtually all the samples in the present study. The Isoplot program allows the use of various different models. Model 1 assumes that the only cause for scatter from a straight line is analytical errors. Model 2 can be used for Pb-Pb

isochrons and does not weight the points according to the analytical errors. Model 3 can be used for Rb-Sr or Sm-Nd systems and assumes scatter to be the result of analytical errors plus a normally-distributed variation in the Y-values. This model is useful for sets of samples which may not have had the same initial ratio.

Clearly, the MSWD depends partly on the errors which are input into the program. For Rb-Sr data various different error values were used to investigate the effects on the MSWD. For instance, for the Ivigtut top granite errorchron, if the errors are set at 0.5% on $^{87}Rb/^{86}Sr$ and 0.05% on $^{87}Sr/^{86}Sr$, the MSWD obtained is 665 and the error on the age is 350 Ma. Using the absolute errors obtained from the spectrometer, which are about 0.1% on $^{87}Rb/^{86}Sr$ and 0.01% on $^{87}Sr/^{86}Sr$, the MSWD is 5810 but the error on the age is reduced to 61 Ma. Values reported in Chapter 7 use errors of 0.1% on $^{87}Rb/^{86}Sr$ and 0.01% on $^{87}Sr/^{86}Sr$. The errors used for the Sm-Nd errorchrons for Ivigtut samples are the absolute errors, which are equal to about 0.1% on $^{147}Sm/^{144}Nd$ and 0.01% on $^{143}Nd/^{144}Nd$. Errors used for Pb errorchrons are 0.1% on both $^{206}Pb/^{204}Pb$ and $^{207}Pb/^{204}Pb$.

C.3 Calculation of ε_{Nd} and Nd model ages.

The epsilon value (ε_{Nd}) is a measure of the deviation of a sample or sample suite from the expected value in a uniform reservoir and can thus be used to compare samples of different ages. ε_{Nd} for a sample for the present day is calculated as:

$$\varepsilon_{Nd} = \left\{ \left[\frac{\left(\frac{^{143}Nd}{^{144}Nd}\right)_s}{\left(\frac{^{143}Nd}{^{144}Nd}\right)_{CHUR}} \right] - 1 \right\} \times 10^4 \qquad [C:3]$$

where $(^{143}Nd/^{144}Nd)_s$ is the present day $^{143}Nd/^{144}Nd$ ratio in the sample, and $(^{143}Nd/^{144}Nd)_{CHUR}$ is the present day ratio in CHUR (CHondritic Uniform Reservoir). To calculate initial ε_{Nd}, the present day ratios are purely replaced with the calculated initial ratios. Values for CHUR at the present day are $^{143}Nd/^{144}Nd = 0.512638$ (Goldstein *et al.*, 1984) and $^{147}Sm/^{144}Nd = 0.1967$ (Jacobsen & Wasserburg, 1980).

A Nd model age should represent the length of time a sample has been separated from the mantle from which it was originally derived. In order to calculate the model age, an assumption has to be made about the isotopic composition of the original source region: there are two frequently quoted model reservoirs, CHUR and Depleted Mantle (DM). Furthermore, the model age is only valid if the sample represents a single, mantle-derived component. If any crustal contamination has taken place, the Nd model age will represent an average of the time since the crust was removed from the mantle and the time since the mantle-derived component of the sample was formed, and will not represent a geologically useful number. In situations where a depleted mantle source was enriched by volatile-rich fluids prior to separation of the sample magmas, the model age may represent a mantle enrichment age.

In the present study, model ages have been calculated relative to the DM reservoir. The equation used is:

$$T_{DM} = \frac{1}{\lambda} \ln\left[\frac{(^{143}Nd/^{144}Nd)_s - (^{143}Nd/^{144}Nd)_{DM}}{(^{147}Sm/^{144}Nd)_s - (^{147}Sm/^{144}Nd)_{DM}} + 1\right] \qquad [C:4]$$

where T_{DM} is the model age relative to depleted mantle, λ is the decay constant (6.54×10^{-12} a^{-1}), $(^{143}Nd/^{144}Nd)_s$ is the ratio in the sample at the present day and $(^{143}Nd/^{144}Nd)_{DM}$ is the ratio in the depleted mantle at the present day. Reference values for DM are: $^{143}Nd/^{144}Nd = 0.51316$ (Goldstein *et al.* 1984) and $^{147}Sm/^{144}Nd = 0.2137$ (Peucat *et al.*, 1988).

C.4 Lead isotopes: initial ratios and μ values

Initial ratios of lead isotopes at specified ages have been calculated using Pb, Th and U concentration values measured by XRF. It is known that these concentrations may have been changed by recent weathering and the initial values are therefore only approximate. Calculations were carried out using an unpublished spreadsheet written by Rob Ellam. Knowing the relative ratios of the Pb isotopes, and assuming that the $^{235}U/^{238}U$ ratio is 1/137.88, the atomic weights of the different isotopes can be calculated. These can then be used to work out present-day values for $^{238}U/^{204}Pb$, etc. and the initial ratios can be calculated using the three standard equations for the three decay schemes. These equations are of the form:

$$\left(\frac{^{207}Pb}{^{204}Pb}\right)_s = \left(\frac{^{207}Pb}{^{204}Pb}\right)_i + \left(\frac{^{238}U}{^{204}Pb}\right)_s \left(e^{\lambda t} - 1\right) \qquad [C:5]$$

which are similar to those for Rb-Sr and Sm-Nd. The decay constants for Pb are: λ_1 ($^{238}U \rightarrow ^{206}Pb$) = 1.55125 x $10^{-10}a^{-1}$, λ_2 ($^{235}U \rightarrow ^{207}Pb$) = 0.98485 x $10^{-9}a^{-1}$, λ_3 ($^{232}Th \rightarrow ^{208}Pb$) = 0.049475 x $10^{-9}a^{-1}$ (Steiger & Jager, 1977).

Apparent μ_1 and μ_2 values for the two-stage model were calculated based on the equation

$$\frac{^{206}Pb}{^{204}Pb} = a_0 + \mu_1(e^{\lambda_1 T} - e^{\lambda_1 t_1}) + \mu_2(e^{\lambda_1 t_1} - e^{\lambda_1 t_2}) \qquad [C:6]$$

where a_0 = 9.307, which is the primeval $^{206}Pb/^{204}Pb$ ratio of the Earth (Tatsumoto *et al.* 1973), T is the age of the Earth (4.57 Ga), t_1 is the time in the past when the lead was removed from the source reservoir, μ_1 is the $^{238}U/^{204}Pb$ ratio of the source reservoir, and μ_2 is the $^{238}U/^{204}Pb$ ratio of the rock. t_2 is set at 0, assuming that the Pb continued to evolve until the present day. Any

two-stage lead will lie on a secondary isochron which has a slope

$$m = \frac{1}{137.88}\left[\frac{e^{\lambda_2 t_1} - 1}{e^{\lambda_1 t_1} - 1}\right] = \frac{\left(\frac{^{207}Pb}{^{204}Pb}\right)_{t_2} - \left(\frac{^{207}Pb}{^{204}Pb}\right)_{t_1}}{\left(\frac{^{206}Pb}{^{204}Pb}\right)_{t_2} - \left(\frac{^{206}Pb}{^{204}Pb}\right)_{t_1}} \qquad [C:7]$$

The single-stage isochron for time t_1 has slope

$$m = \frac{1}{137.88}\left[\frac{e^{\lambda_2 T} - e^{\lambda_2 t_1}}{e^{\lambda_1 T} - e^{\lambda_1 t_1}}\right] = \frac{\left(\frac{^{207}Pb}{^{204}Pb}\right)_{t_1} - b_0}{\left(\frac{^{206}Pb}{^{204}Pb}\right)_{t_1} - a_0} \qquad [C:8]$$

where a_0 is the primeval $^{206}Pb/^{204}Pb$ ratio of the Earth and b_0 is the primeval $^{207}Pb/^{204}Pb$ ratio. If t_1 is set at 1.2 Ga for the Gardar, the slopes of the two isochrons can be calculated and the resulting equations solved simultaneously for the Pb isotope ratios at time t_1. Values for μ_1 and μ_2 can then be calculated from the standard equations of radioactive decay.

Models with three or more stages cannot be solved by such simple methods, but the parameters presented in this study for the three-stage model were obtained from a graphical model program written by Tom Andersen (in press).

Appendix D: Representative electron probe data

Amphiboles, Ivigtut

Analysis no.	95/1A(1)	95/1A(2)	95/1A(3)	95/1A(4)	95/1A(5)	95/1A(6)
SiO_2	39.88	40.08	39.79	40.04	44.42	42.29
Al_2O_3	7.13	7.07	7.12	7.14	3.71	5.22
Na_2O	2.80	2.91	2.97	3.06	2.01	2.71
K_2O	1.29	1.31	1.29	1.29	1.06	1.98
FeO	32.03	31.94	32.40	32.14	34.47	33.23
MgO	1.48	1.50	1.49	1.41	1.81	1.98
TiO_2	1.94	2.07	1.86	2.00	0.65	1.26
Ca_2O	9.81	9.94	9.88	9.76	8.11	7.63
Ba_2O	0.05	0.02	0.05	0.02	0.05	0.01
MnO	0.54	0.58	0.55	0.50	0.58	0.51
F	0.35	0.46	0.47	0.68	0.16	0.69
Cl	0.46	0.48	0.47	0.48	0.20	0.24
Total	97.76	98.35	98.33	98.52	97.24	97.73

Na-feldspars, Ivigtut

Analysis no.	95/1A(7)	IV 53(1)	95/7(1)	BB25 I(1)	J4 VI(1)	BB25 II(1)
SiO_2	70.59	67.71	67.82	67.99	68.29	68.31
Al_2O_3	20.39	19.23	19.40	18.91	19.37	19.16
Na_2O	7.24	10.99	11.87	11.90	11.71	11.65
K_2O	0.10	1.03	0.14	0.04	0.06	0.05
FeO	0.26	0.28	0.16	0.38	0.37	0.45
MgO	0.01	0.02	0.01	0.02	0.01	0.01
TiO_2	0.01	0.00	0.00	0.01	0.00	0.00
Ca_2O	0.01	0.33	0.07	0.01	0.01	0.00
Ba_2O	0.00	0.07	0.07	0.00	0.03	0.03
MnO	0.02	0.00	0.00	0.00	0.01	0.02
F	0.10	0.59	0.00	0.00	0.00	0.00
Cl	0.00	0.00	0.00	0.00	0.00	0.00
Total	98.74	100.25	99.55	99.26	99.85	99.69

K-feldspars, Ivigtut

Analysis no.	95/1A(8)	IV 53(2)	95/7(2)	BB25 I(2)	BB25 II(2)
SiO_2	65.54	63.36	64.16	64.17	64.05
Al_2O_3	18.16	17.75	18.04	18.17	18.19
Na_2O	0.37	0.56	0.23	0.24	0.26
K_2O	14.97	15.75	16.32	16.33	16.16
FeO	0.18	0.08	0.09	0.02	0.07
MgO	0.02	0.01	0.00	0.00	0.01
TiO_2	0.06	0.00	0.00	0.00	0.01
Ca_2O	0.01	0.00	0.00	0.01	0.00
Ba_2O	0.10	0.33	0.06	0.04	0.03
MnO	0.01	0.00	0.03	0.02	0.02
F	0.00	0.02	0.00	0.00	0.08
Cl	0.00	0.07	0.05	0.00	0.00
Total	99.42	97.92	98.98	98.99	98.88

	Biotites, Ivigtut					
Analysis no.	95/1A(9)	95/1A(10)	95/1A(11)	IV 53(3)	IV 53(4)	IV 53(5)
SiO_2	34.77	35.10	36.30	34.17	34.09	35.37
Al_2O_3	8.95	10.76	10.13	9.64	9.45	9.96
Na_2O	0.06	0.09	0.11	0.04	0.03	0.02
K_2O	8.74	8.52	8.01	8.56	8.84	8.82
FeO	36.86	35.12	38.06	37.43	36.31	37.02
MgO	1.59	1.66	0.96	2.08	1.56	1.45
TiO_2	3.29	3.56	3.27	2.50	3.54	3.35
Ca_2O	0.17	0.05	0.14	0.10	0.04	0.02
Ba_2O	0.08	0.06	0.11	0.01	0.10	0.06
MnO	0.19	0.12	0.22	0.17	0.20	0.21
F	0.31	0.29	0.24	0.83	0.96	0.89
Cl	0.36	0.36	0.37	0.32	0.53	0.40
Total	95.37	95.68	97.92	95.86	95.65	97.56

	Biotites, Ivigtut		
Analysis no.	95/7(3)	95/7(4)	95/7(5)
SiO_2	37.53	35.54	39.82
Al_2O_3	10.52	10.07	10.85
Na_2O	0.03	0.03	0.11
K_2O	8.71	8.61	8.91
FeO	35.42	35.74	33.22
MgO	2.17	2.11	2.10
TiO_2	1.00	0.99	1.95
Ca_2O	0.01	0.03	0.16
Ba_2O	0.09	0.17	0.01
MnO	0.15	0.17	0.15
F	2.59	2.84	2.68
Cl	0.19	0.18	0.17
Total	98.40	96.49	100.13

	Zinnwaldites, Ivigtut					
Analysis no.	J4 VI(2)	J4 VI(3)	J4 VI(4)	J4 VI(5)	J4 VI(6)	J4 VI(7)
SiO_2	38.85	38.83	39.11	39.23	39.90	40.28
Al_2O_3	7.25	7.65	7.79	7.99	8.29	8.32
Na_2O	0.08	0.08	0.11	0.07	0.05	0.08
K_2O	8.54	8.70	8.73	8.83	8.90	8.78
FeO	35.47	35.49	34.91	34.15	32.77	33.16
MgO	0.01	0.02	0.00	0.01	0.01	0.01
TiO_2	0.78	0.70	0.63	0.70	0.64	0.57
Ca_2O	0.00	0.00	0.01	0.00	0.01	0.02
Ba_2O	0.00	0.09	0.00	0.05	0.09	0.00
MnO	0.28	0.29	0.29	0.23	0.24	0.22
F	3.78	3.47	3.58	3.55	3.17	3.92
Cl	0.03	0.05	0.06	0.05	0.05	0.05
Total	95.06	95.35	95.22	94.84	94.11	95.39

Zinnwaldites, Ivigtut

Analysis no.	BB25 II(3)	BB25 II(4)	BB25 II(5)	BB25 II(6)	BB25 II(7)	J3 VII(1)
SiO_2	41.46	41.82	40.88	40.52	40.07	40.06
Al_2O_3	7.82	7.72	7.35	7.52	6.72	8.72
Na_2O	0.09	0.11	0.08	0.09	0.05	0.08
K_2O	9.17	9.02	9.00	8.96	8.97	8.91
FeO	29.59	29.62	31.19	31.72	33.04	33.03
MgO	0.20	0.20	0.22	0.19	0.14	0.04
TiO_2	1.03	0.91	0.95	1.27	1.05	0.74
Ca_2O	0.00	0.00	0.00	0.01	0.01	0.06
Ba_2O	0.06	0.00	0.01	0.06	0.00	0.00
MnO	0.13	0.16	0.15	0.12	0.16	0.05
F	4.43	4.92	3.51	3.48	1.58	2.05
Cl	0.02	0.02	0.03	0.03		
Total	94.00	94.49	93.35	93.96	91.80	93.72

Phengites, Ivigtut

Analysis no.	J4 VI(8)	J4 VI(9)	J4 VI(10)	J4 VI(11)	J4 VI(12)	J4 VI(13)
SiO_2	55.71	55.02	56.51	55.64	55.72	56.87
Al_2O_3	14.76	15.13	14.97	15.60	14.87	14.80
Na_2O	0.07	0.07	0.05	0.05	0.06	0.07
K_2O	10.91	10.98	10.54	10.67	10.58	11.00
FeO	5.24	6.28	6.57	5.37	5.08	4.98
MgO	0.02	0.03	0.02	0.00	0.01	0.01
TiO_2	0.09	0.20	0.54	0.13	0.21	0.04
Ca_2O	0.01	0.00	0.00	0.00	0.00	0.00
Ba_2O	0.00	0.04	0.00	0.00	0.03	0.00
MnO	0.06	0.06	0.04	0.06	0.04	0.04
F	8.27	8.81	9.07	9.17	9.36	9.22
Cl	0.00	0.02	0.01	0.01	0.00	0.00
Total	95.13	96.62	98.30	96.70	95.98	97.03

Phengites, Ivigtut

Analysis no.	BB25 II(8)	BB25 II(9)	J3 VII(2)
SiO_2	57.44	54.95	54.31
Al_2O_3	13.67	15.79	17.25
Na_2O	0.05	0.04	0.04
K_2O	10.63	10.74	10.47
FeO	4.13	4.96	6.66
MgO	0.05	0.02	0.01
TiO_2	0.15	0.02	0.00
Ca_2O	0.00	0.00	0.02
Ba_2O	0.08	0.08	0.01
MnO	0.01	0.05	0.02
F	8.61	8.43	6.11
Cl	0.00	0.01	
Total	94.82	95.09	94.91

	Mg-riebeckite, mineralised zone					
Analysis no.	95/58D(1)	95/58D(2)	95/58D(3)	95/58D(4)	95/58D(5)	95/58D(6)
SiO_2	54.19	55.43	54.97	54.22	55.04	55.12
Al_2O_3	0.26	0.12	0.16	0.54	0.16	0.11
Na_2O	7.51	8.41	7.71	7.29	8.18	8.66
K_2O	0.27	0.75	3.20	1.20	2.71	2.62
FeO	20.59	16.42	17.07	16.16	16.16	14.85
MgO	11.75	14.14	11.69	13.14	12.75	13.85
TiO_2	0.83	0.22	0.67	2.26	1.24	1.00
Ca_2O	0.61	0.30	0.05	0.22	0.05	0.03
Ba_2O	0.08	0.00	0.05	0.09	0.12	0.00
MnO	0.05	0.01	0.05	0.05	0.05	0.02
F	0.40	1.12	1.88	0.74	1.85	2.09
Cl	0.00	0.01	0.01	0.00	0.00	0.00
Total	96.53	96.94	97.50	95.92	98.29	98.35

	Mg-riebeckite, mineralised zone					
Analysis no.	95/58D(7)	95/58D(8)	95/58D(9)	95/58D(10)	95/58F(1)	95/58F(2)
SiO_2	55.29	55.46	54.86	55.17	55.28	55.56
Al_2O_3	0.15	0.31	0.27	0.18	0.43	0.45
Na_2O	8.47	8.80	7.62	9.00	7.66	7.55
K_2O	0.68	1.65	0.44	2.87	1.24	0.28
FeO	16.03	15.47	18.54	14.55	14.23	17.83
MgO	14.25	13.46	12.78	12.60	14.42	13.22
TiO_2	0.39	0.70	0.49	1.66	1.98	0.51
Ca_2O	0.25	0.23	0.80	0.02	0.21	0.32
Ba_2O	0.00	0.00	0.00	0.00	0.04	0.02
MnO	0.02	0.01	0.08	0.02	0.04	0.05
F	1.17	1.49	0.62	3.16	0.47	0.27
Cl	0.01	0.00	0.00	0.00	0.01	0.00
Total	96.73	97.56	96.50	99.23	96.02	96.06

	Mg-riebeckite, mineralised zone			
Analysis no.	95/58F(3)	95/58F(4)	95/58F(5)	95/58F(6)
SiO_2	55.03	54.73	54.27	55.26
Al_2O_3	0.43	0.32	0.82	0.55
Na_2O	7.13	7.59	6.43	6.27
K_2O	0.85	1.34	0.65	0.36
FeO	15.58	15.52	15.77	13.80
MgO	14.18	12.81	13.57	15.74
TiO_2	1.66	2.72	1.26	0.58
Ca_2O	0.62	0.49	2.37	2.48
Ba_2O	0.10	0.08	0.00	0.00
MnO	0.12	0.05	0.12	0.14
F	0.32	0.25	0.15	0.42
Cl	0.02	0.00	0.03	0.01
Total	96.03	95.89	95.44	95.61

Biotites, mineralised zone

Analysis no.	95/58D(11)	95/58D(12)	95/58D(13)	95/58A(1)	95/58A(2)	95/58A(3)
SiO_2	35.05	34.92	36.95	37.02	36.43	36.31
Al_2O_3	12.65	11.91	11.31	14.24	14.60	14.48
Na_2O	0.54	0.18	0.23	0.43	0.53	0.51
K_2O	8.66	8.18	9.34	9.14	9.16	9.23
FeO	19.69	20.73	20.93	9.44	9.24	9.85
MgO	11.58	10.58	11.78	19.88	19.50	19.35
TiO_2	6.13	5.60	4.69	3.65	4.52	3.98
Ca_2O	0.06	1.38	0.04	0.11	0.02	0.13
Ba_2O	1.14	1.98	0.16	0.68	1.18	0.93
MnO	0.13	0.11	0.11	0.12	0.10	0.11
F	0.47	0.45	0.47	0.37	0.48	0.37
Cl	0.01	0.01	0.01	0.00	0.01	0.00
Total	96.09	96.02	96.01	95.09	95.76	95.25

Clinopyroxenes, mineralised zone

Analysis no.	95/58F(7)	95/58F(8)	95/58F(9)	95/58F(10)	95/58A(4)	95/58A(5)
SiO_2	49.90	52.33	50.50	48.40	50.56	50.31
Al_2O_3	2.62	1.46	2.05	3.82	1.96	2.30
Na_2O	0.49	2.73	3.36	0.53	0.35	0.42
K_2O	0.01	0.34	0.53	0.01	0.02	0.05
FeO	7.94	15.36	19.54	6.80	5.57	5.88
MgO	15.77	14.68	11.70	14.62	14.48	14.34
TiO_2	1.77	0.46	1.22	2.13	1.41	1.57
Ca_2O	19.87	7.93	7.51	21.45	24.41	24.35
Ba_2O	0.07	0.01	0.00	0.08	0.08	0.07
MnO	0.18	0.45	0.42	0.12	0.15	0.17
F	0.00	0.10	0.04	0.00	0.00	0.00
Cl	0.00	0.04	0.06	0.01	0.00	0.00
Total	98.62	95.88	96.93	97.97	99.00	99.45

Zircons, Ivigtut

Analysis no.	J4 V(1)	J4 V(2)	J4 V(3)	J4 V(4)	J4 V(5)	J4 V(6)
SiO_2	32.14	32.212	31.061	31.272	31.216	31.926
ZrO_2	63.997	64.848	60.913	59.357	62.241	61.925
HfO_2	3.084	1.819	4.399	5.668	2.783	3.643
FeO	0.03	0.098	0.122	0.082	0.92	0.028
Al_2O_3	0.009	0.047	0.037	0.074	0.109	0.008
CaO	0.026	0.062	0.653	0.061	0.215	0.085
Y_2O_3	0.2	0.257	0.435	1.04	0.165	0.869
Yb_2O_3	0.376	0.336	0.52	0.383	0.261	0.55
Er_2O_3				0.287	0.144	0.273
ThO_2	0.019	0.055	0.105	0.53	0.039	0.406
Total	99.881	99.734	98.245	98.754	98.093	99.713

Zircons, Ivigtut

Analysis no.	95/1A(12)	95/1A(13)	95/1A(14)	95/1A(15)	IV 60(1)	IV 60(2)
SiO_2	32.48	32.17	32.21	31.887	31.514	31.86
ZrO_2	61	61.087	64.274	63.553	64.226	63.806
HfO_2	1.372	2.211	1.489	1.809	3.389	3.145
FeO	0.987	1.911	0.515	0.943		
Al_2O_3	0.001	0.009	0.01	0.079		
CaO	0.061	0.103	0.078	0.145		
Y_2O_3	1.029	0.494	0.899	0.305	0.037	0.062
Yb_2O_3	0.233	0.107	0.196	0.163		
Er_2O_3	0.17	0.114				
ThO_2	0.137	0.032	0.079	0.106	0.107	0.096
Total	97.47	98.238	99.75	98.99	99.273	98.969

Appendix E: Geochemical data

Sample type	*Lamprophyre*	*Lamprophyre*	*Lamprophyre*	*Lamprophyre*	*Lamprophyre*	*Lamprophyre*
Sample number	95/12D	95/13	95/16	95/19C	95/31C	95/33
Major elements (wt%)						
SiO_2	35.53	41.67	35.58	35.68	37.70	33.70
Al_2O_3	6.13	8.63	8.11	8.67	11.79	7.88
Fe_2O_3	14.90	14.79	17.86	15.17	19.38	17.80
MgO	14.64	14.23	10.58	12.00	12.87	8.75
CaO	9.81	9.54	11.77	10.28	4.72	13.77
Na_2O	1.55	1.10	1.47	0.92	0.20	1.52
K_2O	1.71	2.33	2.64	4.89	0.02	2.60
TiO_2	3.73	3.27	5.11	3.22	4.51	4.49
MnO	0.18	0.22	0.27	0.23	0.20	0.26
P_2O_5	0.57	0.37	0.83	0.66	0.50	1.02
SUM	88.75	96.14	94.22	91.72	91.89	91.80
Loss on Ignition	10.54	3.89	4.83	7.93	7.40	6.87
TOTAL	99.29	100.03	99.05	99.65	99.29	98.67
Norms						
Qz	0.0	0.0	0.0	0.0	0.2	0.0
Co	0.0	0.0	0.0	0.0	4.5	0.0
Or	0.0	14.5	0.0	0.0	0.1	0.0
Ab	0.0	2.1	0.0	0.0	1.9	0.0
An	5.4	12.4	8.3	5.6	22.4	7.8
Lc	9.1	0.0	13.2	25.1	0.0	13.3
Ne	8.1	4.2	7.3	4.7	0.0	7.7
Ac	0.0	0.0	0.0	0.0	0.0	0.0
Di	32.9	28.2	25.8	9.8	0.0	20.8
Hy	0.0	0.0	0.0	0.0	55.9	0.0
Ol	30.0	28.1	23.7	32.6	0.0	23.5
La	1.6	0.0	5.3	10.5	0.0	10.9
Mt	3.4	3.1	3.8	3.3	4.3	3.9
Il	8.1	6.5	10.5	6.8	9.5	9.5
Ap	1.5	0.9	2.1	1.7	1.3	2.6
Trace elements (ppm)						
Rb	55.9	176.9	104.0	439.2	2.9	219.4
Ba	572.7	380.9	916.2	682.6	-16.0	872.6
Th	7.7	7.0	11.6	8.0	9.1	18.6
U						
Mo						
Ta						
Nb	59.2	52.9	135.2	70.7	75.4	123.9
La	25.4	17.0	59.7	40.1	23.3	72.1
Ce	74.8	70.2	141.0	103.0	83.3	187.0
Sr	695.4	255.2	798.9	359.8	37.5	892.6
Nd	38.3	40.0	83.1	53.6	50.1	102.6
Hf						
Zr	231.2	247.8	525.0	244.0	333.9	329.6
Y	21.2	24.6	34.3	29.1	45.9	37.0
Pb	9.8	5.7	5.3	2.9	9.0	7.8
Zn	122.0	148.4	160.6	107.4	123.9	210.8
Cu	128.2	106.7	119.3	23.4	70.5	132.8
Ni	644.3	573.4	288.1	421.6	603.3	239.4
Cr	530.0	758.3	256.5	600.1	945.6	1496.5
V	258.3	287.1	313.0	292.1	347.6	378.0
Sc	19.9	24.4	15.9	24.2	35.6	29.4
Ga						
Sn						

Sample type	*Lamprophyre*	*Lamprophyre*	*Lamprophyre*	*Lamprophyre*	*Lamprophyre*	*Lamprophyre*
Sample number	95/34B	95/58A	95/67	96/52C	96/54A	81119
Major elements (wt%)						
SiO_2	38.07	33.65	42.36	28.16	35.30	35.13
Al_2O_3	6.92	9.53	12.26	6.28	9.82	9.66
Fe_2O_3	18.48	18.96	15.80	18.36	13.85	17.26
MgO	14.66	8.52	9.08	12.03	9.00	9.33
CaO	8.51	11.93	9.27	10.75	9.39	11.82
Na_2O	0.28	2.16	3.33	0.24	2.05	2.07
K_2O	2.27	2.71	1.52	3.34	0.87	3.16
TiO_2	5.20	5.53	3.54	4.15	2.41	6.00
MnO	0.18	0.22	0.20	0.28	0.21	0.23
P_2O_5	0.52	1.06	0.76	1.81	0.35	0.80
SUM	95.09	94.27	98.12	85.41	83.25	95.46
Loss on Ignition	4.32	4.99	1.76	13.10	16.25	3.85
TOTAL	99.41	99.26	99.88	98.51	99.50	99.31
Norms						
Qz	0.0	0.0	0.0	0.0	0.0	0.0
Co	0.0	0.0	0.0	0.0	0.0	0.0
Or	14.4	0.0	9.3	0.0	6.3	0.0
Ab	1.2	0.0	11.3	0.0	5.3	0.0
An	11.7	9.0	14.5	7.4	18.3	8.2
Lc	0.0	13.5	0.0	17.0	0.0	15.6
Ne	0.8	10.7	9.6	1.3	8.6	10.1
Ac	0.0	0.0	0.0	0.0	0.0	0.0
Di	24.1	17.2	22.8	0.0	29.1	19.3
Hy	0.0	0.0	0.0	0.0	0.0	0.0
Ol	32.2	23.4	20.4	41.4	22.5	21.3
Ln	0.0	8.2	0.0	13.0	0.0	7.7
Mt	3.9	4.1	3.2	4.4	3.4	3.7
Il	10.6	11.3	7.0	9.4	5.6	12.1
Ap	1.3	2.7	1.8	5.0	1.0	2.0
Trace elements (ppm)						
Rb	240.7	93.4	44.7		30.1	115.1
Ba	515.9	2515.1	601.8		256.8	1306.1
Th	10.5	18.3	8.6		3.9	11.8
U						
Mo						
Ta						
Nb	90.8	169.0	73.9		38.7	125.9
La	14.8	84.6	44.8		28.6	48.4
Ce	71.0	183.9	102.0		63.0	131.2
Sr	85.5	769.3	784.9		361.2	1202.7
Nd	39.6	98.1	52.6		36.4	71.5
Hf						
Zr	307.6	605.2	310.7		177.0	462.4
Y	24.3	37.9	30.6		22.3	36.6
Pb	2.8	3.4	13.7		5.3	5.9
Zn	82.5	180.8	159.7		160.1	135.1
Cu	162.0	62.2	73.8		37.8	97.8
Ni	520.5	75.0	239.6		346.2	155.6
Cr	591.4	55.2	364.9		483.4	188.6
V	341.2	310.5	247.4		269.4	393.3
Sc	26.0	24.3	21.4		27.1	24.3
Ga						
Sn						

Sample type	*Lamprophyre*	*Lamprophyre*	*Lamprophyre*	*Lamprophyre*	*Basaltic dyke*
Sample number	81121	81123	81159	86192	95/6B
Major elements (wt%)					
SiO_2	45.00	40.49	37.59	36.17	49.37
Al_2O_3	15.39	10.15	9.83	9.52	16.20
Fe_2O_3	12.33	16.90	17.88	18.77	12.85
MgO	6.83	9.04	8.78	11.03	2.52
CaO	3.78	9.89	9.95	10.03	5.86
Na_2O	3.83	3.04	2.70	1.58	4.83
K_2O	2.89	2.23	1.67	3.50	3.27
TiO_2	3.93	4.33	6.68	5.63	2.16
MnO	0.20	0.20	0.20	0.26	0.15
P_2O_5	0.52	0.63	0.41	0.61	1.42
SUM	94.70	96.90	95.68	97.10	98.63
Loss on Ignition	4.58	2.51	3.71	2.13	1.10
TOTAL	99.28	99.41	99.39	99.23	99.73
Norms					
Qz	0.0	0.0	0.0	0.0	0.0
Co	0.4	0.0	0.0	0.0	0.0
Or	18.3	13.8	10.5	0.0	19.8
Ab	29.1	1.0	0.8	0.0	33.0
An	16.4	7.8	10.4	9.0	13.2
Lc	0.0	0.0	0.0	17.0	0.0
Ne	3.0	14.1	12.7	7.6	4.8
Ac	0.0	0.0	0.0	0.0	0.0
Di	0.0	32.1	31.9	18.3	6.0
Hy	0.0	0.0	0.0	0.0	0.0
Ol	21.0	17.5	15.5	26.5	13.0
La	0.0	0.0	0.0	5.1	0.0
Mt	2.6	3.5	3.8	3.9	2.6
Il	8.0	8.6	13.5	11.2	4.2
Ap	1.3	1.5	1.0	1.5	3.4
Trace elements (ppm)					
Rb	73.4	75.2	53.7	112.6	412.3
Ba	1470.4	761.7	872.7	1218.2	1394.4
Th	5.2	8.9	7.3	12.1	3.7
U					
Mo					
Ta					
Nb	170.3	82.6	92.7	169.2	53.6
La	17.6	35.9	19.8	45.0	37.7
Ce	55.0	102.0	82.0	139.0	107.8
Sr	454.9	865.7	653.5	1401.9	806.8
Nd	32.0	52.8	45.0	67.8	57.0
Hf					
Zr	934.1	352.2	357.9	484.6	237.5
Y	23.7	30.7	25.3	36.5	31.7
Pb	4.3	4.7	3.8	19.2	106.6
Zn	161.0	162.9	100.0	155.5	177.0
Cu	11.1	98.0	69.6	94.5	22.6
Ni	118.7	230.8	144.5	220.1	3.1
Cr	373.6	244.3	248.4	214.8	0.0
V	247.0	254.5	353.2	351.5	44.6
Sc	23.4	18.5	25.0	23.1	15.9
Ga					
Sn					

Sample type	*Basaltic dyke*	*Altered dyke*	*Basaltic dyke*	*Basaltic dyke*	*Basaltic dyke*	*Basaltic dyke*
Sample number	95/10	95/12A	95/12C	95/18B	95/18C	95/42
Major elements (wt%)						
SiO_2	48.93	59.83	47.97	41.74	44.04	45.25
Al_2O_3	13.80	18.81	17.86	14.44	14.87	14.98
Fe_2O_3	15.89	3.22	13.10	17.23	15.84	12.58
MgO	4.38	0.85	7.31	5.39	4.43	9.81
CaO	7.58	4.71	8.97	7.15	7.72	9.34
Na_2O	3.51	9.61	3.19	2.61	3.86	1.81
K_2O	1.17	0.08	0.45	3.44	1.21	1.95
TiO_2	3.18	0.42	1.40	4.76	4.14	1.31
MnO	0.20	0.13	0.18	0.21	0.20	0.24
P_2O_5	0.65	0.15	0.17	1.21	1.11	0.16
SUM	99.29	97.81	100.59	98.18	97.42	97.42
Loss on Ignition	0.00	4.18	-0.29	1.12	2.18	2.04
TOTAL	99.29	101.99	100.30	99.30	99.60	99.46
Norms						
Qz	0.0		0.0	0.0	0.0	0.0
Co	0.0		0.0	0.0	0.0	0.0
Or	7.1		2.7	21.0	7.5	11.9
Ab	30.3		27.1	11.8	29.9	13.7
An	18.8		33.3	18.1	20.5	28.0
Lc	0.0		0.0	0.0	0.0	0.0
Ne	0.0		0.0	6.0	2.2	1.2
Ac	0.0		0.0	0.0	0.0	0.0
Di	12.8		8.5	8.6	9.9	15.5
Hy	17.2		4.4	0.0	0.0	0.0
Ol	2.9		18.4	18.7	15.9	24.2
La	0.0		0.0	0.0	0.0	0.0
Mt	3.2		2.6	3.5	3.3	2.6
Il	6.2		2.7	9.4	8.2	2.6
Ap	1.5		0.4	2.9	2.7	0.4
Trace elements (ppm)						
Rb	23.4	0.6	5.5	181.9	42.4	229.1
Ba	630.0	225.2	206.3	468.7	619.8	244.1
Th	6.6	29.1	3.1	5.1	4.6	2.0
U		1.2				
Mo		1.5				
Ta						
Nb	16.5	39.5	6.8	19.7	23.8	6.0
La	28.3	226.5	0.8	12.7	15.0	6.1
Ce	77.8	348.4	27.4	40.3	59.0	29.3
Sr	299.1	873.5	393.2	479.1	526.1	186.9
Nd	45.7	119.7	14.8	28.6	39.3	17.2
Hf						
Zr	345.4	54.1	91.6	172.0	211.9	88.5
Y	49.1	56.6	20.1	35.9	39.6	26.7
Pb	7.1	19.7	1.7	1.8	1.7	17.1
Zn	144.9	40.8	94.5	114.5	83.3	144.2
Cu	46.0	1.7	60.2	67.3	51.1	108.0
Ni	36.5	3.7	102.5	68.4	53.5	185.0
Cr	41.5	1.9	73.2	34.6	25.7	322.6
V	212.1	29.0	154.2	149.4	107.0	302.3
Sc	28.2	0.0	21.3	20.6	19.3	46.4
Ga						
Sn						

Sample type	*Basaltic dyke*	*Basaltic dyke*	*Basaltic dyke*	*Basaltic dyke*	*Basaltic dyke*	*Altered dyke*
Sample number	95/44D	95/45	95/47	95/49	95/60	95/86B
Major elements (wt%)						
SiO_2	49.57	48.06	48.51		46.01	37.84
Al_2O_3	16.18	13.82	13.53		7.42	15.38
Fe_2O_3	12.47	15.94	16.34		12.87	15.93
MgO	2.64	4.44	4.67		24.61	2.78
CaO	6.39	6.13	7.52		6.31	20.41
Na_2O	4.63	3.27	3.45		0.30	0.17
K_2O	3.07	1.32	1.17		0.09	0.03
TiO_2	2.18	3.19	3.22		0.07	1.07
MnO	0.15	0.18	0.21		0.20	0.26
P_2O_5	1.49	0.71	0.75		0.01	0.85
SUM	98.78	97.06	99.36		97.89	94.71
Loss on Ignition	0.76	2.39	0.03		2.09	2.33
TOTAL	99.54	99.45	99.39		99.98	97.04
Norms						
Qz	0.0	0.4	0.0		0.0	0.0
Co	0.0	0.0	0.0		0.0	0.0
Or	18.6	8.1	7.1		0.5	0.0
Ab	34.1	28.9	29.8		2.6	0.0
An	14.6	20.0	18.4		19.3	44.1
Lc	0.0	0.0	0.0		0.0	0.1
Ne	3.3	0.0	0.0		0.0	0.8
Ac	0.0	0.0	0.0		0.0	0.0
Di	6.6	5.8	12.4		10.4	30.8
Hy	0.0	25.4	17.0		34.8	0.0
Ol	12.5	0.0	4.2		29.6	9.6
La	0.0	0.0	0.0		0.0	7.0
Mt	2.5	3.3	3.3		2.6	3.4
Il	4.2	6.3	6.2		0.1	2.2
Ap	3.5	1.7	1.8		0.0	2.1
Trace elements (ppm)						
Rb	224.1	60.3	40.6	312.6	1.5	-11.7
Ba	1682.3	540.5	613.8	332.0	7.0	109.3
Th	3.5	6.6	5.3	4.8	4.2	19.4
U						
Mo						10.5
Ta						
Nb	51.4	16.1	16.3	17.7	0.5	234.6
La	45.1	31.4	35.0	27.3	-0.2	261.0
Ce	101.0	79.0	79.0	92.6	1.5	485.7
Sr	890.2	303.5	296.0	263.0	8.8	19838.5
Nd	57.2	46.6	45.3	50.0	-2.4	191.0
Hf						
Zr	240.0	321.5	322.6	331.3	4.2	226.3
Y	31.5	46.7	47.2	51.2	2.9	71.4
Pb	28.2	7.9	6.0	6.1	4.9	8.6
Zn	87.3	154.7	151.1	95.3	151.2	69.1
Cu	21.3	50.4	48.1	163.0	7.7	24.8
Ni	3.2	42.9	37.9	34.9	824.3	23.8
Cr	-0.8	65.1	58.0	67.0	167.6	3.9
V	45.8	223.0	214.7	236.2	37.7	59.1
Sc	13.4	32.6	28.4	33.3	13.1	7.9
Ga						
Sn						

Sample type	*Basaltic dyke*	*Basaltic dyke*	*Altered dyke*	*Basaltic dyke*	*Basaltic dyke*	*Basaltic dyke*
Sample number	95/88	95/89A	95/91	95/100	95/114	96/9
Major elements (wt%)						
SiO_2	47.49	49.73	40.04	42.75	51.38	49.01
Al_2O_3	17.62	14.65	11.42	17.36	15.45	15.63
Fe_2O_3	13.12	11.91	24.96	12.34	11.47	13.00
MgO	7.17	3.63	0.98	5.70	3.58	2.78
CaO	9.26	7.39	7.04	7.04	6.75	6.24
Na_2O	3.11	6.07	5.17	3.61	4.57	4.73
K_2O	0.42	1.02	2.18	1.83	1.52	3.19
TiO_2	1.57	1.81	0.08	1.77	1.90	2.26
MnO	0.18	0.36	0.59	0.16	0.17	0.16
P_2O_5	0.18	0.58	0.37	0.24	0.52	1.52
SUM	100.12	97.15	92.82	92.80	97.31	98.52
Loss on Ignition	-0.52	1.90	5.83	6.24	2.39	0.69
TOTAL	99.60	99.05	98.65	99.04	99.70	99.21
Norms						
Qz	0.0	0.0	0.0	0.0	0.0	0.0
Co	0.0	0.0	0.0	0.0	0.0	0.0
Or	2.5	6.3	14.2	11.8	9.3	19.3
Ab	26.6	37.7	6.1	18.6	40.2	32.2
An	33.2	10.1	1.7	28.1	17.8	12.3
Lc	0.0	0.0	0.0	0.0	0.0	0.0
Ne	0.0	8.5	22.8	8.0	0.0	4.8
Ac	0.0	0.0	0.0	0.0	0.0	0.0
Di	9.9	20.2	30.2	6.9	11.2	7.9
Hy	3.7	0.0	0.0	0.0	7.7	0.0
Ol	18.0	9.8	18.4	19.8	6.4	12.8
La	0.0	0.0	0.0	0.0	0.0	0.0
Mt	2.6	2.5	5.5	2.7	2.4	2.7
Il	3.0	3.6	0.2	3.7	3.7	4.4
Ap	0.4	1.4	0.9	0.6	1.3	3.6
Trace elements (ppm)						
Rb	6.1	36.5	143.7	137.1	40.5	186.7
Ba	192.0	940.2	787.0	1619.8	951.3	1824.2
Th	4.0	6.6	15.1	2.8	4.7	4.9
U						
Mo						
Ta						
Nb	8.3	64.2	328.9	15.4	15.7	54.3
La	8.3	84.5	266.1	15.6	44.0	40.6
Ce	30.0	178.4	559.7	34.5	101.0	90.0
Sr	383.2	1175.9	2065.5	1080.9	640.6	804.4
Nd	14.8	94.1	315.2	20.2	55.2	47.7
Hf						
Zr	105.9	313.1	131.9	135.0	280.2	263.3
Y	23.5	47.4	67.0	28.3	33.5	35.0
Pb	1.9	7.7	14.2	14.1	5.9	10.6
Zn	97.8	132.7	887.3	140.8	119.4	79.9
Cu	66.6	25.5	17.6	63.6	36.9	28.9
Ni	100.7	34.3	1.8	129.0	37.2	7.7
Cr	89.3	32.5	-14.0	155.7	38.1	0.0
V	176.3	172.6	20.7	233.2	185.5	54.0
Sc	24.9	22.6	0.1	33.1	23.1	16.8
Ga						
Sn						

Sample type	*Basaltic dyke*	*Basaltic dyke*	*Basaltic dyke*	*Basaltic dyke*	*Basaltic dyke*	*Basaltic dyke*
Sample number	96/11	96/17	96/30A	81165	81167	86170
Major elements (wt%)						
SiO_2	49.57	45.86	46.73	50.19	48.30	43.00
Al_2O_3	15.91	19.00	18.89	15.48	14.23	12.79
Fe_2O_3	12.83	10.97	11.15	12.95	15.65	14.57
MgO	2.48	8.19	7.50	4.76	5.42	9.83
CaO	5.71	8.87	9.17	7.93	7.93	9.51
Na_2O	4.84	2.87	3.06	3.55	3.63	2.79
K_2O	3.36	0.44	0.87	1.03	1.01	0.93
TiO_2	2.14	0.85	1.03	2.03	3.02	2.95
MnO	0.13	0.14	0.15	0.18	0.20	0.19
P_2O_5	1.41	0.17	0.12	0.53	0.53	0.24
SUM	98.38	97.36	98.67	98.63	99.91	96.79
Loss on Ignition	1.01	2.36	1.05	1.38	-0.15	2.98
TOTAL	99.39	99.72	99.72	100.01	99.76	99.77
Norms						
Qz	0.0	0.0	0.0	0.0	0.0	0.0
Co	0.0	0.0	0.0	0.0	0.0	0.0
Or	20.4	2.7	5.3	6.2	6.0	5.8
Ab	33.5	25.2	23.6	30.8	31.2	14.8
An	12.1	39.1	36.1	23.9	19.9	20.6
Lc	0.0	0.0	0.0	0.0	0.0	0.0
Ne	4.7	0.0	1.6	0.0	0.0	5.4
Ac	0.0	0.0	0.0	0.0	0.0	0.0
Di	6.4	4.4	7.9	10.8	13.8	22.2
Hy	0.0	1.6	0.0	18.7	7.5	0.0
Ol	12.8	22.7	21.0	1.8	11.4	21.9
Ln	0.0	0.0	0.0	0.0	0.0	0.0
Mt	2.6	2.3	2.3	2.6	3.2	3.0
Il	4.2	1.7	2.0	4.0	5.8	5.9
Ap	3.4	0.4	0.3	1.3	1.2	0.6
Trace elements (ppm)						
Rb	212.7	44.3	12.7	15.5	21.1	18.0
Ba	1844.6	120.1	221.3	783.5	539.8	200.8
Th	5.6	3.6	3.5	2.8	6.9	6.9
U						
Mo						
Ta						
Nb	54.5	3.7	9.2	12.5	12.0	19.5
La	38.2	9.4	5.9	26.2	28.3	12.7
Ce	98.7	19.5	24.3	73.5	66.6	53.2
Sr	738.5	350.0	514.4	545.1	327.0	459.2
Nd	55.1	11.6	12.0	41.7	37.0	28.6
Hf						
Zr	262.3	77.0	78.2	213.6	249.6	178.7
Y	33.3	13.7	15.7	32.5	38.2	21.6
Pb	18.8	7.0	2.4	5.6	6.2	4.4
Zn	116.0	85.6	77.3	131.2	135.6	109.0
Cu	32.5	20.8	39.6	43.6	43.8	83.2
Ni	6.0	163.7	122.8	46.0	46.0	277.7
Cr	0.0	43.4	75.6	37.3	84.7	447.6
V	46.1	78.3	123.8	203.9	216.5	306.4
Sc	14.5	12.6	16.9	20.0	26.1	23.5
Ga						
Sn						

Sample type	*Basaltic dyke*	*Basaltic dyke*	*Basaltic dyke*	*Basaltic dyke*	*Basaltic dyke*
Sample number	101402	101409B	101414ho	101420	KU11
Major elements (wt%)					
SiO_2	44.28	48.43	54.24	53.09	48.66
Al_2O_3	10.68	16.57	13.21	17.42	13.92
Fe_2O_3	11.14	13.31	10.89	9.42	16.05
MgO	11.50	2.99	8.51	1.90	4.92
CaO	9.59	4.49	7.36	5.88	7.49
Na_2O	2.29	5.95	2.96	4.40	3.60
K_2O	1.52	2.29	0.51	2.25	1.02
TiO_2	1.62	2.46	1.00	1.99	3.02
MnO	0.16	0.13	0.14	0.13	0.20
P_2O_5	0.67	0.66	0.08	0.60	0.73
SUM	93.45	97.29	98.90	97.08	99.61
Loss on Ignition	5.74	1.86	1.33	2.30	0.24
TOTAL	99.19	99.15	100.23	99.38	99.85
Norms					
Qz	0.0	0.0	4.2	1.9	0.0
Co	0.0	0.0	0.0	0.0	0.0
Or	9.7	14.1	3.1	13.8	6.2
Ab	16.8	35.7	25.6	38.7	31.0
An	15.6	12.2	21.7	22.0	19.1
Lc	0.0	0.0	0.0	0.0	0.0
Ne	2.3	9.0	0.0	0.0	0.0
Ac	0.0	0.0	0.0	0.0	0.0
Di	25.1	5.4	12.3	3.6	11.6
Hy	0.0	0.0	28.8	12.8	15.2
Ol	23.2	14.3	0.0	0.0	6.1
La	0.0	0.0	0.0	0.0	0.0
Mt	2.4	2.8	2.2	1.9	3.3
Il	3.3	4.9	1.9	3.9	5.8
Ap	1.7	1.6	0.2	1.4	1.7
Trace elements (ppm)					
Rb	74.4	43.7	12.8	114.0	22.8
Ba	2885.9	1518.5	133.9	954.0	608.4
Th	4.8	6.3	2.6	2.1	6.1
U					
Mo					
Ta					
Nb	47.9	63.1	5.4	27.0	15.2
La	35.8	44.2	3.3	49.1	27.4
Ce	78.2	107.5	10.5	104.2	70.8
Sr	1449.6	1775.2	314.6	920.4	301.8
Nd	42.0	60.0	7.3	46.7	38.8
Hf					
Zr	172.4	318.4	53.5	266.3	304.8
Y	20.4	14.5	11.7	26.1	48.9
Pb	2.4	5.8	2.4	8.9	7.5
Zn	104.4	180.0	104.7	123.6	144.8
Cu	70.1	28.7	50.0	24.6	46.2
Ni	349.0	9.4	210.1	11.9	45.1
Cr	463.0	0.4	389.0	5.7	58.9
V	193.7	57.5	154.3	126.1	200.7
Sc	17.7	3.6	19.7	13.7	24.6
Ga					
Sn					

Sample type	*Alkaline dyke*	*Alkaline dyke*	*Alkaline dyke*	*Alkaline dyke*	*Alkaline dyke*	*Alkaline dyke*
Sample number	95/11A	95/11B	95/23	95/28A	95/30A	95/31A
Major elements (wt%)						
SiO_2	60.61	58.17	56.28	55.08	56.43	57.80
Al_2O_3	18.38	20.70	19.53	21.39	22.51	20.16
Fe_2O_3	7.25	7.49	8.82	7.49	5.80	5.77
MgO	0.06	0.05	0.17	0.17	0.34	1.00
CaO	0.14	0.09	0.45	1.08	0.87	0.19
Na_2O	8.22	6.97	5.24	3.69	5.85	4.74
K_2O	3.78	4.22	7.18	8.20	4.60	7.58
TiO_2	0.09	0.02	0.12	0.02	0.02	0.08
MnO	0.15	0.31	0.23	0.21	0.18	0.08
P_2O_5	0.14	0.10	0.22	0.10	0.15	0.05
SUM	98.82	98.12	98.24	97.41	96.74	97.46
Loss on Ignition	1.13	1.85	1.50	2.40	1.62	2.33
TOTAL	99.95	99.97	99.74	99.81	98.36	99.79
Norms						
Qz	0.0	0.0	0.0	0.0	0.0	0.0
Co	0.8	4.8	2.9	4.9	6.9	4.1
Or	22.8	25.6	43.5	50.0	28.2	46.2
Ab	62.9	59.3	35.7	28.1	51.4	38.6
An	0.0	0.0	0.8	4.9	3.5	0.6
Lc	0.0	0.0	0.0	0.0	0.0	0.0
Ne	4.3	0.6	5.3	2.3	0.0	1.5
Ac	0.0	0.0	0.0	0.0	0.0	0.0
Di	0.0	0.0	0.0	0.0	0.0	0.0
Hy	0.0	0.0	0.0	0.0	7.1	0.0
Ol	6.4	6.9	8.0	7.0	0.5	6.8
La	0.0	0.0	0.0	0.0	0.0	0.0
Mt	2.5	2.6	3.0	2.6	2.0	2.0
Il	0.2	0.0	0.2	0.1	0.0	0.2
Ap	0.3	0.2	0.5	0.2	0.4	0.1
Trace elements (ppm)						
Rb	135.4	200.1	443.2	611.8	377.3	239.8
Ba	487.0	256.6	157.7	238.7	247.5	462.1
Th	26.1	29.6	24.2	19.1	41.7	27.6
U	11.9	10.5	8.2		7.8	14.7
Mo	2.1	2.7	6.1		7.2	1.5
Ta						
Nb	395.5	504.3	235.3	240.7	810.1	308.8
La	199.7	92.8	160.9	174.3	79.8	183.1
Ce	453.8	210.4	285.5	318.2	194.9	351.2
Sr	104.4	39.3	160.0	121.8	139.8	79.4
Nd	136.7	73.6	103.4	128.9	72.8	122.5
Hf						
Zr	1539.9	2037.7	922.0	1173.1	3397.6	839.4
Y	60.4	47.1	61.1	72.3	40.5	43.0
Pb	22.1	28.3	157.0	18.1	19.6	13.1
Zn	110.2	352.8	949.8	118.0	197.3	48.8
Cu	9.7	5.5	63.8	24.5	4.2	4.9
Ni	0.4	1.9	2.8	2.5	2.4	2.6
Cr	0.9	0.7	0.5	-10.8	2.5	0.8
V	4.8	6.2	4.3	6.7	9.7	18.0
Sc	0.1	-0.5	1.1	-4.1	-0.6	0.7
Ga						
Sn						

Sample type	*Alkaline dyke*	*Alkaline dyke*	*Alkaline dyke*	*Alkaline dyke*	*Alkaline dyke*	*Alkaline dyke*
Sample number	95/39A	95/44K	95/48	95/51	95/55	95/57
Major elements (wt%)						
SiO_2	58.03	60.27	58.07	59.96	67.86	58.11
Al_2O_3	15.87	15.84	21.05	15.67	14.79	20.33
Fe_2O_3	10.55	7.14	5.47	7.88	4.76	6.55
MgO	0.21	0.57	0.10	0.71	0.01	0.12
CaO	1.58	3.45	0.14	3.15	0.31	0.06
Na_2O	7.04	6.45	6.84	6.13	6.60	4.95
K_2O	3.20	3.52	5.05	3.61	4.24	7.01
TiO_2	0.54	0.65	0.01	0.75	0.19	0.36
MnO	0.06	0.10	0.12	0.10	0.03	0.20
P_2O_5	0.15	0.24	0.01	0.32	0.01	0.10
SUM	97.23	98.22	96.86	98.29	98.79	97.79
Loss on Ignition	2.16	1.12	2.80	1.00	0.87	2.10
TOTAL	99.39	99.34	99.66	99.29	99.66	99.89
Norms						
Qz	0.0	1.2	0.0	2.2	11.4	0.0
Co	0.0	0.0	4.3	0.0	0.0	4.7
Or	19.6	21.3	31.0	21.9	25.6	42.6
Ab	61.3	55.9	53.7	53.1	53.8	43.1
An	2.3	4.0	0.7	4.7	0.0	0.0
Lc	0.0	0.0	0.0	0.0	0.0	0.0
Ne	0.3	0.0	3.4	0.0	0.0	0.0
Ac	0.0	0.0	0.0	0.0	2.3	0.0
Di	4.2	10.4	0.0	8.0	1.4	0.0
Hy	0.0	3.1	0.0	5.3	5.2	3.7
Ol	7.2	0.0	5.1	0.0	0.0	2.8
La	0.0	0.0	0.0	0.0	0.0	0.0
Mt	3.7	2.5	1.9	2.7	0.1	2.3
Il	1.1	1.3	0.0	1.5	0.4	0.7
Ap	0.4	0.6	0.0	0.8	0.0	0.2
Trace elements (ppm)						
Rb	119.1		438.9	187.9	486.7	208.0
Ba	294.6		137.9	730.7	47.5	243.5
Th	15.3		24.4	16.7	43.0	24.3
U				5.8		18.9
Mo				2.0		10.2
Ta						
Nb	136.9		738.2	143.8	804.0	373.4
La	84.1		18.1	143.4	273.0	29.3
Ce	166.0		106.3	283.8	493.1	122.8
Sr	124.4		27.2	154.8	16.3	181.5
Nd	83.6		41.4	133.1	174.5	42.9
Hf						
Zr	644.3		3726.1	816.3	2734.1	1538.4
Y	54.6		19.8	68.0	156.9	41.4
Pb	7.4		7.9	27.5	56.4	13.2
Zn	33.2		51.2	99.8	142.9	177.5
Cu	1245.8		23.8	21.0	-4.4	2.3
Ni	1.6		3.6	3.2	2.7	2.4
Cr	-7.1		-2.8	1.6	-16.4	2.0
V	3.3		13.4	10.2	3.4	23.4
Sc	6.9		-3.1	5.6	-3.1	-1.4
Ga						
Sn						

Sample type	*Alkaline dyke*	*Alkaline dyke*	*Alkaline dyke*	*Alkaline dyke*	*Alkaline dyke*
Sample number	95/96	95/108	96/10	96/28A	96/32
Major elements (wt%)					
SiO_2	62.70	53.19	60.36	53.76	57.24
Al_2O_3	16.49	19.04	16.69	20.67	20.71
Fe_2O_3	6.12	6.24	7.31	3.56	6.59
MgO	0.00	0.01	0.60	0.00	0.01
CaO	0.29	1.60	2.92	0.36	0.16
Na_2O	9.04	9.53	6.42	11.66	4.52
K_2O	3.99	5.13	3.97	4.33	8.19
TiO_2	0.21	0.03	0.66	0.02	0.03
MnO	0.15	0.24	0.10	0.23	0.23
P_2O_5	0.02	0.04	0.24	0.00	0.03
SUM	99.02	95.05	99.26	94.59	97.71
Loss on Ignition	0.61	4.35	0.74	4.36	1.73
TOTAL	99.63	99.40	100.00	98.95	99.44
Norms					
Qz	0.0	0.0	0.0	0.0	0.0
Co	0.0	0.0	0.0	0.0	4.3
Or	24.2	32.5	23.8	27.3	49.8
Ab	62.0	24.1	55.0	32.2	34.1
An	0.0	0.0	5.1	0.0	0.6
Lc	0.0	0.0	0.0	0.0	0.0
Ne	1.2	27.1	0.0	30.1	2.9
Ac	3.1	3.3	0.0	1.9	0.0
Di	1.2	7.4	7.0	1.7	0.0
Hy	0.0	0.0	4.4	0.0	0.0
Ol	5.6	3.9	0.4	3.4	6.0
La	0.0	0.0	0.0	0.0	0.0
Mt	0.0	0.0	2.5	0.0	2.3
Il	0.4	0.1	1.3	0.0	0.1
Ap	0.1	0.1	0.6	0.0	0.1
Trace elements (ppm)					
Rb	174.6	231.0	220.6	410.8	375.6
Ba	12.6	12.3	549.1	22.8	629.1
Th	40.6	18.9	12.4	38.2	15.5
U	13.2	8.2			
Mo	6.0	4.3			
Ta					
Nb	463.8	413.5	146.4	619.8	420.2
La	374.0	250.3	144.7	103.1	31.9
Ce	718.4	512.4	282.8	309.9	123.3
Sr	45.6	198.6	150.2	35.5	202.1
Nd	277.6	207.0	131.4	141.8	249.0
Hf					
Zr	2203.4	1826.1	809.4	3419.9	1714.3
Y	151.1	73.2	75.4	134.5	83.2
Pb	51.5	32.6	65.4	59.3	21.7
Zn	405.5	343.0	168.9	501.3	451.8
Cu	-0.4	-0.7	28.3	0.0	2.6
Ni	4.1	2.0	9.0	8.4	5.8
Cr	-0.8	1.9	0.0	0.0	0.0
V	1.6	2.4	11.4	3.3	5.5
Sc	0.2	-3.3	3.6	0.0	0.0
Ga					
Sn					

	Kûngnât	Kûngnât	Kûngnât	Kûngnât	Kûngnât	Kûngnât
Sample type	*Gabbro*	*Gabbro*	*Gabbro*	*Gabbro*	*Gabbro*	*Gabbro*
Sample number	95/64	95/74	81129	KU12	KU16	86186
Major elements (wt%)						
SiO_2	46.59	46.13	46.76	46.92	45.17	44.13
Al_2O_3	18.58	16.45	14.54	16.13	15.28	16.47
Fe_2O_3	13.91	15.73	15.33	15.85	15.55	17.55
MgO	3.97	4.51	4.22	5.93	4.25	7.88
CaO	7.21	7.56	8.49	6.58	9.18	7.25
Na_2O	3.84	3.88	4.03	3.86	3.60	3.04
K_2O	1.12	1.46	1.37	1.85	1.09	0.76
TiO_2	4.14	3.28	3.87	2.77	5.07	2.60
MnO	0.18	0.20	0.21	0.19	0.20	0.20
P_2O_5	0.30	0.58	0.54	0.51	0.52	0.27
SUM	99.84	99.78	99.36	100.59	99.92	100.15
Loss on Ignition	-0.67	-0.46	0.45	-0.65	-0.38	-0.86
TOTAL	99.17	99.32	99.81	99.94	99.54	99.29
Norms						
Qz	0.0	0.0	0.0	0.0	0.0	0.0
Co	0.0	0.0	0.0	0.0	0.0	0.0
Or	6.7	8.8	8.2	11.0	6.6	4.5
Ab	32.9	28.1	28.8	27.2	26.5	24.1
An	30.6	23.5	17.9	21.4	22.6	29.5
Lc	0.0	0.0	0.0	0.0	0.0	0.0
Ne	0.0	2.8	3.2	3.1	2.4	1.1
Ac	0.0	0.0	0.0	0.0	0.0	0.0
Di	3.1	9.0	18.0	6.8	16.7	4.3
Hy	0.5	0.0	0.0	0.0	0.0	0.0
Ol	14.7	16.9	12.0	20.9	11.1	27.3
La	0.0	0.0	0.0	0.0	0.0	0.0
Mt	2.8	3.2	3.1	3.2	3.1	3.5
Il	8.0	6.3	7.5	5.3	9.8	5.0
Ap	0.7	1.4	1.3	1.2	1.2	0.6
Trace elements (ppm)						
Rb	13.4	23.0	19.3	29.1	15.2	5.8
Ba	779.0	808.3	979.4	943.3	743.9	492.8
Th	4.5	6.0	3.0	5.3	3.9	8.5
U						1.0
Mo						0.7
Ta						3.1
Nb	20.7	19.4	23.0	21.8	23.7	11.6
La	8.1	19.9	20.1	23.2	11.9	9.1
Ce	32.6	53.9	49.7	50.8	37.5	29.9
Sr	812.8	625.9	667.7	557.9	679.8	550.6
Nd	14.1	28.4	28.7	34.6	22.5	19.2
Hf						2.9
Zr	116.4	158.1	158.7	207.7	140.6	129.0
Y	12.7	25.3	26.0	30.6	23.5	18.9
Pb	2.4	5.3	7.1	4.2	5.3	2.7
Zn	87.4	115.2	109.8	114.4	110.2	116.2
Cu	29.4	52.9	100.6	31.7	56.9	29.5
Ni	19.5	32.7	15.1	61.4	14.9	107.0
Cr	5.4	25.5	6.4	58.2	11.3	110.7
V	145.0	193.9	186.8	202.3	260.5	196.3
Sc	9.8	17.2	29.4	14.0	30.8	9.7
Ga						19.4
Sn						

	Kûngnât	Kûngnât	Kûngnât	Kûngnât	Kûngnât	Kûngnât
Sample type	*Gabbro*	*Metasom. gabbro*	*Metasom. gabbro*	*Metasom. gabbro*	*EBG syenite*	*EBG syenite*
Sample number	58301B	86180b	86184b	86191B	95/62	95/63A
Major elements (wt%)						
SiO_2		39.59	42.80	40.54	59.24	60.04
Al_2O_3		15.51	15.49	14.41	16.10	18.25
Fe_2O_3		14.24	15.87	14.78	7.58	4.25
MgO		6.59	7.08	7.66	0.58	0.54
CaO		6.84	6.28	5.41	2.36	2.37
Na_2O		2.55	3.24	2.54	5.23	5.83
K_2O		6.23	3.40	6.02	5.68	6.03
TiO_2		2.09	2.24	1.75	0.75	0.71
MnO		0.16	0.18	0.21	0.17	0.08
P_2O_5		0.30	0.35	0.14	0.13	0.24
SUM		94.10	96.93	93.46	97.82	98.34
Loss on Ignition		3.03	1.29	2.74	1.39	1.51
TOTAL		97.13	98.22	96.20	99.21	99.85
Norms						
Qz		0.0	0.0	0.0	0.0	0.0
Co		0.0	0.0	0.0	0.0	0.0
Or		0.0	21.1	6.2	34.5	36.4
Ab		0.0	6.8	0.0	45.5	45.7
An		13.4	18.5	11.0	3.8	5.9
Lc		31.1	0.0	25.4	0.0	0.0
Ne		12.6	11.9	12.6	0.0	2.5
Ac		0.0	0.0	0.0	0.0	0.0
Di		11.6	9.7	14.1	6.4	3.8
Hy		0.0	0.0	0.0	4.6	0.0
Ol		21.1	23.5	23.6	0.8	2.3
La		2.2	0.0	0.0	0.0	0.0
Mt		3.1	3.3	3.2	2.6	1.5
Il		4.3	4.5	3.6	1.5	1.4
Ap		0.7	0.9	0.4	0.3	0.6
					0.21	0.33
Trace elements (ppm)						
Rb	5.2	1561.7	312.5	2135.2	80.9	49.4
Ba	448.5	496.7	538.7	509.6	794.5	1913.1
Th	10.6	12.8	9.3	25.8	5.1	2.0
U		1.0	1.0	2.0	2.7	2.0
Mo		0.7	0.6	0.5	2.9	0.9
Ta		1.0	0.8	4.4		
Nb	12.3	17.3	14.5	124.8	43.2	12.9
La	-15.8	16.1	111.4	97.1	29.5	10.8
Ce	18.3	44.3	56.6	210.6	53.6	22.8
Sr	514.7	593.2	459.3	410.9	110.2	546.6
Nd	8.4	29.5	84.7	91.1	29.3	12.8
Hf		2.4	2.9	10.9		
Zr	91.0	122.4	168.0	692.8	189.0	51.9
Y	10.1	34.9	93.9	65.2	20.0	10.3
Pb	1.8	50.0	54.6	43.3	10.0	6.6
Zn	204.5	149.5	243.0	321.0	91.4	45.6
Cu	31.3	17.4	33.0	17.5	8.6	3.5
Ni	76.4	103.3	105.2	108.3	0.8	0.8
Cr	60.1	117.1	125.9	153.6	2.3	1.2
V	1036.1	241.0	199.5	161.9	-4.0	-4.5
Sc	16.8	15.4	10.1	9.8	11.0	4.8
Ga		18.2	20.1	19.9		
Sn						

Sample type	Kûngnât *ELS syenite*	Kûngnât *ELS syenite*	Kûngnât *SE syenite*	Kûngnât *E syenite*	Kûngnât *E syenite*	Kûngnât *WULS*
Sample number	95/71	95/73B	81127	81143	81145	95/75
Major elements (wt%)						
SiO_2	64.98	59.31	59.61	62.97	59.87	61.89
Al_2O_3	16.04	17.92	16.69	16.67	17.05	14.14
Fe_2O_3	4.56	5.38	7.20	4.90	5.89	9.16
MgO	0.49	0.88	0.60	0.25	0.61	0.15
CaO	1.46	2.53	2.44	1.89	2.33	2.27
Na_2O	5.35	5.06	5.16	5.61	5.44	5.65
K_2O	5.68	6.35	6.05	5.86	5.99	4.78
TiO_2	0.55	1.01	0.75	0.47	0.73	0.75
MnO	0.08	0.08	0.16	0.11	0.15	0.20
P_2O_5	0.11	0.29	0.19	0.04	0.15	0.07
SUM	99.29	98.82	98.85	98.76	98.20	99.06
Loss on Ignition	0.57	0.42	0.74	1.11	1.47	0.30
TOTAL	99.86	99.24	99.59	99.87	99.67	99.36
Norms						
Qz	7.5	0.0	0.0	2.8	0.0	4.3
Co	0.0	0.0	0.0	0.0	0.0	0.0
Or	33.9	38.2	36.3	35.2	36.2	28.9
Ab	45.8	42.8	44.4	48.3	46.5	47.1
An	3.0	7.5	4.6	3.1	4.5	0.0
Lc	0.0	0.0	0.0	0.0	0.0	0.0
Ne	0.0	0.4	0.0	0.0	0.3	0.0
Ac	0.0	0.0	0.0	0.0	0.0	1.1
Di	3.1	2.8	5.6	5.4	5.5	9.8
Hy	3.9	0.0	1.9	2.6	0.0	4.9
Ol	0.0	3.9	2.8	0.0	3.3	0.0
La	0.0	0.0	0.0	0.0	0.0	0.0
Mt	1.5	1.8	2.5	1.7	2.0	2.4
Il	1.1	2.0	1.5	0.9	1.4	1.5
Ap	0.3	0.7	0.5	0.1	0.4	0.2
	0.28	0.40				
Trace elements (ppm)						
Rb	224.8	43.4	75.7		77.2	117.9
Ba	733.8	2134.3	446.8		1025.0	26.0
Th	26.2	3.4	1.5		3.3	6.5
U	7.7	2.1			1.0	3.0
Mo	1.8	1.2			2.4	1.1
Ta						
Nb	83.1	15.2	35.0		28.2	82.2
La	101.8	12.7	22.8		26.0	97.9
Ce	192.4	39.3	47.5		54.1	149.7
Sr	200.3	303.1	130.2		278.2	12.9
Nd	73.2	21.5	27.2		26.6	103.5
Hf						
Zr	630.9	151.6	104.2		114.5	228.8
Y	52.9	20.2	15.4		15.3	64.3
Pb	18.8	5.0	9.7		10.2	8.1
Zn	71.6	49.1	88.3		68.7	195.0
Cu	2.4	7.4	17.3		7.3	7.9
Ni	3.4	1.8	1.1		1.7	0.9
Cr	3.8	2.2	-3.6		1.1	0.3
V	8.3	-3.3	7.0		-1.0	0.4
Sc	2.4	1.6	4.6		4.0	0.2
Ga						
Sn						

Sample type	Kûngnât *WLLS*	Kûngnât *lam. WLLS*	Kûngnât *WLLS*	Kûngnât *WLLS*	Kûngnât *WLLS*	Kûngnât *WLLS*
Sample number	95/77B	95/84	95/85	81103	81108	81110
Major elements (wt%)						
SiO_2	58.19	60.78	59.30	60.15	63.39	49.32
Al_2O_3	15.03	15.35	15.33	15.18	16.25	9.17
Fe_2O_3	10.82	8.12	10.10	8.86	5.39	23.87
MgO	0.49	0.26	0.22	0.35	0.14	1.57
CaO	3.18	2.46	2.98	3.10	1.89	6.69
Na_2O	5.33	5.87	5.57	5.35	5.66	3.44
K_2O	5.28	5.55	5.27	5.51	6.14	3.02
TiO_2	1.12	0.74	0.75	0.81	0.46	2.77
MnO	0.19	0.17	0.23	0.17	0.11	0.49
P_2O_5	0.24	0.11	0.11	0.08	0.04	0.60
SUM	99.88	99.42	99.87	99.56	99.47	100.94
Loss on Ignition	0.07	0.32	0.09	-0.05	0.26	-1.26
TOTAL	99.95	99.74	99.96	99.51	99.73	99.68
Norms						
Qz	0.0	0.0	0.0	0.1	2.3	0.0
Co	0.0	0.0	0.0	0.0	0.0	0.0
Or	31.5	33.3	31.4	32.9	36.6	18.0
Ab	44.5	48.7	46.6	45.8	48.4	29.4
An	1.5	0.0	1.3	1.1	0.8	0.7
Lc	0.0	0.0	0.0	0.0	0.0	0.0
Ne	0.5	0.0	0.5	0.0	0.0	0.0
Ac	0.0	1.1	0.0	0.0	0.0	0.0
Di	11.2	10.3	11.4	12.2	7.4	25.1
Hy	0.0	0.0	0.0	3.2	1.8	8.4
Ol	4.3	2.8	3.6	0.0	0.0	3.6
La	0.0	0.0	0.0	0.0	0.0	0.0
Mt	3.7	2.0	3.4	3.0	1.8	8.1
Il	2.2	1.4	1.4	1.6	0.9	5.3
Ap	0.6	0.3	0.3	0.2	0.1	1.4
Trace elements (ppm)						
Rb	90.9	140.1	71.9	109.4	136.6	64.5
Ba	1044.4	295.6	174.5	398.5	225.7	645.3
Th	10.5	11.0	6.8	8.7	6.3	12.9
U	4.2	3.3	2.8	3.1		7.6
Mo	3.1	2.4	1.8	3.5		4.0
Ta	8.3					
Nb	54.9	48.4	11.6	50.9	53.5	112.5
La	54.9	103.3	13.4	49.8	41.0	76.3
Ce	120.5	125.2	35.8	111.4	83.5	177.0
Sr	91.5	48.8	35.9	58.8	48.2	67.4
Nd	63.3	74.4	19.4	57.4	43.2	100.1
Hf	6.2					
Zr	361.1	221.5	73.7	242.6	356.6	247.5
Y	47.9	53.4	16.4	43.6	37.0	74.0
Pb	11.0	8.5	6.1	13.3	13.8	7.6
Zn	127.0	115.3	86.7	110.5	82.1	276.2
Cu	10.8	5.8	13.5	11.0	5.7	33.5
Ni	3.0	1.0	0.9	1.7	2.9	0.5
Cr	0.9	1.2	2.7	1.1	-3.5	3.5
V	-9.6	-1.7	-4.5	-3.4	7.0	-15.9
Sc	13.9	7.4	5.6	9.6	2.1	33.9
Ga	27.1					
Sn						

Sample type	Kûngnât *WLLS*	Kûngnât *WULS*	Kûngnât *WULS*	Kûngnât *WULS*	Kûngnât *Microgranite*	Kûngnât *Microgranite*
Sample number	86200	81132	81133	81134	95/59B	95/59C
Major elements (wt%)						
SiO_2	61.35	62.52	62.81	65.73	64.99	73.02
Al_2O_3	15.46	16.39	15.99	17.13	14.81	11.88
Fe_2O_3	8.38	6.94	6.61	3.05	6.65	4.14
MgO	0.27	0.06	0.12	0.05	0.06	0.04
CaO	2.45	0.42	1.68	0.57	0.45	0.21
Na_2O	5.41	6.47	6.39	6.77	7.54	5.25
K_2O	5.56	5.55	5.27	5.68	4.52	3.80
TiO_2	0.61	0.55	0.56	0.11	0.28	0.15
MnO	0.17	0.16	0.16	0.08	0.14	0.05
P_2O_5	0.05	0.04	0.06	-0.01	0.03	0.01
SUM	99.71	99.09	99.64	99.16	99.46	98.55
Loss on Ignition	0.11	0.61	0.55	0.54	0.66	0.65
TOTAL	99.82	99.70	100.19	99.70	100.12	99.20
Norms						
Qz	1.5	0.2	0.8	2.5	5.0	27.4
Co	0.0	0.0	0.0	0.0	0.0	0.0
Or	33.2	33.4	31.5	34.0	27.4	23.1
Ab	46.2	54.3	53.5	57.2	52.4	41.1
An	1.5	0.0	0.0	0.0	0.0	0.0
Lc	0.0	0.0	0.0	0.0	0.0	0.0
Ne	0.0	0.0	0.0	0.0	0.0	0.0
Ac	0.0	0.9	0.8	0.5	4.8	3.0
Di	9.2	1.7	7.1	2.6	1.9	0.9
Hy	4.3	6.6	3.4	2.3	6.6	4.2
Ol	0.0	0.0	0.0	0.0	0.0	0.0
La	0.0	0.0	0.0	0.0	0.0	0.0
Mt	2.8	1.8	1.7	0.7	0.0	0.0
Il	1.2	1.1	1.1	0.2	0.5	0.3
Ap	0.1	0.1	0.1	0.0	0.1	0.0
Trace elements (ppm)						
Rb	142.5	142.0	124.6		241.8	221.2
Ba	333.8	6.7	32.5		63.7	50.7
Th	8.6	4.4	6.4		22.9	12.9
U	3.3		2.9		16.6	7.9
Mo	0.9		1.4		6.5	1.8
Ta					17.4	
Nb	41.1	55.8	43.8		179.3	147.2
La	54.7	24.4	54.0		167.1	53.2
Ce	106.3	90.1	106.1		352.8	119.5
Sr	53.0	3.0	14.9		13.5	14.3
Nd	53.5	35.2	62.4		117.8	47.5
Hf					12.7	
Zr	105.5	226.0	171.9		538.1	277.8
Y	42.8	20.3	26.9		58.9	36.5
Pb	10.7	7.9	5.9		21.3	17.9
Zn	111.3	95.1	98.6		197.5	147.3
Cu	5.8	8.8	9.2		5.4	-2.0
Ni	2.4	1.5	2.5		3.0	3.1
Cr	3.1	-3.2	1.7		0.7	2.5
V	1.2	5.0	-2.9		-0.5	3.9
Sc	11.8	-1.7	1.3		1.6	0.1
Ga					42.7	
Sn						

Sample type	Kûngnât *Microgranite*	Kûngnât *Microgranite*	Kûngnât *Microgranite*	Kûngnât *Microgranite*	Kûngnât *Microgranite*	Kûngnât *Microgranite*
Sample number	95/66	95/68A	95/68B	95/79A	95/79B	95/80
Major elements (wt%)						
SiO_2	71.33	65.67	62.23	63.47		65.39
Al_2O_3	14.32	16.24	16.72	15.79		14.00
Fe_2O_3	2.64	4.12	5.74	5.85		6.93
MgO	0.22	0.33	0.33	0.00		0.02
CaO	0.45	1.30	1.45	0.69		0.45
Na_2O	4.08	5.90	5.44	7.54		7.50
K_2O	5.24	5.51	6.37	5.34		4.48
TiO_2	0.29	0.32	0.44	0.15		0.31
MnO	0.05	0.11	0.12	0.13		0.12
P_2O_5	0.05	0.05	0.07	0.01		0.02
SUM	98.66	99.55	98.90	98.96		99.21
Loss on Ignition	0.89	0.58	0.55	0.36		0.27
TOTAL	99.55	100.13	99.45	99.32		99.48
Norms						
Qz	25.9	6.7	1.8	0.4		7.8
Co	1.2	0.0	0.0	0.0		0.0
Or	31.5	32.8	38.2	32.5		27.3
Ab	35.1	50.3	46.7	53.0		48.5
An	2.0	1.6	2.4	0.0		0.0
Lc	0.0	0.0	0.0	0.0		0.0
Ne	0.0	0.0	0.0	0.0		0.0
Ac	0.0	0.0	0.0	4.2		5.0
Di	0.0	4.0	3.9	3.1		2.0
Hy	2.4	1.9	3.3	5.1		6.7
Ol	0.0	0.0	0.0	0.0		0.0
Ln	0.0	0.0	0.0	0.0		0.0
Mt	1.3	2.0	2.8	0.0		0.0
Il	0.6	0.6	0.8	0.3		0.6
Ap	0.1	0.1	0.2	0.0		0.0
Trace elements (ppm)						
Rb	286.6	157.7	194.5	488.5	494.6	339.5
Ba	458.6	402.9	241.8	32.4	25.5	18.4
Th	42.0	26.8	24.9	25.8	10.8	11.6
U	13.0	7.4	7.1	8.2	6.3	3.7
Mo	1.8	1.5	5.0	1.4	0.7	4.3
Ta	18.2	13.3	10.8			
Nb	67.2	88.8	122.7	221.2	176.6	66.4
La	85.6	116.3	127.6	156.9	94.3	269.0
Ce	190.3	268.3	263.5	332.8	208.9	451.9
Sr	99.7	81.4	75.2	12.6	12.8	11.3
Nd	58.0	84.0	105.5	139.4	95.2	128.5
Hf	9.9	14.4	20.4			
Zr	342.9	643.1	1066.1	1190.6	539.1	312.2
Y	48.1	52.2	67.2	120.0	82.9	32.3
Pb	18.6	19.8	24.3	13.8	10.8	6.1
Zn	48.1	96.6	143.2	301.8	259.7	235.7
Cu	-0.3	6.9	7.5	-1.1	-0.7	1.1
Ni	4.9	3.0	2.5	2.5	3.7	2.5
Cr	3.2	2.1	3.5	1.1	0.0	2.8
V	12.3	4.9	2.5	-0.6	2.9	1.4
Sc	1.3	1.8	1.6	-1.7	-0.7	-0.5
Ga	24.4	29.9	34.4			
Sn						

Sample type	Kûngnât *Microgranite*	Kûngnât *Microgranite*	Kûngnât *Microgranite*	Kûngnât *Microgranite*	Kûngnât *Microgranite*	Kûngnât *Microgranite*
Sample number	81128	81144	86180A	86184	86185	86190
Major elements (wt%)						
SiO_2	71.20	73.41		75.98	75.22	
Al_2O_3	14.13	13.51		11.67	11.81	
Fe_2O_3	2.54	1.98		2.21	2.31	
MgO	0.29	0.08		0.01	0.04	
CaO	1.15	0.39		0.02	0.06	
Na_2O	4.67	3.84		4.35	4.72	
K_2O	5.06	5.34		4.76	4.12	
TiO_2	0.30	0.23		0.17	0.15	
MnO	0.04	0.04		0.02	0.03	
P_2O_5	0.01	0.03		0.00	0.01	
SUM	99.40	98.85		99.19	98.46	
Loss on Ignition	0.47	1.03		0.12	0.54	
TOTAL	99.87	99.88		99.31	99.00	
Norms						
Qz	21.8	29.5		33.0	32.0	
Co	0.0	0.8		0.0	0.0	
Or	30.1	32.0		28.5	24.9	
Ab	39.8	32.9		34.1	38.7	
An	2.7	1.8		0.0	0.0	
Lc	0.0	0.0		0.0	0.0	
Ne	0.0	0.0		0.0	0.0	
Ac	0.0	0.0		1.6	1.4	
Di	2.6	0.0		0.1	0.2	
Hy	1.2	1.6		2.2	2.3	
Ol	0.0	0.0		0.0	0.0	
La	0.0	0.0		0.0	0.0	
Mt	1.2	1.0		0.0	0.2	
Il	0.6	0.4		0.3	0.3	
Ap	0.0	0.1		0.0	0.0	
Trace elements (ppm)						
Rb	240.2	231.3	2.9	357.7	326.2	112.4
Ba	542.9	423.2	28.4	10.8	16.0	24.7
Th	38.5	34.7	274.9	10.2	15.7	247.0
U	10.7		61.5		9.4	94.8
Mo	1.9		1.3		1.5	3.7
Ta	6.6		70.2		27.8	
Nb	58.2	57.1	1054.4	111.5	128.7	3137.9
La	95.8	100.5	882.2	20.1	23.5	289.4
Ce	176.1	180.2	1621.6	77.2	113.8	747.6
Sr	137.4	57.5	83.3	2.6	8.4	44.5
Nd	57.0	63.3	654.8	26.9	35.6	289.8
Hf	8.2		91.8		33.1	
Zr	276.7	225.2	5076.4	553.7	1221.5	5182.8
Y	48.4	51.4	1366.4	15.2	25.1	423.9
Pb	22.7	4.1	422.9	31.7	32.6	835.8
Zn	39.1	21.2	212.3	118.7	152.8	527.8
Cu	0.2	2.2	-14.4	2.7	-5.4	-42.5
Ni	3.0	3.2	-10.6	3.9	1.8	3.6
Cr	0.3	-10.8	9.2	1.1	6.3	-0.2
V	15.1	11.6	-7.6	5.1	2.6	-0.7
Sc	1.6	0.5	-0.6	-0.9	-2.1	-5.7
Ga	22.9		49.7		33.4	
Sn						

	Kûngnât	Ivigtut	Ivigtut	Ivigtut	Ivigtut
Sample type	*Microgranite*	*Altered granite*	*Top granite*	*Top granite*	*Top granite*
Sample number	86191A	95/PG	95/1A	95/7	95/43B
Major elements (wt%)					
SiO_2		70.63	69.92	70.44	74.93
Al_2O_3		12.90	13.58	13.07	12.13
Fe_2O_3		2.68	3.56	3.40	1.88
MgO		0.02	0.07	0.10	0.04
CaO		0.83	0.96	1.22	0.47
Na_2O		3.10	5.09	4.86	4.39
K_2O		7.07	4.96	4.70	4.42
TiO_2		0.20	0.25	0.25	0.12
MnO		0.06	0.05	0.03	0.03
P_2O_5		0.03	0.04	0.05	0.01
SUM		97.52	98.48	98.11	98.42
Loss on Ignition		1.86	0.93	1.02	0.81
TOTAL		99.38	99.41	99.13	99.23
Norms					
Qz		24.3	19.5	22.1	31.7
Co		0.0	0.0	0.0	0.0
Or		42.9	29.9	28.4	26.6
Ab		27.0	43.1	41.9	37.8
An		0.4	0.0	0.0	0.3
Lc		0.0	0.0	0.0	0.0
Ne		0.0	0.0	0.0	0.0
Ac		0.0	0.5	0.1	0.0
Di		3.2	4.1	5.2	1.8
Hy		0.5	1.0	0.1	0.6
Ol		0.0	0.0	0.0	0.0
La		0.0	0.0	0.0	0.0
Mt		1.3	1.4	1.6	0.9
Il		0.4	0.5	0.5	0.2
Ap		0.1	0.1	0.1	0.0
Trace elements (ppm)					
Rb	8.1	737.7	247.2	419.8	375.7
Ba	20.1	231.6	326.0	254.4	81.1
Th	103.4	42.4	29.8	33.1	21.6
U	166.3	8.6	8.9	9.3	6.8
Mo	24.8	7.6	21.7	100.6	69.5
Ta	427.3	16.1	20.2	21.1	17.1
Nb	6072.4	99.2	147.7	153.9	98.9
La	570.6	130.4	130.9	97.9	33.7
Ce	1349.6	246.3	257.9	220.5	70.0
Sr	59.6	117.8	50.0	80.9	27.3
Nd	321.0	93.3	98.5	103.9	37.3
Hf	347.5	12.5	15.6	15.7	6.9
Zr	24259.7	494.2	604.1	526.1	193.1
Y	174.1	65.2	94.9	113.1	73.9
Pb	197.2	14.4	21.7	13.3	18.0
Zn	591.0	75.3	229.3	58.4	84.5
Cu	-68.8	-0.5	15.9	16.0	0.0
Ni	3.4	4.3	3.4	1.3	2.2
Cr	9.8	0.4	1.3	6.1	4.8
V	0.2	1.5	1.9	6.7	2.8
Sc	-9.0	-0.2	0.4	0.4	-0.2
Ga	119.7	28.9	36.0	39.2	35.3
Sn				3.8	2.0

	Ivigtut	Ivigtut	Ivigtut	Ivigtut	Ivigtut	Ivigtut
Sample type	*Top granite*	*Top granite*	*Altered granite.*	*Top granite*	*Top granite*	*Altered granite*
Sample number	96/1	96/3	96/7	96/13	96/14	J3 VII
Major elements (wt%)						
SiO_2	74.68	74.21	67.05	75.19	70.05	74.75
Al_2O_3	12.71	12.25	13.63	11.47	13.57	13.01
Fe_2O_3	1.67	2.00	1.63	0.92	3.69	1.23
MgO	0.01	0.04	0.00	0.01	0.05	0.00
CaO	0.20	0.87	0.01	1.07	0.90	0.02
Na_2O	4.56	4.17	7.32	3.73	5.13	5.89
K_2O	4.71	4.86	4.87	4.76	4.93	3.80
TiO_2	0.10	0.14	0.04	0.04	0.24	0.03
MnO	0.05	0.05	0.03	0.03	0.07	0.02
P_2O_5	0.00	0.01	0.01	0.01	0.03	-0.01
SUM	98.70	98.59	94.59	97.22	98.65	98.74
Loss on Ignition	0.61	0.63	0.81	0.91	0.82	0.96
TOTAL	99.31	99.22	95.40	98.13	99.47	99.70
Norms						
Qz	29.7	30.1	16.2	34.7	19.5	27.6
Co	0.0	0.0	0.0	0.0	0.0	0.0
Or	28.2	29.2	30.6	28.9	29.7	22.8
Ab	39.1	35.8	45.7	32.5	43.2	46.5
An	0.3	0.4	0.0	0.5	0.0	0.0
Lc	0.0	0.0	0.0	0.0	0.0	0.0
Ne	0.0	0.0	0.0	0.0	0.0	0.0
Ac	0.0	0.0	1.2	0.0	0.7	0.9
Di	0.6	3.2	0.0	1.6	3.9	0.1
Hy	1.1	0.0	1.9	0.0	1.3	1.3
Ol	0.0	0.0	0.0	0.0	0.0	0.0
La	0.0	0.0	0.0	0.0	0.0	0.0
Mt	0.8	1.0	0.0	0.5	1.3	0.0
Il	0.2	0.3	0.1	0.1	0.5	0.1
Ap	0.0	0.0	0.0	0.0	0.1	0.0
Trace elements (ppm)						
Rb	457.0	235.9	720.7	637.8	618.1	507.1
Ba	71.8	151.4	58.4	60.2	289.9	7.7
Th	14.4	16.4	342.8	194.8	28.5	42.5
U	7.9	5.4	80.5	51.3	6.9	15.9
Mo	4.1	8.1	15.7	40.4	8.3	0.6
Ta	24.5	16.7	128.9	111.2	14.4	46.7
Nb	137.6	76.2	1047.3	1262.6	130.3	247.5
La	27.9	47.4	12.5	15.3	95.8	65.0
Ce	100.1	91.9	114.0	123.9	205.6	157.6
Sr	17.2	45.1	152.6	146.2	95.3	44.4
Nd	39.0	47.1	17.8	21.6	91.4	67.7
Hf	10.2	7.2	130.8	121.6	14.1	33.5
Zr	243.6	179.3	3839.6	3509.6	515.9	791.8
Y	50.1	69.6	146.7	165.4	95.0	234.0
Pb	443.9	19.8	833.9	1230.7	17.3	108.5
Zn	85.1	64.3	924.1	536.2	197.2	213.8
Cu	1.0	9.8	64.3	-4.6	1.3	-6.6
Ni	2.2	1.5	-0.7	0.6	1.5	5.4
Cr	5.9	6.6	5.3	5.5	5.8	0.4
V	3.9	2.6	2.7	5.1	1.1	3.2
Sc	0.8	3.0	-2.5	-3.2	1.4	0.2
Ga	42.2	32.2	71.3	62.9	36.1	52.5
Sn	1.8	0.0	188.0	187.5	6.0	14.7

Sample type	Ivigtut *Greisen*	Ivigtut *Altered granite*	Ivigtut *Altered granite*	Ivigtut *Deep granite*	Ivigtut *Deep granite*	Ivigtut *Deep granite*
Sample number	J4 IV	J4 V	J4VI	BB25 I	BB25 II	BB25 III
Major elements (wt%)						
SiO_2	78.47	64.84	73.64	75.16	71.59	71.90
Al_2O_3	9.90	12.52	13.96	12.84	11.58	12.95
Fe_2O_3	1.32	2.54	1.40	0.87	2.65	1.51
MgO	0.06	0.18	-0.01	0.01	-0.02	-0.01
CaO	1.48	7.82	0.05	0.30	1.37	0.03
Na_2O	0.22	0.51	8.47	4.95	5.06	6.30
K_2O	5.43	4.80	1.19	4.41	3.78	3.99
TiO_2	0.05	0.03	0.03	0.05	0.06	0.04
MnO	0.04	0.02	0.02	0.00	0.05	0.03
P_2O_5	-0.03	-0.03	-0.01	0.00	0.00	-0.03
SUM	96.94	93.23	98.75	98.59	96.12	96.71
Loss on Ignition	1.88	2.59	0.90	0.69	1.41	0.97
TOTAL	98.82	95.82	99.65	99.28	97.53	97.68
Norms						
Qz		32.3	22.7	29.4	27.7	24.7
Co		0.0	0.0	0.0	0.0	0.0
Or		30.5	7.2	26.4	23.5	24.5
Ab		4.6	66.3	42.2	40.4	46.2
An		19.0	0.0	0.0	0.0	0.0
Lc		0.0	0.0	0.0	0.0	0.0
Ne		0.0	0.0	0.0	0.0	0.0
Ac		0.0	1.0	0.2	1.9	1.1
Di		5.4	0.3	1.4	5.7	0.3
Hy		0.0	1.4	0.1	0.0	1.5
Ol		0.0	0.0	0.0	0.0	0.0
La		0.0	0.0	0.0	0.0	0.0
Mt		1.3	0.0	0.3	0.0	0.0
Il		0.1	0.1	0.1	0.1	0.1
Ap		-0.1	0.0	0.0	0.0	-0.1
Trace elements (ppm)						
Rb	647.5	757.8	259.3	592.2	1084.0	1006.6
Ba	75.4	411.9	11.0	43.7	24.8	20.9
Th	198.3	217.6	74.9	55.2	117.4	88.8
U		59.2	17.0	26.2	113.6	47.2
Mo		2.6	0.4	1.6	2.8	2.2
Ta		86.4	56.4	107.5	154.1	84.5
Nb	2525.5	919.4	311.1	737.7	1300.0	640.6
La	43.3	14.5	74.6	44.0	61.6	31.9
Ce	153.3	105.6	188.5	155.3	246.5	115.6
Sr	109.5	803.7	32.6	42.8	202.6	27.7
Nd	63.4	36.1	79.2	63.8	89.3	45.2
Hf		78.3	41.5	59.5	100.4	71.7
Zr	2171.6	2828.8	970.3	1835.7	3623.8	2134.4
Y	293.1	152.6	265.4	212.6	390.7	164.9
Pb	217.1	136.5	113.3	6.1	304.9	142.8
Zn	750.6	55.8	291.1	16.7	720.9	386.7
Cu	363.5	1.2	-9.3	-14.8	-20.6	-10.8
Ni	4.5	3.9	3.3	4.9	5.6	4.5
Cr	1.9	0.8	0.4	0.7	0.4	2.2
V	4.7	3.8	4.3	5.5	2.0	2.9
Sc	-2.4	2.2	0.5	-1.3	-0.7	-0.9
Ga		55.4	61.0	60.0	56.1	60.7
Sn		415.3				

Sample type	Ivigtut *Deep granite*	Ivigtut *Deep granite*	Ivigtut *Top granite*	Ivigtut *Top granite*	Ivigtut *Top granite*	Ivigtut *Top granite*
Sample number	BB25 IV	BB25 V	IV53	IV54	IV59	IV61
Major elements (wt%)						
SiO_2	73.72	62.19	68.48	74.78	74.76	70.42
Al_2O_3	12.38	17.60	13.85	12.22	12.61	13.64
Fe_2O_3	1.85	3.49	4.24	1.82	1.76	3.26
MgO	0.02	0.10	0.13	0.00	0.00	0.08
CaO	0.65	0.62	1.17	0.50	0.42	0.99
Na_2O	4.02	6.33	4.44	3.72	4.26	4.68
K_2O	5.07	6.62	5.27	4.77	4.51	4.76
TiO_2	0.13	0.12	0.31	0.09	0.11	0.26
MnO	0.06	0.12	0.10	0.04	0.02	0.06
P_2O_5	0.00	0.01	0.07	0.01	0.00	0.05
SUM	97.89	97.20	98.06	97.95	98.45	98.19
Loss on Ignition	1.25	2.11	0.83	1.22	0.69	0.59
TOTAL	99.14	99.31	98.89	99.17	99.14	98.78
Norms						
Qz	30.1	0.0	19.6	33.9	31.8	22.8
Co	0.0	0.0	0.0	0.1	0.0	0.0
Or	30.6	40.3	31.9	28.8	27.1	28.7
Ab	34.8	51.5	38.4	32.2	36.7	40.4
An	0.8	0.1	2.3	2.5	2.0	2.2
Lc	0.0	0.0	0.0	0.0	0.0	0.0
Ne	0.0	2.1	0.0	0.0	0.0	0.0
Ac	0.0	0.0	0.0	0.0	0.0	0.0
Di	2.2	2.7	2.7	0.0	0.1	2.2
Hy	0.4	0.0	2.2	1.5	1.3	1.6
Ol	0.0	1.5	0.0	0.0	0.0	0.0
La	0.0	0.0	0.0	0.0	0.0	0.0
Mt	0.9	1.7	2.1	0.9	0.9	1.6
Il	0.2	0.2	0.6	0.2	0.2	0.5
Ap	0.0	0.0	0.2	0.0	0.0	0.1
Trace elements (ppm)						
Rb	180.3	564.8	403.5	467.9	472.4	213.7
Ba	14.5	152.2	481.1	121.0	12.7	429.6
Th	25.9	30.0	29.6	18.2	22.3	22.0
U	8.1	8.9				
Mo	37.2	91.8				
Ta	26.8	15.6				
Nb	118.9	77.3	115.3	100.0	125.2	104.5
La	126.0	69.6	121.4	39.7	26.7	123.0
Ce	242.5	153.6	238.2	89.4	64.0	240.8
Sr	15.0	21.8	67.6	39.0	27.7	62.9
Nd	88.5	65.7	91.5	33.7	31.2	83.0
Hf	14.0	16.2				
Zr	473.8	667.8	560.6	241.4	224.9	482.6
Y	61.8	155.3	75.3	91.6	69.8	66.4
Pb	13.4	4.4	26.0	95.2	15.7	11.2
Zn	79.5	30.2	187.0	293.0	158.5	154.1
Cu	-1.3	0.6	11.3	10.8	0.0	3.8
Ni	1.4	2.8	4.2	4.0	3.3	1.6
Cr	0.2	1.4	0.0	0.0	0.0	0.0
V	5.0	4.5	4.1	3.9	5.2	7.1
Sc	-2.1	1.8	4.3	0.0	0.5	1.6
Ga	35.7	55.0				
Sn	2.0	0.5				

Sample type	Ivigtut *Granophyre*	Ivigtut *Granophyre*	Ivigtut *Granophyre*	Ivigtut *Granophyre*	Ivigtut *Granophyre*	Ivigtut *Granophyre*
Sample number	95/25A	95/37B	95/52	96/15	96/18A	96/20
Major elements (wt%)						
SiO_2	75.11	74.73	75.23	74.68	76.45	74.59
Al_2O_3	12.03	11.85	12.07	12.29	12.01	11.93
Fe_2O_3	2.63	1.87	3.04	1.00	1.55	2.71
MgO	0.04	0.04	0.02	0.05	0.15	0.13
CaO	0.06	0.60	0.02	1.20	0.04	0.49
Na_2O	4.82	4.22	4.84	3.94	5.73	7.21
K_2O	4.06	4.78	3.86	4.98	2.12	0.03
TiO_2	0.10	0.08	0.07	0.08	0.05	0.06
MnO	0.02	0.01	0.02	0.01	0.03	0.01
P_2O_5	0.01	0.01	0.01	0.00	0.03	0.04
SUM	98.88	98.18	99.18	98.23	98.16	97.19
Loss on Ignition	0.72	1.05	0.67	0.82	0.59	1.25
TOTAL	99.60	99.23	99.85	99.05	98.75	98.44
Norms						
Qz	31.2	31.4	31.5	31.3	34.9	31.8
Co	0.0	0.0	0.0	0.0	0.3	0.0
Or	24.4	28.9	23.1	30.0	12.8	0.2
Ab	39.9	35.1	41.1	34.0	49.5	62.9
An	0.0	0.0	0.0	1.2	0.0	0.1
Lc	0.0	0.0	0.0	0.0	0.0	0.0
Ne	0.0	0.0	0.0	0.0	0.0	0.0
Ac	1.0	0.9	0.2	0.0	0.0	0.0
Di	0.2	2.7	0.0	1.7	0.0	1.9
Hy	2.5	0.6	2.6	0.0	1.7	1.6
Ol	0.0	0.0	0.0	0.0	0.0	0.0
La	0.0	0.0	0.0	0.0	0.0	0.0
Mt	0.6	0.3	1.3	0.5	0.8	1.3
Il	0.2	0.2	0.1	0.2	0.1	0.1
Ap	0.0	0.0	0.0	0.0	0.1	0.1
Trace elements (ppm)						
Rb	413.7	262.1	285.6	374.2	177.0	2.3
Ba	23.1	200.0	83.4	307.7	112.7	8.4
Th	44.1	11.0	21.7	59.9	218.6	216.4
U	13.7	16.8	10.4	13.3	41.4	142.8
Mo	2.2	11.3	1.7	3.4	5.4	6.2
Ta	41.9	41.8		42.7	144.1	138.7
Nb	358.3	380.9	341.9	333.3	1282.3	1267.6
La	25.6	45.8	64.4	59.2	21.1	21.5
Ce	91.6	131.7	152.6	169.7	166.1	166.9
Sr	27.5	43.2	17.3	45.3	20.4	44.4
Nd	35.0	70.5	64.7	71.4	54.5	54.4
Hf	44.7	38.5		39.1	138.0	133.5
Zr	1564.6	1464.8	1132.3	1237.4	3946.4	3914.6
Y	29.4	87.3	35.1	130.1	380.5	375.3
Pb	33.8	9.3	17.3	13.3	47.4	38.2
Zn	72.9	25.2	65.2	21.6	9.2	20.6
Cu	-0.4	182.5	6.8	67.3	111.9	252.6
Ni	2.7	3.6	2.7	3.7	-2.1	-1.3
Cr	0.6	2.1	2.3	3.8	4.7	4.0
V	2.2	5.1	1.7	4.7	4.2	5.2
Sc	-0.5	-1.9	0.4	1.5	-0.5	-0.6
Ga	46.6	46.2		42.5	62.4	58.9
Sn				124.0	69.5	

Sample type	Ivigtut *Granophyre*	Ivigtut *Granophyre*	Ivigtut *Granophyre*	Ivigtut *Granophyre*	Grønnedal-Íka *L. Ser. syenite*
Sample number	96/21A	96/21B	96/23A	96/23B	95/94
Major elements (wt%)					
SiO_2	74.54	74.97	75.61	74.89	56.71
Al_2O_3	11.67	11.82	12.50	11.90	22.98
Fe_2O_3	2.92	3.08	0.50	1.98	5.01
MgO	0.03	0.02	0.03	0.02	0.28
CaO	0.13	0.10	0.73	0.57	4.09
Na_2O	5.35	5.38	5.21	3.78	7.36
K_2O	2.51	2.58	3.38	4.99	1.28
TiO_2	0.08	0.09	0.06	0.08	0.14
MnO	0.07	0.04	0.00	0.00	0.10
P_2O_5	0.00	0.00	0.00	0.00	0.11
SUM	97.30	98.07	98.02	98.21	98.06
Loss on Ignition	1.56	0.93	0.61	1.01	1.91
TOTAL	98.86	99.00	98.63	99.22	99.97
Norms					
Qz	33.4	33.1	31.9	32.9	0.0
Co	0.0	0.0	0.0	0.0	2.4
Or	15.3	15.6	20.4	30.1	7.7
Ab	46.6	46.5	45.0	32.6	62.4
An	0.4	0.5	0.8	0.8	20.1
Lc	0.0	0.0	0.0	0.0	0.0
Ne	0.0	0.0	0.0	0.0	0.7
Ac	0.0	0.0	0.0	0.0	0.0
Di	0.2	0.0	0.8	1.9	0.0
Hy	2.5	2.6	0.0	0.7	0.0
Ol	0.0	0.0	0.0	0.0	3.8
La	0.0	0.0	0.0	0.0	0.0
Mt	1.4	1.5	0.2	1.0	2.4
Il	0.2	0.2	0.1	0.2	0.3
Ap	0.0	0.0	0.0	0.0	0.3
Trace elements (ppm)					
Rb	224.3	259.0	215.0	321.7	16.0
Ba	88.4	71.3	200.3	254.2	392.4
Th	46.9	62.1	27.0	33.6	4.8
U	15.0	22.4	16.9	21.0	1.5
Mo	3.4	3.1	7.4	8.0	1.2
Ta	45.2	41.9	53.6	42.4	
Nb	375.5	402.1	418.7	351.0	122.8
La	69.6	75.7	109.8	22.5	62.6
Ce	208.7	201.7	339.6	97.8	129.6
Sr	19.3	52.1	52.7	40.2	1184.8
Nd	102.3	99.7	159.1	54.4	53.3
Hf	61.7	57.1	82.0	37.8	
Zr	2176.5	2063.3	2530.6	1483.5	184.0
Y	183.6	185.6	126.3	96.0	22.0
Pb	81.7	73.4	11.8	24.3	5.7
Zn	684.2	879.5	9.3	15.4	91.9
Cu	11.0	19.8	7.3	274.0	3.2
Ni	-0.4	0.7	0.7	1.3	1.4
Cr	6.7	5.7	5.1	5.0	1.0
V	2.1	1.3	6.5	4.1	4.4
Sc	-2.1	-0.7	-3.1	-1.5	-0.4
Ga	48.4	48.0	43.8	44.3	
Sn	57.5		8.5	357.6	

	Grønnedal-Íka	Grønnedal-Íka	Grønnedal-Íka	Grønnedal-Íka	Grønnedal-Íka	Grønnedal-Íka
Sample type	*L. Ser. syenite*	*L. Ser. syenite*	*L. Ser. syenite*	*L. Ser. syenite*	*L. Ser. syenite*	*U. Ser. syenite*
Sample number	95/126	95/127	95/128	96/27	96/29	95/92
Major elements (wt%)						
SiO_2	56.71	53.82	54.71	55.73	53.40	50.01
Al_2O_3	17.83	15.51	22.72	20.56	19.16	25.20
Fe_2O_3	11.62	10.82	4.26	5.02	8.36	3.98
MgO	0.17	0.64	0.27	0.08	0.40	0.33
CaO	0.10	4.87	1.03	0.31	2.35	1.74
Na_2O	4.83	7.03	8.66	7.98	7.47	6.31
K_2O	6.85	4.94	6.52	7.43	5.62	5.98
TiO_2	0.38	0.10	0.12	0.16	0.08	0.13
MnO	0.13	0.36	0.12	0.09	0.24	0.13
P_2O_5	0.02	0.01	0.12	0.02	0.02	0.07
SUM	98.63	98.10	98.53	97.37	97.11	93.89
Loss on Ignition	0.83	1.75	1.93	1.85	2.73	5.81
TOTAL	99.46	99.85	100.46	99.22	99.84	99.70
Norms						
Qz	0.0	0.0	0.0	0.0	0.0	0.0
Co	2.4	0.0	0.0	0.0	0.0	5.7
Or	41.4	30.5	39.2	45.6	34.4	37.8
Ab	41.7	19.9	22.4	21.4	25.9	24.1
An	0.4	0.0	3.9	0.0	2.2	8.7
Lc	0.0	0.0	0.0	0.0	0.0	0.0
Ne	0.1	18.8	28.3	24.6	21.4	17.9
Ac	0.0	4.9	0.0	2.1	0.0	0.0
Di	0.0	22.0	0.4	1.3	8.5	0.0
Hy	0.0	0.0	0.0	0.0	0.0	0.0
Ol	7.7	1.6	3.2	3.6	3.2	3.4
La	0.0	0.0	0.0	0.0	0.0	0.0
Mt	5.6	2.0	2.1	1.0	4.1	2.0
Il	0.7	0.2	0.2	0.3	0.2	0.3
Ap	0.0	0.0	0.3	0.0	0.1	0.2
Trace elements (ppm)						
Rb	163.4	135.3	132.0	189.7	187.2	126.8
Ba	182.8	58.9	146.1	83.2	68.1	555.3
Th	8.7	12.1	7.6	5.7	7.0	9.5
U	5.4	5.3	1.9	0.5	2.8	3.5
Mo	3.6	2.5	1.7	2.4	3.8	1.5
Ta						
Nb	119.6	87.3	83.8	58.2	83.5	79.3
La	36.4	32.3	32.7	35.7	42.8	38.6
Ce	54.2	93.9	70.8	72.4	91.4	92.7
Sr	226.1	235.9	632.3	360.1	283.3	637.2
Nd	22.3	56.6	36.5	32.0	37.2	38.5
Hf						
Zr	227.2	1336.8	510.5	199.8	709.7	556.2
Y	12.9	24.5	16.9	13.2	17.1	16.5
Pb	8.0	5.5	5.7	3.9	12.9	13.1
Zn	138.6	149.7	87.0	68.3	132.7	116.2
Cu	6.6	5.4	5.2	2.2	8.2	3.5
Ni	1.5	1.9	2.2	0.7	2.2	2.2
Cr	1.3	0.8	-0.5	4.8	8.1	3.1
V	2.1	4.1	2.4	3.8	3.2	3.1
Sc	-0.3	-0.7	-1.0	-1.7	3.5	-2.7
Ga						
Sn						

	Grønnedal-Íka	Grønnedal-Íka	Grønnedal-Íka	Grønnedal-Íka	Grønnedal-Íka	Grønnedal-Íka
Sample type	*U. Ser. syenite*	*U. Ser. syenite*	*U. Ser. syenite*	*U. Ser. syenite*	*U. Ser. syenite*	*U Ser. syenite*
Sample number	95/98	95/103	95/105	95/109A	95/119	95/122
Major elements (wt%)						
SiO_2	54.89	54.40	48.04	53.47	53.58	55.27
Al_2O_3	22.09	22.03	25.17	22.54	27.29	23.94
Fe_2O_3	4.54	4.24	5.41	4.86	3.69	4.51
MgO	0.32	0.27	0.51	0.42	0.31	0.18
CaO	1.08	0.77	1.52	1.31	0.02	0.27
Na_2O	9.15	9.57	8.51	9.36	3.91	3.76
K_2O	6.00	5.86	5.14	5.81	7.96	8.32
TiO_2	0.12	0.18	0.35	0.29	0.15	0.13
MnO	0.09	0.12	0.14	0.12	0.09	0.10
P_2O_5	0.13	0.03	0.41	0.18	0.02	0.20
SUM	98.41	97.46	95.20	98.37	97.02	96.67
Loss on Ignition	1.35	2.52	4.39	1.38	2.98	2.93
TOTAL	99.76	99.98	99.59	99.75	100.00	99.60
Norms						
Qz	0.0	0.0	0.0	0.0	0.0	0.0
Co	0.0	0.0	4.0	0.0	12.7	9.1
Or	36.1	35.7	32.1	35.0	48.6	51.0
Ab	25.5	25.1	19.3	22.1	32.9	33.0
An	1.5	0.0	5.2	2.4	0.0	0.1
Lc	0.0	0.0	0.0	0.0	0.0	0.0
Ne	28.9	31.4	30.7	31.8	0.7	0.0
Ac	0.0	0.2	0.0	0.0	0.0	0.0
Di	2.7	3.2	0.0	2.7	0.0	0.0
Hy	0.0	0.0	0.0	0.0	0.0	2.5
Ol	2.5	2.1	4.4	2.7	3.0	1.5
La	0.0	0.0	0.0	0.0	0.0	0.0
Mt	2.2	1.9	2.7	2.4	1.8	2.2
Il	0.2	0.4	0.7	0.6	0.3	0.3
Ap	0.3	0.1	1.0	0.4	0.0	0.5
Trace elements (ppm)						
Rb	191.7	166.8	109.3	146.6	229.9	236.2
Ba	147.1	295.5	2242.5	1080.9	252.0	373.2
Th	2.3	8.5	6.9	6.7	7.1	4.9
U	1.5	5.2	1.0	1.3	1.7	1.9
Mo	1.0	3.6	2.4	2.2	1.0	1.4
Ta						
Nb	40.9	122.9	90.5	68.0	59.8	57.8
La	27.4	33.2	65.3	56.4	65.6	29.3
Ce	50.9	86.1	145.1	107.1	122.7	72.1
Sr	328.2	328.2	1048.1	754.6	157.9	240.0
Nd	25.7	35.9	57.8	45.2	43.8	38.8
Hf						
Zr	189.5	601.6	249.6	256.2	140.1	171.4
Y	9.0	15.0	25.7	19.6	11.7	13.0
Pb	0.6	6.6	3.4	3.9	5.4	3.0
Zn	59.0	109.0	129.3	92.6	78.0	79.7
Cu	3.4	-0.2	12.1	3.0	2.1	5.5
Ni	1.4	2.8	2.9	2.5	1.6	2.2
Cr	2.2	1.7	3.2	2.1	2.6	2.3
V	3.3	4.2	1.4	0.4	1.7	5.1
Sc	1.5	0.0	0.4	0.0	-3.3	-1.2
Ga						
Sn						

	Grønnedal-Íka	Grønnedal-Íka	Grønnedal-Íka	Grønnedal-Íka	Grønnedal-Íka	Grønnedal-Íka
Sample type	*U. Ser. syenite*	*U. Ser. syenite*	*Pxy-rich sy*	*Pxy-rich sy*	*Pxy-rich sy*	*Pxy-rich syenite*
Sample number	96/25	96/48	95/111	95/120	95/121	96/39
Major elements (wt%)						
SiO_2	51.25	56.98	52.36	58.15	51.90	48.36
Al_2O_3	19.68	22.16	21.85	22.87	18.48	12.18
Fe_2O_3	6.00	5.19	6.92	3.36	9.37	17.03
MgO	0.34	0.32	0.54	0.14	0.91	1.83
CaO	2.70	0.16	2.07	0.05	4.01	9.78
Na_2O	8.22	4.98	3.47	5.46	6.64	4.43
K_2O	7.31	7.37	8.34	7.39	4.95	3.42
TiO_2	0.23	0.22	0.23	0.09	0.27	0.35
MnO	0.20	0.11	0.17	0.07	0.29	0.56
P_2O_5	0.08	0.03	0.51	0.02	0.65	1.33
SUM	96.01	97.52	96.45	97.60	97.46	99.26
Loss on Ignition	3.48	2.02	3.09	2.22	1.82	1.13
TOTAL	99.49	99.54	99.54	99.82	99.28	100.39
Norms						
Qz	0.0	0.0	0.0	0.0	0.0	0.0
Co	0.0	5.9	4.8	6.0	0.0	0.0
Or	45.9	44.8	51.3	44.8	30.2	20.6
Ab	0.5	39.7	20.5	41.5	26.8	19.4
An	0.0	0.6	7.2	0.1	6.2	3.3
Lc	0.0	0.0	0.0	0.0	0.0	0.0
Ne	34.6	2.0	5.5	3.2	16.9	10.2
Ac	4.5	0.0	0.0	0.0	0.0	0.0
Di	12.0	0.0	0.0	0.0	8.6	32.0
Hy	0.0	0.0	0.0	0.0	0.0	0.0
Ol	1.3	3.9	5.6	2.5	4.7	2.5
Lu	0.0	0.0	0.0	0.0	0.0	0.0
Mt	0.0	2.5	3.4	1.6	4.6	8.2
Il	0.5	0.4	0.5	0.2	0.5	0.7
Ap	0.2	0.1	1.2	0.1	1.6	3.1
Trace elements (ppm)						
Rb	138.7	250.3	258.0	194.9	139.5	115.8
Ba	655.2	245.7	2268.6	316.1	179.2	125.8
Th	10.3	7.5	13.6	7.3	7.4	12.4
U	8.8	1.6	5.3	2.3	2.6	2.3
Mo	4.1	2.9	3.8	1.3	1.5	2.0
Ta					6.8	
Nb	129.8	77.2	229.5	52.4	76.6	77.3
La	59.6	51.6	112.0	26.1	86.5	162.9
Ce	126.7	84.4	248.3	74.9	220.2	437.2
Sr	1079.8	228.3	810.7	228.0	368.7	646.9
Nd	60.1	39.8	104.6	26.1	121.9	273.6
Hf					11.4	
Zr	555.6	659.1	1065.3	140.5	547.1	987.6
Y	17.7	16.7	35.1	14.0	32.3	63.4
Pb	6.7	7.6	10.5	3.9	3.1	0.4
Zn	135.7	116.4	166.2	74.1	138.6	234.2
Cu	3.6	3.5	6.6	2.5	7.1	12.2
Ni	0.7	2.7	2.1	1.5	1.7	1.7
Cr	4.6	6.6	4.2	1.8	1.5	11.4
V	1.6	4.8	4.8	17.3	4.8	6.7
Sc	-1.4	-0.7	-2.0	-1.3	2.7	3.9
Ga					31.7	
Sn						

	Grønnedal-Íka	Grønnedal-Íka	Grønnedal-Íka	Grønnedal-Íka	Grønnedal-Íka	Grønnedal-Íka
Sample type	*Syenite*	*Syenite*	*Syenite*	*Syenite*	*Xen por syenite*	*Xen por syenite*
Sample number	95/93	95/97	95/106	96/47	95/117	95/118
Major elements (wt%)						
SiO_2	52.72		59.63	53.34	60.42	54.86
Al_2O_3	24.35		21.19	26.46	18.22	18.16
Fe_2O_3	5.83		4.30	4.72	6.74	8.30
MgO	0.36		0.30	0.19	0.08	0.51
CaO	0.97		0.04	0.45	0.23	2.19
Na_2O	7.97		7.08	5.51	8.41	5.74
K_2O	3.69		4.96	5.65	3.55	5.48
TiO_2	0.16		0.28	0.17	0.12	0.24
MnO	0.16		0.06	0.14	0.36	0.29
P_2O_5	0.16		0.03	0.04	0.16	0.48
SUM	96.38		97.87	96.67	98.29	96.26
Loss on Ignition	3.57		1.85	3.29	1.47	2.59
TOTAL	99.95		99.72	99.96	99.76	98.85
Norms						
Qz	0.0		0.0	0.0	0.0	0.0
Co	6.1		4.3	11.0	0.5	0.0
Or	22.7		30.1	34.6	21.5	33.8
Ab	45.8		58.0	43.4	64.7	39.8
An	3.9		0.0	2.0	0.1	7.9
Lc	0.0		0.0	0.0	0.0	0.0
Ne	13.3		1.9	2.7	4.4	6.0
Ac	0.0		0.0	0.0	0.0	0.0
Di	0.0		0.0	0.0	0.0	0.1
Hy	0.0		0.0	0.0	0.0	0.0
Ol	4.6		3.1	3.5	5.0	6.7
La	0.0		0.0	0.0	0.0	0.0
Mt	2.9		2.1	2.3	3.3	4.1
Il	0.3		0.5	0.3	0.2	0.5
Ap	0.4		0.1	0.1	0.4	1.2
Trace elements (ppm)						
Rb	72.0	107.4	137.6	195.6	96.5	191.2
Ba	575.5	35.7	2073.6	499.8	344.4	607.9
Th	4.7	5.1	7.2	8.3	17.0	19.0
U	1.4	3.4	3.6	3.1	12.9	4.3
Mo	1.5	4.1	2.7	3.4	17.2	3.0
Ta						
Nb	119.7	38.6	96.3	111.2	412.4	159.0
La	40.2	27.8	26.6	25.5	214.0	77.7
Ce	96.2	90.1	92.6	34.6	668.2	195.5
Sr	1364.5	135.3	121.8	426.5	185.1	775.7
Nd	46.0	46.0	36.2	17.4	196.5	87.1
Hf						
Zr	281.2	2576.5	1230.2	255.3	2074.3	1874.7
Y	21.1	20.4	10.1	10.1	33.4	37.8
Pb	3.6	3.7	9.0	18.7	9.5	13.6
Zn	123.3	145.2	99.9	144.2	254.2	264.1
Cu	2.9	6.0	2.1	7.2	10.0	10.6
Ni	1.1	1.2	3.2	0.5	3.1	0.7
Cr	0.9	0.5	2.1	3.5	-1.6	1.6
V	1.7	16.7	10.9	5.3	0.3	4.4
Sc	-1.4	3.5	-0.7	0.9	0.0	0.8
Ga						
Sn						

	Grønnedal-Íka	Grønnedal-Íka	Grønnedal-Íka	Grønnedal-Íka	Grønnedal-Íka	Grønnedal-Íka
Sample type	*Xen por syenite*	*Microsyenite*	*Microsyenite*	*Carbonatite*	*Carbonatite*	*Carbonatite*
Sample number	96/37	95/125	96/40	95/101	95/110	95/86D
Major elements (wt%)						
SiO_2	53.57		54.09	0.65	10.83	0.81
Al_2O_3	20.19		19.28	0.20	3.10	0.28
Fe_2O_3	6.39		8.88	4.16	6.73	17.37
MgO	0.56		0.34	0.19	0.21	0.66
CaO	3.76		1.19	50.09	40.44	41.95
Na_2O	7.87		6.72	0.01	0.67	0.13
K_2O	1.69		6.83	0.14	1.79	0.10
TiO_2	0.58		0.21	0.01	0.02	0.01
MnO	0.21		0.21	1.13	0.69	1.33
P_2O_5	0.60		0.06	2.08	2.98	4.23
SUM	95.42		97.81	58.66	67.46	66.88
Loss on Ignition	4.20		1.60			
TOTAL	99.62		99.41	58.66	67.46	66.88
Norms						
Qz	0.0		0.0			
Co	0.0		0.0			
Or	10.5		41.5			
Ab	55.1		24.6			
An	15.5		2.4			
Lc	0.0		0.0			
Ne	8.1		18.4			
Ac	0.0		0.0			
Di	0.0		2.9			
Hy	0.0		0.0			
Ol	4.9		5.4			
La	0.0		0.0			
Mt	3.2		4.3			
Il	1.2		0.4			
Ap	1.5		0.2			
Trace elements (ppm)						
Rb	51.8	136.1	206.6	-1.2	44.3	0.6
Ba	279.2	95.0	51.0	6014.4	1412.9	3187.2
Th	10.3	5.6	5.1	147.7	82.7	129.7
U	3.8	2.9	1.1	-11.6	0.5	26.5
Mo	2.3	3.8	1.2	1.8	235.0	7.0
Ta						
Nb	101.2	51.6	76.9	-1.0	388.2	441.6
La	49.7	4.1	22.6	784.1	786.9	650.3
Ce	120.9	34.8	62.1	2132.4	1949.1	1606.8
Sr	1284.8	110.1	398.5	10058.8	5898.0	16099.9
Nd	70.3	18.0	25.4	1123.9	1061.0	1041.6
Hf						
Zr	780.5	2942.2	525.4	18.4	22.2	31.3
Y	26.2	11.5	6.8	236.2	304.2	412.3
Pb	13.4	2.8	1.2	18.4	20.2	39.3
Zn	178.0	125.3	126.8	74.4	142.5	141.8
Cu	1.8	6.4	22.6	43.8	33.4	34.9
Ni	1.7	1.4	1.2	6.0	5.8	7.6
Cr	5.4	3.7	9.6	-4.6	-6.9	-4.4
V	3.3	6.0	1.8	0.0	1.4	0.0
Sc	2.9	0.5	0.6	23.5	20.9	9.0
Ga						
Sn						

	Grønnedal-Íka	Grønnedal-Íka			
Sample type	*Carbonatite*	*Carbonatite*	*Gneiss*	*Gneiss*	*Gneiss*
Sample number	96/35	96/36	95/37H	95/50A	95/123
Major elements (wt%)					
SiO_2	1.65	3.35	74.12	71.53	64.53
Al_2O_3	0.52	0.95	14.88	15.93	16.94
Fe_2O_3	14.72	18.87	0.53	0.87	3.20
MgO	0.72	0.42	0.35	0.32	0.27
CaO	37.48	39.14	3.07	2.16	1.91
Na_2O	0.18	0.09	4.21	4.59	8.54
K_2O	0.22	0.76	1.18	3.43	3.68
TiO_2	0.01	0.01	0.08	0.09	0.09
MnO	2.93	1.70	0.01	0.02	0.16
P_2O_5	1.73	1.31	0.03	0.05	0.21
SUM	60.15	66.58	98.46	98.99	99.53
Loss on Ignition			0.83	0.87	0.33
TOTAL	60.15	66.58	99.29	99.86	99.86
Norms					
Qz			38.5	26.7	0.0
Co			1.2	0.9	0.0
Or			7.1	20.5	22.1
Ab			36.2	39.3	65.7
An			15.3	10.5	0.0
Lc			0.0	0.0	0.0
Ne			0.0	0.0	1.0
Ac			0.0	0.0	2.3
Di			0.0	0.0	7.1
Hy			1.2	1.4	0.0
Ol			0.0	0.0	0.6
La			0.0	0.0	0.0
Mt			0.3	0.4	0.0
Il			0.2	0.2	0.2
Ap			0.1	0.1	0.5
Trace elements (ppm)					
Rb			95.7	180.1	74.4
Ba	206.2	806.3	429.6	413.8	424.7
Th			0.4	9.9	5.3
U			0.7	2.2	2.7
Mo			0.6	0.6	1.2
Ta					
Nb			2.6	14.3	46.2
La	1055.0	946.8	-1.7	6.0	48.4
Ce	2605.5	2282.1	-3.7	14.7	91.0
Sr	19227.9	15245.4	252.0	210.7	153.7
Nd	1269.6	1171.8	0.8	7.4	46.0
Hf					
Zr			22.9	77.2	318.1
Y			3.3	12.4	18.3
Pb			8.8	22.4	6.6
Zn			14.1	33.8	103.7
Cu			-3.3	2.2	-0.5
Ni			7.4	3.4	1.8
Cr			6.9	1.1	1.9
V			10.6	6.4	12.0
Sc			2.1	1.3	1.8
Ga					
Sn					

Sample type	*Gneiss*	*Gneiss*	*Gneiss*	*Gneiss*	*Gneiss*	*Gneiss*
Sample number	96/22	J3 VIII	J3 IX	81141	KU13	KU14
Major elements (wt%)						
SiO_2	70.10	70.38	75.33	56.25	49.53	71.46
Al_2O_3	16.54	15.30	13.27	24.68	26.72	15.28
Fe_2O_3	1.95	2.59	1.61	2.10	3.35	1.79
MgO	0.67	0.69	0.44	2.22	2.24	0.66
CaO	4.06	3.19	2.56	4.58	13.13	2.41
Na_2O	5.10	5.37	4.86	5.61	3.12	5.55
K_2O	0.49	1.21	0.80	3.44	0.63	1.29
TiO_2	0.17	0.28	0.17	0.11	0.25	0.23
MnO	0.03	0.04	0.02	0.05	0.05	0.02
P_2O_5	0.08	0.08	0.02	-0.01	0.01	0.06
SUM	99.19	99.13	99.09	99.03	99.03	98.76
Loss on Ignition	0.52	0.73	1.22	1.05	1.25	1.05
TOTAL	99.71	99.86	100.31	100.08	100.28	99.81
Norms						
Qz	28.7	26.6	37.9	0.0	0.0	28.1
Co	0.4	0.0	0.0	3.4	0.0	0.5
Or	2.9	7.3	4.8	20.5	3.8	7.7
Ab	43.6	45.9	41.6	44.9	25.6	47.6
An	19.8	14.2	12.2	23.0	57.7	11.7
Lc	0.0	0.0	0.0	0.0	0.0	0.0
Ne	0.0	0.0	0.0	1.7	0.6	0.0
Ac	0.0	0.0	0.0	0.0	0.0	0.0
Di	0.0	1.1	0.5	0.0	6.6	0.0
Hy	3.1	3.0	2.0	0.0	0.0	2.9
Ol	0.0	0.0	0.0	5.2	3.6	0.0
La	0.0	0.0	0.0	0.0	0.0	0.0
Mt	0.9	1.2	0.8	1.0	1.6	0.9
Il	0.3	0.5	0.3	0.2	0.5	0.4
Ap	0.2	0.2	0.1	0.0	0.0	0.1
Trace elements (ppm)						
Rb	36.4	85.4	63.7	1.4	14.4	74.7
Ba	204.3	197.4	153.5	16.3	120.8	201.2
Th	1.4	20.5	13.6	153.8	-1.0	3.2
U	0.5	2.1	2.4	217.7		
Mo	0.6	0.7	0.8			
Ta						
Nb	3.9	14.1	8.5	0.9	0.8	11.8
La	12.8	71.1	35.0	3.3	0.6	13.6
Ce	26.4	131.8	59.6	11.4	0.2	21.5
Sr	455.9	224.2	182.4	13.1	178.2	220.9
Nd	7.9	46.3	21.5	-2.0	-0.7	11.7
Hf						
Zr	82.8	172.0	139.4	4.6	5.9	108.0
Y	7.8	21.0	9.5	10.3	3.3	12.5
Pb	8.9	12.3	16.7	2.7	6.1	23.8
Zn	22.7	64.1	42.1	16.2	41.1	59.3
Cu	6.5	2.9	0.9	53.5	6.8	5.3
Ni	2.7	5.0	3.7	1.8	36.0	6.3
Cr	6.2	3.1	1.7	34.9	137.8	0.1
V	28.6	18.2	11.7	-0.4	100.4	19.7
Sc	8.6	5.1	3.0	925.5	13.8	3.0
Ga						
Sn						

Sample type	*Dyrnaes granite*	Nunarssuit *Helene granite*	Ilimaussaq *Green granite*	OGDC *Microsyenite*	YGDC *Granite vein*
Sample number	85924	101433	Il 100	40553	85974
Major elements (wt%)					
SiO_2	72.32	73.56	71.98	71.32	63.62
Al_2O_3	11.84	12.62	10.37	13.98	13.83
Fe_2O_3	4.17	2.40	5.14	1.68	6.51
MgO	0.04	0.07	0.09	0.37	0.27
CaO	0.48	0.52	0.77	0.76	1.32
Na_2O	4.67	3.91	4.50	3.75	5.49
K_2O	4.77	5.30	4.65	5.11	4.87
TiO_2	0.32	0.23	0.33	0.23	0.36
MnO	0.07	0.03	0.11	0.04	0.11
P_2O_5	0.01	0.02	0.00	0.06	0.04
SUM	98.69	98.66	97.94	97.30	96.43
Loss on Ignition	0.21	0.66	0.27	1.09	1.46
TOTAL	98.90	99.32	98.21	98.39	97.89
Norms					
Qz	26.5	29.3	29.9	28.2	9.7
Co	0.0	0.0	0.0	1.1	0.0
Or	29.0	31.8	28.5	31.1	30.2
Ab	35.3	33.6	28.5	32.7	46.1
An	0.0	1.3	0.0	3.5	0.0
Lc	0.0	0.0	0.0	0.0	0.0
Ne	0.0	0.0	0.0	0.0	0.0
Ac	3.0	0.0	3.7	0.0	1.7
Di	2.1	1.1	3.5	0.0	5.8
Hy	3.3	1.3	4.0	2.1	3.7
Ol	0.0	0.0	0.0	0.0	0.0
Ln	0.0	0.0	0.0	0.0	0.0
Mt	0.0	1.2	0.0	0.8	2.1
Il	0.6	0.4	0.6	0.5	0.7
Ap	0.0	0.0	0.0	0.1	0.1
Trace elements (ppm)					
Rb	262.9	152.6	388.6	177.8	174.5
Ba	79.9	296.6	20.4	795.2	118.6
Th	36.7	14.2	31.8	15.9	17.5
U	31.2	0.7	24.8	3.3	25.5
Mo	5.3	2.7	3.7	0.6	6.1
Ta	19.4	14.9	22.7	28.4	19.5
Nb	139.5	31.5	191.1	15.4	211.9
La	169.0	165.0	161.6	43.4	205.6
Ce	354.4	286.0	338.8	77.4	418.4
Sr	35.1	43.2	22.8	220.1	75.0
Nd	146.2	115.0	156.7	34.0	167.4
Hf	31.9	15.6	31.7	7.5	34.0
Zr	1341.0	565.7	1376.7	204.1	1638.8
Y	101.9	68.3	137.7	18.4	119.5
Pb	69.4	25.9	55.3	23.9	51.6
Zn	193.2	87.9	253.4	32.3	218.3
Cu	2.7	-0.5	-0.8	-1.1	2.8
Ni	2.5	2.4	0.9	4.5	2.1
Cr	7.1	6.0	6.0	2.1	9.1
V	2.4	-0.1	-3.3	14.2	-3.2
Sc	-2.3	-0.2	-0.9	4.1	-1.9
Ga	29.5	27.8	34.9	16.6	32.2
Sn					

	Tugtutoq	Bangs Havn	Tugtutoq	Nunarssuit
Sample type	*Granite*		*Granite*	*Granite vein*
Sample number	40596	101383	50260	NUN1
Major elements (wt%)				
SiO_2	69.96	59.42	68.55	66.23
Al_2O_3	13.45	13.84	13.89	8.49
Fe_2O_3	3.59	11.04	3.68	9.84
MgO	0.02	0.56	0.03	0.04
CaO	0.54	2.83	0.55	0.55
Na_2O	5.10	5.21	5.75	4.47
K_2O	5.01	4.08	5.01	5.10
TiO_2	0.27	1.23	0.22	0.28
MnO	0.06	0.23	0.05	0.16
P_2O_5	0.01	0.24	0.01	0.01
SUM	98.00	98.67	97.74	95.17
Loss on Ignition	0.72	0.35	0.53	0.44
TOTAL	98.72	99.02	98.27	95.61
Norms				
Qz	20.1	6.1	15.7	26.6
Co	0.0	0.0	0.0	0.0
Or	30.4	24.6	30.7	32.7
Ab	42.4	45.0	45.1	16.6
An	0.0	2.4	0.0	0.0
Lc	0.0	0.0	0.0	0.0
Ne	0.0	0.0	0.0	0.0
Ac	1.3	0.0	2.7	7.5
Di	2.4	9.0	2.5	2.6
Hy	2.0	4.6	2.7	10.5
Ol	0.0	0.0	0.0	0.0
La	0.0	0.0	0.0	0.0
Mt	0.9	5.3	0.0	0.0
Il	0.5	2.4	0.4	0.6
Ap	0.0	0.6	0.0	0.0
Trace elements (ppm)				
Rb	210.7	57.9	211.4	808.1
Ba	39.3	1380.2	5.8	55.6
Th	21.7	8.5	21.7	33.2
U	8.6	2.0	7.7	13.4
Mo	12.7	1.0	9.8	3.1
Ta	34.8	8.0	23.7	35.5
Nb	146.4	38.1	126.8	373.8
La	92.1	55.0	190.1	407.3
Ce	196.4	109.1	381.6	793.1
Sr	15.3	160.5	8.6	26.9
Nd	95.8	62.4	158.6	327.3
Hf	20.7	8.7	28.5	22.5
Zr	687.8	455.1	1108.9	1057.4
Y	113.7	75.5	101.2	166.2
Pb	31.9	25.8	34.9	80.3
Zn	100.2	207.3	172.0	698.1
Cu	-1.5	12.0	-1.8	0.3
Ni	1.8	2.7	2.6	2.4
Cr	7.3	0.0	6.8	9.3
V	-0.3	-7.1	-1.0	-2.1
Sc	-1.7	14.6	-1.0	2.8
Ga	41.0	27.7	44.4	41.3
Sn				

The $Fe_2O_3/(FeO+Fe_2O_3)$ ratios used for norm calculations, and the references from which those ratios were taken, are given below:

Lamprophyres, basaltic dykes and gabbros = 0.15 (Upton, 1960)

Kûngnât syenites & all trachytic dykes = 0.25 (Upton, 1960)

Grønnedal-Íka syenites = 0.55 (Bedford, 1989)

Ivigtut and Kûngnât granites = 0.35 (Bailey, 1980, Macdonald *et al.*, 1972)

Means & standard deviations used in figure 6.6

	lamprophyre	s.d.	ne-norm dyke	s.d.	hy-norm dyke	s.d
Rb	122.5	110.4	139.4	116.7	33.9	30.3
Ba	861.8	604.3	1189.6	816.6	522.8	299.7
Th	9.9	4.2	4.6	1.5	4.5	1.7
U						
K_2O	2.3	1.1	2.1	1.0	1.0	0.5
Ta						
Nb	102.0	44.0	37.1	21.6	13.0	6.4
La	38.5	21.1	30.3	22.1	24.3	15.6
Ce	105.9	42.0	77.1	43.3	61.6	31.7
Sr	641.3	386.1	837.5	441.4	422.9	190.4
Nd	57.6	22.4	43.0	22.4	33.8	16.7
Hf						
Zr	393.5	190.7	205.5	76.9	219.3	107.9
TiO_2	4.5	1.2	2.4	1.1	2.2	0.9
Y	30.7	7.2	29.4	9.5	32.6	13.7

All data in ppm except TiO_2 and K_2O, in wt%

Means & standard deviations used in figure 6.9

	gabbro	s.d	E. sy.	s.d	WLLS	s.d.
Rb	20.0	6.3	91.9	67.0	108.0	33.0
Ba	850.8	104.3	1174.6	686.6	445.4	304.8
Th	4.5	1.2	6.9	9.5	9.3	2.4
U			3.1	2.6	4.1	1.8
K_2O	1.4	0.3	5.9	0.2	5.2	1.0
Ta						
Nb	21.7	1.7	36.3	25.7	53.3	30.1
La	16.6	6.3	33.9	34.1	56.2	28.1
Ce	44.9	9.3	68.3	61.9	108.5	42.9
Sr	668.8	93.5	261.4	159.5	57.7	17.8
Nd	25.7	7.8	31.8	21.1	58.8	25.1
Hf						
Zr	156.3	33.5	207.0	212.7	229.8	110.8
TiO_2	3.8	0.9	0.7	0.2	1.0	0.8
Y	23.6	6.6	22.4	15.4	45.0	17.4

	WULS	s.d	granite	s.d
Rb	128.2	12.4	280.5	92.9
Ba	21.7	13.4	205.6	211.8
Th	5.8	1.2	24.2	10.9
U	3.0	0.1	9.3	3.7
K_2O	5.2	0.4	5.0	0.7
Ta				
Nb	60.6	19.6	113.5	53.5
La	58.8	37.0	110.5	71.2
Ce	115.3	30.8	229.7	115.5
Sr	10.3	6.4	46.7	46.0
Nd	67.0	34.4	78.5	38.8
Hf				
Zr	208.9	32.1	604.4	381.8
TiO_2	0.6	0.1	0.3	0.1
Y	37.2	23.7	50.5	27.6

Intrusion						Kûngnât	Kûngnât
Sample type	*Lamprophyre*	*Lamprophyre*	*Basaltic dyke*	*Basaltic dyke*	*Basaltic dyke*	*Gabbro*	*Gabbro*
Sample	95/16	95/58A	95/12C	95/44D	95/88	95/64	95/74
REE (ppm)							
La	54.9	87.3	11	45.5	10.2	11.9	24.2
Ce	122.94	188.91	26.76	108.02	25.17	30.83	56.98
Pr	15.52	23.64	3.72	13.83	3.44	4.15	7.58
Nd	64.2	92.2	17	58	15.9	16.7	31.3
Sm	13.25	17.21	3.91	10.97	3.77	2.89	6.03
Eu	4.36	5.45	1.68	4.58	1.52	2	2.44
Gd	12.17	14.92	4.67	9.84	4.6	3.39	6.18
Dy	7.98	9.22	4.59	6.51	4.42	2.49	4.71
Ho	1.33	1.53	0.93	1.16	0.88	0.49	0.89
Er	2.47	2.53	2.36	2.4	2.26	0.3	2.1
Yb	1.78	1.98	2.38	2.1	2.27	1.18	1.98
Lu	0.24	0.29	0.4	0.33	0.37	0.2	0.33

Intrusion	Kûngnât	Kûngnât	Kûngnât	Kûngnât	Kûngnât	Kûngnât	Kûngnât
Sample type	*Gabbro*	*Met. gabbro*	*Met. gabbro*	*Met. gabbro*	*EBG syenite*	*WULS*	*WLLS*
Sample	86186	86180b	86184b	86191B	95/62	95/75	95/77B
REE (ppm)							
La	14.3	22.6	106	114.2	26.6	83	48.1
Ce	32.9	44.24	63.54	237.91	60.32	141.28	113.92
Pr	4.26	5.63	20.45	26.42	7.66	24.78	14.76
Nd	17.2	21.5	72.9	87.1	29.5	100	57.1
Sm	3.63	4.54	16	16.18	5.54	18.31	10.7
Eu	1.63	1.62	1.98	1.5	2.14	0.65	2.95
Gd	3.72	5.22	18.44	14.5	4.73	16.43	10.3
Dy	3.22	5.26	17.02	13.74	3.84	12.07	8.87
Ho	0.62	1.08	3.27	2.73	0.72	2.29	1.75
Er	1.68	2.89	8.4	7.26	1.67	5.17	3.73
Yb	1.6	2.18	6.2	6.71	1.89	6.23	4.51
Lu	0.27	0.33	0.91	0.97	0.33	1.29	0.79

Intrusion	Kûngnât	Kûngnât	Kûngnât	Kûngnât	Kûngnât	Ivigtut	Ivigtut
Sample type	*Microgranite*	*Microgranite*	*Microgranite*	*Microgranite*	*Microgranite*	*Top granite*	*Top granite*
Sample	95/66	95/80	86180A	86185	86191A	95/1A	96/3
REE (ppm)							
La	73.8	306.9	1064	29.6	655	115.4	47
Ce	169.15	570.24	1988.1	103.48	1408.1	241.32	98.21
Pr	16.05	53.37	197.6	8.48	132.9	27.64	11.19
Nd	50.3	153.1	640	27.6	381	95.3	37.5
Sm	8.57	15.4	159	6	58.1	18.47	7.67
Eu	0.73	0.48	5.6	0.18	2	1.62	0.78
Gd	7.54	8.74	198.5	4.95	41.5	17.53	8.25
Dy	8.08	5.93	240.5	6.07	31.6	16.74	8.65
Ho	1.67	1.19	48.9	1.35	6.3	3.25	1.75
Er	4.26	2.31	132.8	4.34	14.6	7.59	4.26
Yb	5.37	5.24	114	5.98	19.9	7.24	4.28
Lu	0.88	1.05	15.8	1.04	3.7	1.06	0.62

Intrusion	Ivigtut	Ivigtut	Ivigtut	Ivigtut	Ivigtut	Grønnedal-Ík	Grønnedal-Íka
Sample type	*Alt. granite.*	*Alt. granite.*	*Deep granite*	*Granophyre*	*Granophyre*	*L. Ser. syenite*	*U. Ser. syenite*
Sample	96/7	J4VI	BB25 II	96/18A	96/21B	96/29	95/103
REE (ppm)							
La	14.2	62.5	57.5	20.4	73.8	38.8	34.4
Ce	61.86	161.1	186.74	106.72	179.08	82.43	69.83
Pr	7.9	19.91	23.14	15.6	23.34	9.96	7.91
Nd	21.1	68.1	70	51.7	88.6	35.5	28.1
Sm	9.85	21.78	24.78	24.02	25.44	6.09	4.73
Eu	0.3	0.36	0.81	0.82	0.92	1.4	1.28
Gd	12.32	27.28	30.17	32.04	29.57	5.08	3.72
Dy	38.77	37.92	74.63	64.2	32.53	3.67	2.86
Ho	9.16	8.02	16.96	13.65	6.42	0.68	0.53
Er	29.67	22.02	52.06	37	15.95	1.27	1.16
Yb	40.15	23.61	64.3	38.32	15.92	2.11	1.26
Lu	5.93	3.41	9.46	5.46	2.26	0.48	0.19

Intrusion	Grønnedal-Ík	Grønnedal-Ík	Grønnedal-Íka		Nunarssuit	Ilimaussaq	OGDC
Sample type	*Pxy-rich sy*	*Xen por sy.*	*Carbonatite*	*Dyrnaes gran.*	*Helene granite*	*Green granite*	*Microsyenite*
Sample	95/121	96/37	96/35	85924	101433	II 100	40553
REE (ppm)							
La	74.1	53.6	493.8	212.9	168.4	153	43.6
Ce	198.77	124.38	1302.62	427.65	304.67	321.82	85.06
Pr	27.06	16.87	173.42	47	31.83	37.37	9.83
Nd	110.5	67.2	682.4	152.6	97.3	128	31.5
Sm	19.99	12.11	105.68	25.2	16.13	23.43	4.88
Eu	4.25	4.25	31.02	1.2	1.22	1.51	0.7
Gd	15.31	10.05	71.49	20.26	13.54	21.23	3.43
Dy	8.75	6.08	43.16	18.46	11.62	20.92	2.88
Ho	1.45	1.02	7.18	3.73	2.29	4.28	0.57
Er	2.69	1.93	10.93	9.76	5.64	11.55	1.54
Yb	3.09	2.12	6.14	10.14	5.56	11.61	1.9
Lu	0.6	0.37	0.71	1.61	0.93	1.86	0.32

Intrusion	YGDC	Tugtutoq	Bangs Havn	Tugtutoq	Nunarssuit
Sample type	*Granite vein*	*Granite*		*Granite*	*Granite vein*
Sample	85974	40596	101383	50260	NUN1
REE (ppm)					
La	218.3	101.5	54.8	193.2	434.6
Ce	425.5	205.5	124.25	387.6	868.29
Pr	46.15	24.08	16.12	42.67	96.69
Nd	147.6	85.7	63.7	138.7	307.2
Sm	24.57	17.44	13.68	22.38	50.28
Eu	1.43	0.69	3.87	0.72	1.85
Gd	20.17	17.34	14.17	18.14	39.4
Dy	19.6	18.28	13.41	18.56	32.54
Ho	4.03	3.69	2.71	3.87	6.34
Er	10.89	9.96	7.4	10.55	16.75
Yb	12.12	8.79	7.37	10.63	25.43
Lu	2.04	1.3	1.26	1.67	5.06

Appendix F: Radiogenic isotope data

Sample No.	$^{87}Rb/^{86}Sr$	$^{87}Sr/^{86}Sr$	$^{147}Sm/^{144}Nd$	$^{143}Nd/^{144}Nd$	Initial data $^{87}Sr/^{86}Sr$	Initial data ε_{Nd}	T Nd DM
Lamprophyres							
95/13	1.711	0.73397	0.1271	0.512264	0.70357	3.77	1574
95/16	0.287	0.70889	0.1222	0.512266	0.70379	4.59	1487
95/58A	1.233	0.70826	0.1039	0.512233	0.68635	6.86	1286
Basaltic dykes							
95/12A	0.003	0.70329	0.0977	0.511927	0.70323	1.86	1617
95/12C	0.018	0.70376	0.1427	0.512274	0.70344	1.48	1896
95/88	0.027	0.70385	0.1285	0.512309	0.70337	4.43	1520
95/44D	0.605	0.71641	0.1134	0.512011	0.70566	1.00	1742
Alkaline dykes							
95/51	4.301	0.77338	xxx	xxx	0.69697		
95/57	3.831	0.76252	0.1504	0.512354	0.69447	1.82	1935
Grønnedal-Íka							
95/103	1.575	0.72923	0.0971	0.511973	0.69988	3.62	1549
95/110	0.025	0.70348	0.2434	0.512119	0.70301	-17.96	-5456
95/119	7.174	0.77810	xxx	0.511878	0.64444		
95/121	1.142	0.72245	0.3767	0.511965	0.70117	-43.25	-1125
95/127	1.686	0.73333	0.1193	0.512142	0.70192	3.23	1640
96/29	1.970	0.73763	0.1029	0.512035	0.70092	3.87	1545
Ivigtut							
95/1A	17.021	0.98408	0.1167	0.511858	0.69156	-2.93	2039
95/7	16.905	1.00062	0.1284	0.511918	0.71009	-3.56	2210
95/43B	55.199	1.61148	xxx	0.512111	0.66283		
96/3	20.390	1.01199	0.1227	0.511897	0.66156	-3.10	2108
96/7	14.980	0.93936	0.2755	0.513251	0.68191	-0.15	225
96/14	20.810	1.06561	xxx	xxx	0.70797		
BB25 (v)	132.796	2.65076	0.1418	0.512095	0.36853	-2.16	2248
J3 (vii)	35.602	1.41961	0.2174	0.512646	0.80775	-3.03	-22870
J4 (vi)	28.074	1.23939	0.1943	0.512655	0.75691	0.70	3929
BB25(ii)	16.110	1.02112	0.2325	0.512854	0.74426	-1.29	-2507
95/52	79.999	2.05099	0.1549	0.512322	0.67612	0.26	2164
96/18A	31.590	1.22608	0.2568	0.513041	0.68317	-1.37	-421
96/21B	15.381	0.96883	0.1895	0.512535	0.70449	-0.90	3897
96/23B	27.398	1.13567	0.1828	0.512495	0.66480	-0.66	3258
Kûngnât							
95/64	0.043	0.70423	0.1122	0.511918	0.70345	-0.30	1860
95/74	0.111	0.70529	0.1189	0.511940	0.70327	-0.96	1955
95/62	1.764	0.74227	0.1100	0.511884	0.71016	-0.60	1870
95/73B	0.449	0.71138	0.1165	0.511917	0.70321	-1.02	1943
95/75	67.326	1.75428	0.1119	0.511862	0.52911	-1.35	1937
95/77B	3.135	0.75656	0.1153	0.511852	0.69951	-2.10	2019
95/85	8.195	0.84238	0.1169	0.511885	0.69325	-1.70	2000
95/66	9.254	0.85476	0.1010	0.511540	0.68636	-5.87	2182
95/68B	8.374	0.85983	0.1070	0.511757	0.70744	-2.60	1997
95/80	304.332	5.68955	0.0581	0.511371	0.15144	-2.17	1748
Gneiss							
J3 (viii)	1.180	0.74628	0.1037	0.511022	0.72600	-17.28	2943
95/50A	2.628	0.77177	0.1518	0.511919	0.72661	-7.15	3035

Sample No.	$^{206}Pb/^{204}$ Pb	$^{207}Pb/^{204}$ Pb	$^{208}Pb/^{204}$ Pb	Apparent mu_1
Lamprophyres				
95/13				
95/16	20.952921	15.560996	40.213444	7.80
95/58A				
Basaltic dykes				
95/12A				
95/12C	16.382068	15.020844	36.285053	7.49
95/88	16.440447	15.014551	36.533752	7.47
95/44D				
Alkaline dykes				
95/51				
95/57				
Grønnedal-Íka				
95/103	23.843867	15.731080	39.257691	7.69
95/110				
95/119				
95/121				
95/127	21.158882	15.481851	41.883751	7.63
96/29	15.915756	14.871248	36.024502	7.29
Ivigtut				
95/1A				
95/7				
95/43B				
96/3	15.617717	14.992589	38.003851	7.55
96/7	15.825294	14.828084	36.388302	7.22
96/14	19.284229	15.056988	40.029348	7.14
BB25 (v)	29.788768	15.868220	52.521732	7.08
J3 (vii)				
J4 (vi)				
BB25(ii)	19.684347	15.121747	36.660592	7.20
95/52				
96/18A				
96/21B	18.792341	15.096673	38.172226	7.28
96/23B				
Kûngnât				
95/64				
95/74				
95/62	15.916409	14.946779	35.832897	7.42
95/73B				
95/75	16.266376	14.976865	36.565583	7.43
95/77B	16.504457	14.998046	36.635909	7.43
95/85				
95/66	24.389585	15.652360	44.425524	7.47
95/68B				
95/80				
Gneiss				
J3 (viii)	15.287991	14.615228	45.585431	7.28
95/50A	21.906379	15.602534	36.180781	6.09

Sample No	$^{87}Rb/^{86}Sr$	$^{87}Sr/^{86}Sr$	$^{147}Sm/^{144}Nd$	$^{143}Nd/^{144}Nd$	Initial data $^{87}Sr/^{86}Sr$	Initial data ε_{Nd}	T Nd DM
YGDC							
196/494	0.232	0.70668	0.1149	0.512039	0.70281	0.52	1725
50216	6.051	0.79776	0.1039	0.511794	0.69682	-2.63	1891
186227	3.591	0.81449	0.1084	0.511785	0.75459	-3.48	1984
186225a	66.305	1.67359	0.0836	0.511574	0.56758	-3.89	1853
Tugtutoq							
50337	68.036	1.72347	0.1053	0.511924	0.58859	-0.29	1734
50308	66.287	1.74927	0.0703	0.511765	0.64356	1.83	1480
50279	38.489	1.29105	0.0959	0.511713	0.64903	-3.01	1867
50258	164.367	3.39719	0.1052	0.511780	0.65545	-3.09	1933
40593	5.258	0.78924	0.0993	0.511738	0.70153	-3.03	1889
50244	18.084	0.98472	0.0959	0.511690	0.68307	-3.46	1896
50228	78.843	2.04305	0.0981	0.511936	0.72791	1.02	1610
Syenitknold							
216618	0.026	0.70344	0.1125	0.512021	0.70300	0.53	1711
216615	0.217	0.70690	0.0419	0.512073	0.70328	12.11	964
216614	0.062	0.70400	0.1196	0.511997	0.70297	-1.00	1878
216603	0.127	0.70602	0.0879	0.511844	0.70390	0.75	1591
OGDC							
86035	36.752	1.28242	0.0965	0.511863	0.66937	-0.17	1683
2/81	0.217	0.70650	0.1108	0.512042	0.70288	1.19	1652
108180	0.113	0.70481	0.1100	0.512030	0.70292	1.08	1657
86116	1.136	0.72106	0.1054	0.511947	0.70211	0.15	1702
Dykes							
91/80	0.182	0.70618	0.0706	0.511632	0.70314	-0.81	1624
68/80	0.729	0.70918	0.1055	0.511757	0.69702	-3.59	1970
59/80	0.504	0.71205	0.1115	0.511949	0.70364	-0.73	1801
3/80a	24.733	1.04855	0.1771	0.512041	0.63599	-8.75	4605
27/80	0.498	0.71101	0.1063	0.511849	0.70270	-1.91	1855
14/80	0.327	0.70869	0.1017	0.511965	0.70324	1.05	1623

Sample No.	$^{206}Pb/^{204}$ Pb	$^{207}Pb/^{204}$ Pb	$^{208}Pb/^{204}$ Pb
YGDC			
40452	17.937	15.412	37.616
175/80A	16.796	15.277	36.211
YGD 196	18.471	15.349	40.356
186227	16.961	15.281	36.391
50216	17.612	15.340	36.820
186225	18.271	15.379	37.130
OGDC			
2/81	19.886	15.598	38.380
108/80	19.591	15.557	38.528
40430	19.128	15.542	38.240
86116	18.901	15.457	37.969
86035	18.553	15.412	37.943
Central Tugtutoq			
40593	16.184	15.131	36.152
40599	31.989	16.391	52.612
50244	17.835	15.271	37.860
50279	16.316	15.135	36.330
50320	16.684	15.199	36.766
50280	16.775	15.245	37.277
50258	17.127	15.219	37.038
50337	16.598	15.160	36.586
50228	17.945	15.366	37.562
50288	21.175	15.550	37.040
50308	17.239	15.202	37.193
50094	17.344	15.318	36.607
Syenitknold			
216614	17.766	15.381	37.246
216618	17.523	15.336	37.031
216615	18.265	15.414	37.730
212198	18.076	15.399	37.542
216603	19.684	15.577	36.580
Dykes			
36/80	19.795	15.615	38.004
59/80	23.888	16.305	41.587
78/80	18.255	15.365	37.461
91/80A	16.108	15.145	35.740
14/80	19.519	15.511	36.702
27/80B	16.761	15.254	36.205
50094	17.347	15.325	36.638
68/80	18.459	15.455	37.809
117/80A	19.161	15.444	38.219
3/80A	18.038	15.371	37.149

Appendix G: Stable isotope data

Sample	Description	$\delta^{18}O_{SMOW}$	$\delta^{13}C_{PDB}$
95/86E	Gronnedal-Ika carbonatite: calcite	7.845	-4.677
95/86D	Gronnedal-Ika carbonatite: calcite	8.239	-4.377
96/33	Gronnedal-Ika carbonatite: calcite	7.01	-4.576
14849Sid	Gronnedal-Ika carbonatite: siderite	8.612	-5.025
96/35	Gronnedal-Ika carbonatite: siderite	7.386	-4.972
KUSid1	Kungnat SE pegmatite	10.3045	-6.554
KUCal1	Kungnat SE pegmatite	6.507	-5.032
KUCal2	Kungnat gabbro vugh	8.481	-6.753
KUCal3	Kungnat W pegmatite	7.861	-3.859
81126	Kungnat SE pegmatite	9.253	-6.415
95/76	Kungnat W pegmatite	8.9765	-7.1805
IvSid2	Ivigtut Siderite	8.029	-8.285
BGJU1	Ivigtut Siderite	8.41	-8.06
IvSid1	Ivigtut Siderite	7.776	-8.202
IvSid1b	Ivigtut Siderite	7.988	-7.252
Ivig. Sid.	Ivigtut Siderite	7.957	-8.032
BB25 iv	Siderite, w/in Ivigtut granite	9.152	-7.7
J3 iv	Siderite, from Ivigtut greisen	7.997	-7.052
81162	lamprophyre	10.309	-5.672
86167	lamprophyre	10.0865	-4.6935
96/52C	lamprophyre	9.946	-5.234
96/54A	lamprophyre	10.244	-4.972
95/12E	siderite from dyke mineralisation	7.648	-7.194
95/58	siderite from dyke mineralisation	7.468	-8.409

Appendix H: Average modal mineralogy

	Grønnedal-Íka L. Ser. foyaite	Grønnedal-Íka L. Ser. c-g. brn. sy.	Grønnedal-Íka U. Ser. foyaite	Grønnedal-Íka Pxy-rich syenite
Alkali feldspar	50-70%	40-50%	50-60%	
Plagioclase				
Quartz				
Nepheline	10-15%	30-40%	15-20%	5-10%
Cancrinite	5%	<5%	<5%	5%
Olivine				
Pyroxene	5-20%	10%	10%	up to 60%
Amphibole				
Mica	5%		<5%	5-10%
Opaque oxides	5%	<5%	<5%	10-15%
Other accessories		<5%		5-10% (apatite)
Calcite				
Siderite				

	Grønnedal-Íka U. Ser. coarse sy.	Grønnedal-Íka Xen. porph. sy.	Grønnedal-Íka Carbonatite
Alkali feldspar	35%	65-70%	
Plagioclase			
Quartz			
Nepheline	50%	10%	
Cancrinite			
Olivine			
Pyroxene		15%	
Amphibole			
Mica	10%		
Opaque oxides		<5%	
Other accessories	5%	<5%	5%
Calcite		5-10%	75%
Siderite			20%

	Lamprophyre	Brown Dyke	Alkaline dyke
Alkali feldspar			60-80%
Plagioclase	<20%	60-70%	
Quartz			
Nepheline			
Cancrinite			
Olivine		10-20%	
Pyroxene	<10%	10-20%	<10%
Amphibole	20-40%		
Mica	20-40%		10-30%
Opaque oxides	10%	5-10%	5-10%
Other accessories		<5%	
Calcite	<20%		
Siderite			

	Ivigtut Top granite	Ivigtut Albitised granite	Ivigtut Granophyre	
Alkali feldspar	60-65%		50%	
Plagioclase		40-50%		
Quartz	25-30%	25%	40%	
Nepheline				
Cancrinite				
Olivine				
Pyroxene				
Amphibole	<10%			
Mica	<10%			
Opaque oxides	5%		5%	
Other accessories		20-30%	5%	
Calcite				
Siderite		10%		

	Kûngnât WLLS	Kûngnât WULS	Kûngnât Eastern syenite	Kûngnât Ring-dyke gabbro
Alkali feldspar	65-70%	70%	75-85%	
Plagioclase				65%
Quartz		10%		
Nepheline				
Cancrinite				
Olivine	5%		<5%	15%
Pyroxene	10-15%	10%	5-10%	10%
Amphibole	5-10%	5%	<5%	
Mica				5%
Opaque oxides	5%	5%	5%	5%
Other accessories				
Calcite				
Siderite				

	Kûngnât Late granite
Alkali feldspar	45%
Plagioclase	15%
Quartz	30%
Nepheline	
Cancrinite	
Olivine	
Pyroxene	
Amphibole	
Mica	10%
Opaque oxides	
Other accessories	
Calcite	
Siderite	